Compressive Sensing Based Positioning Algorithms to Locate Transmitting Nodes in Wireless Networks.

By

Audri Biswas

A thesis submitted to Macquarie University

for the degree of

Doctor of Philosophy

Department of Engineering

May 2018

MACQUARIE
University
SYDNEY·AUSTRALIA
FACULTY OF SCIENCE AND ENGINEERING

Examiner's Copy

Typeset in LaTeX 2_ε.

Except where acknowledged in the customary manner, the material presented in this thesis is, to the best of my knowledge, original and has not been submitted in whole or part for a degree in any university.

Audri Biswas

Acknowledgements

I would like to especially thank my principal supervisor, A/Prof. Sam Reisenfeld, for the patient guidance, encouragement, advice and the technical support he has provided throughout the duration of my candidature. I am extremely privileged to have a supervisor like him, who genuinely cared about the well-being of his students and showed true enthusiasm towards the outcome of my work. Without his unconditional dedication, support and guidance, this dissertation would not have been possible. He is undoubtedly one of the best scholars, teachers, and a role model, I have ever had the honor of meeting and working with. He is one those pure Engineers that truly understands the theory and has the ability to convert the concept into a working prototype. If I ever get the opportunity, I would never miss a chance of working with him again.

I would also like to extend my gratitude to all the academic and professional staffs of School of Engineering, Macquarie University who provided logistical and general support during my candidature. In particular, I would like to make a special mention about Prof. Candace Lang, who played an integral role in supporting me during the rough times of the candidature. My acknowledgment goes out to all the PhD students of School of Engineering, who provided a much need laugh and entertainment during the hectic PhD schedule. I thoroughly enjoyed the random conversations in the kitchen about the future of Engineering and the impact of PhD students on the workforce.

I would acknowledge the support of Mark Hedley and Zhou Chen from CSIRO, Australia and Leonardo Goratti from CREATE-NET, Italy for extending their helping

hands in guiding and advising me during the early stage of my PhD candidature.

Special acknowledgment goes out to Macqurie University, for awarding me with Macquarie University International Scholarship (MQIS) during my undergraduate years and Macquarie University Research Excellence Scholarship (MQRES) that provided me with the funding to undertake this research.

This section goes out to those special people in my life. Firstly my parents Prabir Biswas and Bichitra Das. I have been extremely fortunate in my life to have such parents, who never hesitated to sacrifice their comfort for the sake of my happiness. Their unconditional love and unparallel support provided me the motivation to go through the rough hurdles of PhD. I am blessed to call myself their son. Secondly, to all my extended families who were an excellent source of encouragement, whenever I felt down. Lastly to my beautiful wife Nishita Paul. She was always there supporting me during the best and worst part of PhD. Despite the long hours and weekends at University, she always welcomed me home with her brightest smile. This PhD would not have been possible without her love and support. Words will fall short if I had to thank her for all that she has done for me. She is my strength and undoubtedly the best gift from God.

To my parents and my beautiful wife.

List of Publications

0.1 Patent

- A. Biswas, S.Reisenfeld: Direction of Arrival Estimation, Australian Provisional Patent, 2016904636, PCT filed 28th October, 2017.

0.2 Conference

- A. Biswas and S. Reisenfeld, "*New high resolution direction of arrival estimation using Compressive Sensing*," 2017 IEEE 22nd International Workshop on Computer Aided Modeling and Design of Communication Links and Networks (CAMAD), Lund, 2017, pp. 1-6.

- S. Maric, A. Biswas and S. Reisenfeld, "A complete algorithm to diagnose and alleviate the effects of physical layer attacks," 2017 International Conference on Signals and Systems (ICSigSys), Sanur, 2017, pp. 29-34.

- A. Biswas, S. Reisenfeld, L. Goratti, M. Hedley and Z. Chen, "*Multiresolution Compressive Sensing algorithm to detect off-grid direction of arrival*," 2016 10th International Conference on Signal Processing and Communication Systems (ICSPCS), Gold Coast, QLD, 2016, pp. 1-6.

- A. Biswas, S. Reisenfeld, M. Hedley, Z. Chen, and P Cheng. "*Localization of primary users by exploiting distance separation between secondary users*," 2015

Cognitive Radio Oriented Wireless Networks - 10th International Conference, CROWNCOM, Doha, Qatar, 2015, Revised Selected Papers, pp. 451 462

0.3 Journal

- A. Biswas, S. Reisenfeld, "*Highly Accurate Off-Grid Direction of Arrival Estimation using a Novel Iterative Technique*," To be Submitted.
- A. Biswas, S. Reisenfeld, "*A Novel Signal Processing Technique to Estimate the Off-Grid Direction of Arrival using a Uniform Linear Array*," To be Submitted.
- A. Biswas, S. Reisenfeld, "*Performance comparison of a Uniform Circular Array and Uniform Linear Array using an Iterative Compressive Sensing Framework*," To be Submitted.
- A. Biswas, S. Reisenfeld, M. Hedley and Z. Chen, "*Effective sensor positioning to localize target transmitters in a cognitive radio network*", EAI Endorsed Transactions on Cognitive Communications, vol. 16, no. 6, pp. 4, 2016.

Abstract

Over the decades, the Wireless Cellular Network (WCN) and Wireless Local Area Network (WLAN) have transformed into a gigantic eco-system feeding billions of portable devices with an astronomical amount of the digital data. With modernization and miniaturization of computer electronics, this amount of data is set to hit a record high in the next few years. Unfortunately, current infrastructures of WCN and WLAN are struggling to cope with the global demand due to severe scarcity of spectral resources and outdated infrastructure. This lead to extensive research on the upcoming Fifth Generation (5G) wireless network technology. The 5G technology aims to increase the data rate by two orders of magnitude compared to the predecessor technology 4G. The technologies listed to be the key enablers for 5G include, spatial multiplexing, device-to-device communication, beam-forming and cognitive radio networks (self-configuration networks). In this regard, geo-location information of the wireless devices is crucial in bounding the large-scale interference between the devices to a level producing acceptable performance degradation. Moreover, accurate positioning information plays a critical role in determining exclusion zones for wireless devices in networks, and this enables maximal spectrum reuse and spectrum efficiency.

The thesis introduces several novel algorithms. Algorithms are introduced which accurately determine the Direction Of Arrival (DOA) of the signal at a receiver. Using these techniques at two or more receiving locations, the position of the radio transmitter may be determined with great accuracy using triangulation. In addition, the thesis proposes an algorithm to determine the position of a transmitting source using the

Received Signal Strength (RSS) at several locations. The new DOA and RSS based positioning algorithms are based upon the framework of compressive sensing (CS), which is an emerging signal processing technique that offers superior recovery of a signal using limited observations, especially when the signal is sparse in some given bases.

For CS implementation of the DOA estimation, the problem is initially modeled with the assumption that actual DOA is one of a quantized set of angles. With this assumption, a dictionary matrix may be constructed which can be used in the CS algorithm to find an estimated DOA which is an element of the set of quantized positions. In practical situations, the actual DOA is not always equal to an element of the quantized set of grid points, and this implies that the estimated DOA will have some quantization error. Since the number of antenna elements is typically much smaller than the number of quantization points, the matrix formulation of the solution of the vector indicating the DOA represent an under-determined set of equations. Compressive sensing is used to determine the sparsest solution to the matrix equation.

A fundamentally new iterative algorithm to estimate the DOA of an incoming signal in a wireless network is introduced in the thesis. This algorithm, which utilizes compressive sensing as a foundation, eliminates the error induced due to discrete grid quantization. This enables the estimation error performance of the algorithm to achieve the theoretical Cramer Rao Lower Bound (CRLB) using just two iterations. The algorithm requires extremely low computational complexity for implementation and is general in nature. The proposed algorithm is demonstrated by applying it to two antenna array geometries, the Uniform Circular Array (UCA) and Uniform Linear Array (ULA). For both the UCA and the ULA, the CRLB performance is achieved by the new algorithm. The relative performances of the UCA and ULA were compared.

The thesis also considers a novel multiresolution DOA estimation algorithm based on CS that illustrates superior performance compared to the traditional techniques. The multiresolution approach is also shown to be effective in reducing the computational complexity of the estimation process.

A novel RSS based localization algorithm is presented that offers improvement in

the structure of the dictionary matrix by selectively eliminating observations from closely placed sensors. Similar observations lead to ill-conditioned dictionary matrices and as a result, degrades the performance of CS processing. The study illustrates that different random distributions of sensors have unique effects on the structure of the measurement matrices.

An in-depth analysis on the impact of different parameters on the structure of the dictionary matrix is presented. The analysis suggests that careful manipulation of antenna array geometry parameters can significantly enhance the structure of the dictionary matrix and therefore improve the estimation accuracy of the algorithm.

In summary, the thesis investigates localization techniques based on compressive sensing processing. Several new, high-performance algorithms were described and their performances and computational complexities were analyzed. The thesis establishes a connection between the mathematical properties of the dictionary matrix and the performance of the new localization techniques. Within classes of antenna array geometries, the dictionary matrix properties are used as an enabler for the selection of antenna elements spacings that provided optimized DOA estimation performance.

Contents

List of Figures

List of Tables

1

Introduction

1.1 Motivation

The inception of wireless communication dates back to 1897 with Marconi's successful demonstration of wireless telegraphy [4]. In the early days, a variety of consumer applications adopted wireless system including: 1) television transmission using radio transmitters, 2) point-to-point microwave circuits that formed the backbone of the telephone network. Unfortunately, the wireless technology was replaced with modern wired connections including optical fibre cable. The fast transmission speed of an optical fibre provides a competitive advantage over the wireless systems and offers a reliable low error rate data transmission. Surprisingly after the deployment of mobile handsets in the early 1990s, which is primarily based on Wireless Communication Systems (WCS), an opposite trend was observed. Wired telephone technology slowly

started fading away and is partially replaced by hand-held mobile phones that were part of a wireless cellular networks (WCN) [5].

One of the major reasons behind the popularity of WCN is the flexibility of accessing a cellular network virtually anywhere and at any time. This clearly indicates that customers are now ready to sacrifice the reliability and performance of wired networks for the ease and accessibility of WCNs. Traditionally WCN suffered from limited spectral capacity and maximum network congestion. Such drawbacks prompted researchers to explore alternatives in order to provide the service needed. The hard work in research paid off with the development of Wireless Local Area Network (WLAN). A new standard (Wi-Fi) was published in 1997 and began its journey with two variants, called 802.11b (operating on the 2.4 GHz band) and 802.11a (operating on the 5.8 GHz band) [6, 7]. WLAN offered high data rates at the expense of limited network coverage (50 meters) compared to WCN (50 km). The backhaul of a WLAN is usually supported by wired connections (copper or optical fibre). Soon after the innovation of Wi-Fi standards, engineers and researchers immediately dived into the development of prototypes that would comply with it. Thanks to advanced electronics, miniaturization, and computerization of consumer devices became a reality. This led to ground-breaking innovations such as tablets, laptops, smart-phones, iPods, wearable smart-devices that are now able to connect themselves to the internet with the help of Wi-Fi. The popularity of Wi-Fi was boosted due to the ability to connect multiple devices to the internet at the same time. Often coupled with wireless capabilities, these smart electronic devices have an unprecedented capacity to connect and share information amongst themselves and with their users, leading to the promise of smarter systems. Currently, the field of wireless communication has evolved into a monstrous eco-system feeding billions of smart devices with an enormous amount of digital data. According to CISCO's visual networking index [8–10],

- The annual global internet traffic will reach 3.3 Zetabyte (ZB; 1000 Exabytes [EB], EB; 1 billion Gigabytes [Gb]) by 2021. This is expected to be a 175% increase from the 2016 global traffic of 1.2 ZB and accounts for a threefold increase in the next 4 years.

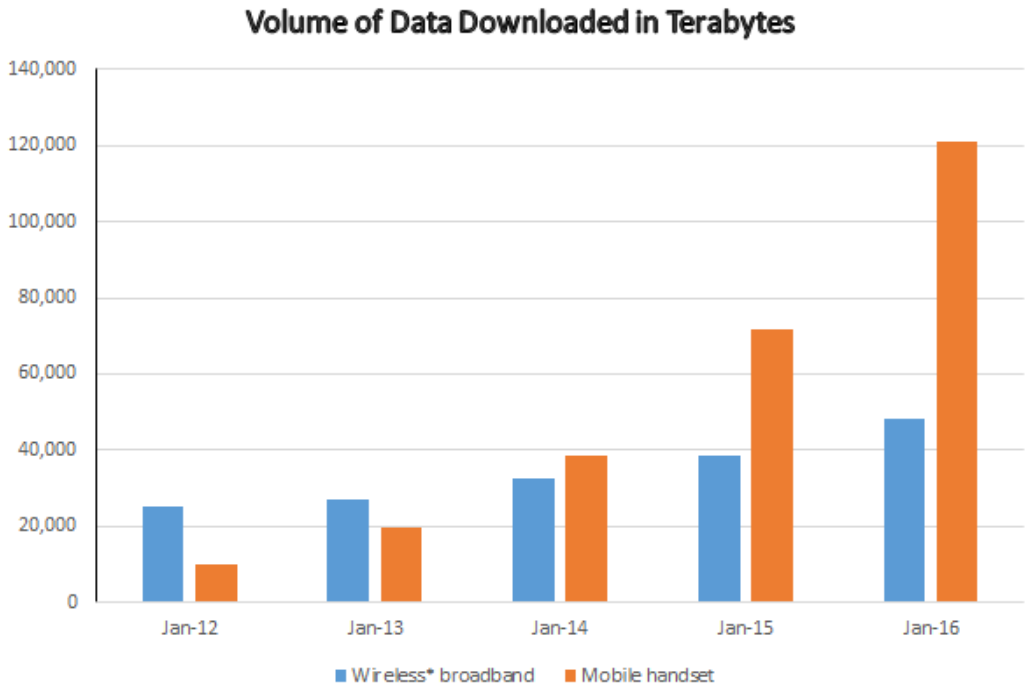

Fig. 1.1: Data downloads by Australian residents in terabytes (TB). Data collected from ABS.

- Traffic from wireless and mobile devices will account for more than 63% of the total internet traffic by 2021. Wireless devices will account for 63% of the aggregated internet traffic, while wired devices will account for 37%. In 2016, wired traffic accounted for 51%.

- The number of devices connected to the internet will be three times as high as the global population by 2021. Due to the exponential increase in the number of devices and their capability, internet traffic per capita will increase to 35 GB, from 13.5 GB in 2016.

The forecast clearly indicates that the smart sharing and wide connectivity of wireless devices will exert a serious strain on the existing wireless technologies. Australia is also not far behind in this global trend. The data from the Australian Bureau of Statistics (ABS) and Australian Communication and Media Authority (ACMA) [11–13] are combined to generate the bar diagram shown in Fig. 1.1. According to the

statistics,

- The total volume of data downloaded in the three months ended 31 December 2016 was 2.6 million Terabytes (or 2.6 Exabytes). This is a 23.3% increase in data downloads when compared with the three months ended 30 June 2016 and a 50.8% increase in the year between December 2015 and December 2016.

- The volume of data downloaded via mobile handsets for the three months ended 31 December 2016 was 146,050 Terabytes. This was a 20.6% increase in data downloads via mobile handsets from the three months ended 30 June 2016 and a 61.0% increase in downloads in the year ended 31 December 2016.

In reality, the evolution of the wireless technology fails to match up to the ever-growing demand for large data. In order to cater for the connectivity boom, an overhaul of the existing technology is mandatory. In the past few decades, the WCN went through several iterations of improvements. Since its inception, the WCN evolved from its legacy standard of the first generation (1G) to the existing fourth generation (4G) with current research focusing on the advancement of 4G and the implementation of the upcoming fifth generation (5G) technology [14, 15]. The prime emphasis of 5G will be on data rates and efficiency, with heavyweights such as Qualcomm and Nokia looking at technologies which can cope with traffic growth of 1000 times [16]. A summary of the standards, technologies adopted by the different generations are listed in Table. 1.1

Generations	**Standards**	**Technology**	**Data Switching**	**Data Rate.**
1G	AMPS, TACS	Analog	Circuit	NA
2G	GSM, CDMA, EDGE	Digital	Circuit	236.8 kbps
3G	UTMS, CDMA2000, HSPDA	Digital	Packet	384 kbps
4G	LTE Advanced, WiMax	Digital	Packet	100 Mbps
5G	Massive MIMO, D2D, M2M	Digital	Packet	10 Gbps

TABLE 1.1: A summary of the evolution of Wireless Cellular Networks.

Parallel to the development of the WCN, WLAN technology has significantly expanded

its capability to provide high speed to Wi-Fi customers [17, 18]. The different generations of the WLAN and their corresponding technologies and data rates are listed in Table. 1.2.

Generations	Protocol	Frequency	Data Rate.
1st	802.11	2.4 GHz	2 Mbps
2G	802.11a, 802.11b	5 GHz, 2.4 GHz	54 Mbps, 25 Mbps
3G	802.11g	2.4 GHz	54 Mbps
4G	802.11n	5 GHz, 2.4 GHz	600 Mbps
5G	802.11ac	5 GHz	1.63 Gbps
5G	802.11ad	60 GHz	4.63 Gbps

Table 1.2: A summary of the evolution of Wireless Local Area Networks.

1.2 Emerging Technologies for 5G WCN

Although there has been no confirmed consensus on the architecture of 5G, researchers have explored and proposed several alternatives that will offer cost-efficient improvements compared to the existing 4G WCN [19–23]. The primary technologies and approaches that can be adopted to satisfy the requirements of 5G can be classified as follows.

1.2.1 Heterogeneous Networks (HetNets)

To cater for the high volume of digital data, one of the possible solutions can be reducing the cell size. 5G will consist of a multi-tier heterogeneous networks consisting of macro-cells integrated with large numbers of micro-cells coexisting at the same time. Small cells will have a different flavour, as their area of coverage is smaller than macro cells. By reducing the cell size, the spectral efficiency can be improved through efficient frequency reuse [24]. At the same time, small cells also offer better network

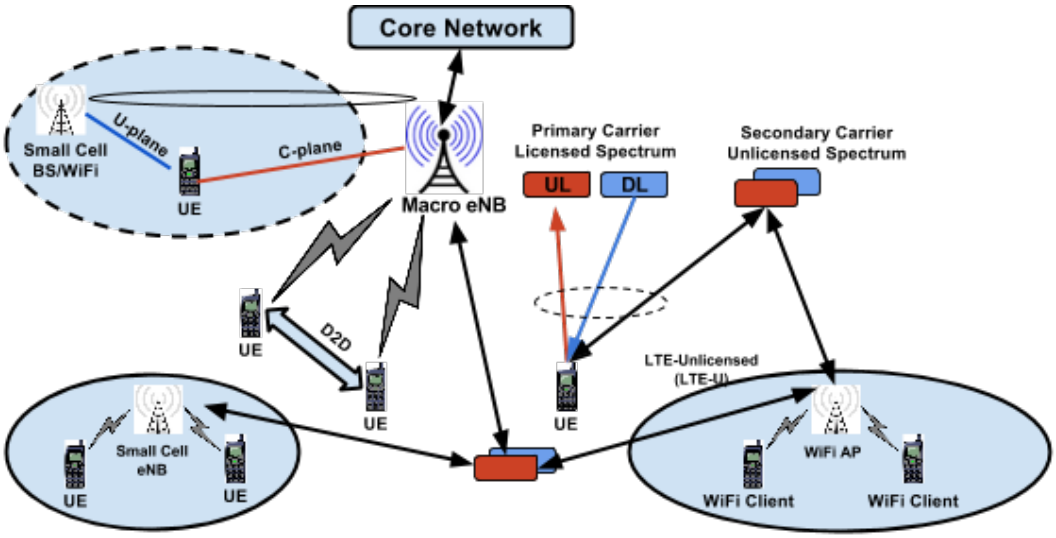

Fig. 1.2: A HetNet based 5G wireless network [1].

coverage as they can be easily deployed indoors such as home, office, university campus, public vehicles etc. The concurrent operations of different classes of cells will make 5G networks more dense than existing 4G [25]. High density and unplanned deployment of small cells introduce inter-cell interference, which has been considered to be one of the biggest drawbacks of HetNets. Additionally, due to the irregular shape and size of the cell, inter-tier interference (between micro and macro cells) can be introduced [26]. To overcome this issue, sophisticated power control and resource allocation techniques need to be considered. However, with accurate location information of the small cells and macro cell, the aforementioned issues regarding inter-cell and intra-cell interference can be significantly reduced [27].

1.2.2 Device-to-Device communication

Device to Device (D2D) communication has been widely praised to be a feasible solution for high-density network problems [28, 29]. D2D communication forms a direct link between two independent terminals in order to share information. In the current 4G cellular network, no standards are defined to establish a point-to-point (P2P) link between two devices. As a result, all communication is required to be routed via a Base Station (BS), which is extremely inefficient, especially when the devices are placed in

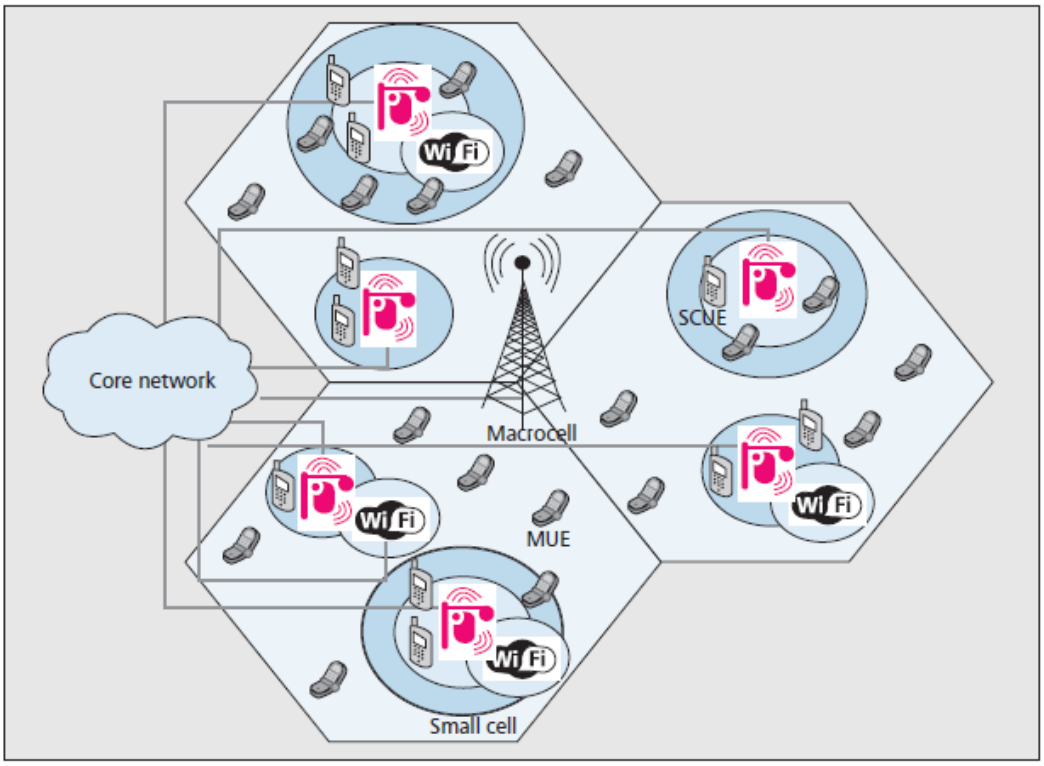

Fig. 1.3: Coexistence architecture of several wireless technologies to enable reliable high-speed data rate for 5G.

close proximity to each other. In scenarios where a large number of devices are involved, this extra routing can result in internet traffic congestion, leading to bottlenecks and latency in the communication process. Wireless D2D communication underlaying cellular architecture can significantly improve the spectral efficiency, increasing the overall throughput of the network [30]. In addition, network controlled D2D communication will reduce the extra overhead and routing functionality of the macro BS. However, D2D connections can be a major source of interference to other cell users (macro and micro) if appropriate regulations are not imposed. Additionally, discovering neighboring nodes and establishing a link can be challenging, especially when a large number of nodes are available [31]. But with sufficient positioning knowledge of the cellular devices in a given cell, D2D communication will offer superior performance in terms of network coverage, capacity, spectral efficiency and power consumption [32].

1.2.3 Merging of WCN and WLAN

Offloading cellular traffic to WiFi and small cells is seen by operators as a key solution for handling the demanding growth in mobile data traffic. This is considered as a collaborative network system, where users have the ease to enjoy the best of each world. Data offloading to WiFi is particularly attractive due to the low cost-per-bit and availability of sufficient spectrum (2.4 GHz and 5 GHz) [33, 34]. The proposal aims to lighten the burden on the cellular network, and at the same time it will concurrently provide a higher throughput to the users. Although in theory, the proposal is very promising, especially in dense areas offloading can be very complicated. One of the reasons is guaranteeing a smooth handover between these two radio access technologies. An unplanned offloading may result in an increase in the overall interference, causing a degradation to the throughput and Quality of Service (QOS) of the network [35]. Moreover, in situations where there is a high concentration of cellular devices, WLAN may not be well equipped to handle the number of users [36]. The efficiency of the handover process and the interference mitigation technique is directly dependent on the positioning of the node with respect to the BSs for WLAN and WCN. Accurate geo-spatial information of the cellular devices can assist the BSs in offloading excess traffic in specific areas with lower density networks. The process reduces network traffic congestion and improves the QOS of the network.

1.2.4 Cognitive Radio

Joseph Mitola III was credited with introducing the concept of Cognitive Radio (CR) through the platform of Software Defined Radio (SDR). The cognitive cycle by Mitola can be characterized in three states [37, 38] :

- Awareness - is the ability if the radio to measure, sense and be aware of its environment and internal states. A radio may exhibit different levels of awareness such as spectrum awareness, location awareness, user awareness and network awareness.

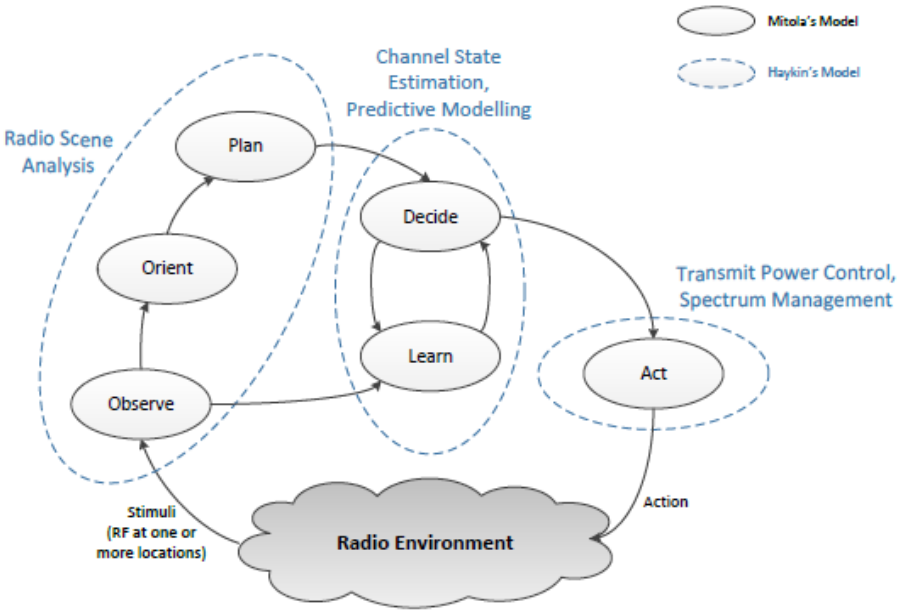

Fig. 1.4: Summary of Mitola's and Hykin's model of cognitive radio [2].

- Cognition - it's the ability to process the information gathered from the awareness stage of the cognitive process to make intelligent decisions about the operating behavior of the radio in order to achieve the performance requirement of the network.

- Adaptability - is the capability of dynamically adjusting certain operating parameters such as transmit power, carrier frequency, and modulation strategy without requiring any modification to the hardware components. This quality enables CR to readily integrate into an unknown environment without compromising the balance of the network.

Dynamic spectrum access (DSA) is one the recognizable features of the CR that aims to overcome the apparent spectrum scarcity problem by ensuring smart spectrum allocation and effective utilization of the spectrum resources. DSA has two main objectives: 1) highly reliable communication without affecting other users in the networks, 2) efficient utilization of the radio spectrum. A Cognitive Radio Network (CRN) usually

consists of two sets of users, primary/licensed users (PU) and secondary/unlicensed users (SU) [39]. Since SUs have lower priority, the channel use is constrained by a maximum acceptable level of interference to PUs. DSA provides a promising solution by enabling both PUs and SUs to coexist in the frequency channel without causing harmful interference to each other. DSA technology is based on the concept of learning the radio environment information of the (PUs). The knowledge is then subsequently used for transmitting parameter selection in the secondary user channel. This selection must be made with the dual requirements of SU communication effectiveness and bounded interference to PUs [40]. The bounded interference to PUs can only be maintained if the PU locations and received power levels from other PUs are known by SUs. In a CRN, often user terminals suffer from a hidden node problem, where an SU is unaware of the existence of another PU placed beyond the network range of the SU. This phenomenon interrupts a communication link and reduces the throughput of the network. Avoiding these problems is challenging, and requires complete geographical information of both the SU and the PU. Therefore, to satisfy the performance requirement of a CR positioning information of the users is of paramount importance.

1.2.5 Massive MIMO

Multiple-input/ multiple-output (MIMO) technology has attracted a lot of attention in the field of research on the upcoming 5G cellular network for its advancement in improving the reliability and capacity of the network. Massive MIMO is an upgraded version of the existing MIMO technology, where a large number of antenna elements are placed in a specific antenna geometry to enable high data rate transmission. The introduction of mmWave frequency in wireless communication is responsible for paving the path of MIMO development. At higher frequency the channel bandwidth is abundant, offering 100× greater throughput than what is available in the traditional cellular bands [41]. Moreover, due to the small wavelength of mmWave signals, dozens or even hundreds of antenna elements can be bundled at the BSs, WiFi Access Points (APs) and even at the portable cellular device. This makes the MIMO system incorporated

with mmWave frequency a perfect recipe for the high capacity channel in dense networks [42]. With the use of a large number of antennas in a massive MIMO structure, the noise, fading and hardware defects can be averaged because signals from a large number of antennas can be combined together in the free space. This increases the robustness of massive MIMO against fading and failure of the antenna elements. Massive MIMO aims to increase the capacity of a BS by several orders of magnitude while simultaneously improving the radiated energy-efficiency.

Beamforming

Beamforming (BF) is a classic signal-processing technique, where multiple antennas are adaptively phased to create a concentrated beam [43]. The technique provides antenna array gains, thereby improving the signal-to-noise ratio (SNR) and an additional radio link margin that mitigates the propagation loss. Also, BF helps to reduce the co-channel interference because of the spatial selectivity of the directional antennas. In D2D communication, BF promises highly directional adaptive antennas that can be steered in various directions, to shine a concentrated beam towards a user [44]. However, without accurate positioning knowledge, BF can lead to wastage of spectral resources and may introduce unwanted interference for other users [45, 46].

Spatial Multiplexing

Due to the advancement of MIMO technology integrated with BF techniques, Spatial Multiplexing (SM) is a reality in WCN as well as in WLAN. SM involves sampling a spatial domain into multiple pieces, enabling each of the antenna elements to shine a concentrated beam simultaneously and in parallel on the same RF channel [47]. In a typical cellular network design, the approach allows the BS to serve a large number of cellular devices simultaneously, given that the cells do not overlap. For SM to work well, the channel must provide sufficient decorrelation between the different closely spaced antennas [48]. The technique offers multiplexing gain that increases the throughput of the network by several orders of magnitude. Location information of the cell devices

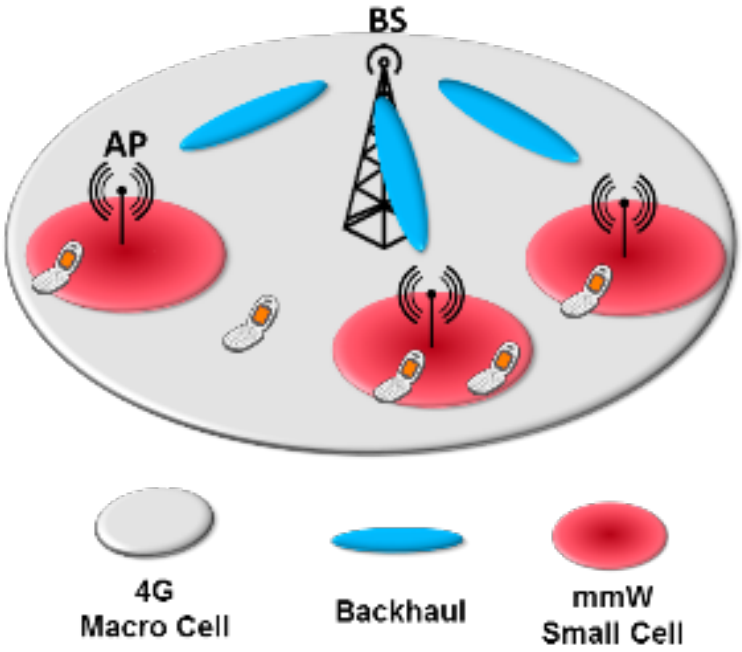

Fig. 1.5: Beamforming enabled spatial multiplexing of multiple cell users using MIMO [3].

can greatly enhance the process, by helping the BS to direct a beam towards the intended users [49]. Moreover, location information will considerably improve the energy efficiency of the total output RF power of BS by restricting it from radiating towards unwanted users. This is crucially important as existing infrastructures are subject to large amount of power consumption.[50].

Jammer Identification

With the widespread use of WCNs and WLANs, the security of wireless communication has attracted considerable attention. Radio jamming is a technique adopted by unauthorized users to deliberately block and interrupt wireless channels for authorized users. It is usually conducted by using a transmitter to transmit at high power, so that it overrides any signal at the receiver [51]. Radio jamming poses an unacceptable risk to public safety by potentially preventing the transmission of emergency communications. Cellular jammers do not distinguish between social or other cell phone conversations

and an emergency call to a family member or a 911 emergency responder. Similarly, GPS and Wi-Fi jammers maliciously disrupt both routine and critical communications services. Jammers could also block more than just cell phone calls; these devices could disrupt important communications services that operate on adjacent frequencies or, worse, they could disrupt all communications within a broad frequency range [52]. To mitigate these challenges, massive MIMO channels are used for directing an antenna null towards an intended jammer and reducing the chances of a possible network failure. This is possible due to the availability of large null spaces that can be exploited for directing a concentrated beam. However, without correctly detecting the geographic position of the jammer, the process to null-out a jammer is challenging. Moreover, the position information helps to carry out the location consistency check, that can be used to differentiate between a legitimate user and a jammer [53, 54].

1.3 Challenges and Objectives

The journey of the localization algorithms initially started by studying the position of the sun and moon and using their positions to navigate travelers on the ground and sea with coarse precision. Early technologies were supported by the compass, that relied on the earth's magnetic field for navigation purposes. Currently, the most reputable localization technology, the Global Positioning System (GPS), started its journey as an aid for the military services. The research was fostered by the Department of Defence (DoD) of the United States of America (USA) when its first Navigation System with Timing and Ranging (NAVSTAR) satellite was launched in 1978 [55]. GPS became available for civilian applications in the early 1990s and today almost all smartphones and automobiles are equipped with this technology. Miniaturization of chips and low-cost electronics are considered to be the major contributors to escalating GPS's popularity. Currently, GPS provides two levels of service: Standard Positioning Service (SPS) which uses the coarse acquisition (C/A) code on the L1 frequency, and Precise Positioning Service (PPS) which uses the P(Y) code on both the L1 and L2 frequencies. The PPS service is reserved for military purposes and is restricted for

civilian use. Among the top GPS performers, users could expect positional accuracies within approximately 5 m of the true position in open-sky settings, 7 m in young forest conditions, and 10 m under closed canopies [56]. Apart from the numerous benefits, GPS technology also has its fair share of drawbacks. The main GPS error source is due to inaccurate time-keeping by the receiver's clock. Microwave radio signals traveling at the speed of light from at least four satellites are used by the receiver's built-in computer to calculate its position, altitude, and velocity. Small discrepancies between the GPS receiver's onboard clock and GPS time, which synchronizes the whole global positioning system, mean that distances calculated can drift significantly. Since GPS technology relies on satellite signals, the received signal is always a distorted version of the transmitted signal. This is due to reflections, refractions, scattering and shadowing of the electromagnetic waves by structural obstacles [57]. In cases of heavy distortion especially in an indoor environment (tunnel, building, etc), pin pointing a user becomes a difficult task for existing GPS.

According to the CiSCO visual networking index, by the end of 2021, the number of portable devices that requires an accurate location information will be hitting the 11 billion mark [58]. In reality, equipping each of these devices with a GPS unit is not a cost-effective solution and requires an extensive revamp of the existing network infrastructure. In order to cater for the surge of smart devices and to maintain a reliable connectivity between them, innovative cost-effective positioning systems are mandatory. The challenges of localization technology in a world of inter-connected devices are relatively complex. A large number of smart applications are hosted on these devices that demand for different precision accuracy in order to adapt to a diverse radio environment. The accuracy and precision requirements for these applications are quite diversified and range from centimeters in gaming to meters in indoor geo-location, to tens of meters in turn-by-turn direction, and hundreds of meters for Location Based Service (LBS) in targeted areas [59]. Some of the open challenges in positioning a transmitting device are listed as follows [60–63]:

- Positioning a cellular device in crowded environments during outdoor events such as stadiums, or indoors, such as large lecture halls, is an existing challenge for

a number of smart-applications environments. GPS is restricted by its limited accuracy and is not suitable for determining two closely spaced devices with superior accuracy.

- Indoor localization systems are still in their infancy and are mostly dominated by the influence of interference, line-of-sight obstructions, and multi-path. The most commonly used technologies for indoor localization are WiFi, Radio Frequency Identification (RFID) and Bluetooth, with localization ranges of a few meters. The aforementioned wireless technologies have a limited signal coverage and only performs for a short range. Due to degradations of satellite signal strength, GPS fails miserably in indoor settings.

- Finding cost-efficient positioning systems that can be purchased off the shelf is another long-standing problem. The products that offer superior accuracy are either restricted due to government regulation or are beyond the purchase range of a civilian.

- The requirement of a large number of static nodes or sometimes referred as anchor nodes in order to accurately locate a smart device. The number of nodes significantly increases in indoor scenario compared to outdoor which in many cases are not a realistic option.

- Another challenge for localization is positioning flying smart robots in indoor and outdoor areas. 3D localization needed for these flying robots demands accuracy on the order of the size of these robots to navigate them intelligently without any crash incident.

Current technologies fail to address the challenges listed above and even if they are available, they are not cost-effective. A summary of the existing positioning technologies is listed in Table. 1.3. This gives an indication of the accuracy of these technologies with their respective disadvantages.

Technology	Accuracy	Disadvantages.
GPS	6 m - 10 m	slow computation, processing time, susceptible to reflection
Cellular	4 m - 7 m	heavily patented and limited modification
Bluetooth	8 m - 15 m	coverage range is limited
WiFi	1 m - 5 m	short range, multipath and obstruction from structures
RFID	5 m - 10 m	short range, limited coverage

TABLE 1.3: A summary of existing positioning technologies with their respective accuracies and disadvantages.

1.4 Compressive Sensing: A Solution

To cater for this diverse range of limitations, the solution is required to be robust and agile, with the intelligence to select suitable techniques that satisfy the needs of the respective applications. Compressive Sensing (CS) is an emerging technique, that has created significant hype in the field of signal processing. The technique offers the reconstruction of a signal using lower sampling rate than the celebrated Nyquist-Shannon theorem and has attracted considerable interest in research areas of information theory, computer science, image processing, electronics engineer, and acoustics. CS-based techniques are build upon the framework that many physical quantities are intrinsically or extrinsically sparse and can be represented by a few nonzero expansion coefficients, with respect to suitable expansion bases. CS asserts that one can recover a certain signal from far fewer samples or measurements than traditional methods use. To make this possible, CS relies on two characteristics: 1) sparsity, which expresses the idea that the information rate of a continuous signal may be much smaller than suggested by its bandwidth, and 2) incoherence which pertains to the system modality [64–67].

Despite the ground-breaking success of the CS, its development is thus far focused on a signal with sparse representation in finite discrete dictionaries. However, in practical applications such as radar, array processing, and remote sensing, the signals encountered are specified by a continuous parameter. In order to reduce the computational complexity, researchers have adopted a procedure of discretizing the continuous parameter space into a set of finite grid points. CS relies on a pattern matching technique

where the observation signal is matched with a predefined finite dictionary matrix, which is rectangular in shape (i.e, the number of rows are smaller than the number of columns). While this strategy resulted in significant reduction in sampling rate (lower than Nyquist-Shannon), discretization has its own set of drawbacks [68–70] -

- The structure of the dictionary matrix is often dictated by the physical properties of the sensing process (e.g., the laws of wave propagation) as well as by constraints associated with the respective grid points. As a result, the luxury of selecting a structured dictionary matrix is limited.

- In cases when the true parameter does not lie on the grid points, the signals cannot be sparsely represented by a discrete dictionary. This results in a mismatch between the observed signal and the dictionary matrix that causes the poor reconstruction of a signal.

- It is difficult to characterize the performance of discretization using standard compressed sensing analyses. While on one hand, finer discretization introduces high coherence of signals at the grid points, on the other hand, coarser discretization leads to insufficient information in the dictionary matrix.

- Although finer grids yield an improvement in signal reconstruction error, very fine grids often lead to instability in the structure of the dictionary matrix.

- Even at the finest grid resolution, the signal reconstruction error will always be bounded by the error induced due to grid quantization. As a result, the reconstruction error will never converge to the theoretical Cramér-Rao lower bound (CRLB) of signal estimation.

The biggest question is whether it is possible to develop a localization algorithm taking advantage of the strengths of CS while simultaneously suppressing the respective drawbacks?

1.5 Main Contributions

This thesis highlights the innovation of three fundamentally new localization approaches based on the framework of CS. In this thesis, we consider range-based localization schemes that include accurately determining the position of a node using the received signal strength (RSS) in one case and the direction of arrival/angle of arrival (DOA/AOA) information another case. Along with the introduction of three fundamentally noble localization techniques based on RSS and DOA, the thesis focused on answering some of the open-ended questions arising from the drawbacks of the known CS technologies. Some of the key scientific contributions of this thesis are as follows

- A fundamentally new high-resolution DOA estimation algorithm has been proposed. The algorithm has the ability to determine the DOA of an incoming signal impinging on a antenna array from any possible direction in the range $[-\pi, \pi)$. Simulation results indicate that the MSE of the estimate is on the theoretical Cramér-Rao lower bound (CRLB) of DOA estimation. And no other algorithm can perform better than the CRLB.

- A simple iterative signal processing technique has been proposed that utilizes the largest two coefficients of the recovered sparse vector using CS technique, to estimate a DOA that may not be an element of the quantized grid points. The technique offers an innovative solution to the legacy problem of grid quantization in CS processing and can be adopted for any estimation algorithm based on CS. The simplicity and effectiveness of the algorithm are detailed in the convergence proof for the technique.

- A comparison analysis of the computational complexity of the algorithm is also presented. It has been shown through extensive simulations that the algorithm achieves the CRLB using only a single snapshot (i.e, one time instant) of the incoming signal. On the other hand, traditional DOA-based estimation techniques rely heavily on a large number of snapshots to converge to an accurate

estimate. Compared to the existing technique, our proposed algorithm has significantly lower computational complexity, making it an attractive option for practical hardware implementation. In addition high performance filtering techniques may be effectively applied to sequences of DOA estimate

- The performance of the proposed algorithm is demonstrated by applying it to two well-known antenna array geometries, the Uniform Circular Array (UCA) and the Uniform Linear Array (ULA). For both these antenna geometries, the algorithm achieved the CRLB performance. The results also suggest that the proposed technique can be adapted for a wide range of antenna geometries, indicating the robustness and compatibility of the algorithm.

- For both a UCA and a ULA, an in-depth analysis was carried out to investigate the impact of different antenna parameters on the performance of the algorithm. The analysis led to the establishment of a relationship between the number of antenna elements and the number of discrete grid points that is required for any CS framework to effectively recover the sparse vector. To the best of our knowledge, no other paper in the literature has addressed this issue.

- For both the antenna geometries, we analyzed the influence of the approximate sparsity level of the recovered sparse vector on the MSE performance of the algorithm. Especially for estimating a DOA in between the discrete grid points, the importance of sparsity level is crucial. It has been illustrated through simulation results that, in order to accurately detect the DOA of a transmitting source, the approximate sparsity level of the recovered vector is required to be twice the number of sources available.

- We present a detailed study on the structure of the dictionary matrices for both UCA and ULA. Especially for a UCA, the study indicated that antenna parameters, such as the number of antenna elements and the inter-element spacing, play a crucial role in determining the fitness of the dictionary matrices. Based on the study, we propose a simple but effective way of selecting optimal antenna

parameters that not only improves the structure of the matrix but also reduces the DOA estimation error. Some interesting features of UCA geometry have been discovered in this process that may motivate future theoretical research on UCA antennas. To the best of our knowledge, there has been no prior literature on such work and this will undoubtedly be the first dissertation to identify the significance of this research outcome.

- The structure of the dictionary matrices is analyzed from the perspective of a transform operation. A set of well-known transform operations are integrated with the aim to study their respective impacts on the dictionary matrices of both the UCA and the ULA. The research suggests that Discrete Cosine Transform (DCT) and Discrete Fourier Transform (DFT) performs similarly to the benchmark Karhunen-Loève Transform (KLT). It also highlights that the addition of a transform operation does not provide any significant improvements to the condition of the dictionary matrices.

- A performance comparison between the two antenna geometries UCA and ULA are presented. The comparison clearly outlines the advantages and disadvantages of both UCA and ULA when incorporated with a CS-based DOA estimation algorithm. The simulation results show that, for a restricted angular domain between $[-\pi/2, \pi/2)$, ULA offers a better estimate than UCA. However, when a UCA with optimal array parameters is considered, the UCA has a superior performance to the ULA.

- A novel multiresolution DOA estimation algorithm based on CS has been proposed that has superior performance compared to the traditional DOA estimation approaches. The multiresolution approach achieves a reduction in the MSE by a factor of ten when compared to high-resolution beam scan techniques. It has also been shown that the algorithm achieves a reduction in computation complexity by a factor of nine when compared to a traditional CS algorithm using finer resolution.

- A novel RSS localization algorithm based on a CS platform is described in this thesis. The proposed technique selectively eliminates sensors such that they are separated by a minimum geographic distance. The method yields a selective set of sensors that improve the localization accuracy by 20% and reduces the error by 57% when compared to a random deployment of sensors. The research provides an in-depth analysis on the impact of different random distribution techniques on the structure of the dictionary matrix and on the estimation process.

1.6 Organization

This dissertation follows the non-traditional "Thesis-by-Publication" format which has been approved by the Macquarie University Higher Degree Research Office. It consists of a general introduction, background, and a list of my major scientific publications. The thesis materials are the original texts and graphics of my publications, published or in review, that have been reformatted to improve readability.

1.6.1 Included in Thesis Dissertation

The thesis dissertation consists of the following publications which are presented in order from Chapter 3 to Chapter 7 respectively.

- A. Biswas, S. Reisenfeld, "*Highly Accurate Off-Grid Direction of Arrival Estimation using a Novel Iterative Technique*," To be Submitted.

- A. Biswas, S. Reisenfeld, "*A Novel Signal Processing Technique to Estimate the Off-Grid Direction of Arrival using a Uniform Linear Array*," To be Submitted.

- A. Biswas, S. Reisenfeld, "*Performance comparison of a Uniform Circular Array and Uniform Linear Array using an Iterative Compressive Sensing Framework*," To be Submitted.

- A. Biswas, S. Reisenfeld, L. Goratti, M. Hedley and Z. Chen, "*Multiresolution Compressive Sensing algorithm to detect off-grid direction of arrival*," 2016 10th

International Conference on Signal Processing and Communication Systems (ICSPCS), Gold Coast, QLD, 2016, pp. 1-6.

- A. Biswas, S. Reisenfeld, M. Hedley and Z. Chen, "*Effective sensor positioning to localize target transmitters in a cognitive radio network*", EAI Endorsed Transactions on Cognitive Communications, vol. 16, no. 6, pp. 4, 2016.

1.7 Author Contribution

In all the publications listed above, I was responsible for conducting all the major investigations, analyses, simulations, data processing, drafting and writing. A/Prof. Sam Reisenfeld, my principal supervisor, has provided invaluable support, guidance and advice at every stage in generating the publications. He also played a pivotal role in the process of reviewing the technical content and proofreading all the chapters of this thesis. Dr Mark Hedley and Dr Zhou Chen from CSIRO supported me through the investigation of the system model for the last two chapters. Dr Leonardo Goratti from CREATE-NET was responsible for directing towards the research of DOA estimation and supported me in proof reading chapter 5. Dr Keith Imrie from Macquarie Univesity added valuable contributions to the thesis by editing the chapters in order to reduce inconsistencies and proof reading the content.

1.8 Dissertation Outline

The thesis has been structured as follows

- Chapter 2 provides an overview of the framework of CS. The chapter will highlight the mathematical model of CS signal-recovery techniques and will provide a brief summary of the existing CS algorithms in the literature. An analysis of the construction of dictionary matrix will be presented, followed by the introduction of quantifiable parameters that will be used to characterize the structure of the

matrix. A comprehensive review of the literature available on CS-based localization and CS-based DOA estimation algorithm will be presented. The literature will be used to compare some of the key contribution achieved in this dissertation.

- In Chapter 3, we analyze the effect of the proposed algorithm by applying it to a UCA as the receiving node. The paper focuses on both on-grid and off-grid DOA estimation cases and describes the iterative algorithm that eliminates the quantization error in the CS framework and enables the estimation error to converge to the CRLB using just two iterative operations. The performance of the algorithm is validated by comparing the MSE with the theoretical CRLB as well as well-known DOA estimation techniques. Moreover, an analytic approach is used to evaluate the impact of the antenna parameters of a Uniform Circular Array (UCA) on the construction of the dictionary matrix. It will be shown via mathematical analysis as well as through MATLAB simulations that careful manipulation of antenna parameters can significantly improve the structure of the dictionary matrix, hence resulting in an accurate estimate.

- In Chapter 4, we apply the proposed high-resolution DOA estimation algorithm to a ULA as the receiving node. A ULA possesses some unique features in terms of the construction of the dictionary matrix which are highlighted in details in this chapter. An MSE performance comparison is presented to validate the effectiveness of the algorithm when compared with well-known techniques. A relationship between the number of antenna elements and the number of discrete angular grid points is established in this paper. The relationship shows a parametric trade-off between computational complexity and estimation accuracy of the proposed algorithm.

- Chapter 5 provides a comparison study for the problem of direction-of-arrival (DOA) estimation using the uniform circular array (UCA) and uniform linear array (ULA) antenna geometries. The advantages and disadvantages of each of the antenna geometries are highlighted with respect to being integrated with the CS-based estimation algorithm. The paper also provides a detailed analysis of

the structure of the measurement matrices that are constructed using the array response vector (ARV) for each of the two antenna geometries. The analysis indicates that careful exploitation of the antenna array parameters of a UCA can greatly enhance the DOA estimate, eventually leading to a lower MSE than that of a ULA.

- Chapter 6 describes the novel multi-resolution CS-based DOA detection algorithm, which can perform independently of the transmitter being located at a quantized grid point and uses fewer signal snapshots to detect the incoming DOA. The algorithm shows the power of the multi-resolution technique in significantly reducing the computational complexity when compared to traditional CS-based approaches. Extensive simulation results are presented that shows that the technique outperforms the high-resolution beam-scan technique by achieving a lower MSE of the DOA estimate.

- Chapter 7 showcases a novel RSS-based localization algorithm built on the framework of CS techniques. The chapter evaluates the ability of different CS based techniques to determine the location of a node that is positioned at some discrete geo-location grid points. Two different deployment strategies of sensor nodes are analyzed and their impact on the localization accuracy is verified via extensive simulation. The influence of the sensor deployment strategies on the structure of the dictionary matrix is investigated.

- Chapter 8 outlines the conclusion of the dissertation, highlighting the major findings and innovations of our work. A list of future research directions is also provided in this chapter.

2

Literature Review

In this chapter, we aim to provide an overview of the some of the existing estimation techniques while detailing out their respective advantages and disadvantages. The reader will also be introduced to the theory of Compressive Sensing and different CS-based schemes that have been highlighted in the literature. In addition to that, a detailed literature review on various CS-based DOA estimation methods will be presented, mainly emphasizing on scenarios, where the transmitting source is located in between the grid points. Finally, the chapter will provide a comparison of our contribution against some of leading research outcome in this field.

2.1 Range Measurement

In order to accurately locate a cell user or a wireless node in a network, the details of the position estimation process, theoretical limits, practical limitations and sources of error should be well understood. The problem of localization is the process of finding location information of an unknown transmitting node in a given coordinate system. The localization process consists of two steps: 1) distance measurement between neighboring nodes and 2) geometric calculation using the distance measurements to position the node in a coordinate system. The family of distance measurement technique can be classified into two categories as follows [71]

- Range based - In range based techniques, the location of a node is computed by measuring the distance between an unknown node and an Anchor Node (AN), where ANs are special nodes that are aware of their geographic location in advance either from GPS or by from Global Position System (GPS) or by virtue of being manually placed. A signal sometimes known as pilot or beacon is exchanged between the AN and an unknown node. The physical properties of communication signal such as timing, directionality or signal strength are being utilized for estimating the distance.

- Range Free - In the range-free cases, there is no need for distance measurement, as a result they do not rely on having a dedicated AN. With range-free techniques, instead of estimating distances between sensor nodes, other approaches are used to determine an unknown nodes location at a coarser granularity. These approaches can be grouped into techniques based on area, hop count, and neighborhood information. Estimation of the distance in range-free techniques is based on measuring the number of hops between any pairs of the nodes and distance estimation through numerical or statistical methods using the information concerning the number of connections for each sensor.

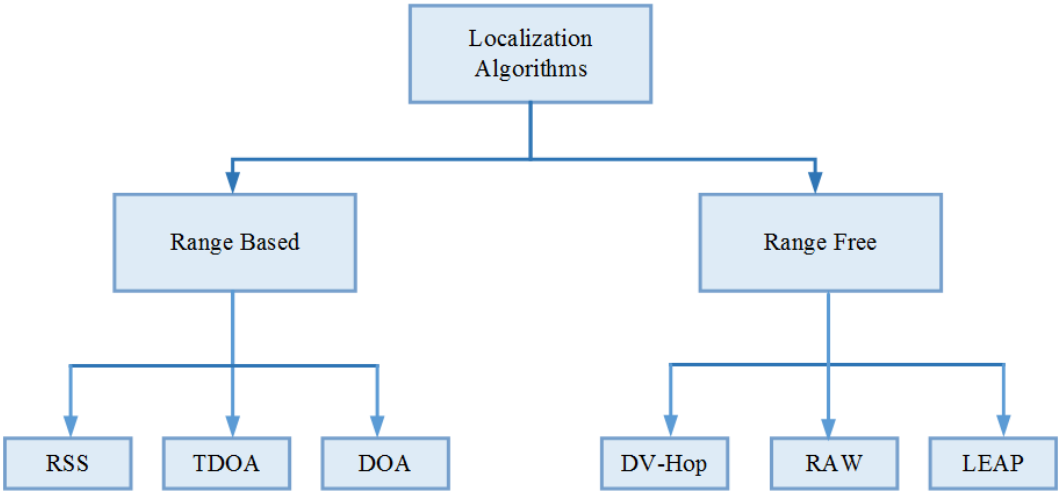

Fig. 2.1: Flowchart detailing the categories of various range-based and range-free localization techniques.

A flow chart showing different localization approaches is shown in Fig. 2.1. Range-free localization scheme is outside the scope of this thesis and our proposed algorithm focuses only range-based techniques. A popular family of range-based distance measurement methods includes the Received Signal Strength (RSS), Time of Arrival (TOA), Time Difference of Arrival (TDOA) and Angle of Arrival (AOA) or Direction of Arrival (DOA) [72, 73].

2.1.1 Signal Strength

Received Signal Strength

In a WCN or in a WLAN, a wireless node transmits a radio signal that propagates in the surrounding of the transmitter. RSS (Received Signal Strength) or RSSI (Received Signal Strength Indicator) is defined as the voltage measured when a transmitted signal is being received at the receivers end. The RSS is often measured as power which is the square of the received voltage. In free space the signal power decays proportionally to the square of the distance between the transmitter and receiver. Apart from the decay, a signal traveling between two neighboring nodes also experiences a fast fading due to multipath and shadowing which is due to the presence of obstacles in the Line

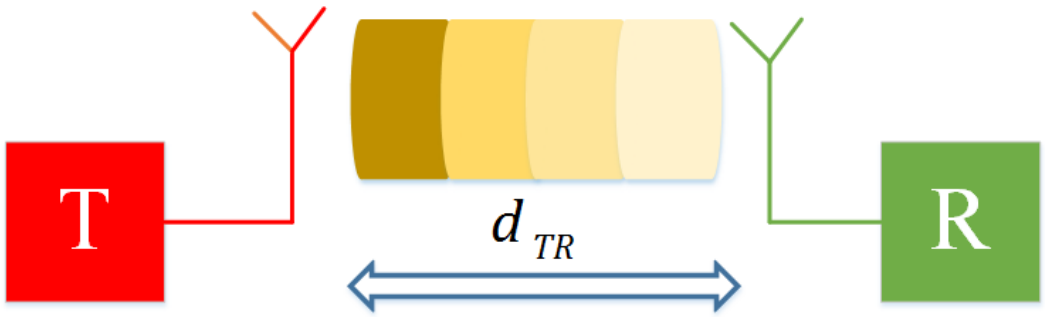

Fig. 2.2: Degradation of signal power over distance d_{TR}.

of Sight (LOS) of the transmitted signal. Ideally, averaging the RSS measurement over a sufficiently long time interval excludes the effects of multipath fading and shadowing, which results in a pathloss model. In a typical model, where the transmit power and pathloss model in known is priori, the received power can be obtained as follows

$$P_R = P_T - PL(d_{TR}) \tag{2.1}$$

where P_R and P_T are the received and transmitted power respectively measured in dB. The pathloss model in dB is represented as $PL(d_{TR})$ which is a function of the distance between the transmitter T and the receiver R. The pathloss in dB can be expressed as

$$PL(d_{TR}) = K + 10\eta \log_{10}(\frac{d_{TR}}{d_0}) + \alpha, \tag{2.2}$$

where

d_{TR} is transmission distance in meters,

d_0 is the reference distance of the antenna far field,

η is the propagation loss exponent,

α is the shadowing loss in dB.

k is a unit-less constant that relies on the antenna characteristics and the average channel attenuation and $K = 10\log_{10}(k)$ [74]. α accounts for the random attenuation of signal strength due to shadowing, where α, in dB, is a Gaussian random variable with

zero mean and standard deviation $\sigma_{dB} = 5.5$ dB. This model was used in [75] for both multipath and log-normal shadowing characterization. After few steps of mathematical manipulations the distance can be retrieves as

$$d_{TR} = d_0 10^{(PL(d_{TR}) - K - \alpha)/10\eta)}. \tag{2.3}$$

Error in Measurement

To date, implementations using RSS based approaches have enjoyed a cost advantage by not requiring specialized hardware. This makes RSS-based techniques very attractive from a cost-performance standpoint to engineers wishing to offer integrated RSS-based positioning solutions. However, one of the major drawbacks in the anomalies in accurately measuring the true RSS. The radio environment in a WCN or a WLAN is notoriously unpredictable and changes dynamically for different scenarios [76]. As a result, claiming to have prior knowledge of the shadowing and multipath effect is not a realistic assumption. For short range communication and LOS signal RSS achieves a reasonable estimate, however, it degrades significantly in case of long range. This is due in part because, in reality, propagation in any cell is far from a purely circular pattern based on an ideal path loss model [77]. Theoretical RSS models in their purest form do not provide for the measurement or consideration of variations seen within actual sites, typically assuming only well-known values for path loss and shadow fading [78].

2.1.2 Timing

Time of Arrival

Time of Arrival (TOA) systems is based on the precise measurement of the arrival time of a signal transmitted from a mobile device to several receiving sensors. Because the transmitted signals travel with a known velocity (approximately the speed of light $c = 3 \times 10^8$m/s), the distance between the mobile device and each receiving sensor can be determined from the elapsed propagation time of the signal traveling between

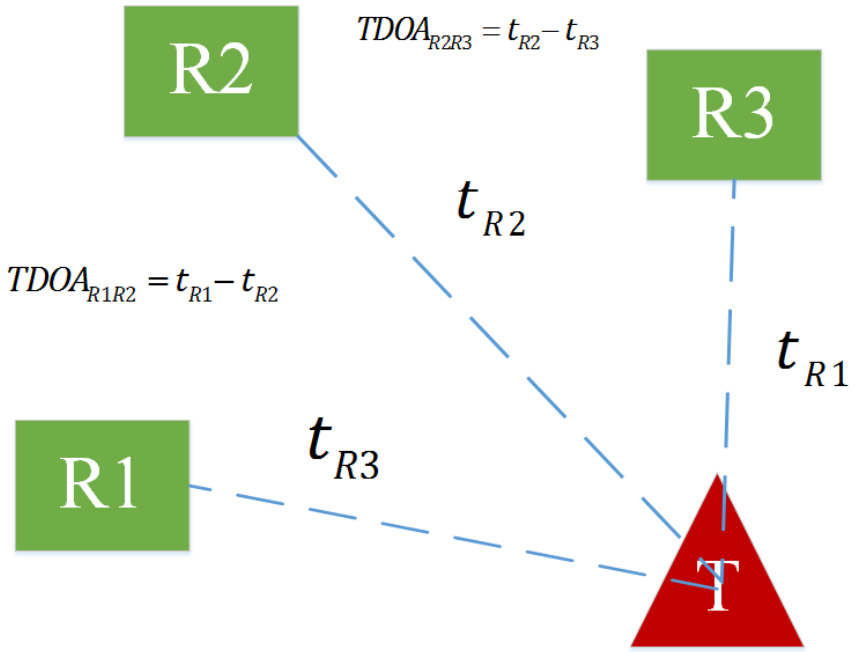

Fig. 2.3: Illustration of time delay of a signal when received at receiver placed at different geographic location.

them. The TOA technique requires very precise knowledge of the transmission start time(s) and must ensure that all receiving nodes, as well as the transmitted nodes, are accurately synchronized with a precise time source. Let us consider a transmitter T that radiates a signal at time t_T that is being received at the receiver R at time t_R, then the time delay due to signal propagation between the transmitter T and receiver R is

$$t_{TR} = t_R - t_T, \tag{2.4}$$

and the transmission distance is calculated as

$$d_{TR} = c \times t_{TR}. \tag{2.5}$$

Time Difference of Arrival

Time synchronizing both receiver R and transmitter T may not be a practical option especially in a scenario where the receiver is in a passive mode. To overcome this issue, Time Difference of Arrival (TDOA) has been introduced. TDOA techniques are based on estimating the difference in the arrival times of the signal from the source at multiple receivers. Because of this, TDOA does not require the use of a synchronized time source at the point of transmission (i.e. the transmitter) in order to resolve time-stamps. In TDOA techniques, a transmission with an unknown starting time is received at various receiving sensors, with only the receivers requiring time synchronization. In this approach, at least three time-synchronized receiving sensors are required. As shown in Fig. 2.3 , when a source T transmits a signal, the receiving nodes R_1, R_2 and R_3 receives the signal with time-stamps t_{R1}, t_{R2} and t_{R3} respectively. The TDOA of the signal between the receivers $R1$ and $R2$ can be expressed as

$$TDOA_{R1R2} = t_{R1} - t_{R2} \tag{2.6}$$

and the distance between the receivers can be calculated as

$$d_{R1R2} = c \times TDOA_{R1R2}. \tag{2.7}$$

The distance equation in 2.7 is used to construct a hyperbola with foci at the locations of both receiving sensors A and B. This hyperbola represents the locus of all the points in the x-y plane, the difference of whose distances from the two foci is equal to d_{R1R2} meters. TDOA implementations are rooted upon a mathematical concept known as hyperbolic lateration which will be discussed in Section 2.2.

Sources of Error

A drawback of the TOA and TDOA approaches is the requirement for precise time synchronization of all stations. Given the high propagation speeds, very small discrepancies in time synchronization can result in very large errors in location accuracy [79].

For example, a time measurement error as small as 100 nanoseconds can result in a localization error of 30 meters. TOA-based positioning solutions are typically challenged in environments where a large amount of multipath, interference, or noise may exist. In case of multipath scenarios, the signals arrive very soon after the LOS signal, and their contributions to the cross-correlation obscure the location of the peak from the LOS signal which contaminates the time measurements. Moreover, the LOS signal can be severely attenuated compared to the late-arriving multipath components, causing it to be embedded inside the noise, causing large positive errors in the TOA estimate [80, 81].

2.1.3 Directionality

Direction of Arrival

The Direction of Arrival (DOA) or Angle of Arrival (AOA) method utilizes the multi-array antennas to estimate the direction of arrival of the signal of interest. Thus a single DOA measurement restricts the source location along a line in the estimated DOA. If at least two such DOA estimates are available from two antennas at two different locations, the position of the signal source can be located at the intersection of the lines of bearings from the two antennas. To estimate the DOA, algorithms are used that exploit the phase differences or other signal characteristics between closely spaced antenna elements of an antenna array and employ phase-alignment methods for beam/null steering. The spacing of antenna elements within the antenna array is typically less than 1/2 wavelength of all received signals [82]. This is required to produce phase differences on the order of radians or less to avoid ambiguities in the DOA estimate. The resolution of DOA estimates improves as the baseline distances between antenna elements increase. However, this improvement is at the expense of ambiguities. As a result, DOA estimation methods are often used with short baselines to reduce or eliminate the ambiguities and at other times with long baselines to improve resolution.

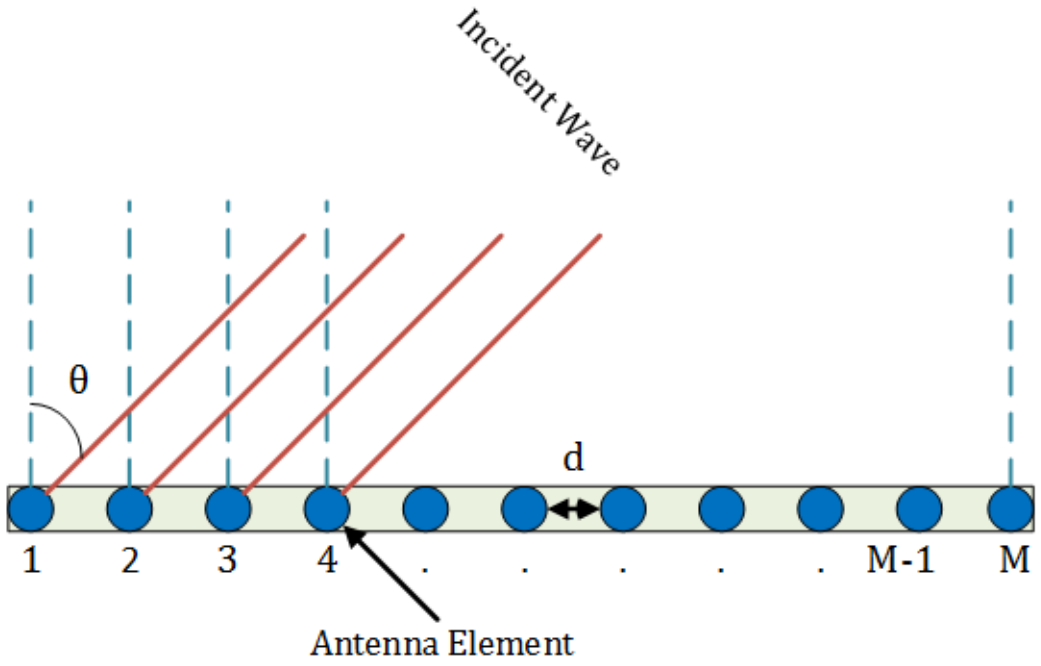

Fig. 2.4: A uniform linear array with M elements, where θ is the azimuth angle of arrival of the received signal

Let us consider M isotropic antenna elements placed in a straight line with an inter-element spacing of $d = \lambda/2$, where λ is the signal wavelength. A travelling plane wavefront impinges on the antenna elements from some unknown direction θ. The incoming wave satisfies the narrowband assumption that the phase difference between the upper and lower band edges of the propagation across the entire array is small. The complex output at the antenna array is given as

$$\mathbf{X_{ULA}} = \mathbf{A_{ULA}}(\theta)P_{ULA} + \boldsymbol{\eta_{ULA}}, \tag{2.8}$$

where $\mathbf{X_{ULA}}$ is an $M \times 1$ array output vector corrupted with noise. The $M \times 1$ noise vector is represented as $\boldsymbol{\eta_{ULA}}$ where the entries are statistically independent and Gaussian distributed with zero mean and variance σ^2, and P_{ULA} is the complex envelope of the source at the receiving array. In (2.8), $\mathbf{A_{ULA}}(\theta)$ is the $M \times 1$ array response vector (ARV) for an incoming plane wave from the direction θ and is generally

given as

$$\mathbf{A_{ULA}}(\theta) = \begin{bmatrix} 1 & e^{-jk\sin(\theta)d_{ULA}} & \dots & e^{-jk\sin(\theta)(M-1)d_{ULA}} \end{bmatrix}.^{T} \tag{2.9}$$

The ARV_{ULA} in (2.9) represents the relative phases of the received signals at the antenna elements where $k = 2\pi/\lambda$ is the wavenumber or phase propagation factor. The aim of this work is to find the incident azimuth angle θ using the relative phase difference between the antenna elements. Fig. 2.4 shows the system model.

2.1.4 Source of Error

A common drawback that DOA shares with some of the other techniques mentioned are its susceptibility to multipath interference. As stated earlier, DOA works well in situations with a direct line of sight, but suffers from decreased accuracy and precision when confronted with signal reflections from surrounding objects [83]. For accurate DOA estimates, it is crucial that the signals coming from the source to the antenna arrays must be coming from the Line-Of-Sight (LOS) direction. Additionally, the installation of the array is considerably high and are sometimes not cost-effective. Another factor is the issue of antenna array element calibration, especially in case of heavy winds or storms a minute change in the physical arrangement of the array can cause severe degradation in the DOA estimation [84].

2.2 Geometric Calculation

Positioning a node involves obtaining a range measurement by exploiting some if the physical parameters of a transmitted signal. This step is followed by geometric calculation using the range measurements to pin point the position of a transmitting node.

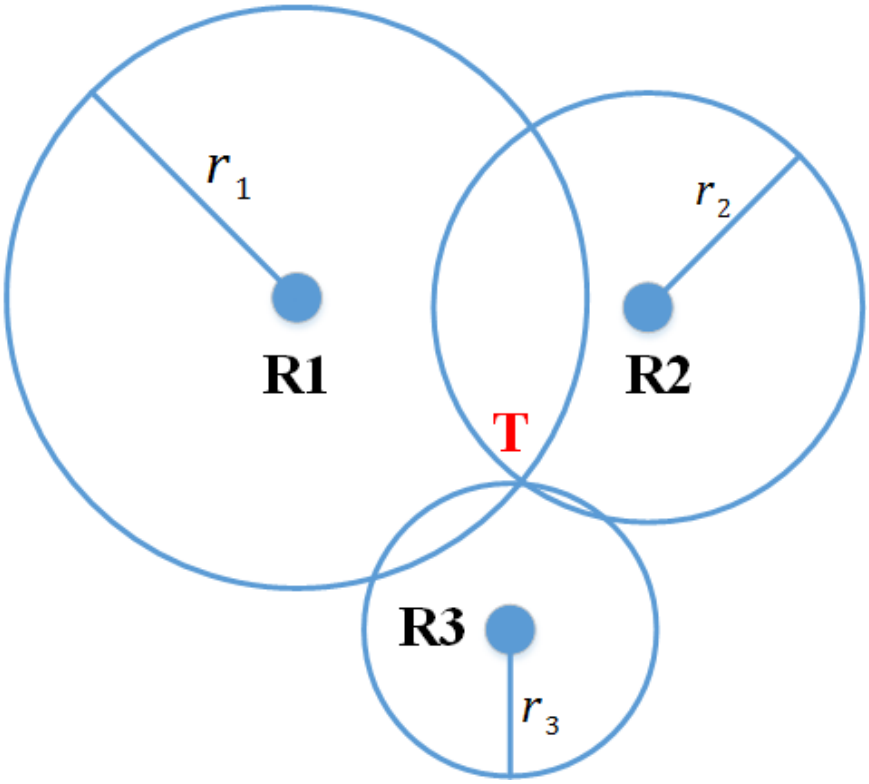

Fig. 2.5: Trilalterion technique to determine the position of a transmitter given that the range is measured using TOA or RSS based techniques.

2.2.1 Trilateration

In geometry, trilateration is the process of determining absolute or relative locations of points by measurement of distances, using the geometry of circles, spheres or triangles. Fig. 2.5 illustrates the concept of trilateration using the range measurement obtained using TOA and RSS techniques. In Fig. 2.5 the three receivers R1, R2 and R3 have measured the distance for the transmitter T to be r_1, r_2 and r_3 respectively. Using each of the calculated distance value a circular plot around the respective receiving sensor is drawn. From the individual perspective of each receiver, the transmitter T is believed to reside somewhere along the locus of their respective circular plots. In some cases, there may be more than one possible solution for the location of mobile device station T, even when using three remote sensors to perform trilateration. In these cases, four or more receiving sensors are can be employed to the improve the accuracy of the result [71, 73].

2.2.2 Hyperbola Intersection

Unlike RSS and TOA techniques, TDOA does not directly provide a range measurement. TDOA implementations are rooted upon a mathematical concept known as hyperbolic lateration. In this approach, at least three time-synchronized receiving sensors are required. The value of TDOA_{R1R2} can be used to construct a hyperbola with foci at the locations of both receiving sensors R1 and R2. This hyperbola represents the locus of all the points in the x-y plane, the difference of whose distances from the two foci is equal to d_{R1R2} meters. Mathematically, this represents all possible locations of mobile device T such that.

$$|d_{TR1} - d_{TR2}| = d_{R1R2} \tag{2.10}$$

The probable location of mobile station T can then be represented by a point along this hyperbola. To further resolve the location of station T, a third receiving sensor at location R3 is used to calculate the message time difference of arrival between sensors R3 and R1. Similarly, one more hyperbola is generated from TDOA_{R1R3}. The intersecting point where these two hyperbolas are used to deduce the position of the transmitter T [71, 73]. Fig. 2.6 illustrates the hyperbolic lateration.

2.2.3 Triangulation

The Angle of Arrival (AOA) technique, sometimes referred to as Direction of Arrival (DOA), locates the mobile station by determining the angle of incidence at which signals arrive at the receiving sensor. Let us consider a transmitter T, with a bearing of θ_a and θ_b respectively from the receivers R1 and R2. Assuming the DOA/AOA are measured accurately at the receivers, geometric relationships can then be used to estimate location from the intersection of two lines of bearing (LoBs) formed by a radial line to each receiving sensor, as illustrated in Figure 2-5. In a two-dimensional plane, at least two receiving sensors are required for location estimation with improved accuracy coming from at least three or more receiving sensors (triangulation). In its purest form that

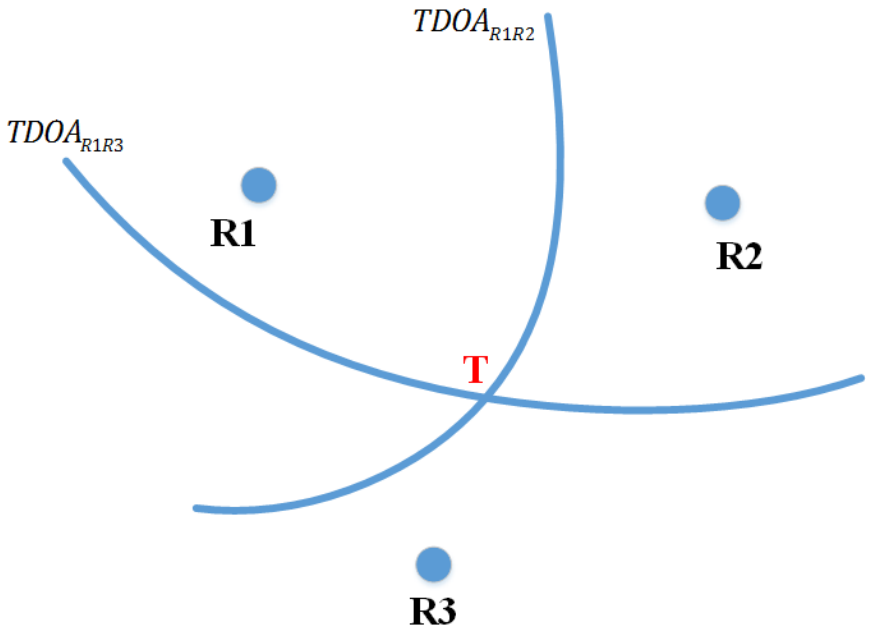

Fig. 2.6: The intersection of two hyperbola resulted from the TDOA measurement between two receivers, to provide the position of transmitter T.

is, (where clear line-of-sight is evident between the mobile device T and receiving phase array sensors R1 and R2), mechanically-agile directional antennas deployed at the receiving sensors are adjusted to the point of highest signal strength [71, 73]. Fig. 2.7 illustrates the triangulation process. In practical commercial and military implementations of DOA, multiple element antenna arrays are used to sample the receiving signal, thereby eliminating the need for more complex and maintenance-intensive mechanical antenna systems. Electronic switching can be performed between arrays or portions of each array, and mathematical computations handled by a background computing system used to extract the angles of incidence.

2.3 Compressive Sensing

The pioneering work of Nyquist and Shannon on sampling continuous-time band signals demonstrates that images, videos, and other data can be extracted from a set of

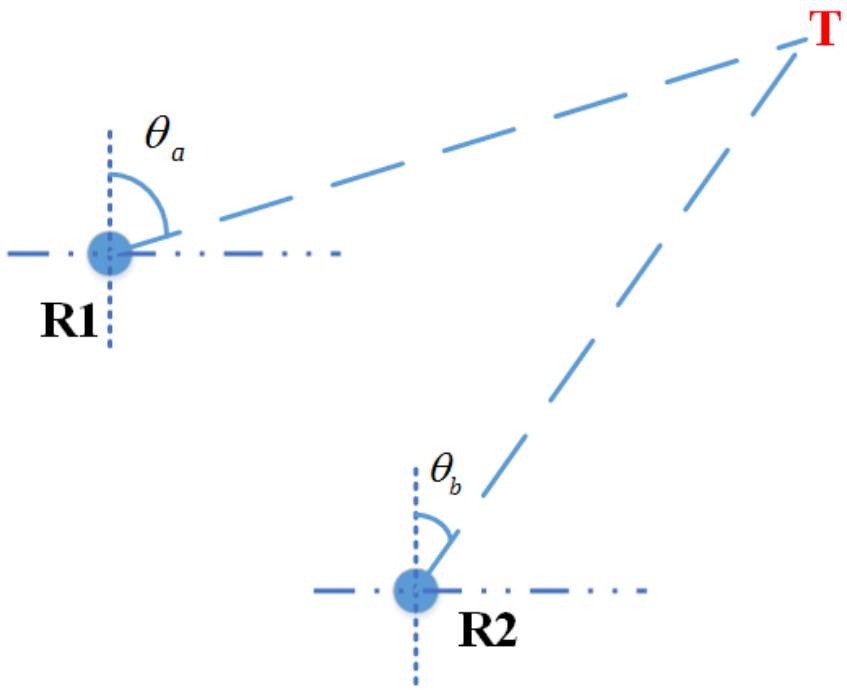

Fig. 2.7: The intersection point of line of bearing to estimation the position of the transmitter.

uniformly spaced samples taken at the so-called Nyquist rate of twice the highest frequency present in the signal of interest. Unfortunately, in many emerging applications, the resulting Nyquist rate is so high that it becomes too costly, or even physically impossible, to build devices capable of acquiring samples at the necessary rate. Thus, despite extraordinary advances in computational power, the acquisition and processing of signals in application areas such as imaging, video, medical imaging, remote surveillance, spectroscopy, and genomic data analysis continue to pose a tremendous challenge. To address the computational challenges involved in dealing with high dimensional data, we turn our focus towards compression techniques that aims at finding the most concise representation of a signal that is able to achieve a feasible level of acceptable distortion. One of the well-known techniques for signal compression is transform coding, that relies on obtaining a basis that provides sparse or compressible representation of a signal on a basis of interest. The sparse representation refers to a signal of length N, that can be represented with $K << N$ coefficients. In other words, both sparse and compressible signals can be represented with high fidelity by preserving only the values and locations

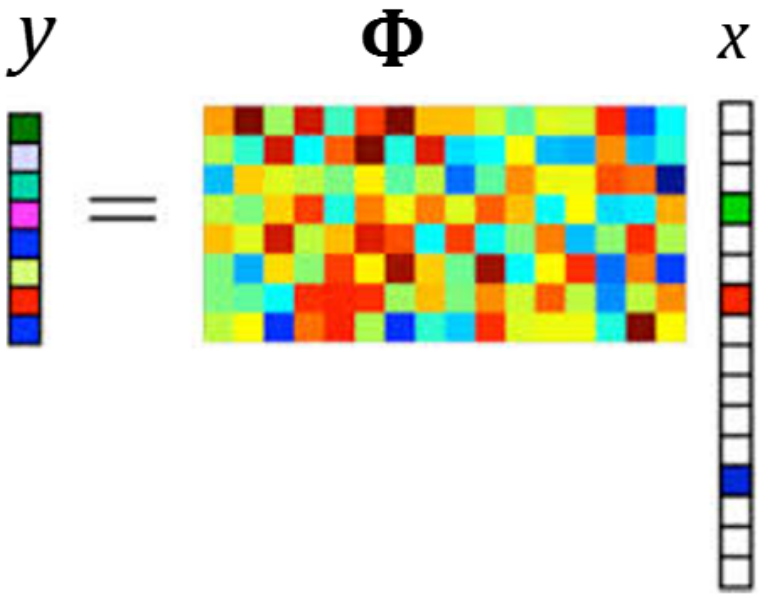

Fig. 2.8: Framework of Compressive Sensing technique.

of the largest coefficients of the signal. This process is called sparse approximation and forms the foundation of transform coding schemes that exploit signal sparsity and compressibility, including the JPEG, JPEG2000, MPEG, and MP3 standards.

Compressive Sensing (CS) is a new framework for signal acquisition that enables a significant reduction in the sampling and computation cost for sensing signals that have a sparse representation on a given basis. In classical Nyquist-Shannon theorem, the signal is first sampled at high data rate and then the sampled data is compressed. While sensing a compressible signal CS relies on finding ways to directly sense the data in a compressed form and this is the fundamental idea behind CS. The field of CS gained enormous popularity due to the work of Candès, Romberg, and Tao and of Donoho, who showed that a finite-dimensional signal having a sparse or compressible representation can be recovered from a small set of linear, nonadaptive measurements [85–88]. The design of these measurement schemes and their extensions to practical data models and acquisition systems are central challenges in the field of CS.

CS differs from classical sampling in three important respects [64, 89],

- First, sampling theory typically considers infinite length, continuous-time signals. In contrast, CS is a mathematical theory focused on measuring finite-dimensional vectors in $\mathbb{R}^N$.

- Second, rather than sampling the signal at specific points in time, CS systems typically acquire measurements in the form of inner products between the signal and more general test functions.

- Thirdly, the two frameworks differ in the manner in which they deal with signal recovery, i.e., the problem of recovering the original signal from the compressive measurements. In the Nyquist-Shannon framework, signal recovery is achieved through sinc interpolation - a linear process that requires little computation and has a simple interpretation. In CS, however, signal recovery is typically achieved using highly nonlinear methods.

2.3.1 Signal Reconstruction

The mathematical framework of CS deals with the recovery of a sparse vector $x_{N\times 1}$, from an observation vector $y_{M\times 1}$ with $M \ll N$. The measurement paradigm consists of the linear projection of the signal vector via a known projection matrix $\Phi_{M\times N}$. As $M \ll N$, the recovery of a sparse vector x from the measurement vector y becomes an undetermined problem with an infinite number of solutions. Therefore, in order to make the solution unique, extra constraints are added to the solution. Sparsity and incoherence are such conditions that are added in CS theory to ensure the mapping of the solution from x to y is one-to-one. Mathematically a vector x is k-sparse when it has a maximum of k non-zero coefficients i.e, such that

$$\Sigma_k = \{x : \|x\|_0 \leq k\}. \tag{2.11}$$

where Σ_k denotes the set of all k-sparse vectors and $||\bullet||_0$ represents the l_0-norm. In the CS framework, an accurate estimation of a sparse vector x can be obtained in the

following reconstruction problem:

$$\min \|x\|_p \quad s.t. \quad \|y - \Phi x\|_2 \leq \zeta, \tag{2.12}$$

where $\|\cdot\|_p$ is the l_p-norm and ζ bounds the amount of noise in the observation data. Φ is the $M \times N$ dictionary matrix that represents a dimensionality reduction, i.e, it maps a vector in $\mathbb{R}^N$ into $\mathbb{R}^M$, where M is typically much smaller than N. The dictionary matrix Φ is the most crucial element in the CS process as the projection from a high dimension to a lower dimension is completely dependent on the characteristics of Φ. The biggest theoretical question is to find out a way to efficiently design Φ to ensure that it preserves the information in vector x without distortion. In [64], Candès and Tao introduced a key notion that has proved to be very useful to study the general robustness of CS; the so-called Restricted Isometry Property (RIP).

Definition 2.3.1 *For each integer k = 1,2.. define the isometry constant δ_k of a matrix Φ as the smallest number such that*

$$(1 - \delta_k)\|x\|_2^2 \leq \|\Phi x\|_2^2 \leq (1 + \delta_k)\|x\|_2^2 \tag{2.13}$$

holds for all k-sparse vector x

A matrix Φ obeys the RIP of order k if δ_k is not to close to one. When this property holds, Φ approximately preserves the Euclidean length of k-sparse vectors, which in turns implies that k-sparse vectors cannot be in the null space of Φ. In case the vector x is in the null space of Φ, there may be infinite solutions and it would be impossible to distinguish a unique solution solely based on the measurement vector y. In other words, the definition of RIP describes that all subsets of k columns taken from Φ are in fact nearly orthogonal. The isometry condition on a measurement matrix Φ has fundamental implications concerning robustness to noise. The uniqueness of a solution is also determined by another crucial characteristic of Φ commonly known as the the spark. The spark of a matrix is the smallest number of columns in matrix Φ that are linearly independent. So the larger the spark, the bigger the signal space, allowing

CS to guarantee exact recovery. According to the theory of CS, when Φ satisfies the RIP condition in (2.13) and spark$(\Phi) > 2K$, there is a high probability of successfully recovering a sparse signal from a noisy measurement [89, 90]. Although spark and RIP provide guarantees for the recovery of a K-sparse vector, verifying that a matrix Φ satisfies any of the above properties has a combinatorial computation complexity, since $\binom{N}{K}$ submatrices must be considered. Therefore it is preferable to use a property of a matrix which is easily computable and provides guarantees of recovery. *Mutual coherence* is one such property that has been repeatedly mentioned in CS theory and has a direct relation to the spark and the RIP property of a dictionary matrix [91, 92]. The *mutual coherence* of a matrix Φ, $\mu(\Phi)$, is the maximum normalized inner product between any two columns ϕ_i and ϕ_j of Φ:

$$\mu(\Phi) = \max_{1 \leq i < j \leq n} \frac{|\langle \phi_i, \phi_j \rangle|}{\|\phi_i\|_2 \|\phi_j\|_2} \tag{2.14}$$

It has been shown in [93] that the *mutual coherence* of a matrix Φ is always bounded in the range $\mu(\Phi) \in [\sqrt{\frac{N-M}{M(N-1)}}, 1]$, where the lower bound is known as the Welch Bound [94, 95]. Note that when $N \gg M$ the lower bound is approximately equal to $\frac{1}{\sqrt{M}}$. Theorem (1.6) of [89] establishes the following relationship between $\mu(\Phi)$ and spark(Φ):

$$\text{spark}(\Phi) \geq 1 + \frac{1}{\mu(\Phi)}. \tag{2.15}$$

By combining (2.15) and the requirement spark$(\Phi) > 2K$, a condition can be introduced for Φ that guarantees uniqueness.

Theorem 2.3.1 (Theorem 1.7 of [89]) *For each measurement vector $y \in \mathbb{R}^m$ there exists at most one signal $x \in \sum_K$ such that $y = \Phi x$ if*

$$K < \frac{1}{2}(1 + \frac{1}{\mu(\Phi)}). \tag{2.16}$$

The Welch bound along with (2.15) provides an upper bound on the level of sparsity K that guarantees uniqueness using coherence. This is another application of the Gershgorin circle theorem [96] that connects the mutual coherence to the RIP property.

2.3.2 Singular values of non-square matrix

The Compressive Sensing framework determines the solution of a rectangular matrix $\Phi_{M\times N}$, where $M \ll N$. Unlike a square matrix, rectangular matrices do not have eigenvalues and do not appear to possess any quantities of comparable significance. However, the use of a symmetric, positive semi-definite square Gram matrix $Q = \Phi^*\Phi$ can be considered and can be formed even if Φ is not square. Since Q is a square matrix, the eigenvalues of Q can be related back to quantify the property of the matrix Φ.

Definition 2.3.2 *The singular values $\rho_1, ..., \rho_m$ (arranged in ascending order) of a $m \times n$ matrix Φ are the positive square roots, $\rho_i = \sqrt{\varrho_i} > 0$, of the non-zero eigenvalues of the associated Gram matrix $Q = \Phi^*\Phi$.*

Since Q is necessarily positive semi-definite, the eigenvalues of Q are always non-negative: $\varrho_i > 0$. This justifies the positive singular values of Q, which is independent of the entries of Φ being positive, negative or complex. The paper [93], also states the number of singular values of a matrix is always equals to the rank of the matrix. The singular values of a matrix play a vital role in providing a geometric interpretation of the action of the matrix. The magnitudes of the singular values can be used to distinguish between a well-conditioned matrix and an *ill-conditioned* matrix.

Definition 2.3.3 *The condition number of a non-square of an $m \times n$ matrix Φ is the ratio between its largest and smallest singular values: $\Upsilon(\Phi) = \frac{\rho_1}{\rho_m}$*

A matrix Φ with a very large condition number is said to be *ill-conditioned*. In particular, it refers to the rate at which the solution x will change with respect to a change

in observation y. In the case of an *ill-conditioned* matrix a small change in y can cause a significance variation to the solution vector x.

2.4 DOA Estimation via CS

The research in the area DOA estimation techniques were mainly dominated by Multiple Signal Classification (MUSIC) [97], and Estimation of Signal Parameters via Rotational Invariance Techniques (ESPRIT) [98] and Capon [99]. MUSIC is equivalent to a large sample realization of the maximum likelihood (ML) method when the signals are uncorrelated [100], and has a super-resolution compared to beamforming [101] under certain conditions. On the other hand, its disadvantages are obvious. The performance of MUSIC deteriorates significantly in the scenarios with small number of snapshots or correlated signals [100]. Sub-spaced based algorithms such as ESPRIT rely on Eigen-value Decomposition (EVD) of the covariance matrix which comes at the expense of high computation complexity. Learning-by-example (LBE) approach based on a support vector machine has been proposed in to estimate DOA of a transmitting source [102–104]. In LBE techniques DOA estimation problem has been recast to a probabilistic framework in order to identify a smaller angular region where the presence of an incoming signal is most probable. LBE approaches enjoys the advantages over the sub-spaced based scenarios where a *prior* knowledge of the number of signals may not be available. While LBE technique is efficient in providing a rough estimate of DOA, it may not as suitable in an application where super-resolution estimation is a requirement. Despite the positive and attractive features of LBE, they also require the evaluation of co-variance matrix similar to MUSIC and ESPRIT which increase the computational complexity of the algorithm.

To overcome such limitations, sparse signal representation (SSR), an emerging area in signal processing, has been proposed. Extensive research has been taken in this specific area [105–108], where the traditional DOA estimation problem is transformed into an SSR platform by inducing the sparsity condition. Compared to existing parameter estimation algorithms, sparsity-based DOA estimation techniques may provide some

advantages, such as being insensitive to source correlation, allowing arbitrary array geometries, working with a single snapshot, and providing certain guarantees for obtaining a global optimum in polynomial time. CS-based techniques rely on discretizing the continuous angular region into a set of finite number of grid points N. However, in many practical applications, such as radar and sonar, the incident DOA may not belong to a subset of the finite number of grid points and can be continuous in angular space. In general, the actual angle of arrival will not be precisely at one of the N grid points. This introduces a mismatch between the observation and the dictionary matrix, forcing the estimate to be incorrect. The degradation of estimation performance in the presence of sensing matrix mismatching is highlighted in algorithms described in [109, 110]. The authors in [111] also investigate the CS-based DOA estimation in the presence of sensing model mismatching errors, proving that the performance of CS-based DOA estimation algorithm degrades dramatically in that case. The results are further re-iterated in [112] where a joint least-absolute shrinkage and selection operator (LASSO) algorithm is used to achieve DOA estimation in the presence of mismatching.

Such drawback of CS-based DOA techniques prompted researchers to focus on the off-grid scenario, where an incoming DOA is between two quantized grid points. One of the early approaches to solving this problem was to finely quantize the angular domain. A dense angular grid leads to a high coherence dictionary matrix violates the Restricted Isometry Property (RIP) condition for the sparse signal recovery [65]. Moreover, a finer quantization implies to a large N which exponentially increases the computational complexity of the algorithm. To reduce the computational complexity an adaptive grid-refinement process is proposed in [113, 114]. The process involves a two-stage strategy where a coarse estimate (closest matched grid point) is obtained using a finite set of angular grid points, which is then followed up with a refinement of specific target area around the corresponding estimate. The technique significantly reduces the computation, however closely placed grid points increase the similarity between the columns of the dictionary matrix. A large similarity introduces ambiguities in the estimation process and degrades the performance of the estimator [115, 116].

Sparse Bayesian learning (SBL) is another reputed technique which has been adopted

for sparse signal recovery in CS. In such cases, the original deterministic problem is reformulated in its probabilistic counterpart then efficiently solved with the Relevance Vector Machine(RVM) [117]. The work in [118–122] also introduced Bayesian framework in the DOA estimation problem offering some sophisticated alternatives. The work in [123] employed a block sparse Bayesian algorithm based on SBL and performs superiorly compared to Bayesian algorithm based on singular value decomposition (SVD) for DOA estimation based on the off-grid model[124]. The algorithm in [124] claims to reduce the computational workload of the signal recovery process and the sensitivity to noise by using the SVD technique. Although the embedded statistical learning theory can be computationally challenging for hardware implementation and will greatly increase the latency in the estimation process. The author in [125] investigates the off-grid model for DOA estimation and proposed a sparse total least squares (STLS) method based on the Gaussian assumption of off-grid distance, which, however, is not satisfied in the off-grid DOA estimation problem. Although aforementioned techniques are mathematically attractive, the embedded statistical model of Bayesian algorithm can give rise to challenges in hardware implementation while greatly increasing the latency in DOA estimation process.

Off-grid DOA estimation techniques using co-prime arrays are proposed by authors in [112, 126], however, the performance analysis against the theoretical bound was not included in the simulation. The work presented in [127, 128] adapts the nearest grid search to obtain a coarse estimate and proposes an expected likelihood (EL) based approach to reduce the bias due to grid quantization. However, the EL process can be computationally challenging does not complete elimination of grid bias. The work in [129] proposes taking centroids of the maximum coefficients of the nearest angular grids to estimate the off-grid DOA. However, when the coefficients do not appear accurately on the neighboring grids, the error can be significantly large.

Compared to the prior literature, our novel algorithm provides a signal-processing solution for high-resolution DOA estimation. The technique offers an innovative solution to the legacy problem of grid quantization in CS processing and can be adopted for any estimation algorithm based on CS. The algorithm completely eliminates the

grid induced quantization error and achieves the Cramér-Rao lower bound (CRLB) of DOA estimation. The core of the invention is an iterative interpolation technique that results in an error discriminant which is robust and offers superior accuracy to the prior techniques. From a computational complexity point of view, our iterative algorithm is strongly convergent and obtains the final estimate using only a single snapshot of the incoming signal.

3

Highly Accurate Off-Grid Direction of Arrival Estimation using an Uniform Circular Array.

3.1 Abstract

Precise estimation of the Direction of Arrival (DOA) of an incoming signal is of critical importance in determining the location of a transmitting source. Especially in military and upcoming 5G cellular communication, precise localization of a transmitter can lead to effective interference mitigation and jammer identification techniques. Compressive Sensing techniques have been applied in several DOA estimation approaches mainly due to the advantage of estimating the DOA using a measurement collected at a single time

instant (i.e. snapshot). However, to integrate the CS framework on a DOA estimation problem, the incoming DOA is assumed to be sparse in an apriori known basis. The basis is usually constructed by sampling the angular domain of coverage into finite number of angular grid points and the incoming DOA is assumed to be exactly aligned on the quantized grid points. In reality, no physical field is sparse in any apriori known basis. No matter how finely, the angular domain is sampled, the source DOA may never lie on the centre of the grid cell and hence introducing a basis mismatch. The mismatch between the original observation and dictionary matrix constructed using finite grid points introduces an error induced due to grid quantization. The additional error restricts the estimation error to be on the theoretical Cramér-Rao lower bound (CRLB). In this paper we analyze the off-grid DOA estimation cases and proposes a fundamentally new, iterative algorithm that eliminates the quantization error in CS framework and enables the estimation error to converge to the CRLB using just two iterative operations. The performance of the algorithm is validated by comparing with well known Root-MUSIC and Beam-forming DOA estimation techniques. Results from the simulation suggests that using single snapshot of the incoming signal, the proposed algorithm outperforms the traditional DOA estimation techniques. Moreover an analytic approach is conducted to evaluate the impact of antenna parameters of a Uniform Circular Array (UCA) on the construction of the dictionary matrix. It will be shown that with optimal antenna parameters, the structure of the dictionary matrix can be significantly improved hence increasing the estimation accuracy. A relationship between the number of antenna elements and the number angular grid points has been established in this paper. The relationship shows a systematic trade-off between computational complexity and estimation accuracy.

3.2 Introduction

The first attempt of Direction Finding (DF) or Direction of Arrival (DOA) estimation dates back to 1907 and was soon followed by the introduction of phased array antennas in 1919 [130]. Major advances have been made over the decades to improve the

resolution of DF, however, the underlying concept did not change much. DOA estimation has been an interesting area of research and is widely popular due to several military applications such as radio communication, radio navigation, sonar and radar technologies [131–138]. Especially in military environments, accurate DOA estimation is crucial in the development of Identification, friend or for (IFF) systems. The IFF systems enable military personnel to identify the bearing and location of unauthorized aircraft, vehicles or transmitting sources that may aim to destabilize military communication systems [139]. In radio jamming environments, the determination of the DOA is critical in producing a null in the receive antenna pattern in the correct direction to null-out the jammer power [140].

In commercial cellular 4G and 5G networks, a precise transmitter position enables optimal channel and power allocation to maximize frequency reuse in a cellular communication system. Accurate positioning information allows base stations to spatially differentiate between several users in a network using beam-forming techniques. Smart antennas or adaptive antennas are widely used for generating several independent beams, enabling a variety of users to be spatially multiplexed simultaneously into the same channel. This results in an uninterrupted communication between users (primary/secondary), hence increasing the throughput of the overall network in a specific geographical region [141–143]. Smart antennas provide several advantages over traditional antennas including increased coverage, improved robustness to multi-path and resistance towards unwanted interference [144].

Apart from beamforming, smart antennas have the ability to determine an incoming signal's DOA from data sampled by the antenna elements. Some of the most celebrated subspace-based methods such as Multiple Signal Classification (MUSIC) [97] and Estimation of Signal Parameters via Rotational Invariance Techniques (ESPRIT) [98] and Capon [99] require a large number of signal snapshots for eigenvalue decomposition (EVD) of the covariance matrix. However in many practical applications, due to processing and physical constraints, the number of snapshots of the signal may be limited to just one. In single-snapshot cases, the EVD-based technique fails due to rank deficiency. To overcome such limitations, sparse signal representation (SSR), an emerging

area in signal processing, has been proposed. Compressive Sensing (CS) has gained popularity in signal processing, due to the effectiveness of CS in recovering a sparse signal with minimal measurements [64]. The technique enables signal reconstruction by using a sample rate much lower than the normal Nyquist, given that the sample signal is sparse in some given basis. Several CS integrate techniques are proposed in [108, 145–147], where the traditional DOA estimate problem is transformed into SSR platform by inducing the sparsity condition.

Unlike MUSIC and ESPRIT, CS-based methods do not require EVD of the observation and can offer superior estimates using a single snapshot of the incoming signal. In CS-based problem formulation, the angular domain of coverage is quantized into angular grid points of N possible DOAs. The array response vector (ARV) associated with each of the N possible DOAs is used to generate a known dictionary matrix. The number of grid points, N, in the quantization is greater than the number of antenna elements, M. Therefore the problem of determining the angle of arrival is represented as an underdetermined set of equations which maps the signal originating at each grid point to the set of complex envelope voltage outputs of the antenna elements. However in many practical applications such as radar and sonar, the incident DOA may not belong to a subset of the finite grid points and can be continuous in angle space. In general, the actual angle of arrival will not be precisely at one of the N grid points. This introduces a mismatch between the observation and the dictionary matrix, forcing the estimate to be incorrect.

This drawback of CS-based DOA techniques prompted researchers to focus on the off-grid scenario, where an incoming DOA is between two quantized grid points. One of the early approaches to solving this problem was to finely quantize the angular domain. A dense angular grid leads to a range of problems, including a high correlation between two adjacent steering vectors, and violation of Restricted Isometry Property (RIP) of the dictionary matrix [65]. Moreover a finer quantization implies a large N which exponentially increases the computational complexity of the algorithm. To reduce the computational complexity an adaptive grid-refinement process in proposed in [102, 113, 114]. The process involves obtaining a coarse estimate (closest matched grid

point) and then refining a specific target area around the corresponding estimate. The technique significantly reduces the computation, however closely placed grid points increases similarity between the columns of the dictionary matrix. A large similarity introduces ambiguities in the estimation process and degrades the performance of the estimator. The work in [118–120] introduces a Bayesian framework in the DOA estimation problem offering some sophisticated alternatives, however the techniques can be computationally challenging for practical implementation. In [112, 126] the author outlines an algorithm to detect an off-grid DOA using co-prime arrays but the performance analysis against the theoretical bound was not included.

This work proposes an innovative and fundamentally new approach that provides a signal processing solution to eliminate the grid induced quantization error in CS-based DOA estimation techniques. The process enables the algorithm to achieve the Cramér-Rao lower bound on estimation error and no algorithm can perform better than the bound. The innovative operation involves the determination of the DOA of a radio signal using the signal complex voltages obtained at the outputs of antenna elements configured in a Uniform Circular Array (UCA). The symmetric geometry of UCA greatly reduces the effect of mutual coupling and offers a wider azimuth angular coverage than the Uniform Linear Array (ULA) [148]. The problem of determining the angle of arrival is represented as an underdetermined set of equations which can be solved using CS to recover a sparse vector. The index corresponding to the dominant coefficient of the sparse vector is chosen to be the coarse estimate of the incoming DOA. The work in [127, 128] adapts a similar technique to obtain a coarse estimate and proposes an expected likelihood (EL) based approach to reduce the bias due to grid quantization. However, the EL process can be computationally challenging. The work in [129] proposes taking centroids of the maximum coefficients of the nearest angular grids to estimate the off-grid DOA. However, when the coefficients does not appear accurately on the neighboring grids, the error can be significantly large.

The crucial contribution of this paper is an iterative interpolation technique that results in an error discriminant which is robust and offers superior accuracy compared to the prior techniques. The error discriminant is obtained by rotating the angular grids

in both clockwise and anticlockwise directions by a factor of $\frac{1}{2}$ the grid quantization interval. The two sets of rotated grid points are used to create two modified dictionary matrices that are feed into the CS algorithms to obtain two new sparse vectors. This unique processing results in two scaler magnitude which are the input parameters of the error discriminant function. The iterative process continues until the error discriminant is less than some user-defined threshold. At each stage of the iteration, the coarse estimate is updated with the error discriminant until the stopping criterion is satisfied. Simulation results suggest that the proposed iterative algorithm is strongly convergent and the final estimate achieves the theoretical Cramér-Rao lower bound (CRLB) [B.1] of DOA estimation using just two iterations. In addition to the innovation of the unique algorithm, the paper also proposes an analysis on the antenna array geometry of the UCA that enhances the performance of CS-based DOA estimation techniques. The analysis focuses on the influences of the number of antenna elements and radius of the UCA on the structure of the dictionary matrix. The results from the analysis suggest that at an optimal antenna geometry, the similarity between of the columns of the dictionary is significantly reduced resulting in a superior DOA estimation. The paper also establishes a relationship between the number of antenna elements (M) and the number of quantized grid points (N) that is required to achieve the CRLB.

The paper is organized in the following manner. Section 3.3 discusses the background on CS and parameters to evaluate the structure of the dictionary matrix. Sections 3.4-3.5 provide the system model. This leads to the development of the proposed iterative algorithm and architecture is presented in Section 3.6. Analysis and simulation results are presented in 3.7. Section 3.8 provides the conclusions.

3.3 Background

This section provides a overview on compressive sensing and the associated parameter that are used to analyse the effectiveness of the measurement matrix.

3.3.1 Compressive sensing

Compressive sensing is a mathematical framework that deals with the recovery of a sparse vector $x_{N\times 1}$, from an observation vector $y_{M\times 1}$ with $M \ll N$. The measurement paradigm consists of linear projection of the signal vector via a known projection matrix $\Phi_{M\times N}$. As $M \ll N$, the recovery of a sparse vector x from the measurement vector y becomes a undetermined problem with an infinite number of solutions. Therefore, in order to make the solutions unique, extra constraints are added to the solution. Sparsity is such a constraint added in CS theory that ensures that the mapping of the solution from x to y is one-to-one. In the CS framework, an accurate estimation of a sparse signal x can be obtained in the following reconstruction problem:

$$\min \|x\|_p \qquad s.t. \qquad \|y - \Phi x\|_2 \leq \zeta, \tag{3.1}$$

where $\|\cdot\|_p$ is the l_p-norm and ζ bounds the amount of noise in the observation data. A vector x is said to be K-sparse, if $\|x\|_0 = K$. In [64], Candès and Tao introduced the following isometry condition on a measurement matrix Φ which has fundamental implications concerning robustness to noise. The paper states that a matrix Φ satisfies Restricted Isometry Property (RIP) of order k, if there exists a $\delta_k \in (0, 1)$ such that

$$(1 - \delta_k)\|x\|_2^2 \leq \|\Phi x\|_2^2 \leq (1 + \delta_k)\|x\|_2^2 \tag{3.2}$$

holds for all k-sparse vectors x. In cases when Φ satisfies the above condition in (3.2) and the spark$(\Phi) > 2K$, there is a high probability of successfully recovering a sparse signal from a noisy measurement [89, 90]. The spark of a matrix suggest the smallest number of columns in matrix Φ that are linearly independent. So the larger the spark, the bigger the signal space, allowing CS to guarantee exact recovery. Although spark and RIP provides guarantees for the recovery of a K-sparse vector, verifying that a matrix Φ satisfies any of the above properties has a combinatorial computation complexity, since $\binom{N}{K}$ submatrices must be considered. Therefore it is preferable to use a property of a matrix which is easily computable and provides guarantees of

recovery. *Mutual coherence* is one such property that has been repeatedly mentioned in CS theory and has a direct relation to the spark and the RIP property of a dictionary matrix [91, 92]. The *mutual coherence* of a matrix Φ, $\mu(\Phi)$, is the maximum normalized inner product between any two columns ϕ_i and ϕ_j of Φ:

$$\mu(\Phi) = \max_{1 \leq i < j \leq n} \frac{|\langle \phi_i, \phi_j \rangle|}{\|\phi_i\|_2 \|\phi_j\|_2} \tag{3.3}$$

It has been shown in [93], that the *mutual coherence* of a matrix Φ is always bounded in the range $\mu(\Phi) \in [\sqrt{\frac{N-M}{M(N-1)}}, 1]$, where the lower bound is known as the Welch Bound [94, 95]. Note that when $N \gg M$ the lower bound is approximately equal to $\frac{1}{\sqrt{M}}$. The theorem (1.6) of [89] establishes the following relationship between $\mu(\Phi)$ and spark(Φ):

$$\text{spark}(\Phi) \geq 1 + \frac{1}{\mu(\Phi)}. \tag{3.4}$$

By combining (3.4) and the requirement spark$(\Phi) > 2K$, we can introduce a condition of Φ that guarantees uniqueness.

Theorem 3.3.1 (Theorem 1.7 of [89]) *For each measurement vector $y \in \mathbb{R}^m$ there exists at most one signal $x \in \sum_K$ such that $y = \Phi x$, if*

$$K < \frac{1}{2}(1 + \frac{1}{\mu(\Phi)}). \tag{3.5}$$

The Welch bound along with (3.4) provides an upper bound on the level of sparsity K that guarantees uniqueness using coherence. This is another application of the Gershgorin circle theorem [96] that connects the coherence to the RIP property.

3.3.2 Singular values of non-square matrix

The Compressive sensing framework determines the solution of a rectangular matrix $\Phi_{M\times N}$, where $M \ll N$. Unlike a square matrix, the rectangular matrices do not have eigenvalues and do not appear to possess any quantities of comparable significance. However, the use of a symmetric, positive semi-definite square Gram matrix $Q = \Phi^*\Phi$ can be considered and can be formed even if Φ is not square. Since Q is a square matrix, the eigenvalues of Q can be related back to quantify the property of the matrix Φ.

Definition 3.3.1 *The singular values $\rho_1, ..., \rho_m$ (arranged in ascending order) of a $m \times n$ matrix Φ are the positive square roots, $\rho_i = \sqrt{\lambda_i} > 0$, of the non-zero eigenvalues of the associated Gram matrix $Q = \Phi^*\Phi$.*

Since Q is necessarily positive semi-definite, the eigenvalues of Q are always non-negative: $\lambda_i > 0$. This justifies the positive singular values of Q, which is independent of the entries of Φ being positive, negative or complex. The book in [93] states that the number of singular values of a matrix is always equals to the rank of the matrix. The singular values of a matrix play a vital role in providing a geometric interpretation of the action of the matrix. The magnitudes of the singular values can be used to distinguish between a well-conditioned matrix and an *ill-conditioned* matrix.

Definition 3.3.2 *The condition number of a non-square of a $m \times n$ matrix Φ is the ratio between its largest and smallest singular values: $\Upsilon(\Phi) = \frac{\rho_1}{\rho_m}$*

A matrix Φ with a very large condition number is said to be *ill-conditioned*. In particular, it refers to the rate at which the solution x will change with respect to a change in observation y. In the case of an *ill-conditioned* matrix, a small change in y can cause a significance variation to the solution vector x.

3.4 Problem Formulation

Let us consider a planar array of M isotropic elements equally distributed along a circular ring of a UCA with radius r and angular separation of $2\pi/M$ radians. The inter-element spacing $d = 2r\sin(\frac{\pi}{M})$, is the length of the straight line between two adjacent antenna elements. The angular positions of the antenna elements of the UCA are represented by γ, where $\gamma_m = 2\pi(m-1)/M$. An electromagnetic plane wave impinges on the phased antenna array from some unknown DOA with azimuth and elevation angles θ and ψ respectively. The azimuth angle θ is calculated relative to the x plane and the elevation angle ψ is calculated relative to the $x-y$ plane as shown in Fig. 3.1. The incident signal is considered to be narrow-band and impinges on the antenna elements with equal strength. Under the following assumption, the complex voltage output of the m^{th} antenna array can be written as

$$v_m = s^{inc}\tau_m(\theta,\psi) \tag{3.6}$$

where

$$\tau_m(\theta,\psi) = e^{-jbr\cos(\theta-\gamma_m)\cos(\psi)}. \tag{3.7}$$

and

s^{inc} represents the magnitude of the impinging wave,

b is the angular wavenumber $(2\pi/\lambda)$,

γ_m is the angular position of the m^{th} element,

λ is the free-space wavelength of the wave.

The angular position of the m^{th} antenna element is calculated relative to the first element on the UCA ring. The model assumes that the elevation angle, $\psi = 0$ and that all the antenna elements are on the $x-y$ plane. As ψ is constant, for simplicity τ_m is considered to be a function of the incoming azimuth angle, θ. $\tau_m(\theta)$ represents the phase shift due to the increased travel distance of the incoming signal from an angle θ

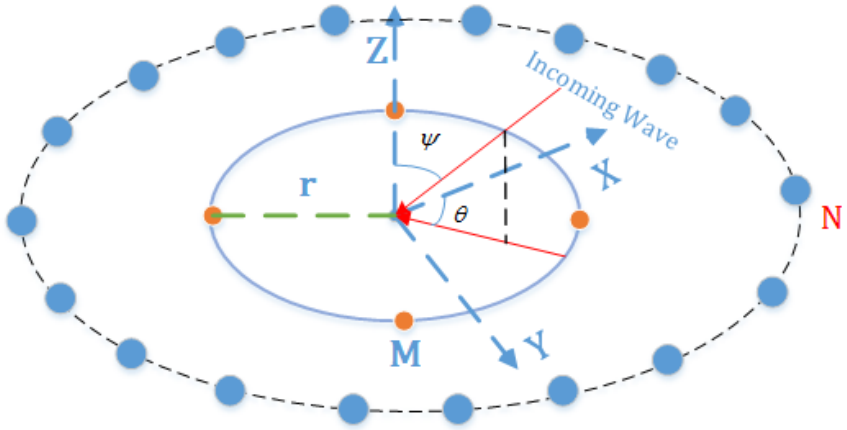

Fig. 3.1: A typical UCA with M elements, where θ and ϕ represent the azimuth and elevation angles of a received signal.

in reference to the first element of the antenna array while it is being received by the m^{th} element of the UCA.

3.5 DOA estimation using Compressive Sensing

This section combines the received open-circuit voltage information at each antenna element to formulate a sparse-matrix problem, which may be solved using CS techniques to identify the DOA of an unknown target. To incorporate the architecture of CS into the system model, the entire 2π radian angular domain is uniformly discretized into N possible DOAs, $\Theta = \{\hat{\theta}_n, 1 \leq n \leq N\}$, as shown in Fig. 3.1. Considering the practical implementation of the model, the incoming DOA θ can be anywhere in the range of $[-\pi, \pi)$. In Section 3.3, we established the relationship between the output of each antenna element and the DOA of the target. In matrix form the output of the antenna array can be rewritten as

$$\mathbf{V} = \mathbf{\Phi}(\Theta)\mathbf{S} \tag{3.8}$$

where

$$\mathbf{\Phi}(\Theta) = \begin{pmatrix} \tau_1(\hat{\theta}_1) & \tau_1(\hat{\theta}_2) & \cdots & \tau_1(\hat{\theta}_N) \\ \tau_2(\hat{\theta}_1) & \tau_2(\hat{\theta}_2) & \cdots & \tau_2(\hat{\theta}_N) \\ \vdots & \vdots & \ddots & \vdots \\ \tau_M(\hat{\theta}_1) & \tau_M(\hat{\theta}_2) & \cdots & \tau_M(\hat{\theta}_N) \end{pmatrix} \tag{3.9}$$

and $\mathbf{V} = \{v_m, 1 \leq m \leq M\} \in \mathbb{C}^{M\times 1}$ is a column vector representing the complex output at each antenna element of the UCA. The dictionary matrix is represented as $\mathbf{\Phi}(\Theta) \in \mathbb{C}^{M\times N}$, where each column corresponds to the M-element array response vector, for an incoming plane wave arriving from the direction $\hat{\theta}_n$. The phase shift $\tau_m(\hat{\theta}_n)$ is calculated using (3.7). The vector $\mathbf{S}$ is an $N \times 1$ vector of coefficients, where s_n^{inc} represents the magnitude of the complex envelope of the wave arriving from $\hat{\theta}_n$. The complex voltage outputs of the antenna elements in (3.8) are corrupted with the additive noise vector $\boldsymbol{\eta} \in \mathbb{C}^{M\times 1}$. The entries of $\boldsymbol{\eta}$ are statistically independent and Gaussian distributed with zero mean and variance σ^2. The effect of noise on the output observations can be expressed as

$$\mathbf{V_n} = \mathbf{\Phi}(\Theta)\mathbf{S} + \boldsymbol{\eta}. \tag{3.10}$$

The system defined in (3.10) is an under-determined set of equations, where $M \leq N$, and can be formulated as a CS problem to recover an estimate $\hat{\mathbf{S}}$ of the original sparse vector $\mathbf{S}$ via convex optimization as shown in (3.1). Therefore

$$\hat{\mathbf{S}} = \min_{\mathbf{S}\in\mathbb{C}^N} \|\mathbf{S}\|_0 \quad s.t. \quad \|\mathbf{V_n} - \mathbf{\Phi}(\Theta)\mathbf{S}\|_2 < \epsilon \tag{3.11}$$

where $\|\cdot\|_0$ is the l_0-norm and ϵ is the regularization parameter that is being determined by the noise or quantization level. Since our model assumes a single transmitting source among the N possible DOAs, the recovered sparse vector will have only one nonzero element. The index n of the non-zero element refers to the angular grid $(\hat{\theta}_n)$ corresponding to the source DOA.

3.6 Iterative Compressive Sensing for DOA Estimation

To solve for the problem defined in (3.10), the CS algorithm searches for the n^{th} column, ϕ_n, of the dictionary matrix, $\mathbf{\Phi}$ such that $|\langle \mathbf{V_n}, \phi_n \rangle|$ has the maximum correlation. The inner-product operation in vector space is represented as $|\langle \bullet, \bullet \rangle|$. The n^{th} element of the recovered vector $\hat{\mathbf{S}}$ in (3.10), corresponds to the column ϕ_n of $\mathbf{\Phi}$, which is chosen to be the incoming DOA. The scalar amplitude of the n^{th} element of $\hat{\mathbf{S}}$ refers to the correlation coefficient between $\mathbf{V_n}$ and ϕ_n. The DOA of the incoming signal can be anywhere in the range $[-\pi, \pi)$. For a random DOA, the probability of exact grid alignment is almost zero. However, it can sometimes be on the angular grid. In general, the DOA will have some angular separation from a discrete grid point, i.e. $\theta = \hat{\theta}_n + \Delta\theta$, where $(-\omega/2) < \Delta\theta < (\omega/2)$ and $\omega = 2\pi/N$ is the quantized grid interval. Conventional CS processing as described in (3.11) in Section 3.5 fails to detect the incoming DOA accurately. As the incoming DOA is between two discrete grid points, a dictionary mismatch is introduced between the processed observation vector, $\mathbf{V_n}$, and the measurement matrix, $\mathbf{\Phi}$. This forces the optimized solution vector, $\hat{\mathbf{S}}$, to converge to an incorrect DOA. Instead of searching for the column with maximum correlation, CS searches for several columns with relatively high correlation coefficients. In a greedy algorithm such as CoSaMP, the number of columns to search can be pre-defined by specifying the sparsity of the recovered vector.

One such instance is illustrated in Fig. 3.2, where the CS algorithm is modified to extract two discrete grid points per source. For an incoming off-grid DOA (shown in blue), the recovered vector $\hat{\mathbf{S}}$ generates two peaks (shown in red) on the neighboring discrete grid points $\hat{\theta}_a$ and $\hat{\theta}_b$. Since the incoming DOA θ is closer to $\hat{\theta}_a$, the grid point corresponding to $\hat{\theta}_a$ has a higher amplitude than for $\hat{\theta}_b$. This indicates that the amplitudes of the grid points are dependent on the relative angular separation of the original DOA from the respective neighboring grid points. The proposed Iterative Compressive Sensing based DOA estimation (ICSDOA) algorithm aims to exploit the

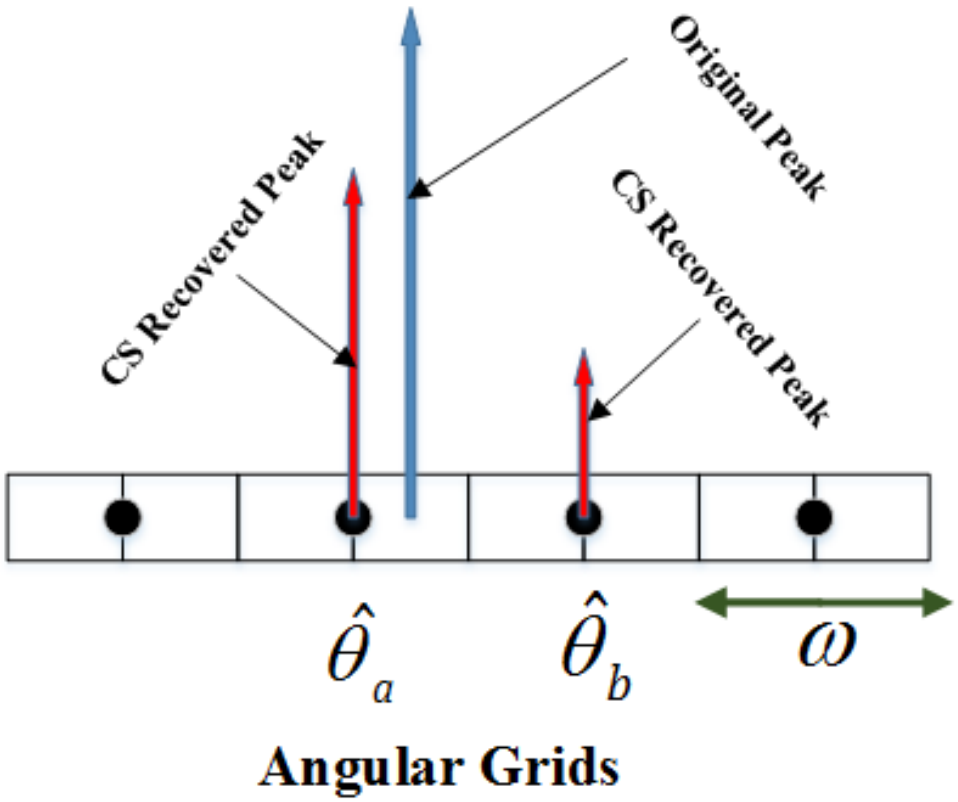

Fig. 3.2: Blue peak indicates original off-grid DOA, whereas red peaks are amplitudes on the neighboring grid points closest to the original source DOA.

amplitude on the closest grid to estimate the DOA of a source.

The estimation algorithm comprises a two-stage strategy where, at the first stage, an index corresponding to the maximum complex envelope of the recovered vector is chosen as a coarse estimate $\breve{\theta}_0$, which may be obtained from

$$n_{max} = \arg\max_{n}\{|\hat{\mathbf{S}}[n]|\} \tag{3.12}$$

such that

$$\hat{\mathbf{S}} = \min_{\mathbf{S}\in\mathbb{C}^N} \|\mathbf{S}\|_0 \quad s.t. \ \|\mathbf{V_n} - \mathbf{\Phi}(\Theta)\mathbf{S}\|_2 < \epsilon$$

and

$$\breve{\theta}_0 = \Theta(n_{max}).$$

where $\hat{\mathbf{S}}$ is the recovered sparse vector after CS processing on (3.11) and Θ represents

Algorithm 1: ICSDOA

Input: $\mathbf{V_n}$, $\mathbf{\Phi}(\Theta_0)$, $\breve{\theta}_0$, n_{max}, Ω

Output: Estimate of Original DOA θ_{est}

1 Initialize $t = 1$

2 Define new measurement matrix $\mathbf{\Phi}(\Theta_{t-1} + \frac{\omega}{2}\overline{u})_{2\pi}$

3 Compute CS to recover vector $\hat{\mathbf{S}}_t$

4 Calculate $\alpha_t = |\hat{\mathbf{S}}_t[n_{max}]|$ and $\beta_t = |\hat{\mathbf{S}}_t[n_{max} - 1]|$

5 Define $\Delta\Theta_t = (\frac{\alpha_t - \beta_t}{\alpha_t + \beta_t})\frac{\omega}{2}$

6 Check

(I) If $(|\Delta\Theta_t| > \Omega)$.

Update $\Theta_t = (\Theta_{t-1} + \Delta\Theta_t\overline{u})_{2\pi}$,

Update $\breve{\theta}_t = \Theta_t(n_{max})$

Update $t = t + 1$

Repeat Steps 2 to 6

(II) Else

$\theta_{est} = \breve{\theta}_t$

the set of N discrete azimuth angular grid points.

At a moderate Signal-to-Noise Ratio (SNR), there is a high probability that the coarse estimate $\breve{\theta}_0$ obtained from the first stage is the quantized grid point closest to the original incoming DOA. That is, the incoming DOA θ may be on either side of the coarse estimate $\breve{\theta}_0$, i.e. $\theta \in [\breve{\theta}_0 - \frac{\omega}{2}, \breve{\theta}_0 + \frac{\omega}{2})$, where $\omega = \frac{2\pi}{N}$ is the angular grid separation. The first stage is followed by an iterative algorithm in the second stage, which updates $\breve{\theta}_0$ at each iteration. In the second stage, the CS operation is carried out once to obtain an optimized sparse vector $\hat{\mathbf{S}}_t$ where t is the number of iterations. The new sparse vectors is recovered by applying the CS operation to the modified measurement matrix $\mathbf{\Phi}(\Theta + \frac{\omega}{2}\overline{u})_{2\pi}$ where $\overline{u}$ is the $N \times 1$ vector with all elements equal to 1 and, for a vector

W, $(W)_{2\pi}$ is defined as

$$(W)_{2\pi} = \text{modulo}(W + \pi\overline{u}, 2\pi\overline{u}) - \pi\overline{u} \tag{3.13}$$

where (3.13) describes the 2π modulo operation on each of the elements in W. The process bounds the elements in vector W in the range $[-\pi, \pi)$. The two dominant coefficients corresponding to the n_{max} and $n_{max} - 1$ index of the recovered vector $\hat{\mathbf{S}}_t$ are respectively stored as α_t and β_t. This action is similar to rotating the angular grid points Θ by $\frac{\omega}{2}$, in both clockwise and anticlockwise directions. However, by exploiting the coefficient of the n_{max} and $n_{max} - 1$ index of $\hat{\mathbf{S}}_t$, both α_t and β_t are obtained using a single rotation of the grid points. The process significantly reduces the computation complexity of the algorithm. When $\alpha_t > \beta_t$, it indicates that the original DOA is greater than the coarse estimate ($\theta > \breve{\theta}_0$) whereas when $\alpha_t < \beta_t$, the original DOA is smaller than the coarse estimate ($\theta < \breve{\theta}_0$). The process identifies the direction of the original DOA with respect to the coarse estimate. The scalars α_t and β_t are used to obtain a phase error discriminant $\Delta\Theta_t$, which is then used to produce a new set of grid points and hence an update of the coarse estimate. The iterative algorithm can be described as follows

For $t = 1, 2, ...,$ and $\Delta\Theta_0 = 0$ and $\Theta_0 = \Theta$

define

$$\alpha_t = |\hat{\mathbf{S}}_t[n_{max}]| \tag{3.14}$$

$$\beta_t = |\hat{\mathbf{S}}_t[k_{max}]| \tag{3.15}$$

where

$$k_{max} = \begin{cases} n_{max} - 1, & \text{for } 2 \leq n_{max} \leq N \\ N, & \text{for } n_{max} = 1 \end{cases}$$

and

$$\hat{\mathbf{S}}_t = \min_{\mathbf{S}_t \in \mathbb{C}^N} \|\mathbf{S}_t\|_0 \;\; s.t. \;\; \|\mathbf{V_n} - \mathbf{\Phi}(\Theta_{t-1} + \frac{\omega}{2}\overline{u})_{2\pi}\mathbf{S}_t\|_2 < \epsilon$$

$$\Delta\Theta_t = \left(\frac{\alpha_t - \beta_t}{\alpha_t + \beta_t}\right)\frac{\omega}{2} \tag{3.16}$$

$$\Theta_t = (\Theta_{t-1} + \Delta\Theta_t\overline{u})_{2\pi} \tag{3.17}$$

$$\breve{\theta}_t = \Theta_t(n_{max}) \tag{3.18}$$

At each iteration, $\Delta\Theta_t$ from (3.16) is used to update Θ_t in (3.17) to produce a new set of quantized grid points. A new measurement matrix is constructed at each iteration using the updated Θ_t, and the iteration continues. The stopping criterion of the algorithm is determined by a user-defined threshold Ω, such that $|\Delta\Theta_t| < \Omega$. A complete sequential breakdown of the algorithm is given in Algorithm 1.

3.6.1 Convergence of ICSDOA

Suppose that $p(\theta)$ is an angular discriminant function such that

$$\breve{\theta}_0 = p(\theta)$$

where θ is the actual angle of arrival in the noiseless case and $\breve{\theta}_0$ is the coarse estimate. Therefore

$$e_0 = \theta - p(\theta)$$

$$\breve{\theta}_1 = \breve{\theta}_0 + p(e_0) = \breve{\theta}_0 + p[\theta - p(\theta)]$$

$$e_1 = \theta - \breve{\theta}_1 = \theta - \breve{\theta}_0 - p[\theta - p(\theta)] = e_0 - p(e_0)$$

$$\breve{\theta}_2 = \breve{\theta}_1 + p(e_1) = \breve{\theta}_1 + p[\theta - \breve{\theta}_1]$$

$$e_2 = \theta - \breve{\theta}_2 = \theta - \breve{\theta}_1 - p[\theta - \breve{\theta}_1] = e_1 - p(e_1)$$

$$\breve{\theta}_{k-1} = \breve{\theta}_{k-2} + p(e_{k-2}) = \breve{\theta}_{k-2} + p[\theta - \breve{\theta}_{k-2}]$$

$$e_{k-1} = \theta - \breve{\theta}_{k-1} = \theta - \breve{\theta}_{k-2} - p[\theta - \breve{\theta}_{k-2}] = e_{k-2} - p(e_{k-2})$$

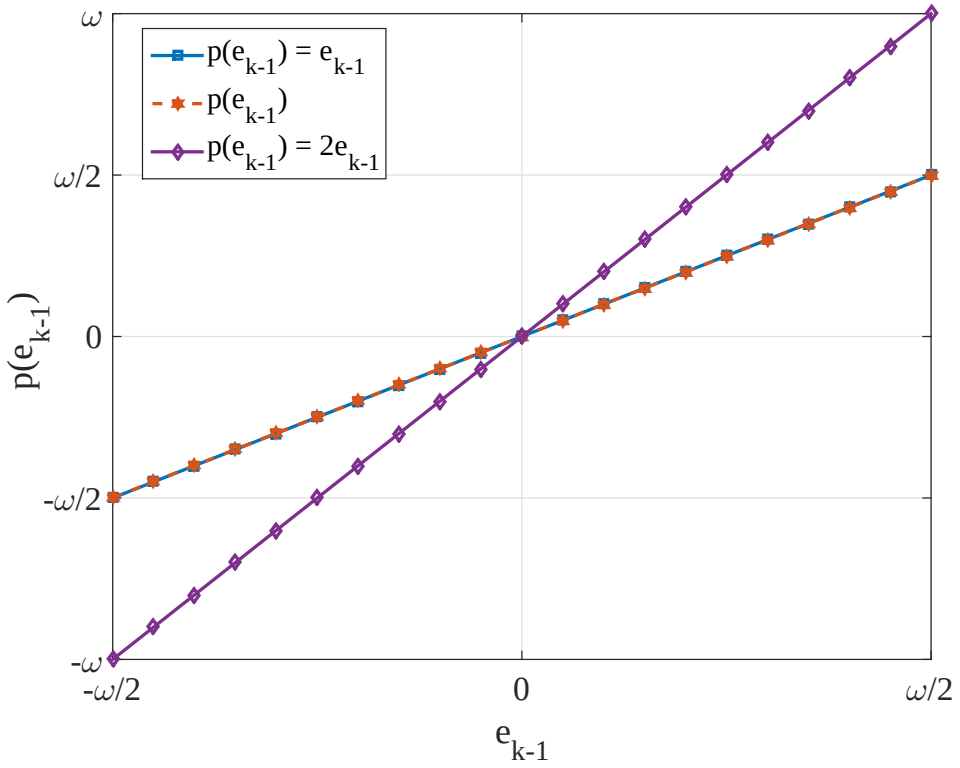

Fig. 3.3: The error discriminant as a function of the difference between the incoming DOA θ and the updated estimate at each iteration $\breve{\theta}_{k-1}$. The figure illustrates the result for no noise case.

In general, for $k = 1, 2, ...$

$$\breve{\theta}_k = \breve{\theta}_{k-1} + p[\theta - \breve{\theta}_{k-1}]$$

$$e_k = \theta - \breve{\theta}_k = \theta - \breve{\theta}_{k-1} - p[\theta - \breve{\theta}_{k-1}]$$

It follows by induction that,

$$e_k = e_{k-1} - p(e_{k-1})$$

Theorem 3.6.1 *Let $p(e)$ be a continuous function, with $p(e) = 0$ for $e = 0$. For $e > 0$, $0 < p(e) < e$ and for $e < 0$, $e < p(e) < 0$. Let e_k, (for $k = 1, 2, 3...$) be a real sequence such that $e_k = e_{k-1} - p(e_{k-1})$, then*

$$\lim_{k\to\infty} e_k = 0$$

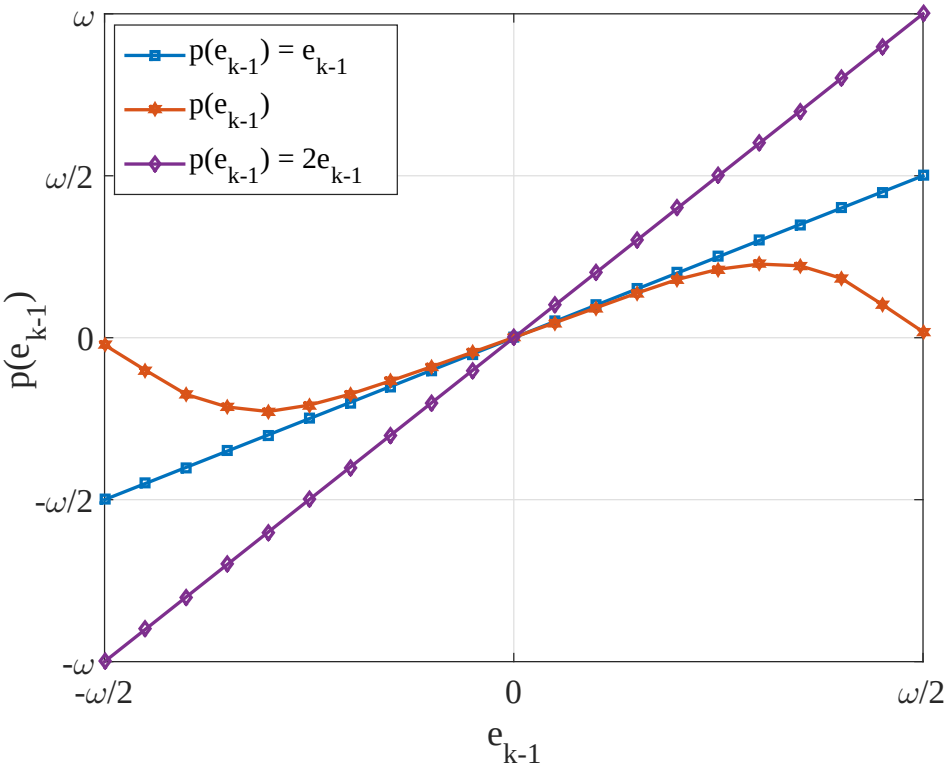

Fig. 3.4: The error discriminant as a function of the difference between the incoming DOA θ and the updated estimate at each iteration $\breve{\theta}_{k-1}$.The figure illustrates the result for SNR = 15 dB .

and the convergence is monotonic.

Proof :

Case : 1

$$e_0 > 0$$

$$e_1 = e_0 - p(e_0)$$

Therefore,

$$0 < e_1 < e_0$$

In general,

$$e_k = e_{k-1} - p(e_{k-1})$$

Therefore,

$$0 < e_k < e_{k-1}$$

and

$$\lim_{k\to\infty} e_k = 0.$$

Case : 2

$$e_0 < 0$$

$$e_1 = e_0 - p(e_0)$$

Therefore,

$$e_0 < e_1 < 0$$

In general,

$$e_k = e_{k-1} - p(e_{k-1})$$

Therefore,

$$e_{k-1} < e_k < 0$$

and

$$\lim_{k\to\infty} e_k = 0.$$

Theorem 3.6.2 *Let $p(e)$ be a continuous function, with $p(0) = 0$. For $e > 0$, $e \leq p(e) < 2e$ and for $e < 0$, $2e < p(e) \leq e$. Let e_k, (for $k = 1, 2, 3...$) be a real sequence such that $e_k = e_{k-1} - p(e_{k-1})$, then*

$$\lim_{k\to\infty} e_k = 0.$$

Proof :

Case : 1

$$e_0 > 0$$

$$e_1 = e_0 - p(e_0)$$

Therefore,

$$-e_0 < e_1 \leq 0$$

$$e_2 = e_1 - p(e_1)$$

$$0 \leq e_2 < -e_1$$

In general, if k is even,

$$-e_k < e_{k+1} < 0$$

if k is odd,

$$0 \leq e_{k+1} < -e_k$$

Therefore

$$\lim_{k\to\infty} |e_k| = 0.$$

and

$$\lim_{k\to\infty} e_k = 0.$$

Case : 2

$$e_0 < 0$$

$$e_1 = e_0 - p(e_0)$$

Therefore,

$$0 \leq e_1 < -e_0$$

$$e_2 = e_1 - p(e_1)$$

$$-e_1 < e_2 \leq 0$$

In general, if k is even,

$$0 \leq e_{k+1} < -e_k$$

if k is odd,

$$-e_k < e_{k+1} \leq 0$$

Therefore

$$\lim_{k\to\infty} |e_k| = 0.$$

and

$$\lim_{k\to\infty} e_k = 0.$$

3.7 Simulation and Analysis

In this section, detailed analysis and extensive simulations are carried out to validate and verify the effectiveness of the proposed algorithm in estimation the DOA of a transmitter. Additionally, the impact of various operating parameters such as number of antenna elements, number of angular grid points on the performance of the algorithm is also presented in this section.

3.7.1 SNR and Performance Parameter

The Signal to Noise (SNR) at the antenna elements has a significant impact on the DOA estimation accuracy of a transmitting source. In order to determine the robustness of the proposed ICSDOA algorithm, the following noise sensitivity test has been considered. The SNR is calculated at the receiver as the ratio of the sum of the received power at m antenna elements to σ^2, where σ^2 is the variance of the complex Gaussian noise. The measured data are characterized by SNR in dB, defined as

$$\mathrm{SNR}_{\mathrm{dB}} = 10\log_{10}\left[\frac{\sum_{m=1}^{M}|v_m|^2}{M\sigma^2}\right] \tag{3.19}$$

where v_m, $m = 1, ...M$, is the noiseless complex voltage observation at each antenna element. To validate that the algorithm has the same performance for any given angle of arrival, U different incoming DOAs are selected from a uniform distribution in the range $[-\pi, \pi)$. For statistical consistency, I Monte Carlo trials are carried out. The results in this section aim to validate the effect of noise sensitivity of the proposed algorithm in determining the actual incoming DOA of a signal. Compressive Sampling Matching Pursuit (CoSaMP) has been used as the platform for the CS operation. The Performance parameter of the algorithm is characterized as the Mean Square Error (MSE), where MSE is defined as

$$\mathrm{MSE} = \frac{\sum_{u=1}^{U}\sum_{i=1}^{I}|\theta_{org,u,i} - \theta_{est,u,i}|^2}{UI} \tag{3.20}$$

where $\theta_{org,u,i}$ is the original DOA of the source and $\theta_{est,u,i}$ is the DOA of the source estimated for the u^{th} scenario and the i^{th} Monte Carlo trial. The MSE of the proposed algorithm will be compared with the Cramér-Rao lower bound, given in [149] as

$$\mathrm{CRLB} \geq \frac{\sigma^2}{Mb^2r^2}, \tag{3.21}$$

where M, b and r are defined in Section 3.4. The expression of CRLB in (3.21) shows that the error variance is independent of the incoming DOA and is only dependent on

M and r of the UCA. CRLB will be used as a benchmark in the following simulation to validate the effectiveness of the model in recovering an accurate estimate of the original sparse vector. An estimator achieving the CRLB is considered to be efficient and it is not possible for any estimator to perform better than the theoretical CRLB. A detailed derivation of the CRLB is presented in Appendix B.1.

3.7.2 Sparse Vector Coefficients

The process of obtaining the coarse estimate involves finding the index of the sparse vector corresponding to the maximum magnitude as shown in (3.12). The sparse vector, $\hat{\mathbf{S}}$, is an output of the CS processing on the measurement matrix $\mathbf{\Phi}$ and the noisy observations $\mathbf{V_n}$. Greedy CS algorithms such as CoSaMP [67] use the approximate sparsity level, l and ϵ as an input in estimating $\hat{\mathbf{S}}$. The greedy algorithms have the ability to output an optimized solution vector while satisfying the sparsity requirement of a user. On the other hand, the L1-optimization algorithm such as Basis-Pursuit [65] does not take the sparsity level, l as an input. This causes the solution vector $\hat{\mathbf{S}}$ recovered using L1-optimization techniques to have a large number of non-zero elements. In the proposed ICSDOA algorithm, the non-zero element of $\hat{\mathbf{S}}$ refers to an estimate of the possible incoming DOA. A solution vector with a large number of non-zero elements will introduce ambiguity in the estimation process, hence degrading the accuracy of the estimation. In this simulation, the approximate sparsity l of the solution vector $\hat{\mathbf{S}}$ will be varied to observe the impact on the MSE performance of the ICSDOA algorithm.

In Section 3.6, the second stage of the algorithm generates the error discriminant, $\Delta\Theta$ which is then used to update the coarse estimate. The error discriminant function uses the inputs α and β which are the respective magnitudes of the complex envelopes corresponding to the index representing the coarse estimate. The magnitudes are obtained by rotating the angular grid points Θ in both the clockwise and anticlockwise direction by a grid interval of $\omega/2$. The results in Fig. 3.5 and Table. 3.1 illustrates the impact of l on the generation of α and β and the output of $\Delta\Theta$. The simulation uses CoSaMP CS algorithm to recover the sparse vector. The approximate sparsity of $\hat{\mathbf{S}}$ will be varied in the range $l \in [1, 3]$. The UCA geometry is constructed with $M = 9$

antenna elements uniformly placed around a ring and an inter-element spacing of $\lambda/2$. The signal to noise ratio is kept constant at 20 dB. A signal is assumed to be impinging on the UCA from a $\theta = 26.67°$.

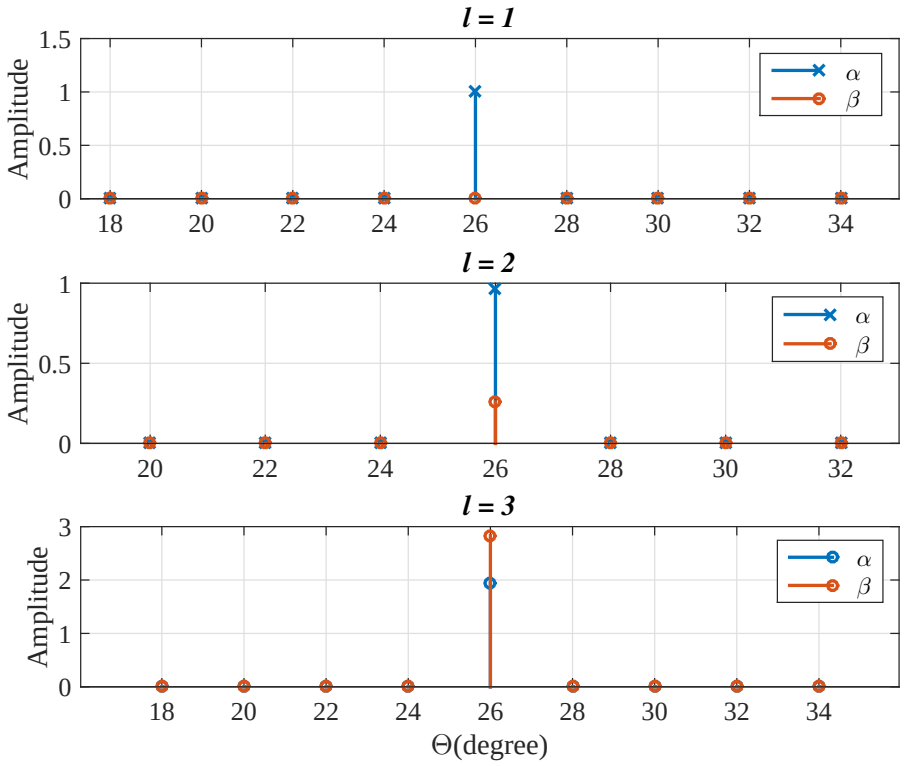

Fig. 3.5: Output of α and β with respect to varying sparsity of the recovered vector.

The plots in Fig. 3.5 shows the effect of l on the output of α and β. The x-axis is the quantized grid points representing the incoming DOA in degrees and the vertical axis is the corresponding magnitudes of α and β. The coarse estimate, $\breve{\theta}_0 = 26°$ is the quantized grid point closest to the incoming DOA, $\theta = 26.67°$. For $l = 1$ and 2, $\alpha > \beta$, which indicates that $\theta > \breve{\theta}_0$ and is true for the test case. However in case $l = 3$, $\alpha < \beta$ and as a result, the estimate is deviating away from the original DOA. For the 3 different cases of l, the error discriminant $\Delta\Theta$ is calculated using (3.16). The value of the error discriminant has been calculated using the first iterative operation of the ICSDOA algorithm. The result presented in the tables are in degrees. The results in Table. 3.1, show the error discriminant calculated using the sparsity level

Sparsity	Initial Estimate	Error Discriminant	Final Estimate.
l = 1	26	1	27
l = 2	26	0.423	26.423
l = 3	28	−0.381	27.62

Table 3.1: Error discriminant calculated in degrees for varying sparsity level of the CoSaMP algorithm

$l = 2$ enables the ICSDOA to achieve an estimate with minimum error. The 2nd best performance case is when the sparsity level is $l = 1$. It can also be referred as nearest quantized grid estimation. The worst performance among the three different sparsity is $l = 3$. In case of $l = 3$, the off-grid incoming DOA is approximated using 3 dominant coefficients causing ambiguity in the estimation process. The result reiterates the fact that, to estimate any incoming DOA in between grid points, the sparsity of the recovered vector $\hat{\mathbf{S}}$ should be set to 2.

To further validate the results presented in Fig. 3.5 and Table. 3.1, an MSE performance test was carried out by varying the SNR from -10 dB to 25 dB. A number of incoming DOAs are considered, selected from a uniform distribution. The MSE of the proposed algorithm is then compared with the theoretical CRLB for estimation accuracy. For this simulation, the number of Monte Carlo runs is set to be 1000. The results in Fig. 3.6 reiterate the prior analysis on the sparsity level of CoSaMP algorithm. The red plot representing $l = 2$ is the best performing among them and achieves the theoretical CRLB for SNR(dB) > 7. Although all three plots approach the bound for SNR = 6 dB, the plots for $l = 1$ and $l = 3$ deviate away from the bound for higher SNR. It can be concluded from the analysis that, the error discriminant function converges to the original estimate rapidly, especially when the approximate sparsity level for the recovery vector $\hat{\mathbf{S}}$ is set to be twice the number of sources detected.

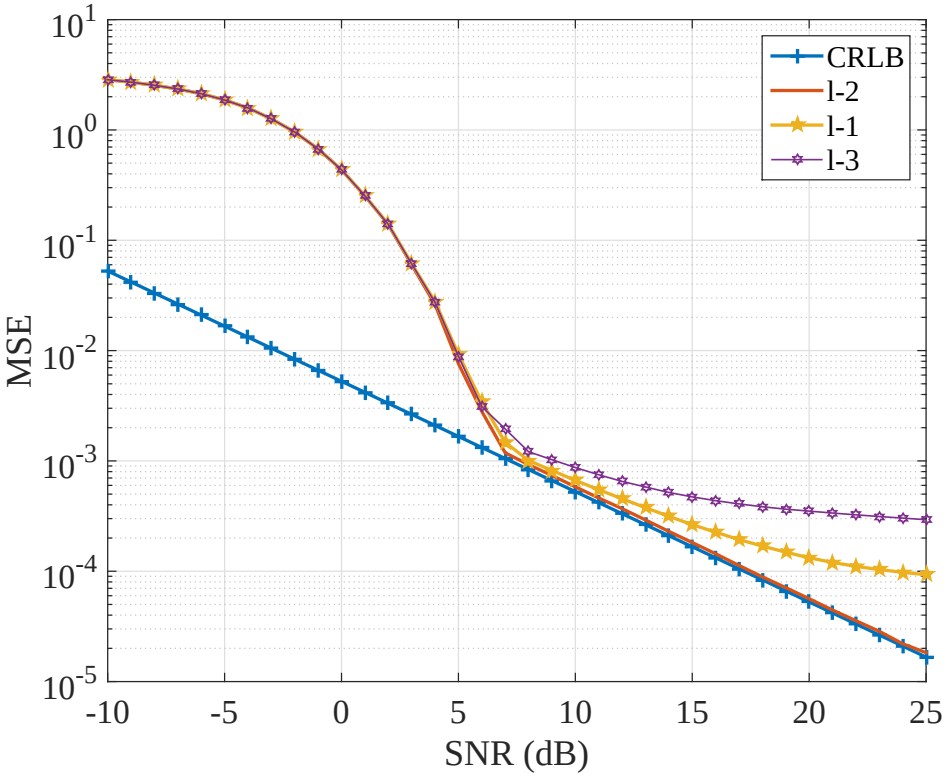

Fig. 3.6: MSE performance of the proposed algorithm with respect to varying sparsity level of the CoSaMP algorithm.

3.7.3 Number of Antenna Elements

The construction of the measurement matrix has a significant influence on the MSE performance of the proposed algorithm. As discussed in Section 3.3.1, for a measurement matrix to guarantee a unique solution via CS, both μ and Υ should have the smallest value in order to satisfy the RIP property. This section analyses the influence of the number of antenna elements M and the radius of the UCA r in the construction of a measurement matrix.

In the first simulation, the mutual coherence of Φ is calculated by varying M and r in the ranges $[6, 21]$ and $[\lambda, 10\lambda]$ respectively. A contour plot is presented in Fig. 3.7 to show the impact of varying M and r on the mutual coherence of the measurement matrix Φ. The angular region in the range $[-\pi, \pi)$ is quantized into $N = 180$ grid points with $\omega = 2\pi/N$. A red dotted line is drawn through the contour plot to distinguish the

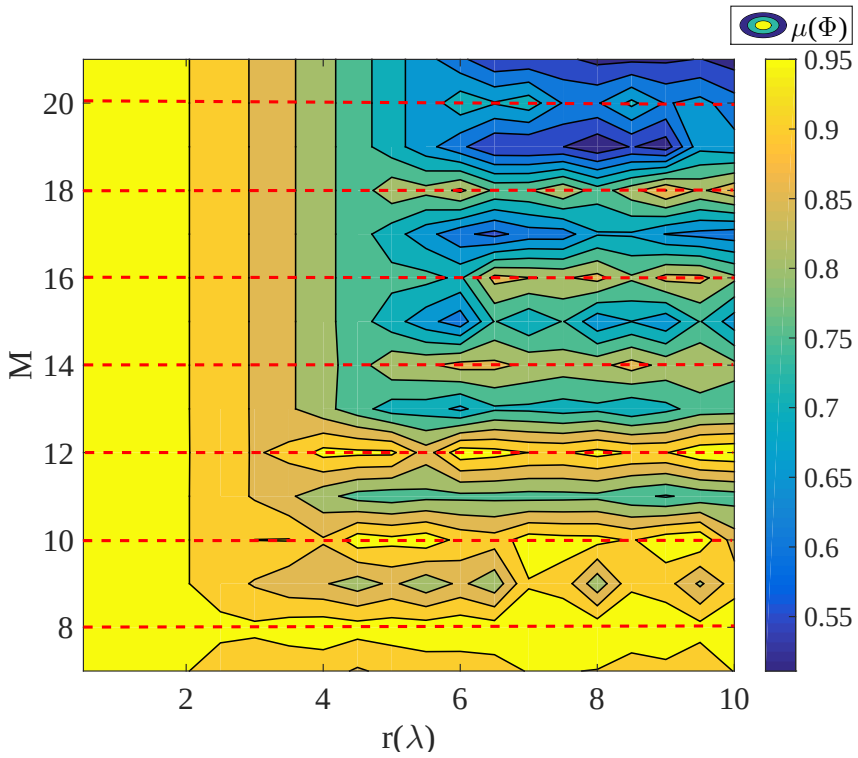

Fig. 3.7: A contour plot showing the mutual coherence of Φ for varying M and r.

effect of an even number of antenna elements as a function of radius. It is evident from the plot that, for $r < 2\lambda$, the mutual coherence of Φ is on the higher side for all M. However, for $r > 2\lambda$, $\mu(\Phi)$ has a sharper drop for odd M than even M. According to prior research on ULA [127], an increase in M causes the rank of Φ to increase, which influences Φ to achieve a lower mutual coherence. However, an interesting observation is presented for the case of a UCA. The complex output of an antenna element can be expressed as in (3.7) such that

$$v_m = s^{inc}\tau_m(\theta,\psi) = s^{inc}e^{-jbr\cos(\theta-\gamma_m)\cos(\psi)}. \tag{3.22}$$

Considering $s^{inc} = 1$ and $h = br\cos(\psi)$, using trigonometric identities (3.22) can be written as

$$v_m = \cos(h\cos(\theta-\gamma_m)) - j\sin(h\cos(\theta-\gamma_m)). \tag{3.23}$$

In (3.23), $\cos(\theta - \gamma_m)$ can be rewritten as

$$\cos(\theta - \gamma_m) = \cos(\theta)\cos(\gamma_m) + \sin(\theta)\sin(\gamma_m). \tag{3.24}$$

Due to circular symmetry in the UCA, for an even number of antenna elements M, $\gamma_1 = 0$ and $\gamma_{\frac{M}{2}+1} = \pi$; as a result for any incoming DOA θ

$$\cos(\theta - \gamma_m) = -\cos(\theta - \gamma_{\frac{M}{2}+1}) \tag{3.25}$$

then

$$v_1^* = v_{\frac{M}{2}+1}. \tag{3.26}$$

The centro-symmetric property of the UCA with even M causes the steering vector to have indistinguishable observations and reduces the dimensionality of Φ. This forces Φ to have a higher mutual coherence, especially when constructed with even M. The centro-symmetric nature of the UCA has been adopted in several DOA estimation techniques to reduce computation [150][151], however, in CS-based methods, the similarity in observations has an adverse effect on the DOA estimation. To illustrate the impact of odd and even number of antenna elements, the minimum $\mu(\Phi)$ for $M = 11$ is compared with $M = 12$. It can be seen that with 11 antenna elements $\mu(\Phi)$ is reduced by a factor of 10. In other words, it suggests that when an odd number of elements are used to construct Φ with $r > 2\lambda$, the mutual coherence between the steering vectors for two distinct DOAs can be significantly minimized. This also indicates that a UCA constructed with an odd number of elements reduces the ambiguity among two incoming DOAs. Additionally, the contour plot also suggests that a UCA constructed using odd M with $r > 2\lambda$, yields lower mutual coherence for Φ.

3.7.4 Radius of UCA

Conventional theory on antenna design [82] suggests having an inter-element separation $d \in [\frac{\lambda}{2}, \lambda]$ between the antenna elements to avoid ambiguity between the steering vectors

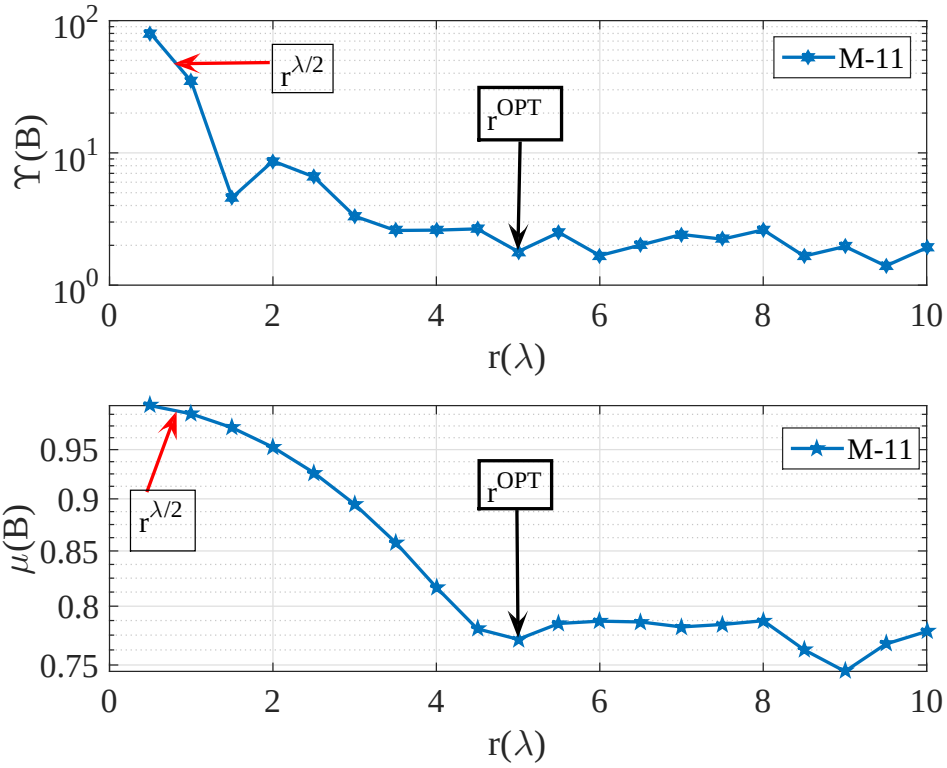

Fig. 3.8: Variation of $\mu(\Phi)$ and $\Upsilon(\Phi)$ with respect to changes in r for $M = 11$

of distinct DOAs. For $d < \frac{\lambda}{2}$, the effect of mutual coupling becomes dominant, whereas for $d > \lambda$ grating lobes are introduced, which splits the main beam into several side beams reducing the efficiency of beam-forming. The inter-element spacing $d = \frac{\lambda}{2}$ has been used as an optimum separation to perform a trade-off between mutual coupling and grating lobes. However, the expression of CRLB in (3.21) suggests that the variance of an unbiased estimator is inversely proportional to the square of the radius. This means an increase in radius will cause the CRLB to decrease significantly. The contour plot of $\mu(\Phi)$ in Fig. 3.7 and the expression of CRLB in (3.21) influenced further research to look for an optimum radius of UCA that enhances the MSE performance of the proposed algorithm.

Let $r^{\lambda/2}$ be the radius of a UCA with M elements such that the inter-element spacing d, between the elements is restricted to $\lambda/2$. The expression of $r^{\lambda/2}$ is derived

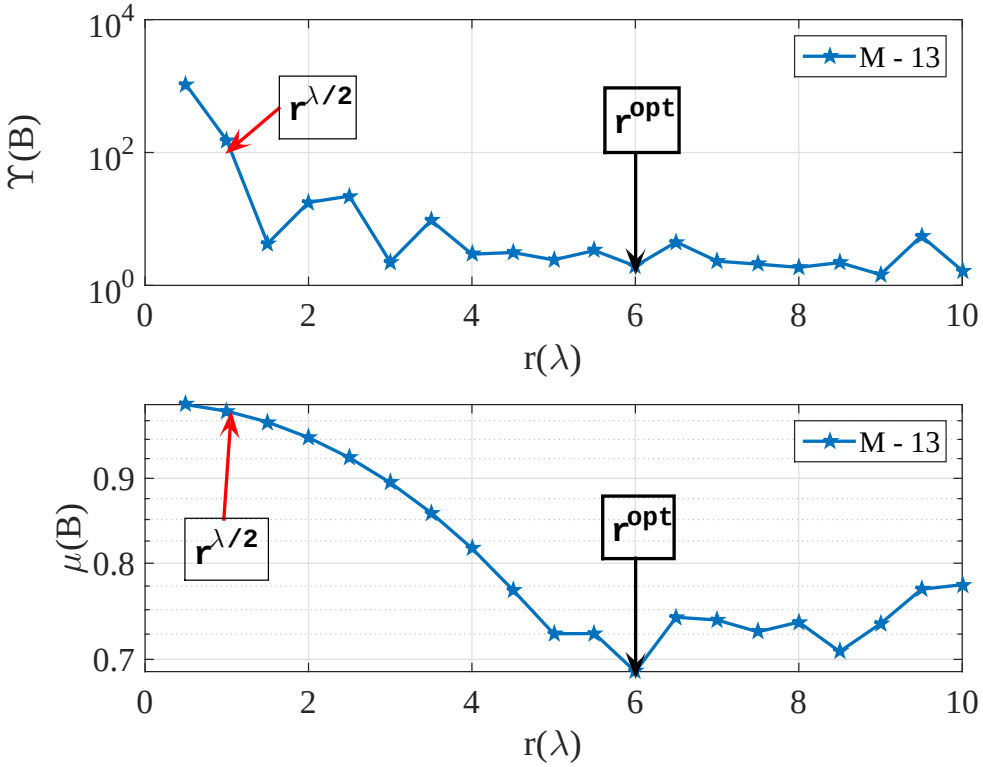

Fig. 3.9: Variation of $\mu(\Phi)$ and $\Upsilon(\Phi)$ with respect to changes in r for $M = 13$

from the definition of $d = \lambda/2$ in Section 3.3 as

$$r^{\lambda/2} = \frac{\lambda}{4sin(\frac{\pi}{M})}. \tag{3.27}$$

For each $M \in [6, 21]$, $r^{\lambda/2}$ is calculated using (3.27) and is found to be in the range $[\lambda/2, 2\lambda)$. From the contour plot in Fig. 3.7 it is evident that $\mu(\Phi)$ associated with $r^{\lambda/2} \in [\lambda/2, 2\lambda)$ is relatively high compared to $\mu(\Phi)$ for $r > 2\lambda$. To gain a deeper understanding into the array geometry further analysis is carried out to observe the influence of r on the structure of Φ.

From this point onwards the analysis will be restricted to an odd number of antenna elements. Two UCA cases have been considered where the geometry consists of $M = 11$ and 13 antenna elements respectively. For each case r is varied between 0.5λ and 10λ with an increment of 0.5λ. The physical size of the antenna array is a practical constraint in terms of implementation, the array analysis has been restricted to $r \leq 10\lambda$.

The graphs in Fig. 3.8 and 3.9 show the variation in $\Upsilon(\Phi)$ and $\mu(\Phi)$ with respect to a varying radius of UCA. The red arrow in the graphs in Fig. 3.8 and 3.9 indicate $r^{\lambda/2}$, where the inter-element spacing is restricted to $\lambda/2$. On the other hand, a black arrow has been drawn to indicate the radius point on the graph such that both the $\Upsilon(\Phi)$ and the $\mu(\Phi)$ are simultaneously minimized. In cases of $M = 11$ and 13, the radius appears to be at 5λ and 6λ. When the plot for $M = 11$ is considered, it can be seen that, at the radius point (indicated by black arrow), both $\Upsilon(\Phi)$ and $\mu(\Phi)$ are reduced by a factor of 12 and 20 respectively compared to $r^{\lambda/2}$. The sharp drop of $\Upsilon(\Phi)$ and $\mu(\Phi)$ greatly improves the matrix structure, enabling CS algorithms to take full advantage of the independent columns in generating an accurate and unique solution. From the analysis, it can be concluded that both $\Upsilon(\Phi)$ and $\mu(\Phi)$ should be used in conjunction to determine the appropriate radius for CS processing. The optimum radius, represented as r^{OPT}, is the point where $\Upsilon(\Phi)$ as well as $\mu(\Phi)$ are simultaneously minimized. The optimum radius is chosen such that the RIP property of the dictionary matrix Φ is preserved. This allows Φ to ensure maximum incoherence between the columns and efficient utilization of the vector space.

To validate the effectiveness of the optimum radius, r^{OPT}, an MSE performance comparison has been carried out against the theoretical CRLB. To provide accurate statistical validation of the simulation results, 10 different DOAs are randomly selected from a uniform distribution in the range $[-\pi, \pi)$. For each DOA, 1000 Monte Carlo trials are carried out. Two graphs are presented in Fig. 3.10 and 3.11, that illustrate the effect of external noise on the performance of two UCA geometries when constructed with a radius $r^{\lambda/2}$ and r^{OPT} respectively. Fig. 3.10 shows the MSE performance of a UCA with 11 antenna elements and Fig. 3.11 shows the performance of a UCA with 13 elements. In both cases, it can be observed that the UCAs constructed with radius r^{OPT} approach their respective CRLB for SNR > 7 dB. The results also strongly support the prior analysis on selecting an optimum radius, $r^{OPT} > r^{\lambda/2}$ such that the structure of Φ can be enhanced. The reduction in $\mu(\Phi)$ for r^{OPT} enabled the measurement matrix to achieve the theoretical CRLB, hence increasing the DOA estimation accuracy by 15

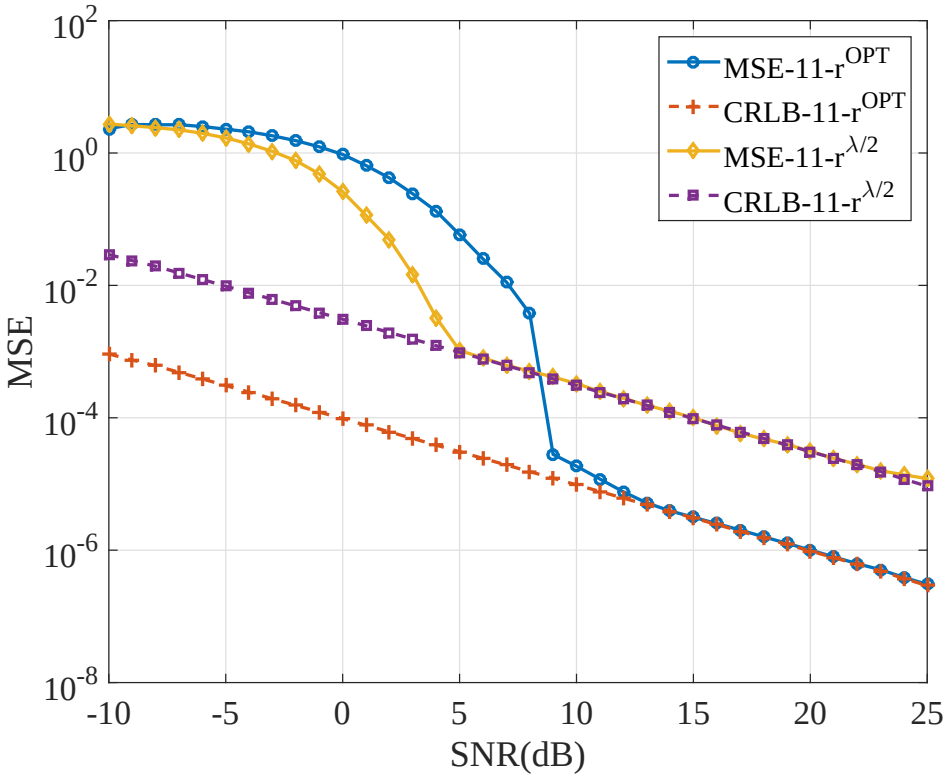

Fig. 3.10: MSE performance of UCA with M=11 constructed with radius $r^{\lambda/2}$ and r^{OPT}.

dB. However, a UCA constructed with $r^{\lambda/2}$ also achieved the CRLB for SNR $>$ 5 dB and stays on the bound for higher SNR. In the SNR region between 0 dB and 7 dB, UCA with $r^{\lambda/2}$ provides a better MSE performance than with r^{OPT}. The results show a systematic trade-off between the size of the antenna and the estimation performance of the UCA. When r^{OPT} is used as the radius of a UCA with $M = 13$ elements, the area of the UCA is increased by a factor of 25, whereas the estimation accuracy is improved by 16 dB.

3.7.5 Angular Grid Quantization

One of the integral parameters used in the construction of the measurement matrix Φ is the quantized angular grid points, Θ. The set of angular grid points is dependent on the quantization interval, $\omega = 2\pi/N$, that is on N. This section analyses the robustness of the proposed algorithm against a varying number of grid points, N. For

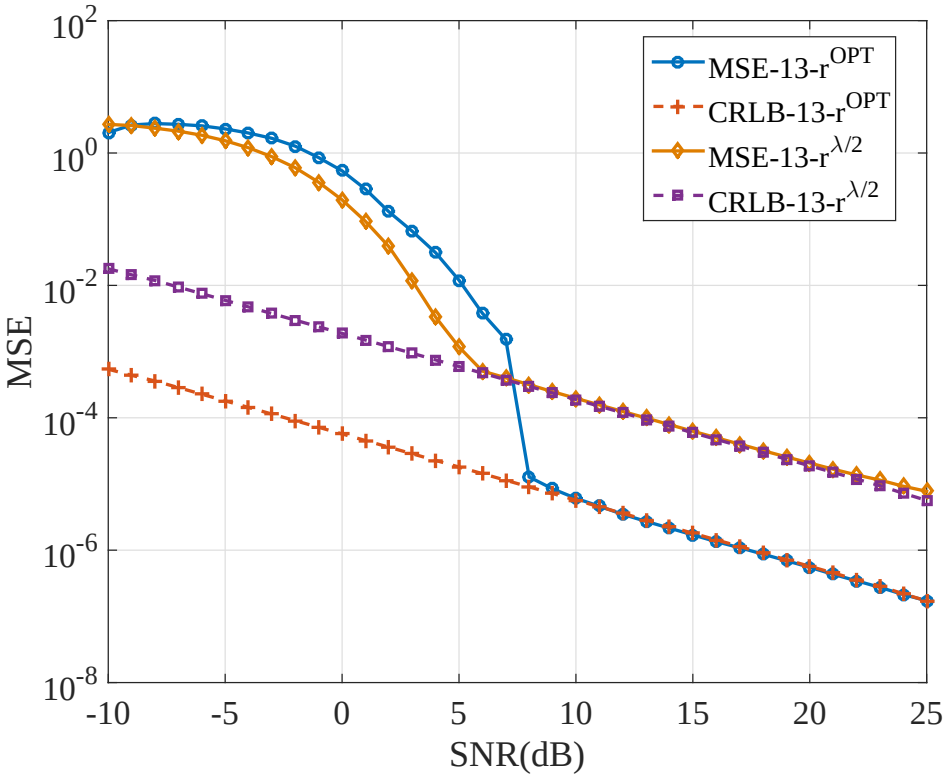

Fig. 3.11: MSE performance of UCA with $M = 13$ and radius $r^{\lambda/2}$ and r^{OPT}.

the analysis in this section the radius of the UCA will be such that the inter-element spacing between the antenna elements is $\lambda/2$. For this simulation, two different UCA geometries are considered with varying $M \in [9, 13]$. A signal is impinging on the UCAs from an incoming DOA of $\theta = 0.99$ radians. To provide a statistical validation, 1000 Monte Carlo runs are carried out. An Error Ratio (ER) is introduced as a performance parameter for this simulation such that

$$\text{Error Ratio (dB)} = 10 \log_{10} \left(\frac{\text{MSE}}{\text{CRLB}} \right). \tag{3.28}$$

The Error Ratio is the ratio of the MSE of the estimate against the respective theoretical CRLB error of the UCA geometries. It provides an indication of the performance difference between the estimation error and the CRLB error on a dB scale. In Fig. 3.12, the plots for two UCA geometries are presented and they show the change in ER with respect to a varying number of grid points. Both the UCA geometries perform in

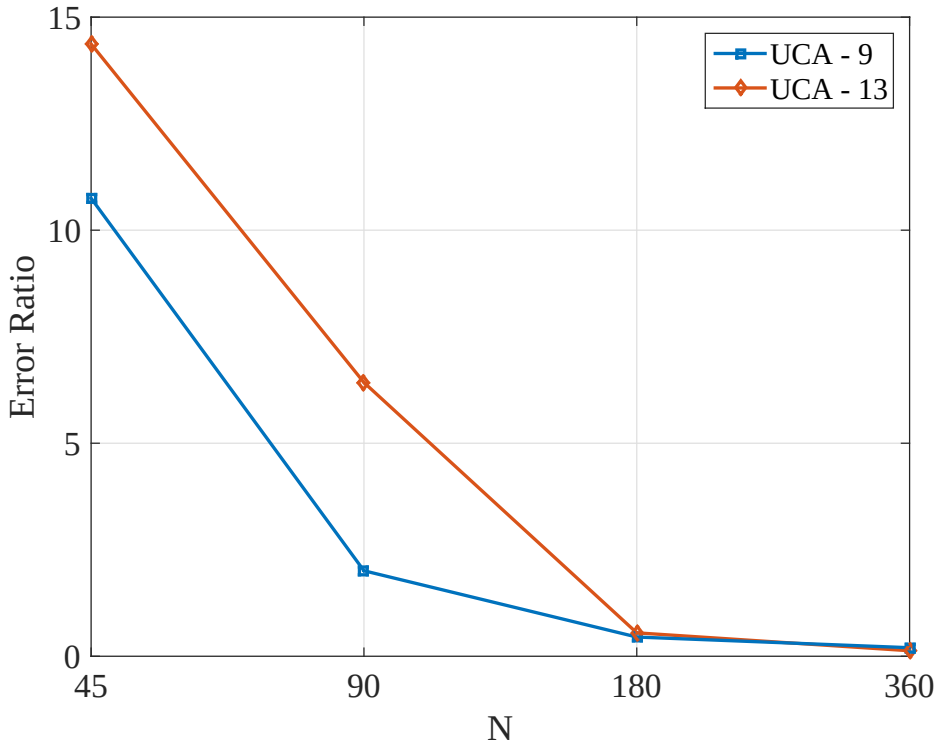

Fig. 3.12: Error Ratio of the two antenna geometries as a function of the number of angular grid points.

a similar fashion, where the ER decreases monotonically for increasing N. This means that, with finer quantization of the 2π angular domain, ER is close to zero and the MSE is on the CRLB. However, with coarser quantization of the 2π angular region (i,e. $N \ll 90$), UCA-9 has a lower ER than UCA-13. At $N = 90$, the ER for UCA-13 is twice that of UCA-9. The result from the analysis suggests that UCAs with smaller M are more robust to the variation in quantization level than UCA with larger M.

The expression of CRLB in (3.21) suggests that the error variance decreases with an increase in M. However, the results in Fig. 3.12 indicate that, at coarser quantization of the angular region, MSE increases with M. To further investigate the effect of N, the phase response of the UCA geometries are calculated for any incoming DOA, with θ in the range $[-\pi, \pi)$. The phase response for a UCA with M antenna elements corresponding to an incoming DOA, θ, is $f(\theta)$ given as

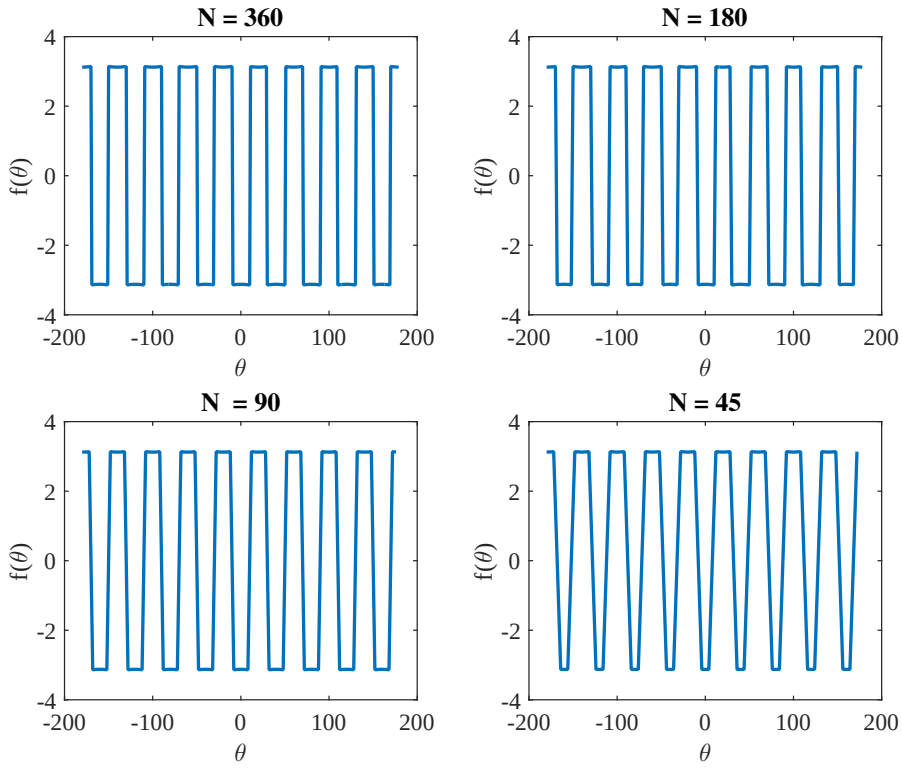

Fig. 3.13: Phase response of UCA-9 for varying number of angular grid points.

$$f(\theta) = \arg(AF), \tag{3.29}$$

where

$$AF = \sum_{m=1}^{M} e^{-jbr\cos(\theta-\gamma_m)} \tag{3.30}$$

The expression of γ_m is given in Section 3.4 that indicates the position of the m^{th} antenna element relative to the 1^{st} element of the UCA. Fig. 3.13 and 3.14 shows two graphs for each of the respective UCA geometries. The graphs have several sub-graphs showing the influence of varying quantization level (i.e, N) on $f(\theta)$. The number of peaks that appears for each of the antenna geometries is $M-2$ and is directly dependent on M [82]. So, for a UCA with larger M, the $f(\theta)$ changes more frequently than with a smaller M. In such cases, when the angular region is coarsely quantized, the consistency of $f(\theta)$ is effected. Especially in the case of UCA-13, the change in shape of $f(\theta)$ remains consistent up until $N = 90$ and changes sharply for $N = 45$.

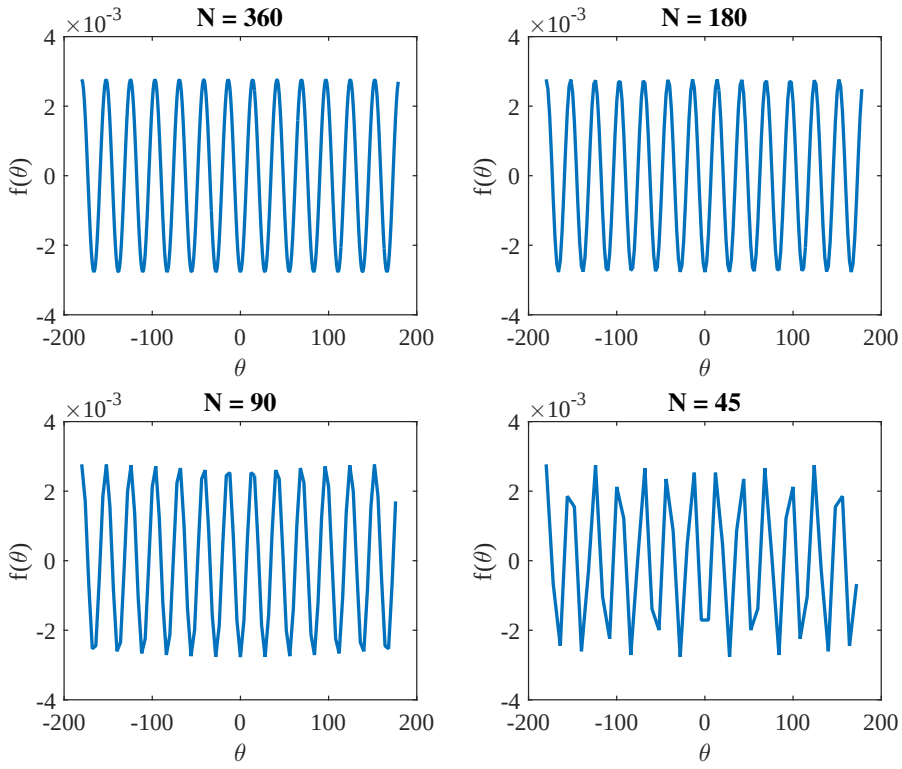

Fig. 3.14: Phase response of UCA-13 for varying number of angular grid points.

This can be associated to the under-sampling of the 2π angular region. At $N = 45$, there are not sufficient samples to reconstruct the entire region of angular coverage. As a result, the CS processing on the measurement matrix Φ fails to resolve the incoming DOA accurately. It can concluded from the results that there is systematic trade-off between the number of antenna elements and the required number of grid quantization points. For a UCA geometry with large M a finer quantization of the angular region is required in order to achieve its respective CRLB.

3.7.6 Transform Operation

The transform operation or sparsifying basis helps to de-correlate the columns of the measurement matrix, allowing CS to maximize the utilization of the column space. A

popular family of transform matrices are the Karhunen-Loève Transform (KLT), Discrete Cosine Transform (DCT), Discrete Fourier Transform (DFT), Orthogonal transform [129, 152–154]. Although KLT is used as a benchmark to judge the performance, the dependency of KLT on measurement makes it computationally more expensive. DFT, on the other hand, is based on a fixed support set but the complex entries of a DFT matrix can significantly alter the information of a complex measurement matrix. The entries of a DCT matrix are real and provide excellent de-correlation and energy compaction properties. A data-processing technique has been adopted in [129] to decorrelate the rows, which are the observations of the complex open-circuit voltages from N angular grid points. Let X be the processing operator

$$\mathbf{X} = \mathbf{Y}\mathbf{\Phi}^{+} \tag{3.31}$$

where $\mathbf{Y} = (\mathbf{H}^{*}\mathbf{\Phi})$ and the $M \times M$ transform matrix is represented as $\mathbf{H}$, where $\mathbf{H}^{*}$ is the conjugate transpose of $\mathbf{H}$. In (3.31) $\mathbf{\Phi}^{+}$ is the Moore-Penrose pseudoinverse of a matrix $\mathbf{\Phi}$. Applying the operator $\mathbf{X}$ on both sides of (3.31) yields

$$\mathbf{Y}\mathbf{\Phi}^{+}\mathbf{V_n} = \mathbf{Y}\mathbf{\Phi}^{+}\mathbf{\Phi}\mathbf{S} + \mathbf{Y}\mathbf{\Phi}^{+}\boldsymbol{\eta}$$

$$\tilde{\mathbf{V}} = \mathbf{B}(\Theta)\mathbf{S} + \mathbf{E}. \tag{3.32}$$

After the data processing, $\tilde{\mathbf{V}} = \mathbf{Y}\mathbf{\Phi}^{+}\mathbf{V_n}$ is the noisy processed observation vector and $\mathbf{B} = \mathbf{Y}\mathbf{\Phi}^{+}\mathbf{\Phi}$ is the processed measurement matrix. The noise vector $\mathbf{E}$ is the new processed measurement noise. The modified system in (3.32) can also be cast into CS framework similar to (3.11) to recover the sparse $\hat{\mathbf{S}}$ vector. The iterative process described in Section 3.6 can be used to estimate the DOA of an incoming signal.

This section details the impact of various transform matrices in estimating the incoming DOA. The simulation is carried out with a UCA geometry using $M = 9$ antenna elements with an inter-element spacing of $d = \lambda/2$. The angular domain in the range $[-\pi, \pi)$ is quantized into $N = 180$ grid points with grid interval $\omega = 2\pi/180$.

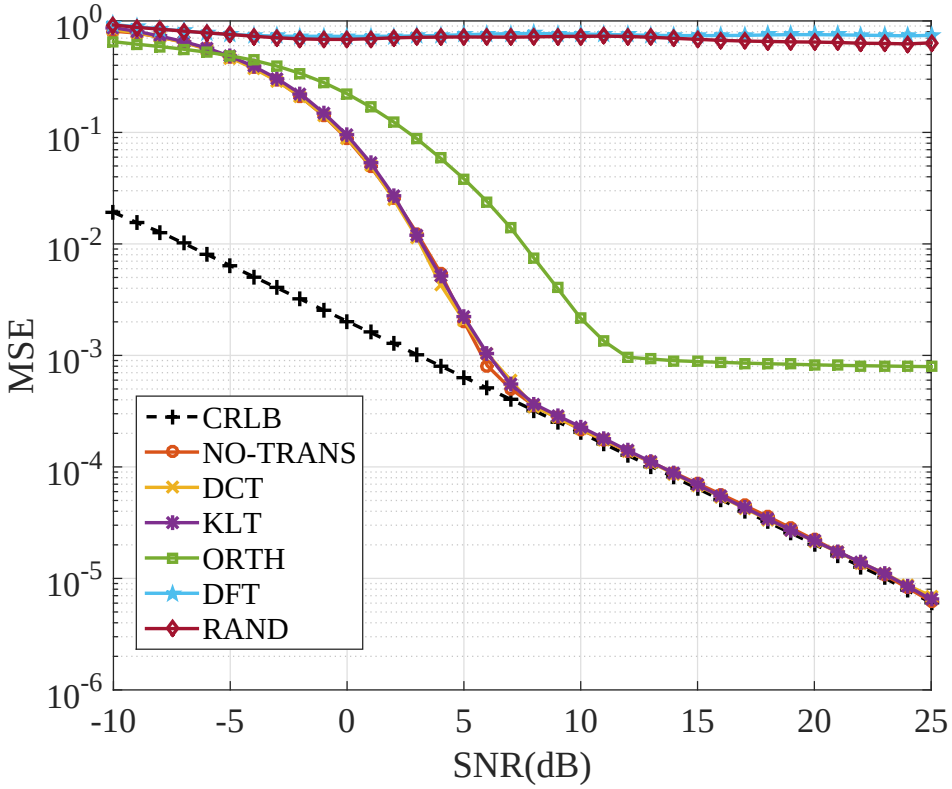

Fig. 3.15: The impact of various transform operations on the MSE performance of the proposed algorithm.

To illustrate the robustness of the algorithm, 100 DOAs are taken randomly from a uniform distribution in the range $[-\pi, \pi)$. For each scenario, 1000 Monte Carlo trials are carried out to provide a statistical validation. The MSE performance of each transform is compared to the theoretical CRLB. The legend NO-TRANS represents the case where the sparse vector is recovered using (3.11) without the influence of any transform operation. The ORTH legend indicates the traditional Gram-Schmidt Transform. It is clear from the graph that, the plots for KLT, DCT and NO-TRANS are performing extremely close to the CRLB with DCT slightly better than both KLT and NO-TRANS. Although ORTH performs better than DFT, it fails to reach the mark of higher performing transforms. This gives a clear indication that the inclusion of the transform operation does not offer any significant advantages in improving the DOA estimate. To reduce the computational complexity of the algorithm, the transform operations can be avoided for further simulations.

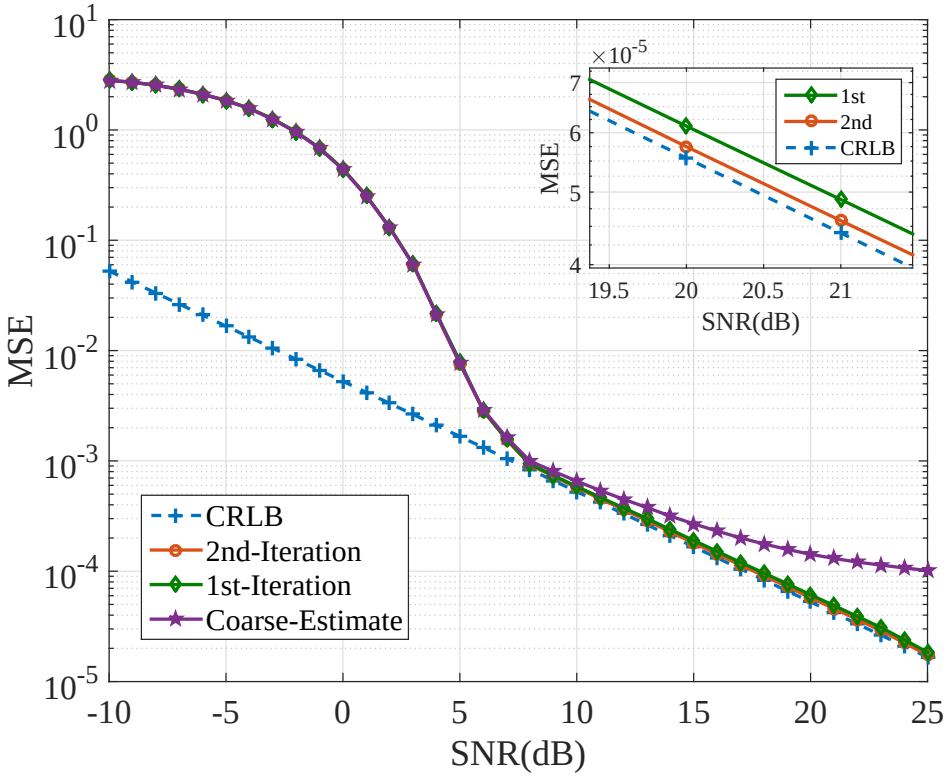

Fig. 3.16: Plots showing the fast convergence of the proposed algorithm. The MSE result for each iteration is compared to the theoretical bound.

3.7.7 Fast Convergence of Proposed algorithm

This section graphically illustrates the fast convergence of the proposed algorithm. For this simulation, a UCA geometry is considered as a receiving node with $M = 9$ antenna elements with radius $r = r^{\lambda/2}$ (i.e, inter-element spacing $d = \lambda/2$). The simulations are carried out with $U = 100$ different DOAs randomly selected from a uniform random distribution in the range $[-\pi, \pi)$. For each DOA, $I = 1000$ Monte Carlo runs are carried out to provide a statistical validation. The spatial angular domain in the range $[-\pi, \pi)$ is quantized into $N = 180$ angular grid points with a quantization interval of $\omega = 2\pi/180$. The SNR is varied between -10 dB and 25 dB with an interval of 1 dB. The first set of simulations aims to demonstrate the ability of the proposed algorithm to approach the theoretical CRLB using just a few iterations. In Fig. 3.16 the y-axis and the x-axis represent the MSE and SNR in dB respectively. Four different plots

are presented in Fig. 3.16, where the purple plot refers to the coarse estimate that was obtained using (3.12). The coarse estimate indicates the quantized grid point that is closest to the original incoming DOA. The green plot represents the MSE of the estimate obtained using the 1st iteration of the ICSDOA algorithm and the red plot indicates the MSE of the estimate using the 2nd iteration. As the plots for both the iterations are extremely similar, a magnified version of the plots is presented inside Fig. 3.16 to provide a better visualization. For low SNR cases (i.e. SNR < 5 dB), the MSE of all the three plots are relatively much higher than the CRLB. This is can be associated with an inaccurate coarse estimate due to noise causing inaccurate peak values in the CS processing. At low SNR, the CS algorithm fails to obtain an accurate match to the closest grid points and as a result, further iterations of the algorithm do not converge to an accurate estimate. A steep drop in the estimation error for all three plots can be observed for SNR > 6 dB. The Coarse-Estimate plot deviates from the CRLB at high SNR, due to errors induced due to grid quantization. However, the plots for the 1st and 2nd iterations approach the CRLB and performs close to the bound. The difference in MSE performance between the iterative operations are extremely small. This indicates the fast convergence of the proposed algorithm towards the bound using just two iterations.

3.7.8 DOA Estimation Performance Comparison

An MSE performance comparison of the proposed ICSDOA algorithm against the Beam-Forming and Root-MUSIC DOA estimation techniques are presented in the following simulations. Root-MUSIC is a modified version of the traditional MUSIC DOA estimation technique and offers superior MSE performance with a relatively large number of snapshots. The Beam-Forming technique, on the other hand, relies on a scanning procedure to estimate a DOA with maximum signal strength and is dependent on the grid quantization of the angular domain. In order to maintain consistency among all three techniques, the simulation will be carried out using a single time instant (i.e. snapshot $= 1$). Two sets of simulations are considered, where the UCA geometries are

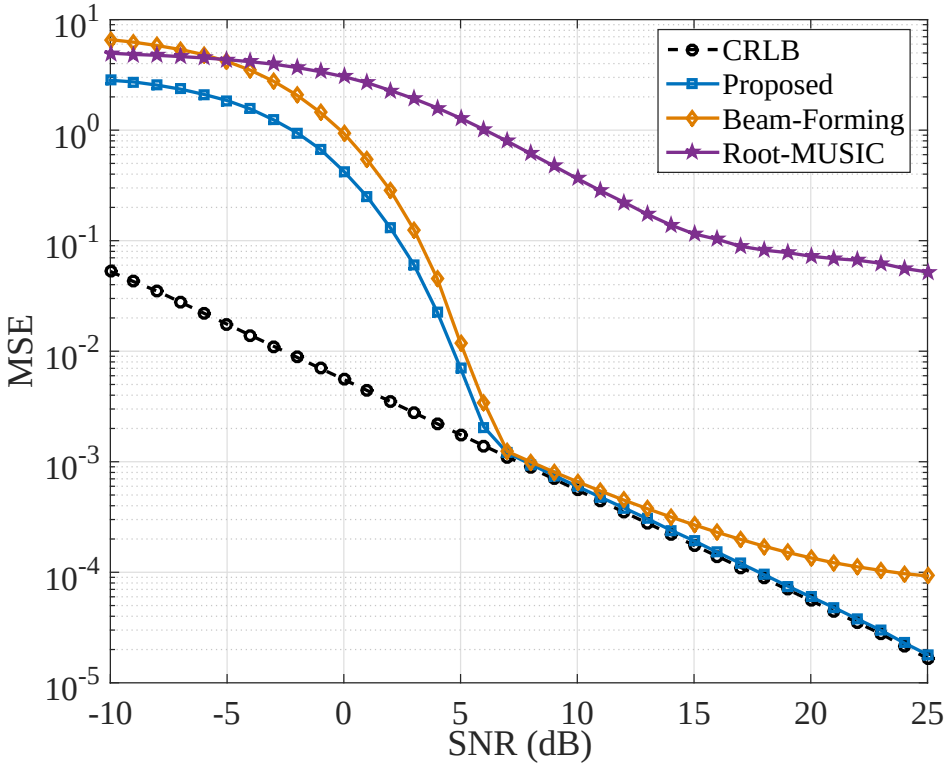

Fig. 3.17: MSE performance comparison of the proposed algorithm against benchmark DOA techniques such as Root-MUSIC and Beam-Forming. The radius of the UCA geometry is $r = r^{\lambda/2}$

constructed around a ring with radius $r^{\lambda/2}$ and r^{OPT} respectively. The remaining simulation parameters such as M, N, U, I and the SNR are similar to the prior simulation in Subsection 3.7.7. The performance of the DOA estimation techniques is compared to the theoretical CRLB, and the results are shown in Figs 3.17 and 3.18.

The plots are shown in Fig. 3.17 illustrate the MSE performance of different DOA estimation techniques when the radius of the UCA geometry is $r = r^{\lambda/2}$. For SNR < 5 dB, the estimation errors for all the techniques are extremely high with ICSDOA performing better than others. However, for SNR > 6 dB, the MSE for both the Beam-Forming and the proposed ICSDOA techniques approach the theoretical bound, while Root-MUSIC is performing the worst among all three. The plot for Beam-Forming remains extremely close to the bound in the SNR range [5 dB, 10 dB), before deviating away from the CRLB for SNR > 15 dB. The Beam-Forming method is dependent

on the grid interval, i.e. $\omega = \pi/180$. Therefore the MSE of Beam-Forming is lower bounded by an error induced due to grid quantization, and the error increases with an increase in the grid interval ω. However, with finer grid quantization Beam-Forming has the capability to perform on the bound. But finer grid quantization forces N to be large, hence significantly increasing the computational complexity. The plot for Beam-Forming can be related back to the plot for a coarse estimate in Fig. 3.16, which is also lower bounded by the error induced due to grid quantization. On the other hand, the performance of the EVD-based technique Root-MUSIC is independent of the grid quantization but relies heavily on the number of snapshots of the incoming signal. The high MSE of Root-MUSIC is associated to the fewer signal snapshots used in this simulation. The simulation result clearly illustrates that iterative operation of ICSDOA completely eliminates the error induced due to grid quantization, whereas the CS processing enables the proposed algorithm to perform with fewer signal snapshot, hence making the algorithm robust and computationally more feasible than Beam-Forming and Root-MUSIC.

Fig. 3.18 shows the comparison in DOA estimation when a modified UCA geometry is introduced. The UCA is constructed with $M = 9$ elements placed at a radius $r = r^{OPT}$. In Subsection 3.7.4, r^{OPT} refers to an optimum radius, that enhances the RIP property of the measurement matrix Φ. It has been shown that at r^{OPT} both the mutual coherence and condition number of Φ is simultaneously reduced. This allows Φ to take advantage of the minimum coherence between the column vectors and an efficient utilization of the vector space. The MSE performance for the modified geometry is slightly different from the results in Fig. 3.17. For the optimum radius case, the MSE of the ICSDOA algorithm approaches the bound at SNR = 15 dB and remains on the bound for higher SNR. In a similar fashion, the plot for Beam-Forming also shows a dip around SNR = 15 dB but fails to match the performance of ICSDOA due to grid quantization error. The CRLB for UCA with $r = r^{OPT}$ is 16 dB lower than with $r = r^{\lambda/2}$ from the previous simulation. This once again verifies the analysis presented in Subsection 3.7.4, and ensures that for higher SNR, the estimation accuracy can be improved by 16 dB, when the UCA is constructed with $r = r^{OPT}$. This also shows the

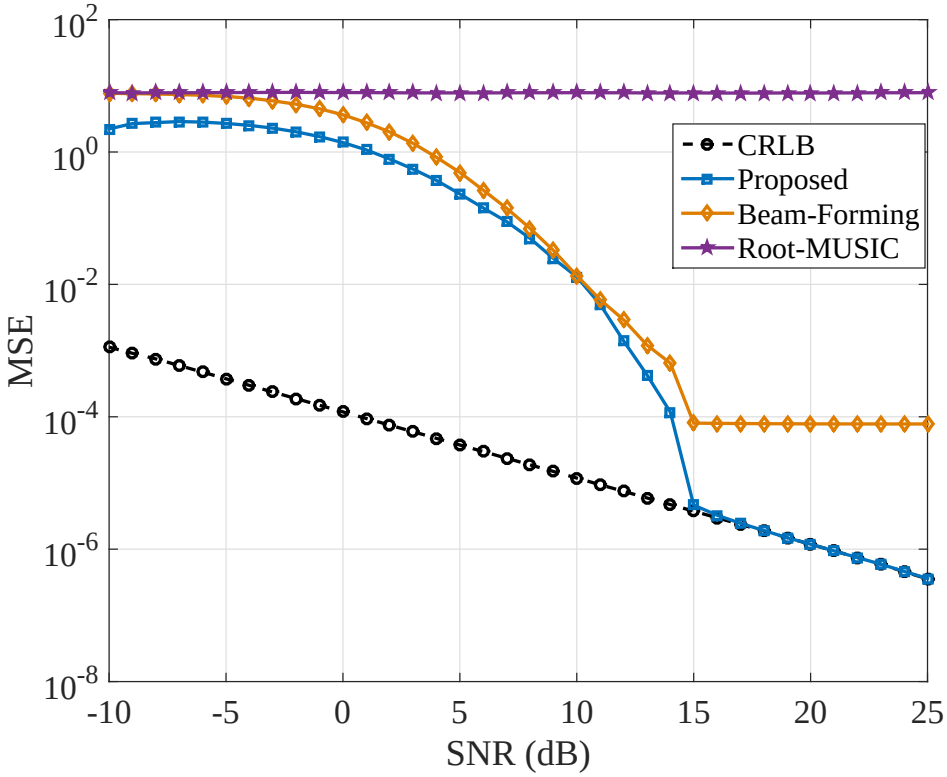

Fig. 3.18: MSE performance comparison of the proposed algorithm against benchmark DOA techniques such as Root-MUSIC and Beam-Forming. The radius of the UCA geometry is $r = r^{OPT}$

power of the ICSDOA in achieving a lower bound by outperforming the Root-MUSIC and Beam-Forming technique.

3.7.9 Computational Complexity

This section discusses the complexity of our proposed algorithm in converging to an estimate. The graph in Fig. 3.16 clearly indicates that the ICSDOA algorithm achieves the CRLB in just 2 iterations. Algorithm-1 indicates that the proposed iterative algorithm uses one CS operations in each iteration to compute the output of an error discriminant. The CoSaMP CS algorithm has been used to retrieve the sparse vector from the under-determined system of equations. According to [67], the computational complexity of the CoSaMP algorithm is given as $O(MN)$. The proposed algorithm

consists of three major stages, coarse estimate, error-discriminant output, and update. The first stage uses only 1 CS operation to retrieve the initial sparse vector and is followed up with the search for the index representing the dominant complex envelope. In total the complexity of the first stage in terms of big O notation can be expressed as $O(MN) + O(N) = O(MN)$. The second stage relies on the rotation of the N angular grid points by a $\frac{1}{2}$ the quantization interval. This process introduces a total of MN multiplications resulting a complexity of $O(MN)$. This step is followed by a CS processing on the rotated grid points which introduces another $O(MN)$ operation. Unlike the first stage, the algorithm does not require a maximum search operation to find the complex envelope. Instead, the algorithm can easily access the vector using the index obtained from the first stage to extract the scalers α and β. The error discriminant calculation in this stage is a simple scalar arithmetic operations with a combined time complexity of O(1). Therefore, in the second stage for each iteration in estimating the error discriminant, the respective complexity can be written as $O(MN)+O(MN)+O(1) = O(2MN)$. The third stage is the update phase, where the output of the error discriminant is used to update the N quantized grid points Θ. The operation is a basic addition with a time complexity of $O(N)$. The total breakdown in terms of time complexity is given in Table 3.2

Processing	Operation	Complexity
Coarse Estimate	$1 \times CS$ + max search	$O(MN)$
Error Discriminant	$2 \times CS$ + $\Delta\Theta$ output	$O(2MN)$
Update	N Additions	$O(N)$

TABLE 3.2: Computational-complexity of proposed algorithm

Eigenvalue decomposition (EVD) based or subspace based DOA estimation methods such as MUSIC, Root-MUSIC and ESPRIT, have a computation complexity of $O(M^2N+M^2)$ and $O(M^3+M^2)$. MUSIC and Root-MUSIC are computationally more complex due to their spectral search and subspace estimation using the EVD of the covariance matrix. From Table. 3.2, it can be concluded that the total time complexity

of the algorithm is $O(MN + 2cMN + N)$, where c is the number of iterative operation required to converge to the estimate. The complexity of our algorithm is highly dependent on the number of error discriminant estimates. According to the convergence test, the error discriminant approaches the stopping criterion with just two iterations. In comparison to the EVD based methods, our proposed technique offers lower complexity ($O(5MN)$) than MUSIC and Root-MUSIC, however, it has higher complexity than ESPRIT.

3.8 Conclusion

This paper proposes a novel approach in estimating the DOA of a transmitting source. A new signal processing paradigm has been proposed in this work that completely eliminates quantization error in grid based estimation techniques and allows the error to be on the theoretical CRLB. A two-stage based estimation process has been introduced in the paper, where a coarse estimate is initially calculated to obtain the nearest quantized grid points. Later an iterative loop is initiated that exploits the two dominant complex envelopes of the recovered sparse vector to generate an error discriminant. Simulation results have been presented to validate that two coefficient case is the most effective in minimizing the estimation error The iterative loop halts when the error discriminant is lower than some user-defined threshold. Since convergence is achieved in two iterations the algorithm may be halted after the second iteration. To verify the robustness of the proposed ICSDOA algorithm, extensive statistical analysis has been carried out with noise inherent to the UCA processing. The end results validated the claim that the ICSDOA approaches the CRLB using just 2 iterative operations. Comparison results indicate that ICSDOA algorithm significantly out-performs other well-known techniques such as Root-MUSIC, ESPRIT, and Beam-Forming in scenarios where single snapshot cases are considered.The computation complexity of the algorithm is calculated to be $O(5MN)$ which is lower than EVD based DOA estimation algorithm such as MUSIC and Root-MUSIC and slightly higher than ESPRIT. However, ESPRIT requires large number of signal snapshots that inherently pushes the

computational complexity higher than ICSDOA. Moreover, the paper also analyses the impact of array geometry parameters such as the number of antenna elements and radius of the UCA on the construction of the dictionary matrix. Result illustrates that with an odd number of antenna elements and an optimum array radius, the mutual coherence between the columns of the dictionary matrix can be significantly reduced. The optimum array radius is deduced by obtaining a radius such that the condition number, as well as the mutual coherence of the dictionary matrix, is simultaneously minimized. The simulation result shows that using the optimal radius, the MSE can be reduced by 16 dB than that of traditional $\lambda/2$ element spacing. However, in case of larger radius, the array size also increases so there is a systematic trade-off between the size of UCA and precision of DOA estimation. A detailed analysis on the influence of the number of antenna elements and the grid quantization on the MSE performance of the algorithm is also presented in this paper. It can be concluded that UCA with a large number of antenna elements require finer quantization of the angular grids to achieve the theoretical bound. Although larger number of antenna elements yield better estimation accuracy of DOA, it also increases the processing time of the algorithm. There is a systematic trade-off of performance as a function of computational complexity. The algorithm can be easily extendable to multiple scenario cases while considering that the number of sources detected is directly proportional to the number of antenna elements. In case of multiple scenarios, an angular separation of two grid quantization level is required between the sources for effective estimation of incoming DOAs.

As part of future work, it is also of great interest to extend the algorithm using multiple receiving UCA antennas to deduce the location of the transmitting source in a network using triangulation. We are also currently working on prototyping the algorithm into a working product to validate the performance of the algorithm in a realistic environment. Incorporating large number sources and analyzing the performance in various multi-path environments is another important topic for future work.

4

A Novel Signal Processing Technique to Estimate the Off-Grid Direction of Arrival using a Uniform Linear Array

4.1 Abstract

This paper proposes a new Direction of Arrival (DOA) estimation technique using a Uniform Linear Array (ULA) antenna as the receiving node. In upcoming 5G cellular communication systems, a precise DOA estimation is integral for the purpose of spatial multiplexing. In a wireless network, spatial multiplexing refers to a technique of assigning independent communication channels to individual users, thereby efficiently reusing the spectrum resources. Spatial multiplexing can provide a viable solution to

the problem of spectrum scarcity. Traditional DOA estimation techniques require eigenvalue decomposition of the covariance matrix at different time instants (i.e. snapshots), which causes an unavoidable increase in the computational complexity of the algorithm. The proposed technique is based on the emerging theory of Compressive Sensing (CS), whereby an estimate can be achieved with a single measurement collected using a single snapshot. In CS-based DOA estimation techniques, the potential angular domain of coverage is uniformly sampled into a finite number of angular grid points and the incoming DOA is assumed to be exactly on the grid points. However, in reality, the probability of having a source DOA on a grid point is extremely low. This introduces a mismatch between the output of the ULA antenna elements and the dictionary matrix constructed with a finite number of grid points. The mismatch causes ambiguity in the estimation process, hence degrading the performance of the algorithm. This paper proposes a novel iterative signal processing technique, that completely eliminates the error induced due to grid quantization. This enables the estimation error to be on the theoretical Cramér-Rao lower bound (CRLB) of DOA estimation. Simulation results show that the proposed technique outperforms renowned DOA estimation techniques such as ESPRIT, Root-MUSIC and Beam-Forming in reducing the error to a minimum. The paper also establishes a relationship between the number of antenna elements and the number of angular grid points in order to enhance the performance of the proposed algorithm.

4.2 Introduction

The evolution of the Internet of Things is expected to interconnect more than 50 billion smart devices by 2020 [155]. The exponential growth of wearable devices along with smart vehicles will push the capacity of wireless communication to the limit. According to CiSCO's visual-networking index, global wearable devices will hit the 600 million mark by 2020 from just 97 million in 2015. In order to accommodate the large capacity demand of the wireless devices, an overhaul is required of the existing communication systems. In a conventional wireless system, a base station

serves users by allocating channels by means of a variety of multiple access schemes such as Frequency-Division Multiple Access (FDMA), Time-Division Multiple Access (TDMA), Code-Division Multiple Access (CDMA) and Orthogonal Frequency-Division Multiple Access (OFDMA). However as the spectral resource (frequency bandwidth) is limited, mainly due to spectrum scarcity and government regulations, alternatives are proposed to efficiently utilize the allocated spectrum. Spatial sectorization is an emerging field of research whereby the spatial domain is separated into different angular intervals representing an individual cells [156–161]. This allows base-station incorporated with Multiple Input Multiple Output (MIMO) antennas to shine directional beams to the cells (provided the cells do not overlap). The technique allows multiple sets of cellular users to be spatially multiplexed simultaneously using the same channel. The Spectral efficiency and capacity of the network can be significantly enhanced by this method, offering a suitable solution to the problem of spectrum scarcity. In order to successfully adopt the technique, accurate estimation of the Direction of Arrival (DOA) information of incoming signals from the cell is of paramount importance.

Traditional subspace-based methods such as Multiple Signal Classification (MUSIC) [97] and Estimation of Signal Parameters via Rotational Invariance Techniques (ESPRIT) [98] require the array sensor to have a linear geometry. Additionally, aforementioned techniques require the computationally expensive eigenvalue decomposition (EVD) of the data covariance matrix for DOA estimation. The performance of the estimator is dependent on a large snapshot realization of the maximum likelihood (ML) in the case of uncorrelated sources. However, with a limited number of signal snapshots, the performance degrades significantly, mainly due to the rank deficiency of the covariance data matrix. Compressive Sensing (CS) has gained popularity in signal processing due to its effectiveness in recovering a sparse signal with minimum measurements [64, 93, 162]. The computationally inexpensive technique motivated researchers to explore DOA estimation as a sparse recovery problem. CS-based DOA estimation methods do not require the EVD of the covariance matrix and can offer superior results using a single snapshot of the incoming signal. This enables CS to be computationally more attractive for a variety of applications.

In CS-based problem formulation, the angular region of coverage is sampled into a grid of N possible DOAs. The number of grid points, N, in the quantization is greater than the number of antenna elements, M. Therefore, the problem of determining the angle of arrival is represented as an underdetermined set of equations which maps the signal originating at each grid point to the set of complex envelope voltage outputs of the antenna elements. Several CS-based techniques are proposed in the literature [106, 118, 146, 147, 163], where the sources are placed strictly on a subset of the quantized grid points. However, in a realistic scenario, the simplistic assumption of having a source DOA on the quantized grid may not be true, as the source DOA can be anywhere in the region of $[-\pi/2, \pi/2)$. In [112] the author outlines an algorithm to detect an off-grid DOA using co-prime arrays, but a performance analysis against the theoretical bound was not included. The work in [108] offers some insight. However, noise sensitivity analysis suggests that the algorithm deviates from the bound at large a Signal-to-Noise Ratio (SNR). The work in [119, 120] introduces a Bayesian framework in the DOA estimation problem offering some sophisticated alternatives, however, the techniques can be computationally challenging for practical implementation.

In this paper, an innovative and fundamentally new approach has been proposed which provides a signal processing solution that eliminates the grid-induced quantization error in CS-based DOA estimation techniques. This allows the algorithm to achieve the Cramér-Rao lower bound (CRLB) on estimation error, and no algorithm can perform better than the bound. The new algorithm involves the determination of the DOA of a radio signal using the signal complex voltages obtained at the outputs of antenna elements configured in a Uniform Linear Array (ULA). As the number of quantized angular grid points is much greater than the number of antenna elements ($N \gg M$), the problem of determining the angle of arrival is represented as an underdetermined set of equations which can be solved using CS to recover a sparse vector. The index corresponding to the absolute maximum amplitude of the sparse vector is chosen to be the coarse estimate. Prior work in [102, 113, 114, 164] adopts a similar approach in obtaining a coarse estimate. However, they rely on adaptive grid refinement around the target area to determine the off-grid DOA. The process reduces the computational

complexity, but a denser grid introduces ambiguity in the detection process by affecting the Restricted Isometry Property (RIP) property of the dictionary matrix[65].

The fundamental contribution of this paper is an iterative processing loop, where the N quantized angular grid points are rotated in both clockwise and anticlockwise directions by half the grid quantization interval. The unique processing results in an error discriminant which is then used to update the coarse estimate at each iteration. The iterative process stops when the error discriminant is close to zero or less than some user-defined threshold. The architecture of the iterative process is described in details in Section 4.5. Simulation result indicates that the algorithm is strongly convergent and achieves the CRLB using just two iterative operations. In addition to the algorithm, the paper also establishes a relationship between the number of antenna elements (M) and the number of quantized angular grid points (N) in order to enhance the performance of CS-based DOA estimation techniques. The analysis suggests that, for a large number of antenna elements, a finer grid quantization is required in order for a ULA geometry to achieve its respective CRLB. A comparative performance is presented to illustrate that the proposed algorithm outperforms traditional Root-Music, ESPRIT and Beam-Forming DOA estimation algorithms using a single snapshot of the incoming signal.

The outline of the paper is as follows. The system model is presented in Sections 4.3-4.4. Section 4.5 discusses the structure of the algorithm in details. A brief background on the structure of the dictionary matrix in CS is provided in Section 4.6. Analysis and simulations are presented in Section 4.7. And finally the conclusion and future work are presented in Section 4.8.

4.3 Problem Formulation

This work assumes a set of M isotropic antenna elements placed in a straight line with an inter-element spacing of $d = \lambda/2$, where λ is the signal wavelength. A traveling plane wavefront impinges on the antenna elements from some unknown direction θ. The incoming wave satisfies the narrowband assumption that the phase difference between the upper and lower band edges of the propagation across the entire array is small. At

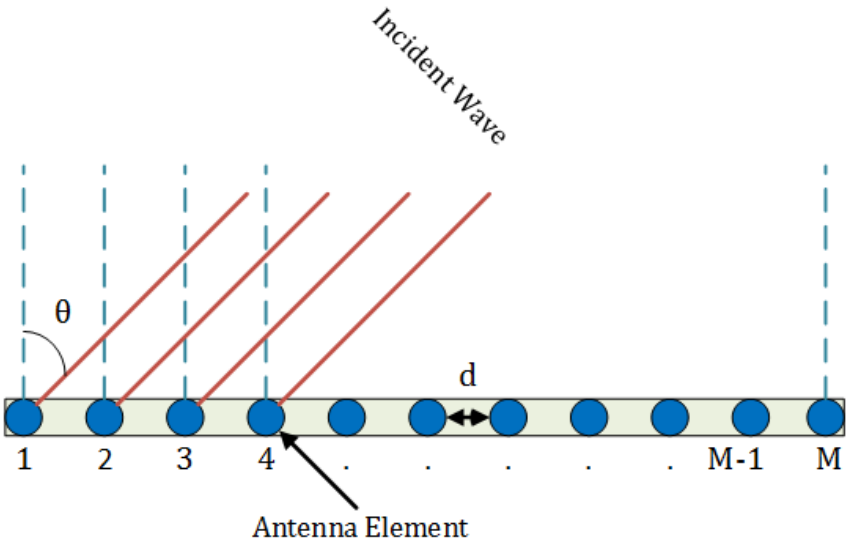

Fig. 4.1: A typical ULA with M elements, where θ is the azimuth angle of arrival of the received signal

the t^{th} instance the output at the antenna elements is given as

$$\mathbf{X}(t) = \mathbf{a}(\theta)p(t) + \mathbf{n}(t) \tag{4.1}$$

where $\mathbf{X}$(t) is an $M \times 1$ array output vector corrupted with noise. The $M \times 1$ noise vector is represented as $\mathbf{n}$(t) where the entries are statistically independent and Gaussian distributed with zero mean and variance σ^2, and $p(t)$ is the complex envelope of the source at the receiving array. In (4.1), $\mathbf{a}(\theta)$ is an $M \times 1$ array response vector (ARV) for an incoming plane wave from the direction θ and is generally given as

$$\mathbf{a}(\theta) = \begin{bmatrix} 1 & e^{-jk\sin(\theta)d} & \dots & e^{-jk\sin(\theta)(M-1)d} \end{bmatrix}^T. \tag{4.2}$$

The ARV in (4.2) represents the relative phases of the received signals at the antenna elements where $k = 2\pi/\lambda$ is the wavenumber or phase propagation factor. The aim of the work is to find the incident azimuth angle θ using the relative phase difference between the antenna elements. Figure 4.1 shows the system model. The phase angle at each element is obtained relative to the phase of a local oscillator signal.

4.4 DOA estimation using Compressive Sensing

This section describes the formulation of a sparse problem that can be solved using compressive sensing techniques to recover the unknown azimuth angle θ of the source. In ULA geometry the spatial coverage is restricted to $[-\pi/2, \pi/2)$. To cast the DOA estimation problem using a ULA as a compressive sensing problem, the estimation of θ must be integrated into a problem of sparse recovery in an over-complete dictionary. Due to the assumption of the model having a single source, the phase contribution on the antenna elements is a sparse representation in a selectively chosen dictionary or basis. To create the dictionary or measurement matrix, the angular domain of $[-\pi/2, \pi/2)$ is quantized into spatial angular grid points with N possible DOAs, $\Theta = \{\hat{\theta}_n, 1 \leq n \leq N\}$. The angular grid separation is represented as ω. The ARV in (4.2) for an incoming plane wave from each of these N unique spatial grids can be combined to create a dictionary matrix described as

$$\mathbf{\Phi}(\Theta) = \left[\mathbf{a}(\hat{\theta}_1) \quad \mathbf{a}(\hat{\theta}_2) \quad \cdots \quad \mathbf{a}(\hat{\theta}_N)\right], \tag{4.3}$$

where $\mathbf{a}(\hat{\theta}_n)$ is the ARV associated with the DOA $\hat{\theta}_n$. Using the definition of the dictionary matrix in (4.3), the array output in (4.1) can be rewritten as:

$$\begin{bmatrix} x_1 \\ x_2 \\ \vdots \\ x_M \end{bmatrix} = \left[\mathbf{a}(\hat{\theta}_1) \quad \mathbf{a}(\hat{\theta}_2) \quad \cdots \quad \mathbf{a}(\hat{\theta}_N)\right] \begin{bmatrix} s_1 \\ s_2 \\ s_3 \\ \vdots \\ s_N \end{bmatrix} + \begin{bmatrix} n_1 \\ n_2 \\ \vdots \\ n_M \end{bmatrix}$$

$$\mathbf{X}(t) = \mathbf{\Phi}(\Theta)\mathbf{S}(t) + \mathbf{n}(t) \tag{4.4}$$

where $\mathbf{S}$(t) is an $N \times 1$ vector of coefficients representing the complex envelope of the arriving signal from each of the N quantized direction of arrival. As the problem formulation has a single source among the N possible DOAs, $\mathbf{S}(t)$ is assumed to be sparse in the angular domain $[-\pi/2, \pi/2)$. In a typical scenario, when the source

transmits strictly from one of the N discrete grid points defined in (4.3), the DOA estimation problem in (4.4) can be cast into the framework of CS. The structure of CS deals with the recovery of a sparse signal from measurements contaminated by noise, which makes the CS framework suitable for DOA estimation. From this point onwards, the explicit dependency on time is ignored. Compressive-sensing based sparse recovery requires the columns of the measurement matrix Φ to be orthonormal. This condition allows accurate projection of the spatial spectrum on the space of bearing angles Θ. To orthonormalize the columns of the matrix Φ a data-processing technique has been adopted as shown in [129]. Let $\mathbf{Q}$ be the processing operator

$$\mathbf{Q} = \mathbf{R}\mathbf{\Phi}^{+} \tag{4.5}$$

where $\mathbf{R} = (\mathbf{H}^{*}\mathbf{\Phi})$ and $\mathbf{H}^{*}$ returns the conjugate transpose of $\mathbf{H}$ where, $\mathbf{H}$ is the $M \times M$ transform matrix. In (4.5) $\mathbf{\Phi}^{+}$ is the Moore-Penrose pseudoinverse of $\mathbf{\Phi}$. Applying the operator $\mathbf{Q}$ on both sides of (4.4) yields

$$\mathbf{R}\mathbf{\Phi}^{+}\mathbf{X} = \mathbf{R}\mathbf{\Phi}^{+}\mathbf{\Phi}\mathbf{S} + \mathbf{R}\mathbf{\Phi}^{+}\mathbf{n}$$

$$\mathbf{V} = \mathbf{Z}(\Theta)\mathbf{S} + \mathbf{E}. \tag{4.6}$$

$\mathbf{V} = \mathbf{R}\mathbf{\Phi}^{+}(\mathbf{X})$ is the noisy processed observation vector and $\mathbf{Z} = \mathbf{R}\mathbf{\Phi}^{+}\mathbf{\Phi}$ is the normalized measurement matrix, while $\mathbf{E} = \mathbf{R}\mathbf{\Phi}^{+}\mathbf{n}$ is the processed measurement noise. The modified problem formulation in (4.6) can also be formulated into a CS problem similar to (4.4). Recovery of $\mathbf{S}$ can be performed by solving the following convex optimization problem:

$$\hat{\mathbf{S}} = \min_{\mathbf{S} \in \mathbb{C}^{N}} \|\mathbf{S}\|_0 \quad s.t. \quad \|\mathbf{V} - \mathbf{Z}(\Theta)\mathbf{S}\|_2 < \epsilon \tag{4.7}$$

where $\|\cdot\|_0$ and $\|\cdot\|_2$ are the l_0-norm and l_2-norm respectively. The regularization parameter is ϵ that is determined by the noise or quantization level. Careful selection of ϵ is crucial in the sparse recovery of the signal. The output of the problem defined

in (4.7) is a reconstructed sparse vector $\hat{\mathbf{S}}$ that approximates the actual spatial vector $\mathbf{S}$. Due to the sparse condition when the direction of arrival is a quantization point, the recovered vector $\hat{\mathbf{S}}$ will contain a single non-zero element. The n^{th} index of the non-zero element refers to the angular grid ($\hat{\theta_n}$) on which the source is located.

4.5 Iterative approach of DOA Estimation

In CS-based DOA estimation techniques, the spatial angular domain is quantized into angular grid points. The quantization process introduces a grid bias or quantization error. In a practical scenario, the true DOA may be never exactly aligned with the discrete azimuth bearing space used to construct the dictionary matrix. The grid bias forces a mismatch between the processed antenna array output $\mathbf{V}$ and the processed dictionary matrix $\mathbf{Z}$. In a typical scenario, the source DOA θ may be between two discrete grid points, i.e. $\theta = \hat{\theta}_n + \Delta\theta$, where $(-\frac{\omega}{2}) \leq \Delta\theta < (\frac{\omega}{2})$, and $\hat{\theta}_n$ is the n^{th} angular grid point. In such cases, the conventional CS processing described in Section 4.4 fails to detect the exact DOA. Instead, the mismatch influences the recovered sparse vector, $\hat{\mathbf{S}}$ in (4.7) to have several non-zero elements which in the ideal case should be just one (as we have just one source). The non-zero elements appear on the discrete grid points closest to the original DOA. During the CS processing of the sparse vector recovery, the optimization algorithm verifies the largest correlation between the observation vector and the columns of the dictionary matrix. The angular grid corresponding to the columns of the dictionary matrix with the highest correlation yields the DOA of an incoming signal. However, in an off-grid scenario, the incoming DOA is between two quantized grid points. To resolve the issue, CS compares the correlation of the observation with the columns of the measurement matrix and generates several peaks at the neighboring angular grid points. The absolute amplitudes of the peaks represent the correlation coefficient of the observation to the relative grid points. One such instance is clearly illustrated in Fig. 4.2. The blue line represents the original DOA and the peak is the magnitude complex envelope of the incoming signal. A CS processing on the observation produces two red peaks at the adjacent grid points. Note

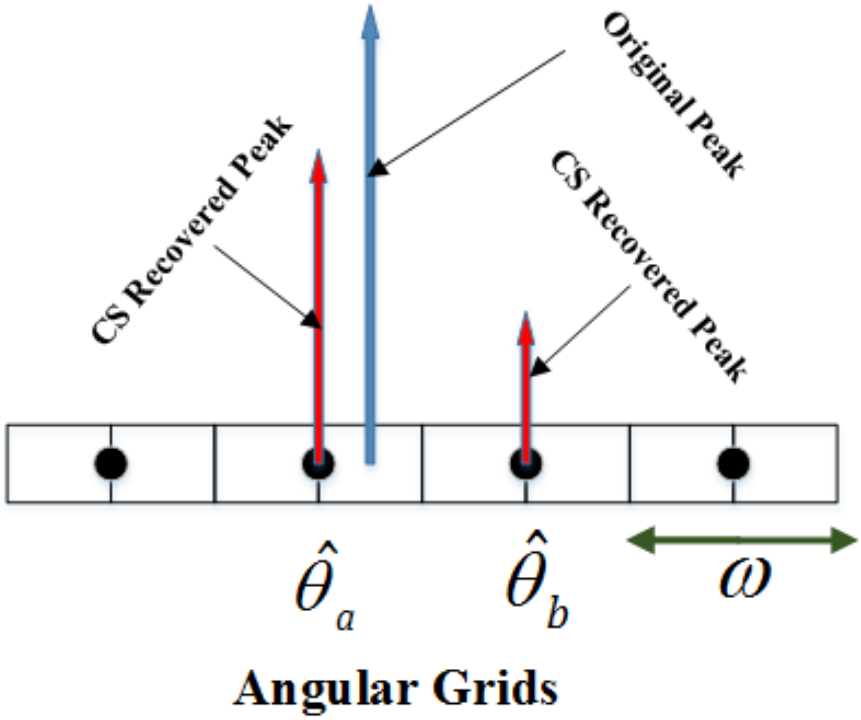

Fig. 4.2: Blue peak indicates original off-grid DOA, whereas red peaks are amplitudes on the neighboring grid points closest to the original source DOA.

that the reconstructed peaks are smaller than the original blue peak. This suggests that CS distributes the weight of the original peak depending on the relative angular separation of the incoming signal from the respective neighboring grid points. This means the further away the DOA is from a grid point, the lower is the amplitude on the grid.

The proposed Iterative Compressive-Sensing based Direction of Arrival (ICSDOA) algorithm exploits the magnitude of the complex envelope on the neighboring grid points to estimate the DOA. The estimation process mainly comprises of three stages, where at the first stage a CS processing is used to obtain a coarse estimate of the original DOA, by solving the optimization problem defined in (4.7). As mentioned earlier, the recovered solution vector will have several non-zero elements, where the n^{th} index corresponding to the non-zero magnitude of the complex envelopes indicate the angular grid point. Among them, the angular grid point with the largest magnitude is chosen to

be the coarse estimate. This also suggests that the coarse estimate corresponds to the columns of the dictionary matrix $\mathbf{Z}$ that has the largest correlation with the observation vector $\mathbf{V}$. The first stage of the estimation process may be obtained according to the following;

$$n_{max} = \arg\max_{n}\{|\hat{\mathbf{S}}[n]|\} \tag{4.8}$$

such that

$$\hat{\mathbf{S}} = \min_{\mathbf{S}\in\mathbb{C}^N} \|\mathbf{S}\|_0 \quad s.t. \ \|\mathbf{V} - \mathbf{Z}(\Theta)\mathbf{S}\|_2 < \epsilon$$

and

$$\breve{\theta}_0 = \Theta(n_{max}).$$

where $\hat{\mathbf{S}}[n]$ is the n^{th} element of the recovered sparse vector $\hat{\mathbf{S}}$, obtained after a CS processing on (4.7). The coarse estimate, $\breve{\theta}_0$, corresponds to the index representing the largest non-zero element of $\hat{\mathbf{S}}$. In [127] and [145], a similar approach has been adopted to obtain a rough estimate of the off-grid DOA.

In the second stage, the algorithm feeds the coarse estimate into a low-computation signal-processing technique to obtain an error discriminant. Assuming that the Signal-to-Noise Ratio (SNR) is moderate and that ϵ in (4.7) is carefully selected, there is a high probability that the coarse estimate obtained from (4.8) is the discrete grid point closest to the original DOA, θ, i.e, $\theta \in [\breve{\theta}_0 - \frac{\omega}{2}, \breve{\theta}_0 + \frac{\omega}{2})$, where $\omega = \frac{\pi}{N}$ is the angular grid separation. This suggests that the original DOA may be on either side of the coarse estimate $\breve{\theta}_0$ with a separation of $|\frac{\omega}{2}|$. Next, an angular rotation of $\frac{\omega}{2}$ a is introduced on the N angular grid points Θ. The angular rotation of the grid points yields a new dictionary, $\mathbf{Z}(\Theta + \frac{\omega}{2}\overline{u})_{2\pi}$ where $\overline{u}$ is the $N \times 1$ vector with all elements equal to 1 and, for a vector W, $(W)_{2\pi}$ is defined as

$$(W)_{2\pi} = \text{modulo}(W + \pi\overline{u}, 2\pi\overline{u}) - \pi\overline{u} \tag{4.9}$$

where, (4.9) describes the 2π modulo operation on each of the elements in W. The process bounds the elements in vector W in the range $[-\pi, \pi)$. A CS operations is

Algorithm 2: ICSDOA

Input: $\mathbf{V_n}$, $Z(\Theta_0)$, $\breve{\theta}_0$, n_{max}, Ω

Output: Estimate of Original DOA θ_{est}

1 Initialize $c = 1$

2 Define new measurement matrix $Z(\Theta_{t-1} + \frac{\omega}{2}\overline{u})_{2\pi}$

3 Compute CS to recover vector $\hat{\mathbf{S}}_c$

4 Calculate $\alpha_c = |\hat{\mathbf{S}}_c[n_{max}]|$ and $\beta_c = |\hat{\mathbf{S}}_c[n_{max} - 1]|$

5 Define $\Delta\Theta_c = (\frac{\alpha_c - \beta_t}{\alpha_c + \beta_c})\frac{\omega}{2}$

6 Check

(I) If $(|\Delta\Theta_c| > \Omega)$.

Update $\Theta_c = (\Theta_{c-1} + \Delta\Theta_c\overline{u})_{2\pi}$,

Update $\breve{\theta}_c = \Theta_c(n_{max})$

Update $c = c + 1$

Repeat Steps 2 to 6

(II) Else

$\theta_{est} = \breve{\theta}_c$

carried out similarly to (4.7), on the rotated dictionary matrix and the output is a new sparse vector $\hat{\mathbf{S}}_c$ where c represents the number of iterative operations. The magnitudes of the complex envelopes corresponding to the n_{max} and $n_{max} - 1$ index of the vector $\hat{\mathbf{S}}_c$ are respectively stored as α_c and β_c. If $\alpha > \beta$ the algorithm indicates that the original DOA is greater than the coarse estimate $(\theta > \breve{\theta}_0)$ whereas if $\alpha < \beta$ the original DOA is smaller than the coarse estimate $(\theta < \breve{\theta}_0)$. The magnitude of the complex envelopes α and β are used to obtain an error discriminant $\Delta\Theta_c$. The second stage of the estimation process can be described as follows, For $c = 1, 2, ...,$ and $\Delta\Theta_0 = 0$ and $\Theta_0 = \Theta$

define

$$\alpha_c = |\hat{\mathbf{S}}_c[n_{max}]| \tag{4.10}$$

$$\beta_c = |\hat{\mathbf{S}}_c[k_{max}]| \tag{4.11}$$

where

$$k_{max} = \begin{cases} n_{max} - 1, & \text{for } 2 \leq n_{max} \leq N \\ N, & \text{for } n_{max} = 1 \end{cases}$$

and

$$\hat{\mathbf{S}}_c = \min_{\mathbf{S}_c \in \mathbb{C}^N} \|\mathbf{S}_c\|_0 \quad s.t \quad \|\mathbf{V} - \mathbf{Z}(\Theta_{c-1} + \frac{\omega}{2}\overline{u})_{2\pi}\mathbf{S}_c\|_2 < \epsilon$$

$$\Delta\Theta_c = \left(\frac{\alpha_c - \beta_c}{\alpha_c + \beta_c}\right)\frac{\omega}{2} \tag{4.12}$$

$$\Theta_c = (\Theta_{c-1} + \Delta\Theta_c\overline{u})_{2\pi} \tag{4.13}$$

A user-defined threshold is used as a stopping criterion such that $|\Delta\Theta_c| < \omega$. At the end of each iteration, the output of the error discriminant is validated against ω, and if the stopping criterion is not satisfied the processes (4.10) to (4.13) are repeated. At each iteration, the N angular grid points represented by Θ_c are updated by adding the error discriminant $\Delta\Theta_c$. This has the effect of an angular rotation of the entire grid. Once the criterion is met, the iterative process stops and the DOA estimate is obtained as

$$\theta_{est} = \Theta_c(n_{max}), \tag{4.14}$$

where n_{max} is found in (4.8). A pseudo-code detailing the steps of the iterative algorithm is presented as 2.

4.5.1 Convergence of ICSDOA

Suppose that $p(\theta)$ is an angular discriminant function such that

$$\breve{\theta}_0 = p(\theta)$$

where θ is the actual angle of arrival in the noiseless case and $\breve{\theta}_0$ is the coarse estimate. Therefore

$$e_0 = \theta - p(\theta)$$

$$\breve{\theta}_1 = \breve{\theta}_0 + p(e_0) = \breve{\theta}_0 + p[\theta - p(\theta)]$$

$$e_1 = \theta - \breve{\theta}_1 = \theta - \breve{\theta}_0 - p[\theta - p(\theta)] = e_0 - p(e_0)$$

$$\breve{\theta}_2 = \breve{\theta}_1 + p(e_1) = \breve{\theta}_1 + p[\theta - \breve{\theta}_1]$$

$$e_2 = \theta - \breve{\theta}_2 = \theta - \breve{\theta}_1 - p[\theta - \breve{\theta}_1] = e_1 - p(e_1)$$

$$\breve{\theta}_{k-1} = \breve{\theta}_{k-2} + p(e_{k-2}) = \breve{\theta}_{k-2} + p[\theta - \breve{\theta}_{k-2}]$$

$$e_{k-1} = \theta - \breve{\theta}_{k-1} = \theta - \breve{\theta}_{k-2} - p[\theta - \breve{\theta}_{k-2}] = e_{k-2} - p(e_{k-2})$$

In general, for $k = 1, 2, ...$

$$\breve{\theta}_k = \breve{\theta}_{k-1} + p[\theta - \breve{\theta}_{k-1}]$$

$$e_k = \theta - \breve{\theta}_k = \theta - \breve{\theta}_{k-1} - p[\theta - \breve{\theta}_{k-1}]$$

It follows by induction that,

$$e_k = e_{k-1} - p(e_{k-1})$$

Theorem 4.5.1 *Let $p(e)$ be a continuous function, with $p(e) = 0$ for $e = 0$. For $e > 0$, $0 < p(e) < e$ and for $e < 0$, $e < p(e) < 0$. Let e_k, (for $k = 1, 2, 3...$) be a real sequence such that $e_k = e_{k-1} - p(e_{k-1})$, then*

$$\lim_{k \to \infty} e_k = 0$$

and the convergence is monotonic.

Proof :

Case : 1

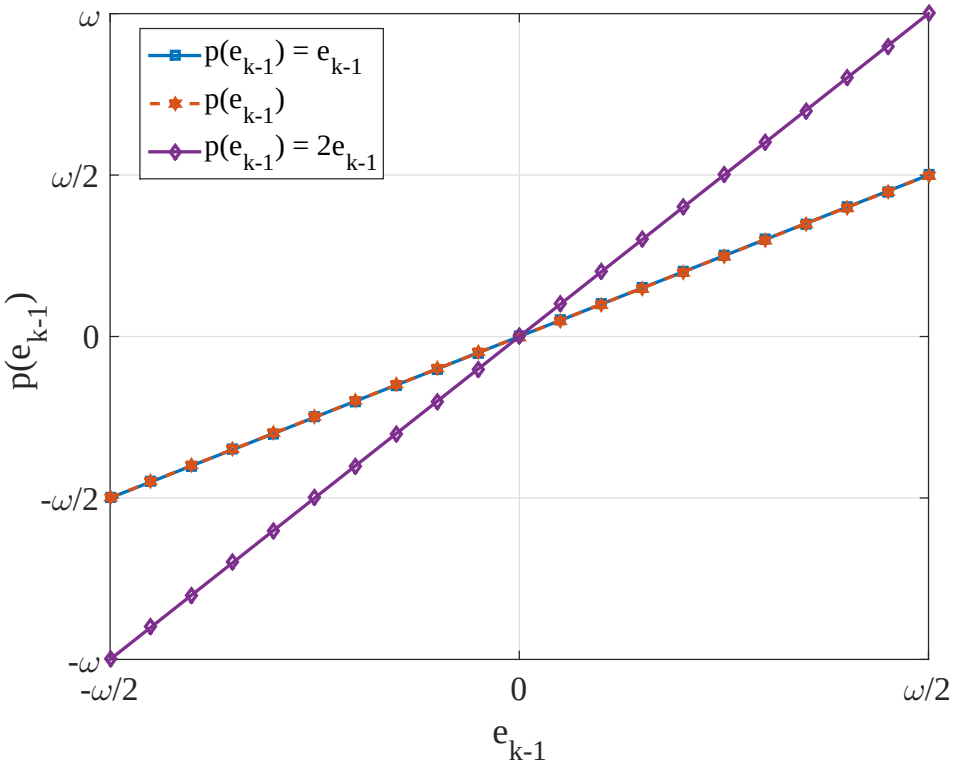

Fig. 4.3: The error discriminant as a function of the difference between the incoming DOA θ and the updated estimate at each iteration $\breve{\theta}_{k-1}$. The figure illustrates the result for no noise case.

$$e_0 > 0$$

$$e_1 = e_0 - p(e_0)$$

Therefore,

$$0 < e_1 < e_0$$

In general,

$$e_k = e_{k-1} - p(e_{k-1})$$

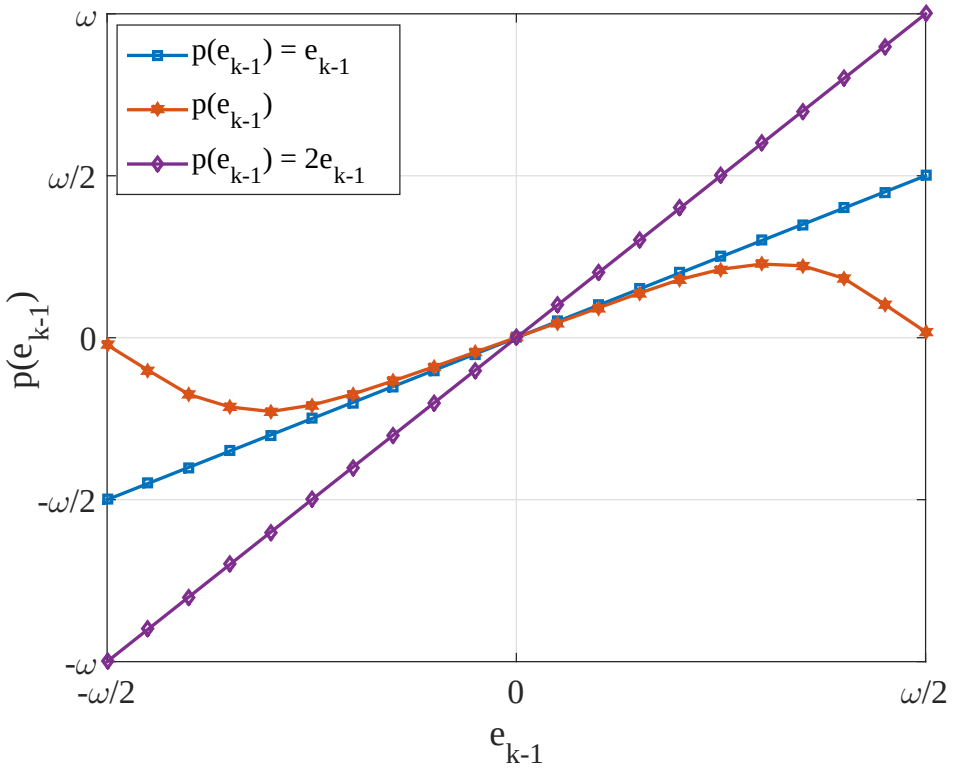

Fig. 4.4: The error discriminant as a function of the difference between the incoming DOA θ and the updated estimate at each iteration $\breve{\theta}_{k-1}$.The figure illustrates the result for SNR = 15 dB .

Therefore,

$$0 < e_k < e_{k-1}$$

and

$$\lim_{k\to\infty} e_k = 0.$$

Case : 2

$$e_0 < 0$$

$$e_1 = e_0 - p(e_0)$$

Therefore,

$$e_0 < e_1 < 0$$

In general,

$$e_k = e_{k-1} - p(e_{k-1})$$

Therefore,

$$e_{k-1} < e_k < 0$$

and

$$\lim_{k\to\infty} e_k = 0.$$

Theorem 4.5.2 *Let $p(e)$ be a continuous function, with $p(0) = 0$. For $e > 0$, $e \leq p(e) < 2e$ and for $e < 0$, $2e < p(e) \leq e$. Let e_k, (for $k = 1, 2, 3...$) be a real sequence such that $e_k = e_{k-1} - p(e_{k-1})$, then*

$$\lim_{k\to\infty} e_k = 0.$$

Proof :

Case : 1

$$e_0 > 0$$

$$e_1 = e_0 - p(e_0)$$

Therefore,

$$-e_0 < e_1 \leq 0$$

$$e_2 = e_1 - p(e_1)$$

$$0 \leq e_2 < -e_1$$

In general, if k is even,

$$-e_k < e_{k+1} < 0$$

if k is odd,

$$0 \leq e_{k+1} < -e_k$$

Therefore

$$\lim_{k\to\infty} |e_k| = 0.$$

and

$$\lim_{k\to\infty} e_k = 0.$$

Case : 2

$$e_0 < 0$$

$$e_1 = e_0 - p(e_0)$$

Therefore,

$$0 \leq e_1 < -e_0$$

$$e_2 = e_1 - p(e_1)$$

$$-e_1 < e_2 \leq 0$$

In general, if k is even,

$$0 \leq e_{k+1} < -e_k$$

if k is odd,

$$-e_k < e_{k+1} \leq 0$$

Therefore

$$\lim_{k \to \infty} |e_k| = 0.$$

and

$$\lim_{k \to \infty} e_k = 0.$$

4.6 Background

Compressive sensing is a mathematical framework that deals with the recovery of a sparse vector $x_{N \times 1}$ from an observation vector $y_{M \times 1}$ with $M \ll N$. The measurement

paradigm consists of the linear projection of the signal vector via a known projection matrix $\Psi_{M\times N}$. As $M \ll N$, the recovery of the sparse vector x from the measurement vector y becomes an under-determined problem with an infinite number of solutions. In the CS framework, an accurate estimation of a sparse signal x can be obtained in the following reconstruction problem, described in [89] as

$$\min \|x\|_p \quad \text{s.t.} \quad \|y - \Psi x\|_2 \leq \zeta, \tag{4.15}$$

where $\|\cdot\|_p$ is the l_p-norm and ζ bounds the amount of noise in the observation data. A vector x is said to be K-sparse if $\|x\|_0 = K$. Accurate recovery of x requires the measurement matrix Ψ to satisfy some strict conditions such as the Restricted Isometry Property (RIP) and Spark$(\Psi) > 2K$ [89]. The Spark of a matrix is the smallest number of columns in matrix Ψ that are linearly independent and the RIP indicates that a subset of the columns chosen from Ψ are nearly orthogonal. Although Spark and RIP provide guarantees for the recovery of a K-sparse vector, verifying that a matrix Ψ satisfies any of the above properties has a combinatorial computation complexity, since each time one must consider $\binom{N}{K}$ submatrices. Therefore it is preferable to use a property of a matrix which is easily computable and guarantees recovery. The *mutual coherence* of a matrix Ψ, $\mu(\Psi)$, is the largest absolute inner product between two columns ψ_i and ψ_j of Ψ:

$$\mu(\Psi) = \max_{1\leq i<j\leq n} \frac{|\langle \psi_i, \psi_j \rangle|}{\|\psi_i\|_2 \|\psi_j\|_2} \tag{4.16}$$

The *Mutual Coherence* of a matrix Ψ is always bounded in the range $\mu(\Psi) \in [\sqrt{\frac{N-M}{M(N-1)}}, 1]$, where the lower bound is known as the Welch Bound [89]. Note that a small $\mu(\Psi)$ indicates that the columns of Ψ are highly independent. If the original signal x in (4.15) satisfies the following requirements

$$\|x\|_0 = K < \frac{1}{2}(1 + \frac{1}{\mu(\Psi)}), \tag{4.17}$$

then, CS algorithms such as Basis Pursuit or other greedy algorithms such as CoSaMP [67] can be used to guarantee the recovery of x from an under-determined set of equations.

4.7 Simulation Results

This section analyzes the effectiveness in estimating the source DOA and the computational complexity of the proposed algorithm and is divided into several subsections aiming to give a detailed insight into some of the key performance parameters of the algorithm. Subsection 4.7.1 details the noise model and an expression for the Cramér-Rao lower bound (CRLB) for DOA estimation using a ULA. The impact of different transform operations in enhancing the performance of the CS operation is discussed in subsection 4.7.3. In subsection 4.7.4, the impacts of the number of antenna elements M and number of quantized grid points N are analyzed. Subsection 4.7.5 evaluates the estimation performance of the algorithm and compares to existing techniques such as Root-MUSIC, ESPIRIT and Beam-Forming. The computational complexity of the algorithms is analyzed in subsection 4.7.6 and a comparison is presented against some of the existing algorithms mentioned above.

4.7.1 SNR and CRLB

In order to determine the robustness of our system model, the following noise-sensitivity test has been considered. The Signal-to-Noise-Ratio (SNR) is calculated at the receiver as the ratio of the sum of the power received from the M antenna elements to σ^2, where σ^2 is the variance of the complex Gaussian noise at each element. The measured data are characterized by SNR in dB, defined as

$$\mathrm{SNR} = 10\log_{10}\left[\frac{\sum_{m=1}^{M}|x_m|^2}{M\sigma^2}\right] \tag{4.18}$$

where x_m, $m = 1, ...M$, is the noiseless complex output at the m^{th} antenna element. To validate the robustness of the proposed ICSDOA algorithm, U different DOAs are selected from a uniform distribution in the range $[-\pi/2, \pi/2)$. For statistical consistency, I Monte Carlo trials are carried out. The results in this section aim to validate the effect of noise sensitivity of the proposed algorithm in determining the actual incoming DOA of a signal. Compressive Sampling Matching Pursuit (CoSaMP) has been used as the platform for the CS operation. The Performance parameter of the algorithm is characterized as the Mean Square Error (MSE), where MSE is defined as,

$$\text{MSE} = \frac{\sum_{u=1}^{U}\sum_{i=1}^{I}|\theta_{org,u,i} - \theta_{est,u,i}|^2}{UI} \tag{4.19}$$

where $\theta_{org,u,i}$ is the original DOA of the source and $\theta_{est,u,i}$ is the DOA of the source estimated for the u^{th} scenario and the i^{th} Monte Carlo trial. The MSE of the proposed algorithm will be compared with the Cramér-Rao lower bound, given in [149] as,

$$\text{CRLB} \geq \frac{\sum_{u=1}^{U}\frac{6\sigma^2}{M(M^2-1)\pi^2\cos^2(\theta_{org,u})}}{U} \tag{4.20}$$

An estimator achieving the CRLB is considered to be efficient and it is not possible for any estimator to perform better than the theoretical CRLB.

4.7.2 Sparse Vector Coefficients

Compressive Sensing involves recovering an approximate sparse vector $\hat{\mathbf{S}}$ that satisfies the condition in (4.7). Greedy CS algorithm such as Compressive Sampling Matching Pursuit (CoSaMP) is a new technique proposed by Needell and Tropp in [67]. The algorithm is based on the prior technique Orthogonal Matching Pursuit, OMP [66], and provides strong guarantees that OMP cannot. One of the key features of the CoSaMP algorithm is the ability to recover an optimized solution vector with sparsity level, l. Unlike CoSaMP, other CS techniques such as Basis Pursuit outputs the sparse vector depending on the relaxation parameter ϵ in (4.7). This causes the solution vector $\hat{\mathbf{S}}$ recovered using Basis Pursuit to have a large number of non-zero elements. In the

proposed ICSDOA algorithm, the non-zero elements of $\hat{\mathbf{S}}$ refer to an estimate of the possible incoming DOA. A solution vector with a large number of non-zero elements introduces ambiguity in the estimation process, hence degrading the accuracy of the estimate.

In Section 4.5, an error discriminant function, $\Delta\Theta$ is used to converge towards the original incoming DOA. The error discriminant function uses the inputs α and β which are obtained using (4.10) and (4.11). The complex envelopes are obtained by rotating the angular grid points Θ in both the clockwise and anticlockwise directions by a grid interval of $\omega/2$. This simulation illustrates the impact of the sparsity level l on the outputs of α and β and the output of $\Delta\Theta$. For this simulation, the CS processing in (4.10) and (4.11) is carried out by varying the sparsity level, l in the range [1,3]. In other words, the simulation forces the CoSaMP algorithm to recover a solution vector with known sparsity, l. The ULA geometry is constructed with $M = 9$ antenna elements uniformly placed in a straight line and an inter-element spacing of $\lambda/2$. The signal to noise ratio is kept constant at 15 dB. A signal is assumed to be impinging on the ULA with a DOA $\theta = 26.34°$.

The plots in Fig. 4.5 show the effect of l on the outputs α and β. The x-axis has the quantized grid points representing the incoming DOA in degrees and the vertical axis is the corresponding complex envelope of α and β. For both $l = 1$ and 2, the algorithm is able to accurately deduce the coarse estimate $\breve{\theta}_0 = 26°$, which is closest angular grid point to the incoming DOA, $\theta = 26.34°$. Moreover with $l = 1$ and 2, $\alpha > \beta$ indicating that $\theta > \breve{\theta}_0$ and is also true in this case. However, with $l = 1$ $\beta = 0$, pushing the error-discriminant to the maximum value of $\omega/2$. The $l = 3$ subplot has a completely different trend, due to several non-zero complex envelopes, it selects $\breve{\theta}_0 = 27°$ to be the coarse estimate. Although the oscillatory nature of the ICSDOA algorithm forces the estimate towards the original DOA, it goes beyond the boundary of convergence. As a result, the estimate obtained with $l = 3$ deviates from θ. For the 3 different cases of l, the error discriminant, $\Delta\Theta$ is calculated using (4.12). The table below shows the estimate of the incoming DOA and are presented in degrees. The results in Table. 4.1,

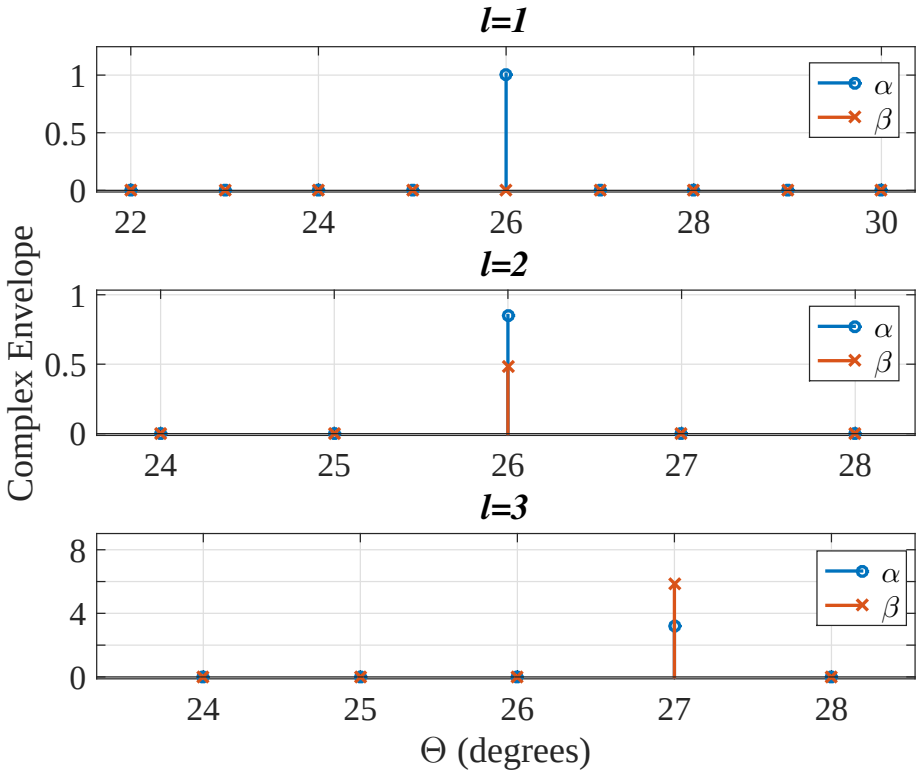

Fig. 4.5: Output of α and β with respect to varying sparsity of the recovered vector.

Sparsity	**Coarse Estimate**	**Error Discriminant**	**Final Estimate.**
$\boldsymbol{l = 1}$	26	0.5	26.5
$\boldsymbol{l = 2}$	26	0.3826	26.3826
$\boldsymbol{l = 3}$	27	-0.2354	26.76

Table 4.1: Error discriminant calculation against changing sparsity level of the CoSaMP algorithm

show the error discriminant generated using $l = 2$ enables the ICSDOA to achieve an estimate with minimum error. It is followed by $l = 1$ and $l = 3$ is the worst among the three. It also indicates that, for an incoming DOA in between the angular grids, the approximate sparsity of the recovered vector, $\hat{\mathbf{S}}$ should be set to 2.

To further validate the results presented in Fig. 4.5 and Table.4.1, an MSE performance test was carried out by varying the SNR from -10 dB to 25 dB. A number of incoming DOAs are considered, selected from a uniform distribution. The MSE of the

proposed algorithm is then compared with the theoretical CRLB for estimation accuracy. For this simulation, the number of Monte Carlo runs is set to be 1000. The plots in Fig. 4.6 reiterates the prior analysis on the sparsity level of the CoSaMP algorithm. The red plot representing $l = 2$ is the best-performing among them and achieves the theoretical CRLB for SNR(dB) > 7. Although all three plots approach the bound for SNR $= 6$ dB, the plots for $l = 1$ and $l = 3$ deviate away from the bound for higher SNR. It can be concluded from the analysis that the error discriminant function converges to the original estimate rapidly, especially when the approximate sparsity level for the recovery vector $\hat{\mathbf{S}}$ is set to be twice the number of sources detected.

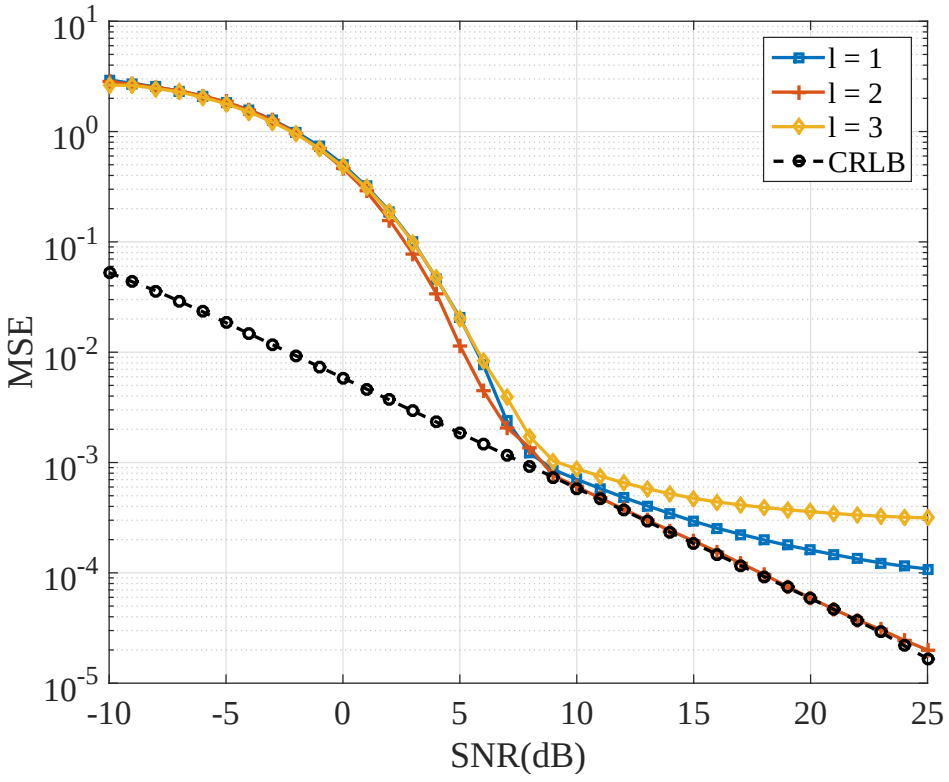

Fig. 4.6: MSE performance of the proposed algorithm with respect to varying sparsity level of the CoSaMP algorithm.

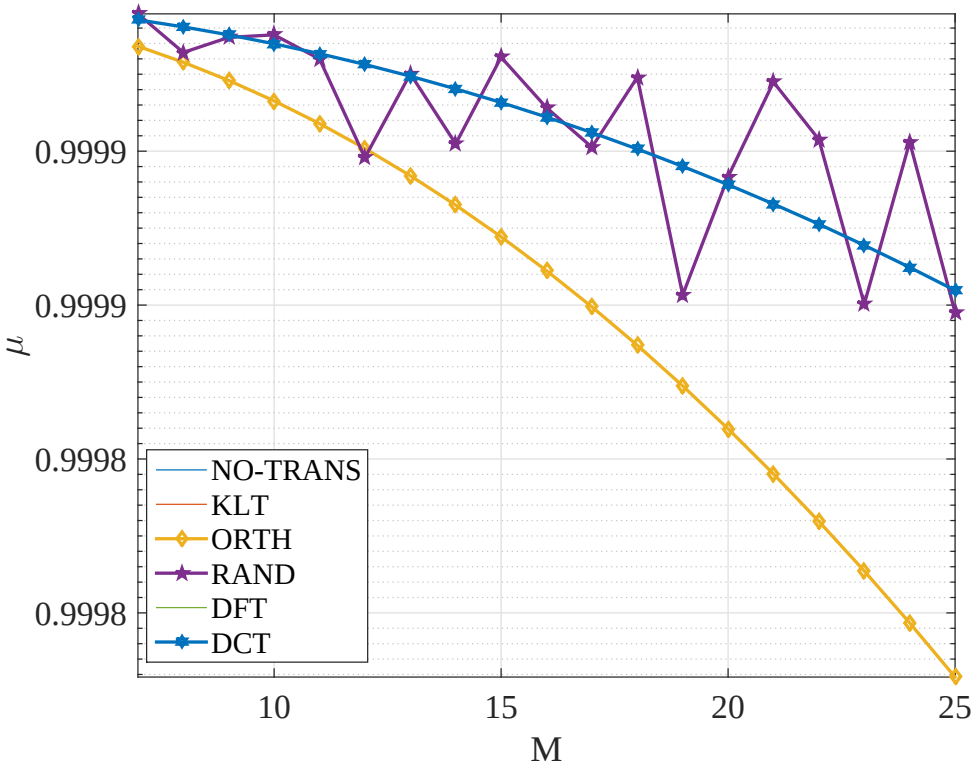

Fig. 4.7: Coherence of measurement matrix Z against the number of antenna elements M, for $N = 90$ grid points

4.7.3 Transform operation

In CS processing, the construction of a measurement matrix plays an integral role in accurately recovering the sparse solution. A transform operation or sparsifying basis helps to de-correlate the columns of the measurement matrix, allowing CS to maximize the utilization of the column space. Moreover, the process enables CS to project the observation directly on to the measurement matrix without any loss of efficiency [165–167]. A popular family of sensing matrices is a random projection, where the entries are random variables from a sub-Gaussian distribution such as Gaussian or Bernoulli. This family of projection matrices is well known to be universally incoherent for all other sparsifying bases. However, it can be computationally quite expensive to use a random matrix for a practical application as they require a large buffering memory due

to their completely unstructured nature. This makes the sampling and recovery process computationally unrealistic in most cases. The Karhunen-Loève Transform (KLT) [152] is a classical procedure that reveals the correlation structure of the signal. KLT is optimal such that it de-correlates the signal into a representation comprising only statistically non-redundant coefficients. In most cases, KLT is used as a benchmark to judge the performance of other transforms. Unfortunately, KLT is data dependent and requires huge computational power to extract a transform matrix. A KLT basis is computed numerically from a sample covariance matrix. In a practical scenario, with a large measurement matrix, the computational complexity increases exponentially. In contrast to KLT, Discrete Fourier Transform (DFT) is based on a fixed support set and is independent of the measurement matrix [154]. The DFT has a lower computational complexity and exhibits good de-correlation and compaction characteristics. But, as the entries of a DFT matrix are complex, it can significantly alter the original magnitude and phase information. The Discrete Cosine Transform (DCT) also provides excellent de-correlation and energy compaction properties [153].

In this section, the impacts of different transform matrices are analyzed in terms of reducing the mutual coherence of the modified measurement matrix $\mathbf{Z}$. In Section 4.4, it has been mentioned that $\mathbf{R} = (\mathbf{H}^*\mathbf{\Phi})$, where $\mathbf{H}$ is the $M \times M$ transform matrix. In Fig. 4.7, to illustrate the influence of $\mathbf{H}$, several transform matrices are considered. The comparison was carried out by constructing $\mathbf{H}$, using KLT, DCT, DFT and a random matrix, where the entries are Gaussian random variables. An orthonormal transform processing technique similar to that in [129] has been considered in the comparison and has a plot legend of ORTH. The NO-TRANS legend in Fig. 4.7 refers to a CS operation without a transform matrix. The plots in Fig. 4.7 indicate the ability of each transform matrix to minimize the coherence among the columns of $\mathbf{Z}$. From the graph, it can be seen that the most effective transform in terms of reducing the coherence of $\mathbf{Z}$, is the orthonormal transform. All three transforms including KLT, DCT, DFT have no significant impact on the coherence of $\mathbf{Z}$, and perform similarly to the NO-TRANS case. Therefore, they are all represented using a single graph (blue). On the other hand, the RAND plot fluctuates for each M and is inconsistent compared to all other

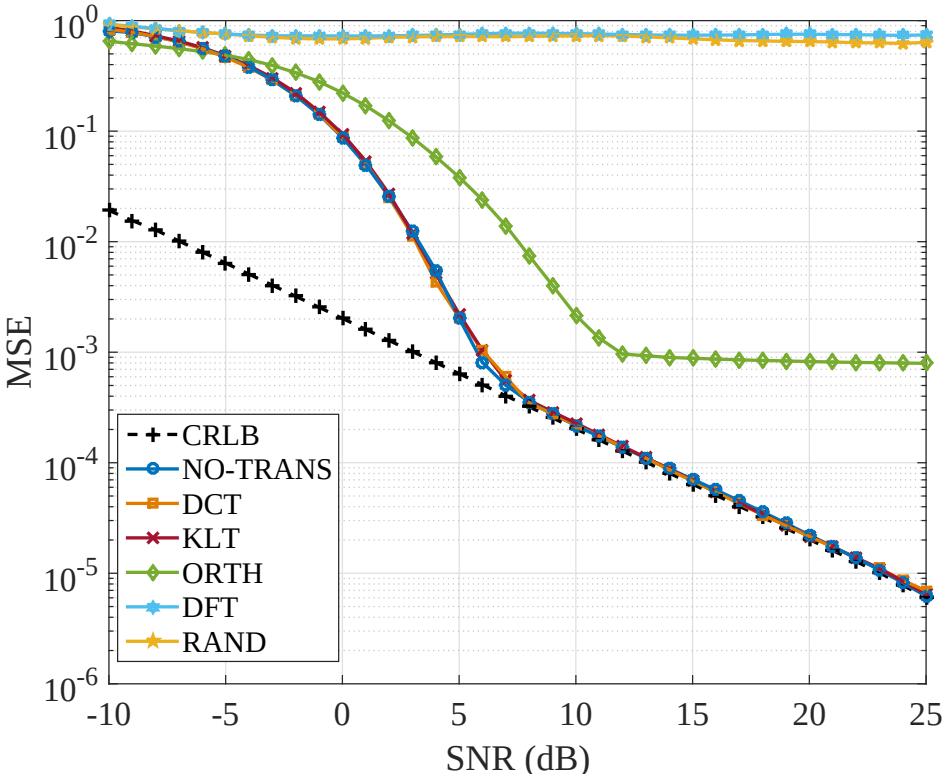

Fig. 4.8: Influence of Transform matrix on Mean Square Error (MSE) of the algorithm

transforms.

The aforementioned transform matrices are used to construct several new dictionary matrices, and each of them is feed into the ICSDOA algorithm to evaluate the impact of the individual transform operation. In this simulation Compressive Sampling Matching Pursuit (CoSaMP) has been used as a CS platform to retrieve the sparse solution vector. For this simulation the angular domain in the range $[-\pi/2, \pi/2)$ is quantized into $N = 90$ angular grid points with $\omega = \frac{2\pi}{N}$. The simulation was carried out using a ULA geometry with $M = 9$ and a constant inter-element spacing of $\lambda/2$. The simulation assumes having a single transmitting source.

The plots in Fig. 4.8 have a different trend than those in Fig. 4.7. The results show that KLT and DCT are the best performing transforms, approaching the CRLB for SNR > 7 dB. In Fig. 4.7, the ORTH transform had the best de-correlating capabilities, however, it failed to accurately project the observation vector $\mathbf{V}$ on to the columns

of **Z**, hence converging to an incorrect estimate. The transform matrix has energy compaction properties, where correlated observations are combined to improve the sparsity of **Z**. However, while enhancing the sparsity, the transform matrix can also alter the information in **Z**, creating a mismatch between the observation vector **V** and measurement matrix **Z**. The mismatch forces the CS algorithm to converge at an incorrect solution, increasing the MSE of DOA estimation. DFT and RAND have complex entries in the measurement matrix which influence the original information of **Z**. This results in an inaccurate DOA estimate as shown in Fig. 4.8. From the results presented and Fig. 4.8, it can be concluded that KTL and DCT, unlike DFT and RAND, preserve the information without altering the complex data of the measurement matrix. ORTH transform achieved to reduce the mutual coherence by compacting the dimensionality of the matrix, but according to the MSE performance in Fig. 4.8, that does not correspond to the best basis of the estimation process. The results indicate, achieving the minimum mutual coherence does not necessarily provide the guarantee of a successful estimation. The problem involves the concept of pattern recognition, where it is crucial for the transformed basis to correlate to the observation rather than having highly independent columns. From the analysis, it is evident that transform operations do not offer any significant advantages over the no transform case. Hence, in order to reduce the computational complexity of the algorithm, the transform operation can be ignored in the further analysis.

4.7.4 Antenna Elements and Grid quantization

The theory of CS suggests that the number of observations required for accurate recovery of the sparse vector is lower bounded by the following inequality

$$M \geq K \ln(N/K), \tag{4.21}$$

where K represents the sparsity of the solution vector. In [64], it has been stated that most K-sparse vectors can be retrieved by ensuring the condition, $M \geq 4K$. This indicates that any CS-based DOA algorithm requires at least $M = 4$ antenna elements

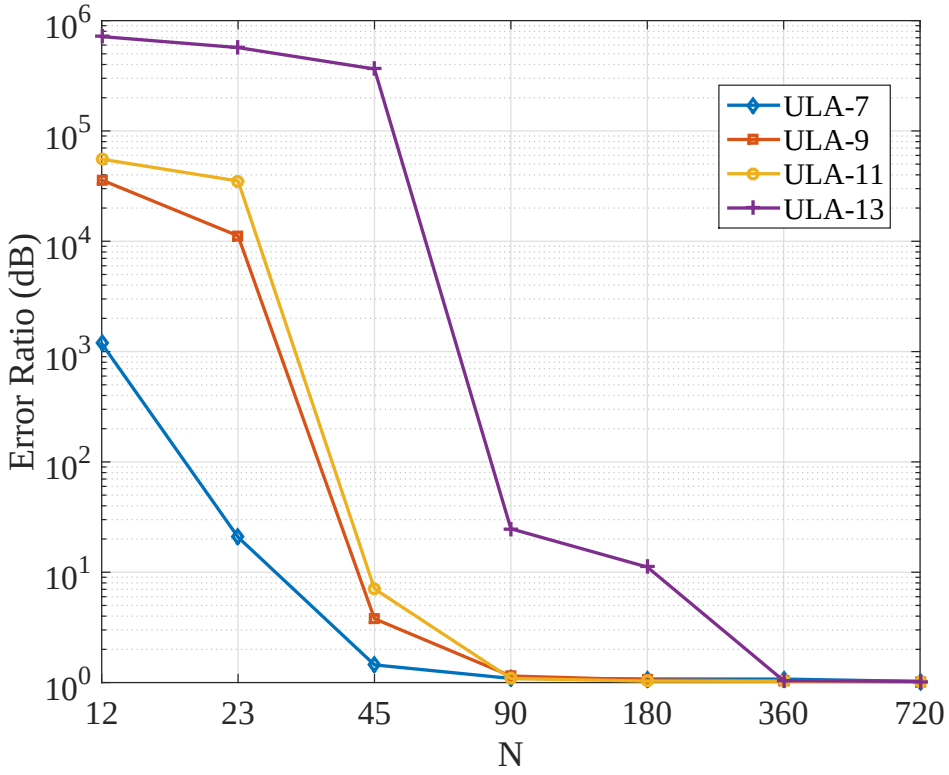

Fig. 4.9: Impact of M and N on the ratio of MSE over CRLB of the proposed algorithm

per transmitting source to deduce the incoming angle of arrival. Another equally important consideration for CS processing is the construction of the measurement matrix [168–170]. The system model adopted for this paper relies on the construction of a deterministic measurement matrix $\mathbf{\Phi}$, where each column represents the ARVs associated with the quantized angular grids Θ. The ARV in (4.2) represents the phase shift due to the increased travel distance of the incoming signal in reference to the first element of the antenna array. The analysis presented in this section highlights the influence of the M antenna elements and N angular grid points on the MSE of the estimated DOA using the proposed ICSDOA algorithm. It also establishes a relationship between M and N and proposes an optimal ratio that enhances the effectiveness of the proposed algorithm.

The first set of simulations is carried out using 4 different ULA geometries with varying $M \in [7, 9, 11, 13]$. The inter-element spacing between the antenna elements

is $\lambda/2$. The angular domain between $-\pi/2$ and $\pi/2$ is quantized into N angular grid points, where N is varied in the range $[12, 23, 45, 90, 180, 360, 720]$. The inter-grid spacing is given as ω, where $\omega = \pi/N$. To provide consistency in the simulation outcomes, 10 DOAs are randomly selected from a uniform distribution in the range $[-7\pi/18, 7\pi/18)$. For each DOA 1000 Monte Carlo trials are carried out while the SNR is kept constant at 15 dB. To evaluate the influence of different N on each of the 4 antenna geometries a new performance parameter, Error Ratio (ER) has been introduced such that

$$\text{Error Ratio (dB)} = 10\log_{10}\left(\frac{\text{MSE}}{\text{CRLB}}\right). \tag{4.22}$$

In (4.22), the ER provides a ratio of the MSE of an estimate using the proposed algorithm against the respective CRLB of the ULA geometries. Moreover, the parameter provides an indication of the deviation of the MSE from the theoretical bound. A higher ER suggests that the estimate is inaccurate and is deviating from the respective error bound. According to (4.20), the CRLB of a ULA is dependent on the number of antenna elements (M) of each ULA geometry. The graph in Fig. 4.9 illustrates that the ER for all the ULA geometries gradually decreases with an increase in N and approach zero for larger N. When looked at closely, it can be seen that ULA-13 requires $N \geq 360$ in order to have an ER close to zero. On the other hand, the plot for ULA-7 approaches the zero mark for $N \geq 90$. Although both ULA-9 and ULA-11 perform close to each other, the ER for ULA-11 is slightly higher than ULA-9. At $N = 90$, the ER for ULA-13 is almost 15 times as large as of ULA-7. Such behavior indicates that ULAs with large M require a finer quantization of the angular domain (i.e. large N) to obtain a precise estimate of the incoming angle of arrival. This suggests that the proposed ICSDOA algorithm integrated with ULA-7 and ULA-9 has an advantage over ULA-11 and ULA-13 in achieving its respective CRLB using a smaller N. The difference in behavior among the ULA geometries can be explained using the theory

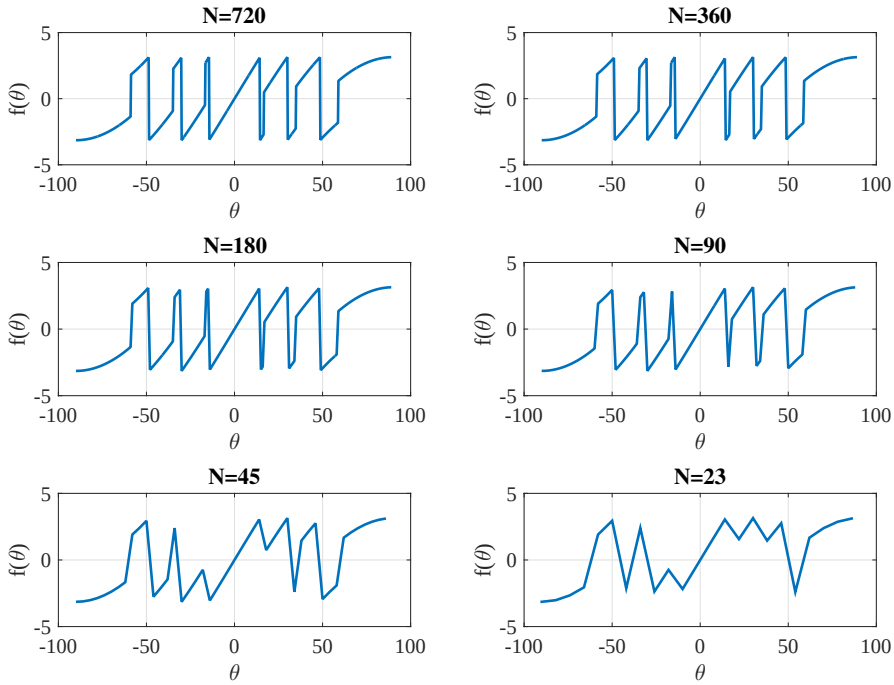

Fig. 4.10: Phase response of ULA-7 for different values of N

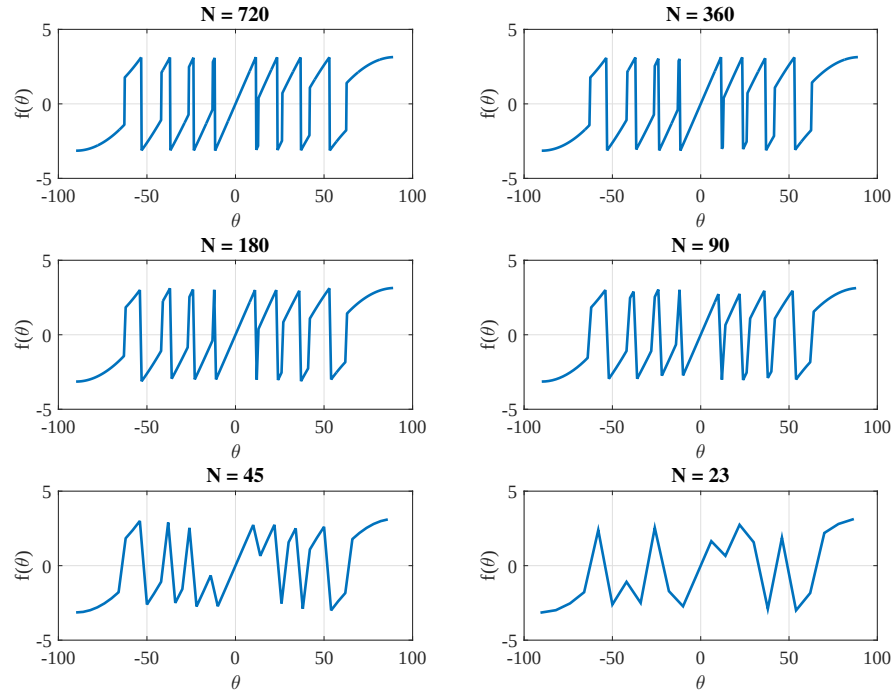

Fig. 4.11: Phase response of ULA-9 for different values of N

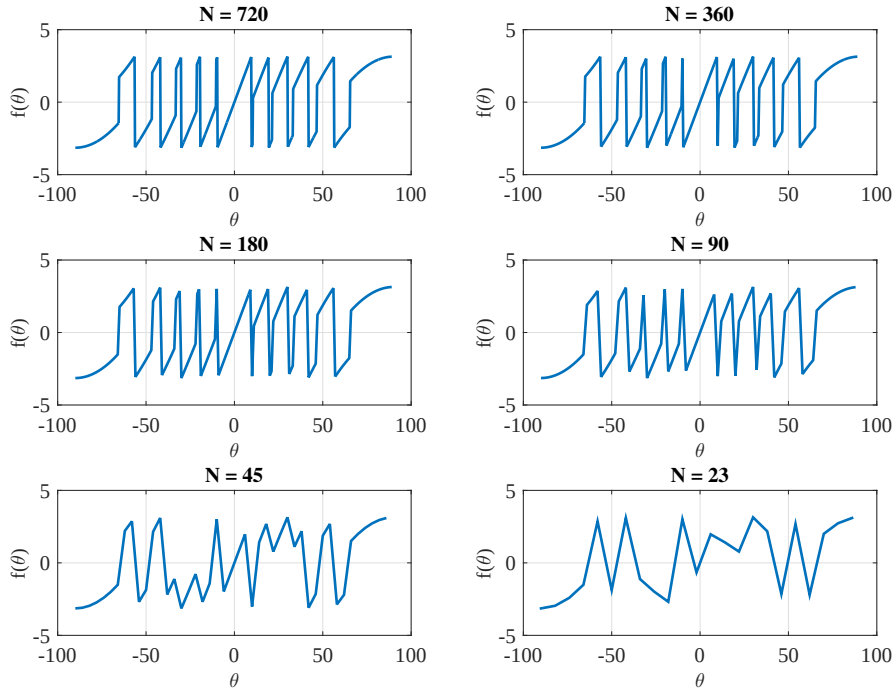

Fig. 4.12: Phase response of ULA-11 for different values of N

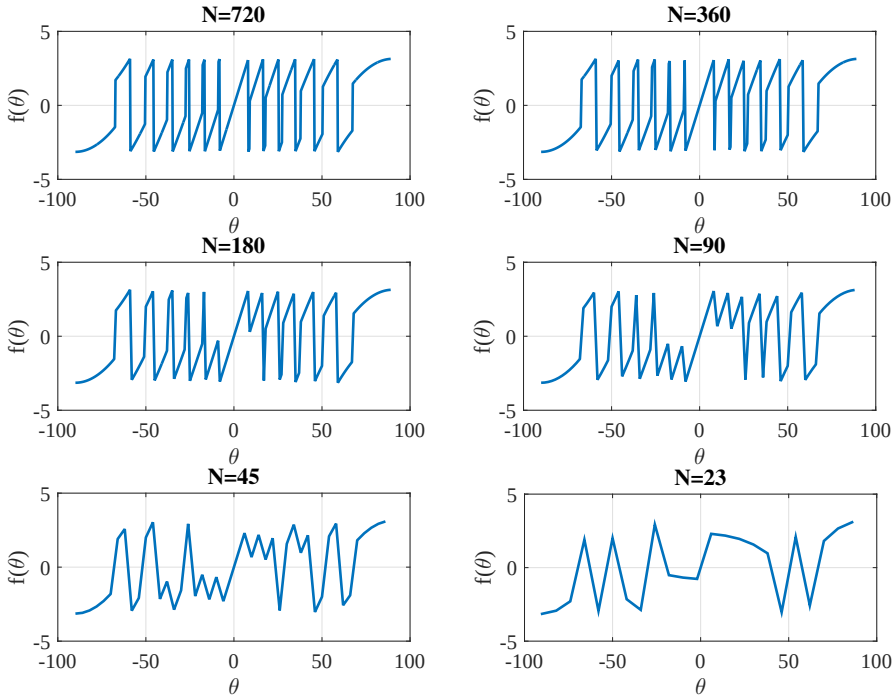

Fig. 4.13: Phase response of ULA-13 for different values of N

of the antenna array by Balanis in [171].

According to the theory, the accuracy of a DOA estimate is directly dependent on the number of antenna elements, given that the angular domain is finely quantized. However, limited research was carried out to study the impact of varying N on different ULA geometries as a DOA estimation problem. To further investigate the effect of N, the phase responses of the ULA geometries are calculated for an incoming DOA in the range $[-\pi/2, \pi/2)$. The phase response of a ULA with M antenna elements corresponding to an incoming angle θ is $f(\theta)$ given as

$$f(\theta) = \arg(AF), \tag{4.23}$$

where

$$AF = 1 + e^{-jk\sin(\theta)d} + \ldots + e^{-jk\sin(\theta)(M-1)d}. \tag{4.24}$$

The graphs in Figs. 4.10, 4.11, 4.12 and 4.13 show the phase responses for each of the 4 ULA geometries. Each graph has several sub-graphs indicating the effect of varying N on $f(\theta)$. The number of sidelobes that appears for each antenna geometry is $M-2$ and is directly dependent on the number of antenna elements M [171]. Let us consider the subgraph with $N = 720$ (finer quantization of angular domain) for all the ULA geometries in Figs. 4.10 to 4.13. The frequency of the pulses in a subgraph increases with an increase in M, which is due to the increased sidelobes. So, for larger M, the phase response of a ULA is more sensitive for varying θ than a ULA with smaller M. Therefore, the sensitivity restricts a ULA with larger M from performing effectively when the angular domain is coarsely quantized (i.e. smaller N). In Fig. 4.10, the sub-graphs for ULA-7 remain consistent until $N = 90$ and change abruptly for $N \leq 45$. This means that at $N = 45$ the angular domain is under-sampled, and does not have enough information to reconstruct the original shape of $f(\theta)$. For ULA-13 the change in shape appears at $N = 180$ and gets worse as N decreases. From the simulation results, it can be concluded that ULA-7 approaches zero ER using half the value of N compared to ULA-13. This allows ULA-7 to achieve its respective CRLB using a smaller number of angular grid points. The analysis establishes a relationship between

M and N that enables ICSDOA algorithm to achieve the CRLBs of respective antenna geometries.

4.7.5 DOA Estimation Performance Comparison

This section graphically illustrates the fast convergence of the proposed ICSDOA algorithm and compares its performance with several well known DOA estimation techniques. In addition, the performances of the DOA techniques are compared to the CRLB. For both sets of simulations, a ULA geometry is considered as a receiving node with $M = 9$ antenna elements with an inter-element spacing $d = \lambda/2$. The simulations considered $U = 100$ different DOAs, where incoming DOAs are chosen randomly from a uniform distribution in the range $[-7\pi/18, 7\pi/18)$. The number of Monte Carlo trials for each scenario is $I = 100$. The spatial angular domain in the range $[-\pi/2, \pi/2)$ is quantized into $N = 180$ angular grid points with a quantization interval of $\omega = \pi/180$. The SNR is varied between -10 dB and 25 dB with an interval of 1 dB.

The first simulation demonstrates the convergence of the proposed ICSDOA in approaching the theoretical CRLB. In Fig. 4.14 the y-axis and the x-axis represent the MSE and SNR in dB respectively. The graph shows 4 plots, where the yellow plot represents the coarse estimate which is obtained using (4.8) in Section 4.5. The coarse estimate refers to the neighboring quantized grid point with maximum amplitude. For low SNR cases the MSEs for all three plots are extremely high. This is because, at low SNR, the CS algorithm fails to converge to a quantized grid point closer to the incoming DOA. As the coarse estimates at low SNR are incorrect, the following iterative operations of ICSDOA are ignored to reduce complexity. However, for SNR $>$ 6 dB, the estimation error drops sharply and approaches the CRLB. The plot for the coarse estimate flattens out at high SNR due to the error induced by grid quantization. The blue and red plots indicate the estimate obtained after the 1st and 2nd iterative operations of the ICSDOA algorithm. From the graph it is clear that using the first iteration the ICSDOA approaches the CRLB for SNR $>$ 6 dB and remains close to the bound for higher SNR. As ICSDOA shows superior performance in reducing the

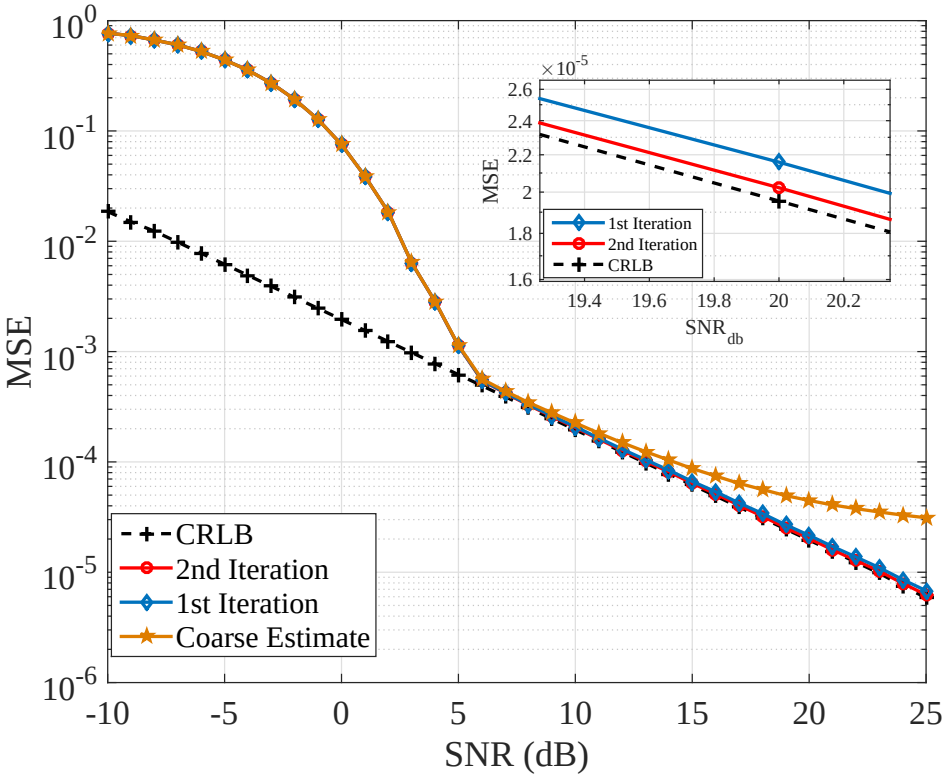

Fig. 4.14: Convergence of algorithm from the coarse estimate to the final estimate in two iterations.

estimation using the 1st recursion, the improvement in the 2nd iterative operation is extremely small. For a better visualization of the difference in performance between two iterative operations, a magnified version of the graph is shown in Fig. 4.14. This gives a clear indication of the rapid convergence with ICSDOA to the CRLB, using just two operations.

In the second set of simulations, shown in Fig. 4.15, the DOA estimation performance of ICSDOA is compared to benchmark DOA estimation techniques such as Beam-Forming, Root-MUSIC and ESPIRIT. As the Root-MUSIC algorithm is a modified version of the well-known MUSIC algorithm, the MUSIC algorithm is excluded from the comparison. All the simulations are carried out using a single time instant (i.e. snapshot = 1). For SNR < 5 dB, the MSE for all the estimation techniques are extremely high. Beam-Forming and ICSDOA perform better than Root-MUSIC and ESPIRIT, with Beam-Forming having a slightly lower MSE than ICSDOA. The plot

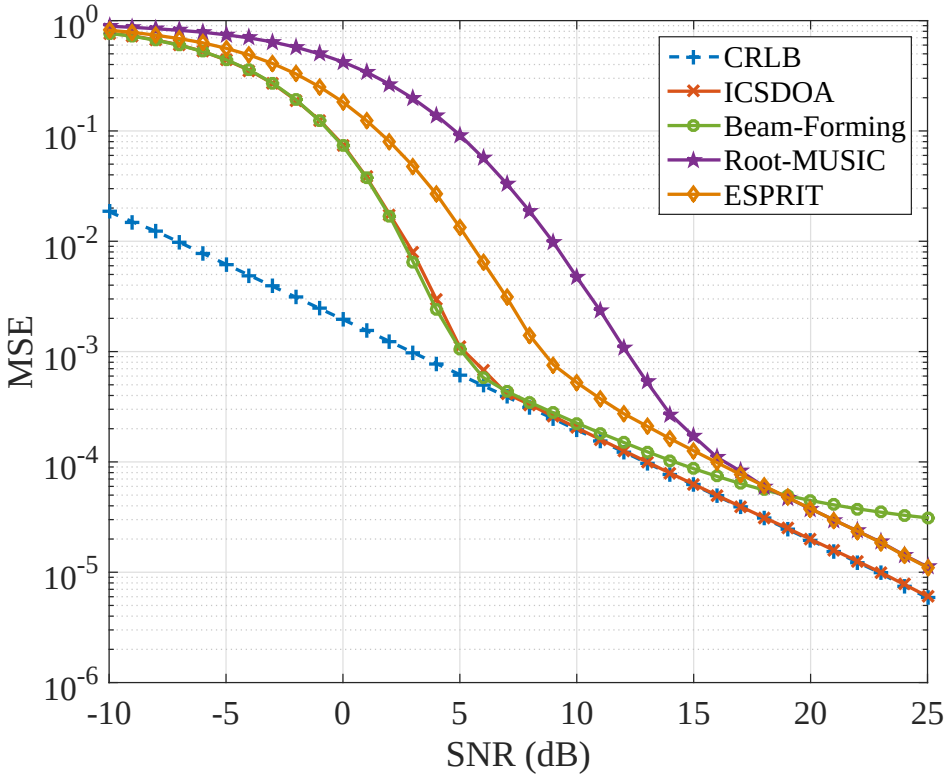

Fig. 4.15: MSE performance comparison of the ICSDOA algorithm against Beam-Forming, Root-MUSIC and ESPRIT.

for Beam-Forming approaches the CRLB for 6 dB <SNR< 10 dB, but deviates away from the CRLB at higher SNR. The Beam-Forming method is dependent on the grid interval, i.e. $\omega = \pi/180$. Therefore the MSE of Beam-Forming is lower bounded by an error induced due to grid quantization, and the error increases with an increase in the grid interval ω. The plot for Beam-Forming can be related back to the plot for the coarse estimate in Fig. 4.14, which also has a lower bound on MSE performance. On the other hand, Root-MUSIC and ESPIRIT have a higher estimation error at low SNR, but overtake the Beam-Forming plot for SNR $>$ 18 dB. This shows that both EVD-based methods perform independently to the grid quantization, but fail to approach the bound due to a smaller number of signal snapshots. However, the proposed ICSDOA algorithm outperforms the above techniques by performing extremely close to the CRLB for SNR $>$ 5 dB and remains on the bound for higher SNR. The iterative

operation of ICSDOA completely eliminates the error resulting from grid quantization, whereas the CS operation allows ICSDOA to achieve superior performance with a single snapshot.

4.7.6 Computational Complexity

This section discusses the complexity of our proposed algorithm in converging to an estimate. The graph in Fig. 4.14 clearly indicates that the ICSDOA algorithm achieves the CRLB in just 2 iterations. Algorithm-2 indicates that the proposed iterative algorithm uses one CS operations in each iteration to compute the output of an error discriminant. The CoSaMP CS algorithm has been used to retrieve the sparse vector from the under-determined system of equations. According to [67], the computational complexity of the CoSaMP algorithm is given as $O(MN)$. The proposed algorithm consists of three major stages, coarse estimate, error-discriminant output, and update. The first stage uses only 1 CS operation to retrieve the initial sparse vector and is followed up with the search for the index representing the dominant complex envelope. In total the complexity of the the first stage in terms of big O notation can be expressed as $O(MN) + O(N) = O(MN)$. The second stage relies on the rotation of the N angular grid points by a $\frac{1}{2}$ the quantization interval. This process introduces a total of MN multiplications resulting a complexity of $O(MN)$. This step is followed by a CS processing on the rotated grid points which introduces another $O(MN)$ operation. Unlike the first stage, the algorithm does not require a maximum search operation to find the complex envelope. Instead, the algorithm can easily access the vector using the index obtained from the first stage to extract the scalers α and β. The error discriminant calculation is a simple scalar arithmetic operations with a combined time complexity of O(1). Therefore, in the second stage for each iteration in estimating the error discriminant, the respective complexity can be written as $O(MN) + O(MN) + O(1) = O(2MN)$. The third stage is the update phase, where the output of the error discriminant is used to update the N quantized grid points Θ. The operation is a basic mathematical addition with a time complexity of $O(N)$. The total breakdown in terms of time complexity is given in Table 3.2

Processing	Operation	Complexity
Coarse Estimate	$1 \times CS$ + max search	$O(MN)$
Error Discriminant	$2 \times CS + \Delta\Theta$ output	$O(2MN)$
Update	N Additions	$O(N)$

Table 4.2: Computational-complexity of proposed algorithm

Eigenvalue decomposition (EVD) based or subspace based DOA estimation methods such as MUSIC, Root-MUSIC and ESPRIT, have a computation complexity of $O(M^2N+M^2)$ and $O(M^3+M^2)$. MUSIC and Root-MUSIC are computationally more complex due to their spectral search and subspace estimation using the EVD of the covariance matrix. From Table. 4.2, it can be concluded that the total computational complexity of the algorithm is $O(MN + 2cMN + N)$, where c is the number of iterative operation required to converge to the estimate. The complexity of our algorithm is highly dependent on the number of error discriminant estimates. According to the convergence test, the error discriminant approaches the stopping criterion with just two iterations. In comparison to the EVD based methods, our proposed technique offers lower complexity ($O(5MN)$) than MUSIC and Root-MUSIC, however, it has higher complexity than ESPRIT.

4.8 Conclusion and Future work

This paper outlines a novel iterative algorithm to detect the DOA of a transmitting source using a ULA antenna as a receiving node. A new signal processing technique has been introduced that utilizes CS operations to develop an error discriminant function. The function enables rapid convergence of a DOA estimate to the theoretical CRLB by eliminating the error induced due to grid quantization. The robustness of the proposed algorithm was verified by conducting extensive statistical analysis with noise inherent in the ULA processing. The results suggest that the algorithm converges to the CRLB

of the DOA estimate with just 2 iterations. At moderate SNR the algorithm outperforms well-known techniques such as Root-MUSIC, ESPIRIT and Beam-Forming by reducing the MSE of performance significantly. The computation complexity of the algorithm is calculated to be $O(5MN)$ which is lower than EVD-based DOA estimation algorithm such as MUSIC and Root-MUSIC and slightly higher than ESPRIT. However, ESPRIT requires large snapshots of the incoming signal to determine the DOA. A detailed analysis on the influence of the number of antenna elements and the grid quantization on the MSE performance of the algorithm is also presented in this paper. It can be concluded that ULAs with a large number of antenna elements require finer quantization of the angular grids to achieve its respective theoretical bound. In other words, ULA with a large M would need a large N, as a result drastically increasing the computational complexity of the algorithm. However, it is worth noting that DOA estimation accuracy of a ULA is directly dependent on M. Hence, there is a systematic trade-off of performance as a function of the computational complexity of the algorithm.

As part of future work, it is of great interest to extend the algorithm using multiple receiving ULA antennas to deduce the location of the transmitting source in a network. One major assumption made in the current research model is that there is only one source. Incorporating a large number sources and analyzing the performance in various multi-path environments is another important topic for future work.

5

Performance comparison of a Uniform Circular Array and Uniform Linear Array using an Iterative Compressive Sensing Framework

5.1 Abstract

This paper provides a comparison study for the problem of direction-of-arrival (DOA) estimation using the uniform circular array (UCA) and uniform linear array (ULA) antenna geometries. The paper focuses on integrating the two antenna geometries with a compressive-sensing based DOA estimation algorithm in order to determine the DOA

of an incoming signal. CS-based approaches offer a competitive advantage over the traditional sub-space based DOA estimation techniques due to their ability to obtain an estimate with minimum measurements (i,e. one snapshot), while completely avoiding the computationally expensive eigenvalue decomposition (EVD). The performance of the antenna geometries is validated by comparing to the theoretical Cramér-Rao lower bound (CRLB) of the respective antenna geometries. Simulation results suggest that ULA achieves a more precise estimate than UCA, especially when the DOAs are in the broad-side region. The paper also provides a detailed analysis on the structure of the measurement matrices that are constructed using the array response vector (ARV) for each of the two antenna geometries. The analysis indicates that careful exploitation of antenna array parameters of a UCA can greatly enhance the DOA estimate, eventually leading a lower MSE than that of ULA.

5.2 Introduction

Smart antennas have been widely used in the area of wireless and cellular communication to overcome the problem of limited channel bandwidth, therefore satisfying the ever-growing demand of large mobile networks. Currently, there is a great interest in integrating smart antennas to the existing cellular infrastructure to maximize the spectral efficiency of the networks. Beam-forming is a technology that allows a base station to simultaneously direct radiation beams towards intended users, and ideally put a null towards un-registered users [142]. The approach offers intelligent alternatives to the interference mitigation problem, while allowing maximum utilization of the spectral resources. However, to place a directional beam towards a user, accurate direction-of-arrival (DOA) information is of paramount importance. The DOA information is also pivotal in several applications such as localization-based services (LBS), jammer identification and adaptive beam-forming [144, 172, 173].

Subspace-based methods, Multiple Signal Classification (MUSIC) [97] and Estimation of Signal Parameters via Rotational Invariance Techniques (ESPRIT) [98] requires eigenvalue decomposition (EVD) of the covariance matrix for DOA estimation. The

EVD process is computationally demanding and relies on a large number of snapshots of the incoming signal for estimation accuracy. Compressive Sensing (CS) is a signal processing technique that is extremely effective in recovering a signal using minimum measurements, given that the incoming signal is sufficiently sparse in some given basis. As the incoming signal is sparse in a given angular dimension, the problem can be cast into a CS problem of sparse vector recovery. In comparison to the aforementioned DOA estimation methods, CS-based DOA estimation techniques offers several advantages: 1) it avoids the computation of an EVD matrix, which demands a complex hardware implementation at the receiver that is not feasible for hand-held devices and 2) it offers a high precision estimate of a DOA using only a single snapshot of the observation. The computationally inexpensive technique has attracted attention and motivated researchers to explore DOA estimation as a sparse recovery problem [108, 146, 147, 174]. Until now, most research in the field of antenna arrays focused on the uniform linear array (ULA) as the form of the antenna geometry. Limited attention has been paid to the uniform circular array (UCA) as an antenna topology for DOA estimation. Unlike, linear arrays, UCAs can provide a wider angular scan coverage in both horizontal and vertical planes. The symmetric geometry of a UCA greatly reduces the distortions in the array pattern due to mutual coupling and the synthesized directional beam patterns can be electronically rotated without a significant change in the beam shape. Moreover, due to the fact that UCAs do not have edge elements, the limitations of end-fire regions can be ignored [175–178].

In a typical CS-based technique, the angular region of coverage is quantized into N possible DOAs, where each DOA represents a grid point on a spatial domain. The number of antenna elements M in a UCA and a ULA is usually smaller than the number of angular grid points N. The complex signals originating from each of the angular grid points are used to create a dictionary matrix that is rectangular in nature. One of the major drawbacks of the CS-based algorithm is the error induced in the estimation due to grid quantization. To eliminate the problem a novel iterative CS-based DOA estimation algorithm (ICSDOA) is proposed in [179] and will be used as a platform to carry out the CS operation. The algorithm has superior performance to traditional EVD-based

approaches and achieves the Cramér-Rao lower bound (CRLB) on estimation error. Simulation results suggest that the proposed algorithm is extremely convergent and is able to provide an accurate DOA estimate using a single snapshot of the signal.

In this paper, we provide a mean-square-error (MSE) performance comparison between the two antenna geometries, UCA and ULA, when incorporated with the ICS-DOA estimation algorithm. The Simulation results suggest that, for a given set of DOAs in the broad-side region, a ULA outperforms UCA in reducing the MSE to a minimum. This is mainly due to the fact that a ULA has a lower CRLB than a UCA. The effectiveness of a CS-based DOA estimation algorithm is heavily dependent on the structure of the dictionary matrix. The paper also provides an in-depth analysis on the influence of different antenna parameters on the structure of the dictionary matrices constructed using UCA and ULA. As the dictionary matrices are rectangular in nature, matrix properties such as mutual coherence and condition number are used as a performance parameter to validate the structure of the matrices. The antenna parameters considered for the analysis include the number of antenna elements M, the number of angular grid points N and the inter-element spacing between the antenna elements. The analysis suggests that careful exploitation of the antenna parameters of a UCA can significantly improve the structure of the dictionary matrix, leading to a lower MSE estimate of a DOA than that of a ULA. Moreover, the impact of M and N on the MSE of each antenna geometry is separately analyzed. Simulation results show that, a ULA with large M requires finer quantization of angular grid points to achieve a minimum error estimate of the incoming DOA.

The outline of the paper is as follows. A background on the CS technique is presented in Section 5.3. Sections 5.4-5.5 provide the system model and the integration of CS framework as a DOA estimation problem. Section 5.6 details the analysis on the dictionary matrices. This is followed by simulation results in Section 5.7 and finally, conclusions are presented in Section 5.8.

5.3 Background

This section provides a brief background information to describe the concept of CS. It also discusses several properties that can used to measure the fitness of a rectangular matrix.

5.3.1 Compressive Sensing

Compressive sensing is a mathematical framework that deals with the recovery of a sparse vector, $x_{N\times 1}$, from an observation vector, $y_{M\times 1}$, with $M \ll N$. The measurement paradigm consists of a linear projection of the signal vector via a known projection matrix $\Psi_{M\times N}$. As $M \ll N$, the recovery of the sparse vector x from the measurement vector y becomes an undetermined problem with a large number of solutions. In the CS framework, an accurate estimation of a sparse signal, x, can be obtained in the reconstruction problem described in [89] as

$$\min \|x\|_0 \quad \text{s.t.} \quad \|y - \Psi x\|_2 \leq \zeta, \tag{5.1}$$

where $\|\cdot\|_p$ is the l_p-norm and ζ bounds the amount of noise in the observation data. The $\min \|x\|_0$ is desired by $\min \|x\|_1$ which is approximately similar in the case of sparse vector. A vector x is said to be K-sparse if $\|x\|_0 = K$. Accurate recovery of x requires the measurement matrix Ψ to satisfy some strict conditions such as the Restricted Isometry Property (RIP) and Spark(Ψ) $> 2K$ [89]. The Spark of a matrix is the smallest number of columns in matrix Ψ that are linearly independent, and the RIP indicates that a subset of the columns chosen from Ψ are nearly orthogonal. Although Spark and RIP guarantees the recovery of a K-sparse vector, verifying that a matrix Ψ satisfies any of the above properties has a combinatorial computation complexity, since each time one must consider $\binom{N}{K}$ submatrices. Therefore it is preferable to use a property of a matrix which is easily computable yet still guarantees recovery. The *mutual coherence* of a matrix Ψ, $\mu(\Psi)$, is the largest absolute inner product between

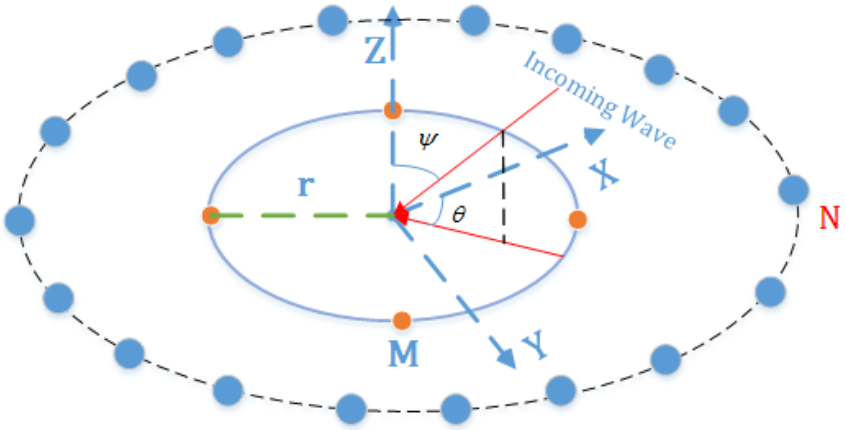

Fig. 5.1: A typical UCA with M elements, where θ and ϕ represent the azimuth an elevation angles of a received signal. The 2π azimuth domain is quantized into N possible angular grid points.

two columns ψ_i and ψ_j of Ψ:

$$\mu(\Psi) = \max_{1 \le i < j \le n} \frac{|\langle \psi_i, \psi_j \rangle|}{\|\psi_i\|_2 \|\psi_j\|_2} \tag{5.2}$$

The *Mutual Coherence* of a matrix Ψ is always bounded in the range $\mu(\Psi) \in [\sqrt{\frac{N-M}{M(N-1)}}, 1]$, where the lower bound is known as the Welch Bound [89]. Note that a small $\mu(\Psi)$ indicates that the columns of Ψ are highly independent. If the original signal x in (1) satisfies the requirement

$$\|x\|_0 = K < \frac{1}{2}(1 + \frac{1}{\mu(\Psi)}), \tag{5.3}$$

then CS algorithms such as Basis Pursuit or other greedy algorithms such as COSAMP [67] can be used to guarantee the recovery of x from an under-determined set of equations.

5.3.2 Singular Values

A rectangular matrix such as $\Psi_{M \times N}$ does not possess any quantifiable parameters such as eigenvalues to determine the structure of the matrix. However, $Q = \Psi^* \Psi$, where Ψ^* is the conjugate transpose of Ψ, is a square matrix and the eigenvalues of Q can be

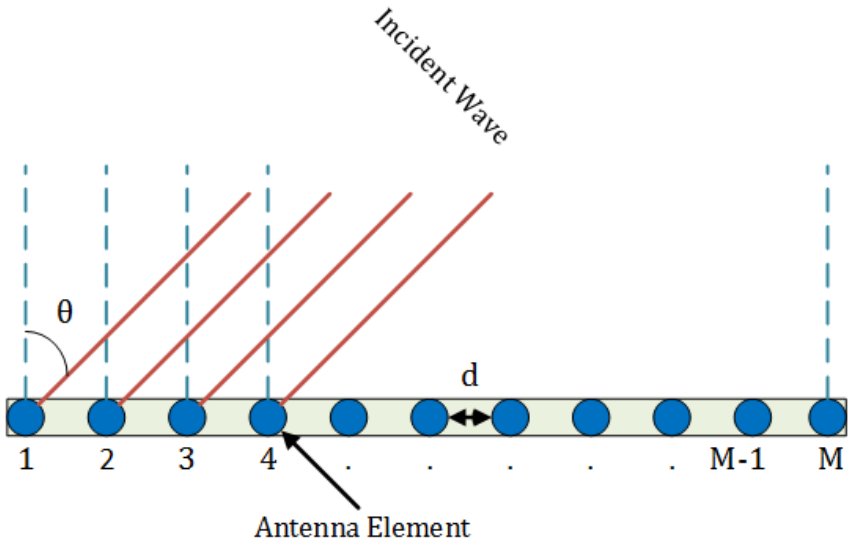

Fig. 5.2: A typical ULA with M elements, where, θ is the azimuth angle of arrival of the received signal

related back to quantify the property of Ψ. The singular values $\rho_1, ..., \rho_m$ (arranged in ascending order) of an $m \times n$ matrix Ψ are the positive square roots of the non-zero eigenvalues of the associated Gram matrix $Q = \Psi^*\Psi$. Singular values of Ψ can be used to introduce another quantifiable parameter known as the condition number, expressed in [93] as

$$\Upsilon(\Psi) = \frac{\rho_{max}}{\rho_{min}}, \tag{5.4}$$

where ρ_{min} and ρ_{max} are the smallest and largest singular values associated with the matrix Ψ. The condition number plays a vital role in providing a geometric interpretation of the action of the matrix. A matrix with a low condition number suggests a strong convergence to an accurate and unique solution to the problem defined in (1).

5.4 Problem Formulation

This section provides the system model for both antenna geometries.

5.4.1 Uniform Circular Array

Let us consider a planar array of M isotropic elements equally distributed around a circular ring of a UCA with radius r, and angular separation of $2\pi/M$ radians. The inter-element spacing $d_{UCA} = 2r\sin(\pi/M)$ is the length of the straight line between two adjacent antenna elements. The angular positions of the antenna elements in the UCA are represented by $\{\gamma_m\}$, where $\gamma_m = 2\pi(m-1)/M$. An electromagnetic plane wave impinges on the antenna elements from some unknown DOA θ. The incident signal is considered to be narrow-band. Under the following assumption, the complex voltage output of the antenna array can be written as

$$\mathbf{V_{UCA}} = \mathbf{A_{UCA}}(\theta)P_{UCA} + \boldsymbol{\eta_{UCA}}, \tag{5.5}$$

where $\mathbf{V_{UCA}}$ is the $M \times 1$ vector output associated with the impinging wave. The $M \times 1$ noise vector is $\boldsymbol{\eta_{UCA}}$ and the entries are assumed to be statistically independent and Gaussian distributed with zero mean and variance σ^2. The Complex envelope of the incoming signal is represented as P_{UCA}. In (5.5), the array response vector associated with an incoming signal from an unknown azimuth angle θ is given as

$$\mathbf{A_{UCA}}(\theta) = \left[e^{-jkr\cos(\theta)} \quad \dots \quad e^{-jkr\cos(\theta-\gamma_M)}\right].^T \tag{5.6}$$

The array response vector of a UCA (ARV_{UCA}) in (5.6) is the phase shift due to the increased travel distance of the incoming signal from an angle θ in reference to the first element when it is received by the mth element of the UCA. The angular wavenumber is k, where $k = 2\pi/\lambda$. The model assumes that the elevation angle $\psi = 0$ and that all the antenna elements are on the same plane. Fig. 5.1 shows the geometry of a UCA and the relative positioning of the antenna elements.

5.4.2 Uniform Linear Array

This work assumes a set of M isotropic antenna elements placed in a straight line with an inter-element spacing of $d = \lambda/2$, where λ is the signal wavelength. A travelling

plane wavefront impinges on the antenna elements from some unknown direction θ. The incoming wave satisfies the narrowband assumption that the phase difference between the upper and lower band edges of the propagation across the entire array is small. The complex output at the antenna array is given as

$$\mathbf{V_{ULA}} = \mathbf{A_{ULA}}(\theta)P_{ULA} + \boldsymbol{\eta_{ULA}}, \tag{5.7}$$

where $\mathbf{V_{ULA}}$ is an $M \times 1$ array output vector corrupted with noise. The $M \times 1$ noise vector is represented as $\boldsymbol{\eta_{ULA}}$ where the entries are statistically independent and Gaussian distributed with zero mean and variance σ^2, and P_{ULA} is the complex envelope of the source at the receiving array. In (5.7), $\mathbf{A_{ULA}}(\theta)$ is the $M \times 1$ array response vector (ARV) for an incoming plane wave from the direction θ and is generally given as

$$\mathbf{A_{ULA}}(\theta) = \begin{bmatrix} 1 & e^{-jk\sin(\theta)d_{ULA}} & \dots & e^{-jk\sin(\theta)(M-1)d_{ULA}} \end{bmatrix}.^T \tag{5.8}$$

The ARV_{ULA} in (5.8) represents the relative phases of the received signals at the antenna elements where $k = 2\pi/\lambda$ is the wavenumber or phase propagation factor. The aim of this work is to find the incident azimuth angle θ using the relative phase difference between the antenna elements. Fig. 5.2 shows the system model.

5.5 DOA estimation using Compressive Sensing

This section describes the formulation of a sparse problem that can be solved using compressive sensing techniques to recover the unknown azimuth angle θ of the source. The spatial coverage of a ULA antenna is in the range $[-\pi/2, \pi/2)$, whereas for a UCA the range is $[-\pi, \pi)$. The circular ring pattern of a UCA offers a wider angular coverage than that of a ULA. To incorporate the architecture of CS into the system model of the UCA and the ULA, the respective angular domain of coverage is quantized into N possible DOAs, where the phase contribution from each of the DOAs are used to create an overcomplete dictionary matrix. For a UCA, the N discrete angular points are represented as $\Theta_{UCA} = \{\hat{\theta}_n, 1 \leq n \leq N\}$. For a ULA, the sampled angular grid

points are represented as $\Theta_{ULA} = \{\tilde{\theta}_n, 1 \leq n \leq N\}$. The angular grid separations for both UCA and ULA are given as $\omega_{UCA} = 2\pi/N$ and $\omega_{ULA} = \pi/N$ respectively, where $\omega_{UCA} > \omega_{ULA}$. The ARVs in (5.6) and (5.8) associated with the N unique spatial grids, Θ_{UCA} and Θ_{ULA} can be combined to create two dictionary matrices described as

$$\mathbf{\Phi_{UCA}}(\Theta_{UCA}) = \left[\mathbf{A_{UCA}}(\hat{\theta}_1) \quad \cdots \quad \mathbf{A_{UCA}}(\hat{\theta}_N)\right], \tag{5.9}$$

$$\mathbf{\Phi_{ULA}}(\Theta_{ULA}) = \left[\mathbf{A_{ULA}}(\tilde{\theta}_1) \quad \cdots \quad \mathbf{A_{ULA}}(\tilde{\theta}_N)\right], \tag{5.10}$$

In Section 5.4, we established the relationship between the output of the antenna geometries and the DOA of the incoming signal. Using the definition of the dictionary matrices in (5.9) and (5.10), the complex voltage output of the antenna arrays in (5.5) and (5.7) can be rewritten as

$$\mathbf{V_{UCA}} = \mathbf{\Phi_{UCA}}(\Theta_{UCA})\mathbf{S_{UCA}} + \boldsymbol{\eta_{UCA}} \tag{5.11}$$

$$\mathbf{V_{ULA}} = \mathbf{\Phi_{ULA}}(\Theta_{ULA})\mathbf{S_{ULA}} + \boldsymbol{\eta_{ULA}} \tag{5.12}$$

where $\mathbf{S_{UCA}}$ and $\mathbf{S_{ULA}}$ are $N \times 1$ vectors of coefficients representing the complex envelope of the incoming signal. The structure of CS deals with the recovery of a sparse signal from measurements corrupted by noise, which makes a CS framework suitable for the DOA estimation problem. The systems of equation in (5.11) and (5.12) can be transformed into a CS problem similar to (5.1) in order to recover the two sparse vectors $\mathbf{S_{UCA}}$ and $\mathbf{S_{ULA}}$. The sparse vector recovery is a convex optimization problem described as

$$\hat{\mathbf{S}}_{\mathbf{UCA}} = \min_{\mathbf{S_{UCA}} \in \mathbb{C}^N} \|\mathbf{S_{UCA}}\|_0 \tag{5.13}$$

subject to

$$\|\mathbf{V_{UCA}} - \mathbf{\Phi_{UCA}}\mathbf{S_{UCA}}\|_2 < \epsilon_{UCA}$$

and

$$\hat{\mathbf{S}}_{\mathbf{ULA}} = \min_{\mathbf{S_{ULA}} \in \mathbb{C}^N} \|\mathbf{S_{ULA}}\|_0 \tag{5.14}$$

subject to

$$\|\mathbf{V_{ULA}} - \mathbf{\Phi_{ULA}} \mathbf{S_{ULA}}\|_2 < \epsilon_{ULA}$$

where $\|\cdot\|_0$ is the l_0-norm and ϵ_{UCA} and ϵ_{ULA} are the regularization parameter that is being determined by the noise or quantization level. Careful selection of the regularization parameter is crucial in sparse recovery of the signal. The outputs of the optimization problem defined in (5.13) and (5.14) are the reconstructed sparse vectors $\hat{\mathbf{S}}_{\mathbf{UCA}}$ and $\hat{\mathbf{S}}_{\mathbf{ULA}}$ that approximates the actual spatial vector $\mathbf{S}_{UCA}$ and $\mathbf{S}_{ULA}$. Due to the sparse condition, the recovered sparse vectors will contain a single dominating non-zero coefficient. The n^{th} index of the vector associated with the non-zero coefficient indicates the discrete angular grid point on which the source is located.

5.6 Analysis of the Dictionary Matrices

This section analyzed the impact of various antenna parameters such as number of antenna elements and inter-element spacing on the structure of the measurement matrices.

5.6.1 Impact of Antenna Elements

This section focuses on the impact of the number of antenna elements on the structure of the dictionary matrices, $\mathbf{\Phi_{UCA}}$ and $\mathbf{\Phi_{ULA}}$. As mentioned in Section 5.3, to enable a CS algorithms to successfully recovery of the sparse vector, it is crucial for the dictionary matrix to satisfy the strict RIP condition. Since verifying the RIP condition can be computationally expensive, properties such as mutual coherence and condition number will be used as a performance parameter for the dictionary matrices. For both UCA and ULA antenna geometries M is varied in the range $[6, 30]$ while the inter-element spacing between the antenna elements is $d_{UCA} = d_{ULA} = \lambda/2$, where λ is the

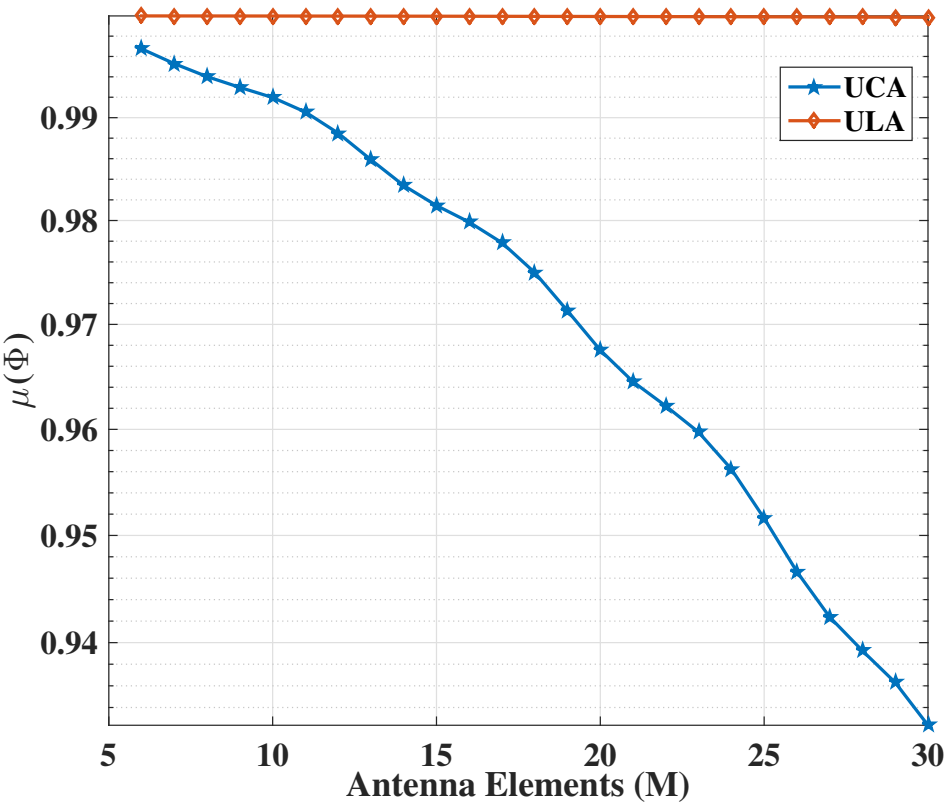

Fig. 5.3: Mutual coherence of Φ_{UCA} and Φ_{ULA} as a function of the number of antenna elements M.

wavelength of the incoming signal. The mutual coherence of the dictionary matrices is calculated using (5.2). Fig. 5.3 shows the variation of the mutual coherence of the two dictionary matrices with respect to increasing M. From the graph, it is evident that the mutual coherence of the UCA geometry decreases as M increases. This indicates that the columns of Φ_{UCA} are highly independent when M is a maximum. On the other hand, in case of ULA, there is no significant impact of M on the mutual coherence of Φ_{ULA}. Although there is a slight reduction in $\mu(\Phi_{ULA})$, when compared to $\mu(\Phi_{UCA})$, the change is insignificant. The analysis suggests that the columns of Φ_{UCA} are highly independent, enabling CS-based DOA estimation algorithms to precisely detect the incoming DOA.

The next set of analysis focuses on a condition number analysis of the dictionary matrices. The condition numbers ($\Upsilon(\Phi_{UCA})$,$\Upsilon(\Phi_{ULA})$) for the antenna geometries are

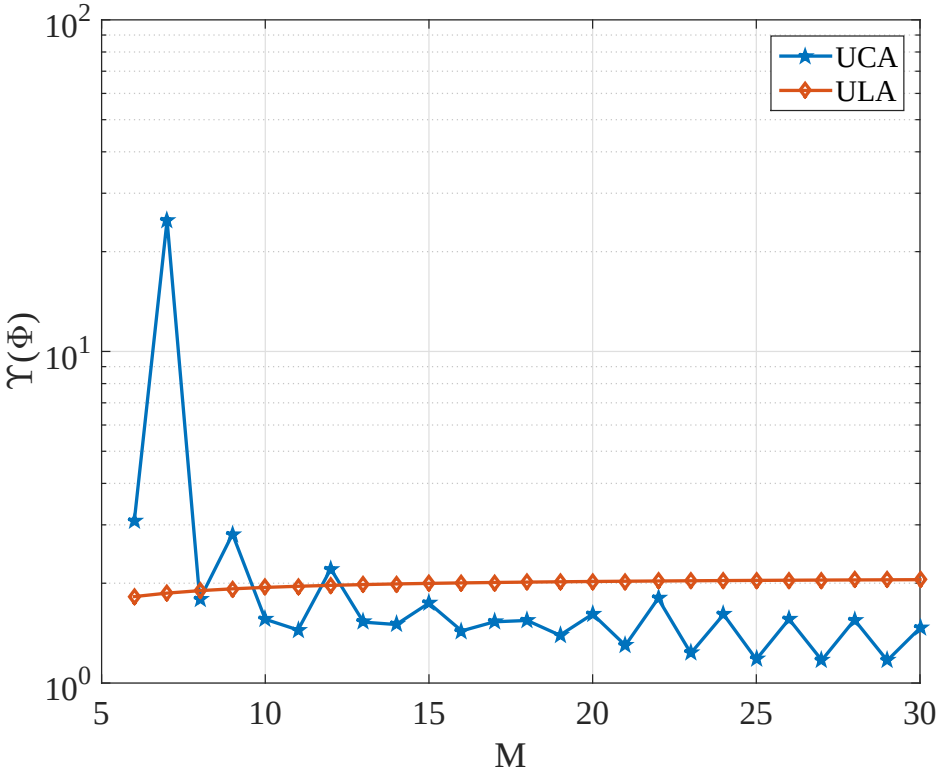

Fig. 5.4: Mutual coherence of Φ_{UCA} and Φ_{ULA} as a function of the number of antenna elements of the antenna geometries.

calculated using (5.4) in Section 5.3. The plots in Fig. 5.4 have a different trend than that of Fig. 5.3. For smaller M (i,e. $M < 10$) $\Upsilon(\Phi_{UCA}) > \Upsilon(\Phi_{ULA})$, suggesting that Φ_{UCA} is ill-conditioned compared to Φ_{ULA}. However, when $M > 12$ $\Upsilon(\Phi_{UCA})$ drops while $\Upsilon(\Phi_{ULA})$ remains unchanged. This shows that M has a higher influence on the mutual coherence of Φ_{UCA} than on that of Φ_{ULA}

5.6.2 Impact of Inter-Element Spacing

Another crucial parameter influencing the construction of the measurement matrix is the inter-element spacing between the antenna elements. Conventional theory on antenna design suggests having an inter-element separation, $d_{UCA} = d_{ULA} \in [\frac{\lambda}{2}, \lambda]$, between the antenna elements to avoid ambiguity between the ARVs of distinct DOAs [82]. This section discusses the impact of d_{UCA} and d_{ULA} on the mutual coherence of the

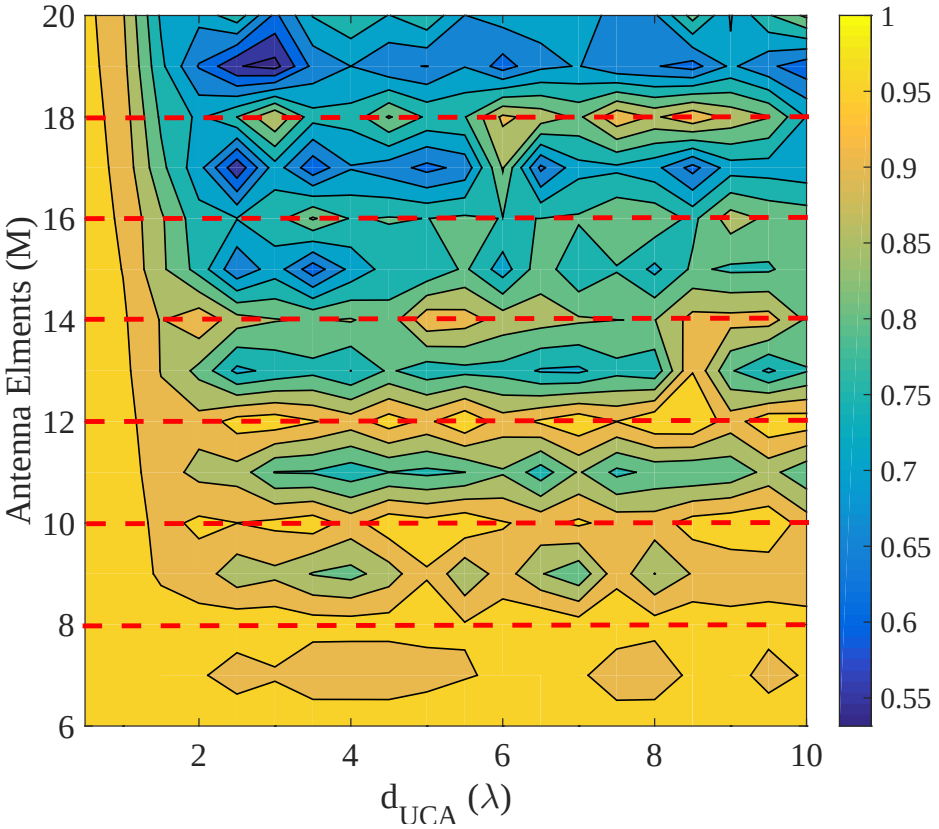

Fig. 5.5: Impact of the number of antenna elements M and the inter-element spacing d_{UCA} on $\mu(\Phi_{UCA})$.

dictionary matrices, Φ_{UCA} and Φ_{ULA} respectively. A contour plot is presented, where the mutual coherence of Φ_{UCA} and Φ_{ULA} are calculated as a function of the number of antenna elements M and the inter-element spacing d_{UCA} and d_{ULA} respectively. For this simulation, the inter-element spacing $d_{UCA} = d_{ULA}$ is a varied in the range $[\lambda/2, 10\lambda]$, whereas M is in the range [6, 20]. The ARV for UCA represented as $\mathbf{A_{ULA}}$ in (5.6) relies on the radius, r of the UCA instead of the inter-element spacing d_{UCA}. The expression for d_{UCA} in Section 5.4 can be rearranged to find an expression for the radius as

$$r = \frac{d_{UCA}}{2\sin(\pi/M)}.$$

Fig. 5.5 and 5.6 shows the variation of $\mu(\Phi_{UCA})$ as a function of the number of

antenna elements M and the inter-element spacing d_{UCA}. First, we will discuss the UCA antenna geometry. In Fig. 5.5, for all M and $d_{UCA} < 2\lambda$, $\mu(\Phi_{UCA})$ takes on high values in the region between 0.9 and 1.0. However, for $d_{UCA} > 2\lambda$, more blue patches can be observed, indicating a reduction in the coherence. It can be seen that the blue patches are more consistent with variation in d_{UCA} especially when M is odd. For an increase in odd M (7,9,11...), the reduction in mutual coherence is much sharper than for even M (8,10,12...), especially when $d_{UCA} > 2\lambda$. On a closer observation it can be seen that, with careful consideration of d_{UCA}, $\mu(\Phi_{UCA})$ for $M = 11$ can be reduced by a factor of 10 when compared with $M = 12$. A red dotted line has been drawn on the contour to differentiate the impact of even numbered M from the odd counterparts. This phenomenon is due to the centro-symmetric property of the UCA, which causes the columns of Φ_{UCA} to be indistinguishable, especially when M is even. A detailed analysis on this topic is provided in in Chapter 3. Moreover, the contour indicates that $d_{UCA} = \lambda/2$ might not be the most suitable inter-element spacing as mentioned in prior research on UCA geometry. The plot shows that, for odd M, a proper selection of inter-element spacing ($d_{UCA} > \lambda/2$) can significantly reduce the mutual coherence of the dictionary matrix. A low mutual coherence enables the CS algorithm to efficiently utilize the columns of a dictionary matrix in order to recover a sparse vector. Especially, in CS-based estimation algorithms, the sparse vector can be recovered with high precision, simply by reducing the mutual coherence of Φ_{UCA}. From the analysis, it can be concluded that the contour plot for Φ_{UCA} provides useful information that can be exploited to construct a dictionary matrix that enhances the performance of CS operations. On the other hand $\mu(\Phi_{ULA})$ responds in a different way to the variation of M and d_{ULA} as shown in Fig. 5.6. The blue areas on the contour in Fig. 5.6 are almost close to 1, indicating maximum coherence among the columns of Φ_{ULA}. The contour also shows that the inter-element spacing d_{ULA} between the antenna elements has limited impact on $\mu(\Phi_{ULA})$. Similarly, there is no evidence to indicate any influence of M on $\mu(\Phi_{ULA})$. The contour plots in Fig. 5.5 and Fig. 5.6 provide a comparison between the two antenna geometries. The result indicates that Φ_{UCA} is more robust and have the advantage of regions of low mutual coherence,

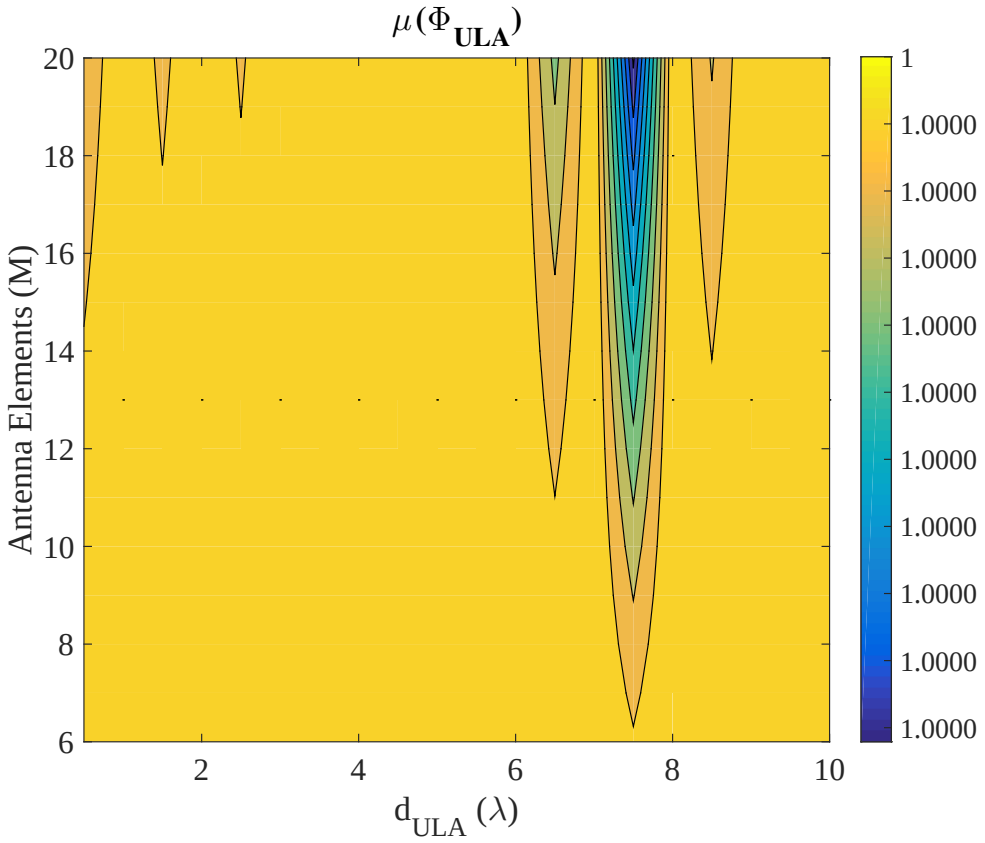

Fig. 5.6: Impact of the number of antenna elements M and the inter-element spacing d_{ULA} on $\mu(\Phi_{ULA})$.

offering maximum utilization of the column space.

5.7 Simulation Results

This section aims to provide an insight into the key performance parameters of the two antenna array geometries when integrated with a CS-based DOA estimation algorithm. Iterative compressive sensing direction of arrival (ICSDOA) estimation algorithm is a novel approach proposed to precisely deduce the incoming angle of arrival of a transmitting source. The algorithm provides a fundamental breakthrough in CS-based estimation techniques by completely eliminating the error due to grid quantization. The algorithm is highly convergent and can be cast into any CS-based estimation algorithms. A detailed description of the proposed ICSDOA algorithm is presented in

Chapter 3 and Chapter 4. The simulation consists of one source, where the signal impinges from any angle in the range $[-\pi/2, \pi/2)$ radians. For the purpose of a fair comparison between the two antenna array geometries, UCA and ULA, the possible angular range of coverage is restricted to $[-\pi/2, \pi/2)$ radians. The signal is assumed to arrive at the antenna elements with equal magnitude in order to perform an unbiased analysis of the accuracy of the method with respect to the angle of arrival.

5.7.1 SNR and CRLB

In order to determine the robustness of our system model, the following noise sensitivity test has been considered. The Signal-to-Noise Ratio (SNR) is calculated at the receiver as the ratio of the sum of the powers received from the M antenna elements to σ^2, where σ^2 is the variance of the complex Gaussian noise. The measured data are characterized by the SNR in dB, defined as

$$\text{SNR} = 10\log_{10}\left[\frac{\sum_{m=1}^{M}|v_m|^2}{M\sigma^2}\right] \tag{5.15}$$

where v_m, $m = 1, ...M$, is the noiseless complex output at the m^{th} antenna element of the respective antenna geometry. To validate the performance of the antenna geometries in accurately estimating an angle of arrival, U different DOAs are chosen from a uniform distribution. For statistical consistency, I Monte Carlo trials are carried out. Compressive Sampling Matching Pursuit (CoSaMP) has been used as the platform for carrying out the CS operation in the proposed ICSDOA algorithm. The Performance parameter of the algorithm is characterized as the Mean Square Error (MSE), where MSE for the antenna geometry is defined as

$$\text{MSE} = \frac{\sum_{u=1}^{U}\sum_{i=1}^{I}|\theta_{org,u,i} - \theta_{est,u,i}|^2}{UI} \tag{5.16}$$

where $\theta_{org,u,i}$ is the original DOA of the source and $\theta_{est,u,i}$ is the DOA of the source estimated for the u^{th} scenario and the i^{th} Monte Carlo trial. The MSE of the proposed algorithm will be compared with the Cramér-Rao lower bound of the UCA and ULA,

given in [149] as

$$\text{CRLB}_{\text{UCA}} \geq \frac{\sigma^2}{Mk^2r^2}, \tag{5.17}$$

$$\text{CRLB}_{\text{ULA}} \geq \frac{\sum_{u=1}^{U} \frac{6\sigma^2}{M(M^2-1)\pi^2\cos^2(\theta_{org,u})}}{U} \tag{5.18}$$

where M, k and r are defined in Section 5.4. An estimator achieving the CRLB is considered to be efficient and it is not possible for any estimator to perform better than the theoretical CRLB.

5.7.2 Effect of Grid Quantization

Firstly, we will discuss the impact of the number of angular grid points N on the MSE performance of each of the antenna geometries (UCA and ULA). The computational complexity of the proposed ICSDOA algorithm in terms of big-O notation, is given as $O(5MN)$[179]. This means that for a constant M, the complexity is directly dependent on N. In order to carry out this simulation, $U = 10$ DOAs are randomly selected from a uniform distribution, given that the DOA falls in the angular coverage of both UCA and ULA. For statistical validation, $I = 2000$ monte carlo runs are carried out. Four cases are considered where each of the antenna geometries is constructed with $M = 9$ and 13 antenna elements respectively. For simplicity, the four antenna structures are represented as UCA-9, UCA-13, ULA-9 and ULA-13. The inter-element spacing between the elements $d_{UCA} = d_{ULA} = \lambda/2$, where λ is the wavelength of the received signal. The number of angular grid points is varied in the range $[45, 90, 180, 360]$, where $N = 45$ is a coarse quantization and $N = 360$ represents finer quantization. The SNR for the simulation is kept constant at 15 dB. According to (5.17) and (5.18), the CRLB of ULA and UCA is dependent on the number of antenna elements (M). To evaluate the influence of N on each of the four different antenna structures a new performance parameter, Error Ratio (ER), has been introduced such that

$$\text{Error Ratio (dB)} = 10\log_{10}\left(\frac{\text{MSE}}{\text{CRLB}}\right), \tag{5.19}$$

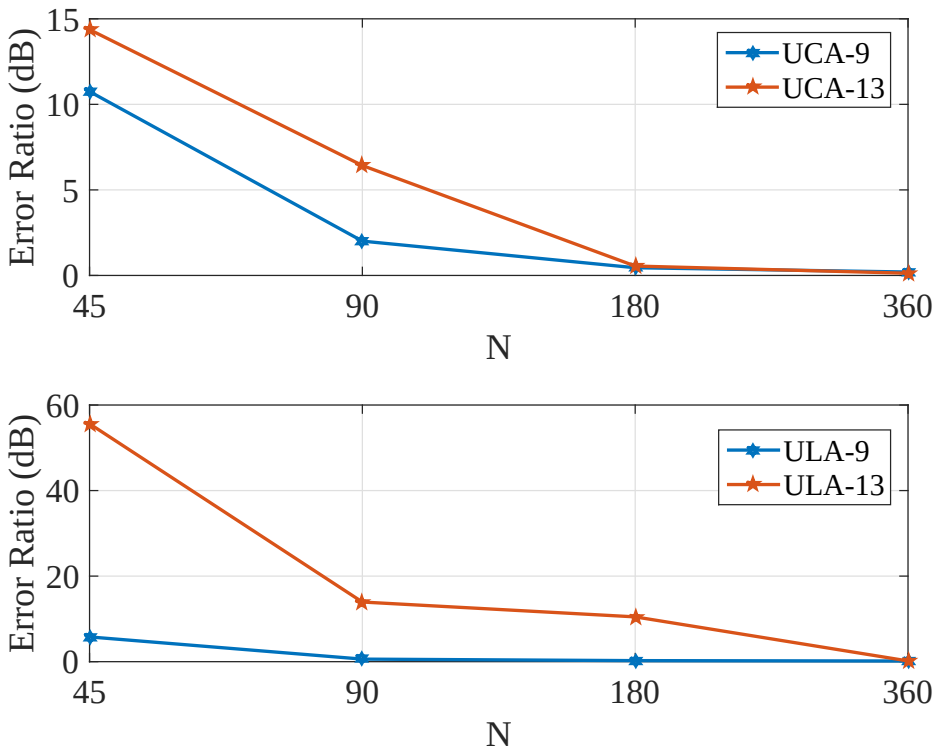

Fig. 5.7: (a) Error Ratio of UCA antenna geometries as a function of N. (b)Error Ratio of UCA antenna geometries as a function of N.

where CRLB represents the theoretical lower bound for the particular antenna geometry. In (5.19), the ER provides a ratio of the MSE of an estimate against the respective CRLB of the antenna structure. Moreover, the parameter provides an indication of the deviation of the MSE from the theoretical bound. A higher ER suggests that the estimate is inaccurate and is moving away from the respective error bound. Fig. 5.7 consists of two subplots with UCA results at the top and ULA at the bottom. For UCA, the ER for both UCA-9 and UCA-13 decreases monotonically with an increase of M. This means that, with finer quantization of the spatial domain, the ER is extremely close to zero, suggesting that the MSE of the estimate is on the CRLB of the respective antenna structure. However with coarser quantization of the angular grid (i,e. $N < 90$), the ER jumps up, with UCA-13 having a higher ER than UCA-9. The

nature of the plots can be associated with under-sampling of the angular grid which makes UCA-9 more insensitive to a variation in the quantization level than UCA-13. The details of the analysis are presented in Chapter 3 and 4. The subplot for ULA in the bottom of Fig. 5.7 have a similar trend to the previous plot. However, the difference in ER values between ULA-9 and ULA-13 is much higher than with its the UCA counterpart. When examined closely, the plot for ULA-13 approaches zero ER with $N = 360$ whereas UCA-13 achieves a similar mark with a coarser grid quantization of $N = 180$. This can be attributed to low mutual coherence of (Φ_{UCA}) as discussed in Section 5.5. A lower mutual coherence enables CS to take full advantage of the column space of the dictionary matrix. This helps CS to accurately resolve the coefficients of the sparse vector even with smaller N, hence reducing the computation complexity of the estimation process. The analysis gives a clear indication of the advantages of the UCA antenna geometry over ULA geometry in estimating an incoming DOA, especially with large M and smaller N. Moreover, the result also portrays the highly sensitive nature of the ULA antenna constructed with large M, as it requires finer quantization of the angular domain (large N) in order to approach its respective CRLB.

5.7.3 Comparison of DOA estimation

The next set of simulations aim to provide insight into the MSE performance of each of the two antenna array geometries under the influence of varying SNR. The MSEs of the estimation are compared to the theoretical CRLBs of the respective antenna geometries. The novel ICSDOA algorithm is used to estimate the DOA of the incoming signal. Similarly to the previous simulation in Section 5.7.2, $U = 10$ DOAs are randomly chosen, with an assumption that the DOAs are the in the range $[-\pi/2, \pi/2)$. The number of Monte Carlo runs for each DOAs is set to $T = 5000$. Two antenna geometries are considered, where both UCA and ULA are constructed with $M = 9$ antenna elements with an inter-element separation of $d_{UCA} = d_{ULA} = \lambda/2$. The number of angular grid points for UCA and ULA is set to be $N_{UCA} = N_{ULA} = 180$, with grid interval $\omega_{UCA} = 2\pi/N_{UCA}$ and $\omega_{ULA} = \pi/N_{ULA}$ respectively. The graph in Fig. 5.8

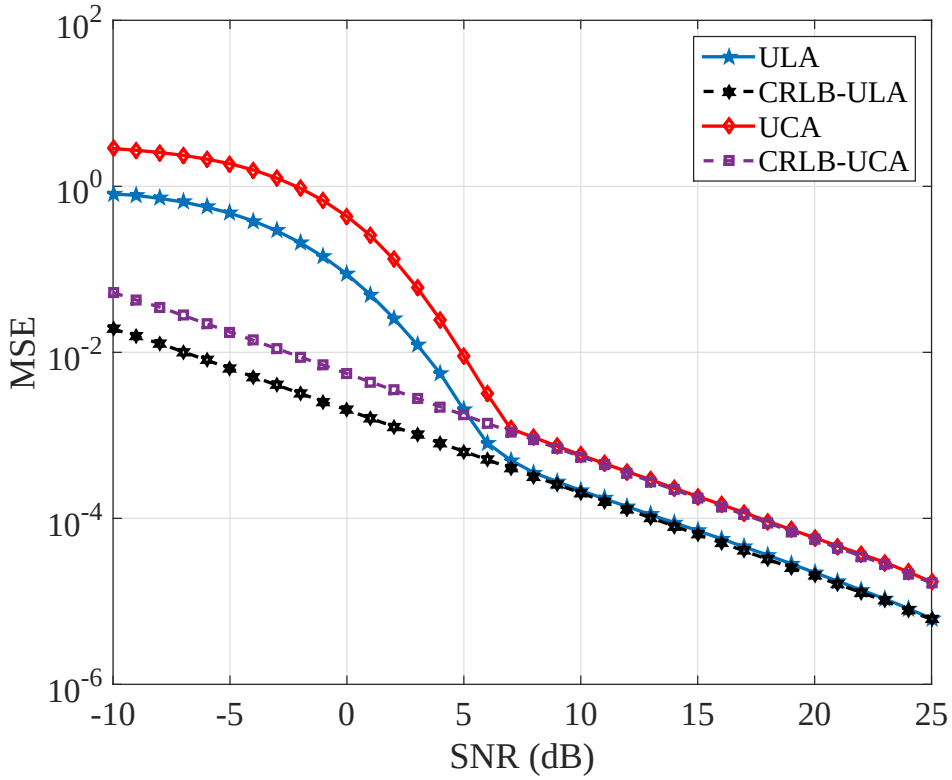

Fig. 5.8: MSE performance comparison of the two antenna geometries with integrated with the ICSDOA estimation algorithm.

shows four plots where the red and blue plots represent the MSE performance of UCA and ULA respectively. On the other hand, the CRLB for both UCA and ULA are shown with the purple and black plot respectively. From the graph, it is clear that the CRLB of ULA is lower than that of UCA. The results clearly match the expressions of CRLBs in (5.17) and (5.18). In (5.18) it can be seen that the CRLB_{ULA} of the error is inversely proportional to $(M(M^2-1))$, given that the remaining parameters are constant. On the other hand the CRLB_{UCA} is inversely proportional to M. This provides an advantage to the ULA geometry in lowering the MSE of the estimation by a factor of M^2. The MSE plots for both the antenna geometries behave in a similar fashion, dipping off at approximately SNR = 6 dB and continuing to be on the CRLBs for higher SNR. For SNR $<$ 5 dB, the MSEs are relatively higher than the CRLBs with ULA having a lower MSE than UCA. The high MSE at low SNR regions can be associated with the inaccurate coarse estimate of the ICSDOA algorithm, where the

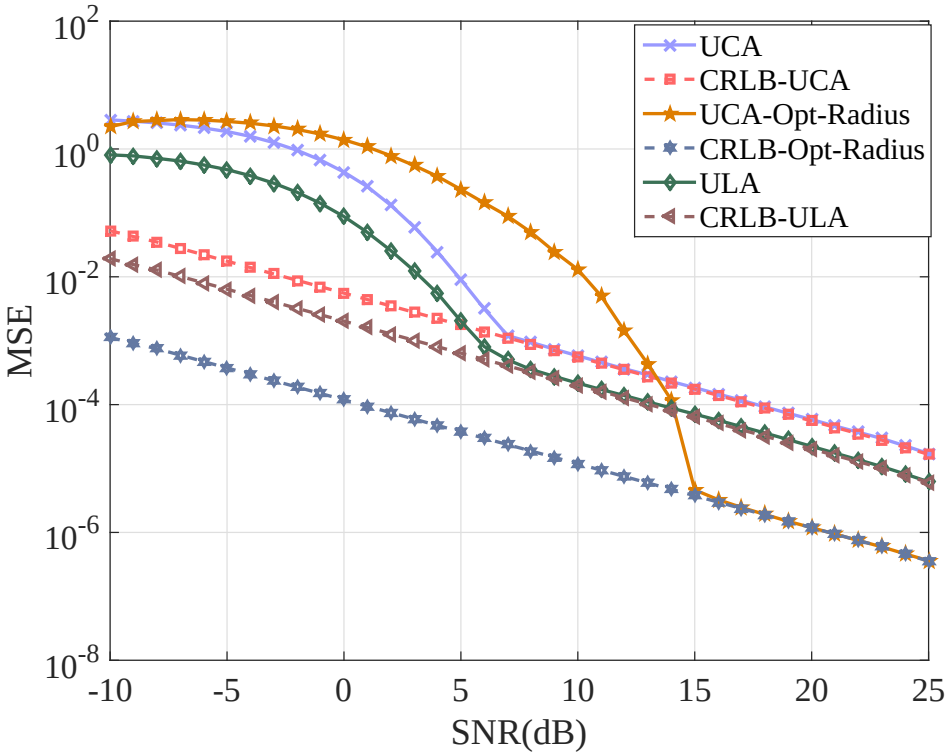

Fig. 5.9: MSE performance comparison between UCA constructed with r^{opt}, UCA constructed with $r^{\lambda/2}$ and ULA constructed with inter-element spacing of $\lambda/2$

underlying CS operation fails to detect the angular grid on which the source is located. The result illustrates an in-depth analysis of the MSE performance comparison of two different phased antenna array geometries when integrated with a CS-based DOA estimation algorithm.

The analysis from Section 5.6.2 proves careful exploitation of the radius of a UCA geometry can yield a modified measurement matrix with a minimum mutual coherence among the columns. Especially, in the CS-based estimation algorithm, minimum mutual coherence is crucial in effectively utilizing the column space of the matrix resulting in an estimate with a low MSE. To verify the theory presented in Section 5.6.2, a new plot has been added to the results in Fig. 5.8. The new plot in Fig. 5.9 refers to a new UCA constructed with $M = 9$ antenna elements and inter-element spacing $d_{UCA} \approx 4\lambda$ ($r = 5.5\lambda$). The antenna parameter d_{UCA} is selectively chosen by analyzing the contour plots in Fig. 5.5 with $M = 9$. The number of grid points $N_{UCA} = 180$ is kept constant

similar to the previous simulation. The plot for UCA-Opt-Radius drops off at higher SNR = 15 dB compared to SNR = 6 dB for the other two plots. However, for SNR > 15 dB, the MSE of UCA-Opt-Radius stays on its respective CRLB. The error bound for the modified UCA is 16 dB and 10 dB lower than CRLB-UCA and CRLB-ULA respectively. This result confirms the influence of $d_{UCA} > \lambda/2$, in reducing the mutual coherence and hence improving the accuracy of the DOA estimate. However, in the SNR region, $[-10dB, 15dB]$ a traditional antenna geometry with $d_{UCA} = d_{ULA} = \lambda/2$ shows superior MSE performance to the modified UCA. Moreover, due to the large radius size, the area of UCA-Opt-Radius increases by a factor of 25 in comparison to a traditional UCA. It can be concluded that with a careful exploitation of the inter-element spacing of a UCA geometry, we can achieve an MSE performance much lower than ULA at the expense of high SNR and a large antenna area.

5.8 Conclusion

In this paper, we investigate the performance of two antenna geometries, namely UCA and ULA in accurately estimating the DOA of an incoming signal that achieves the theoretical CRLB. The estimation algorithm is based on a CS approach that offers superior results with a single snapshot of the incoming signal. Simulation results show that, ULA offers a better DOA estimate than UCA, given that the incoming DOA is in the broad-side region of the antenna geometry. However, an in-depth analysis on the influence of the antenna parameters on the structure of the dictionary matrices is also presented. The investigation illustrates that a UCA with an odd number of antenna elements and an optimum antenna radius significantly reduces the mutual coherence of the dictionary matrix. The improved structure of the dictionary matrix enables a UCA to emhance the DOA estimation accuracy by 16 dB than that of a ULA. Moreover, the impacts of the angular grid resolution on the DOA estimate for the two antenna geometries are separately studied. The result suggests that a ULA with a large number of antenna elements M is sensitive to a lower grid resolution and requires a finer grid quantization to achieve its respective CRLB.

6

Multiresolution Compressive Sensing Algorithm to Detect Off-Grid Direction of Arrival.

6.1 Abstract

The Direction of Arrival (DOA) techniques has been widely used in a variety of applications such as radar, sonar and image processing. Especially in military communication, precise estimation of the DOA, incorporated with smart beam-forming techniques, can provide useful solutions for interference mitigation and jammer identification. Traditional DOA estimation techniques require a large number of snapshots of the incoming

signal to accurately deduce the DOA of an impinging wave, which can significantly increase the computational complexity of the algorithm. We propose a novel Compressive Sensing (CS) based DOA detection algorithm, which is independent of the transmitter being located at a quantized grid point and uses fewer snapshots than the Beam-Scan algorithm to detect the DOA. We evaluated the Mean Square Error (MSE) in estimating the off-grid DOA. Simulation results suggest that the proposed algorithm achieves a reduction in MSE by a factor of ten when compared to the high-resolution Beam-Scan technique.

6.2 Introduction

Over the years, the field of Direction of Arrival (DOA) estimation has witnessed a great surge in research outcomes, mostly due to the immense popularity of smart beam-steering techniques. Smart beam-steering enhances the sensitivity to a particular signal while suppressing other unwanted signals. Apart from beam-forming, precise DOA estimation plays a pivotal role in a wide range of applications such as wireless communications, radar, and medical imaging. Especially in wireless, precise estimation of the DOA of a signal is of paramount importance in an effort to reduce the effect of interference from undesirable transmissions.

DOA estimation techniques integrated into a Cognitive Radio Network (CRN) can provide cutting-edge solutions to the existing issue of spectrum scarcity, especially in the case of the highly dense 5G mobile networks. In CRN a 360° angular domain may be evenly sectorized into N spatial slots. The dedicated spatial slots allow primary/licensed and secondary/unlicensed users to be spatially multiplexed simultaneously into the same channel. This results in an uninterrupted communication between users (primary/secondary), hence increasing the throughput of the overall network in a specific geographical region.

Compressive Sensing (CS) has gained in popularity in signal processing due to the effectiveness of CS in recovering a sparse signal with minimum measurements [64].

The computationally inexpensive technique motivated researchers to explore DOA estimation as a sparse recovery problem [174][107]. In comparison to traditional DOA estimation techniques such as Root Multiple Signal Classification (Root-MUSIC) [97] and Beam-scan [180], CS-based DOA estimation techniques are more attractive due to their ability to resolve closely placed sources with few snapshots, and providing guarantees for obtaining an optimum global solution via convex relaxation [64].

Many CS based DOA [106][163] estimation problems are modeled under the assumption that the continuous angular domain is discretized with N sampling grids and the users are located strictly on a subset of the grids. The assumption provides a simple model, however, it fails to address the underlying practical problem, where a user may be located anywhere off the quantized grid. A weighted average technique was proposed in [129] which exploits the amplitude of the neighboring grids to deduce the original off-grid DOA. Unfortunately, in cases when the peaks do not appear on the neighboring grids, the error for estimating off-grid DOA becomes large. Finer resolution of grids using larger N can be a possible solution to the problem, but as the system of equations is under-defined, a large N will introduce significant rank deficiency and hence degrade the performance of CS [162].

In this paper, we propose a novel Multi-Resolution DOA (MRDOA) detection algorithm, based on CS, to estimate the DOA of a signal arriving from an off-grid source. The first stage of the algorithm focuses on obtaining a sparse solution using convex optimization, where the index of a non-zero coefficient indicates the neighboring grid closest to the original off-grid DOA. The closest grid with the maximum peak is retrieved, then in the next stage, a finer search is carried out on the adjacent grid points. The sequential search will continue until the angular grid separation is less than some user-defined threshold. The estimation problem is formulated with a Uniform Circular Array (UCA) antenna, as a receiving node, on which electromagnetic plane waves arrive from unknown directions. The fact that UCA has a symmetrical geometry and no edge elements greatly reduces the impact of mutual coupling [148]. Both Mean Square Error (MSE) and computational complexity are considered to evaluate the performance of MRDOA. Simulation results suggest that MRDOA appears to achieve a

superior estimation of off-grid DOA in comparison to high-resolution Beam-scan technique. MRDOA also offers lower computational complexity compared to conventional CS techniques using denser grid. Section 6.3 discusses the background of compressive sensing. Sections 6.4-6.5 describe the system model. The algorithm and the integration of transform matrix are presented in Section 6.6 and 6.7. Section 6.8 presents the simulation results which validate the effectiveness of our proposed method. The conclusion is given in Section 6.9.

6.3 Compressive Sensing

The Compressive Sensing technique is an approach to obtain a solution of an under-determined set of equations, for which the solution vector is known to be sparse. A typical example would be the time-frequency pair. A signal which is a linear combination of several frequency components can be easily retrieved by exploiting the sparsity in the frequency domain. The complex Fourier Transform basis functions can be used to represent the time domain signal with a few non-zero coefficients. In such a case the CS algorithm can be used to obtain a sparsest solution vector to a set of under-determined equations. The sparse vector $x_{N\times 1}$ is the solution with the minimum number of non-zero elements. If $y_{M\times 1}$ is the raw observation vector, there exists the following relationship,

$$y = \Phi x, \tag{6.1}$$

where $\Phi_{M\times N}$ is a measurement or dictionary matrix. The theory in [64] and [162] states that, a matrix Φ satisfies *Restricted Isometry Property* (RIP) condition, when all subsets of S columns chosen from Φ are nearly orthogonal. Once this is true, there is a high probability of completely recovering the sparse vector with at least $M = C \times K \times \log_e(N/K)$ measurements (where K is the number of PUs and C is a positive constant) using the l_1-minimization algorithm [64]. This can be can be

expressed as,

$$\min \|\vec{x}\|_1 = \min \sum_i |x_i|$$

subject to

$$\vec{y} = \Phi\vec{x}.$$

In case of external noise the algorithm is modified to a *Second-Order Cone Program* for an optimized solution for a defined threshold ζ. This can be stated as,

$$\min \|\vec{x}\|_1 = \min \sum_i |x_i|$$

subject to

$$\|\vec{y} - \Phi\vec{x}\|_2 \leq \zeta, \tag{6.2}$$

where $\|\cdot\|_p$ is the l_p-norm and ζ is the relaxation constraint for measurement errors. The sparsest solution for $\vec{x}$ is the solution with minimum $\|\vec{x}\|_0$. However, the CS algorithm is effective because the same solution vector usually has the minimum l_0-norm and minimum l_1-norm [64].

6.4 Problem Formulation

Let us consider a planar array of M isotropic elements equally distributed around a circular ring UCA with radius r and angular separation of $360°/M$. The inter-element spacing $d = 2r\sin(\frac{180°}{M})$, is the length of the straight line between two adjacent antenna elements. The angular positions of the antenna elements in UCA are represented by γ, where $\gamma_m = 2\pi(m-1)/M$. A set of P electromagnetic plane waves impinges on the antenna elements from some unknown DOAs. The incident signals are considered to be narrow-band and characterized by the same frequency content. The narrow-band assumption states that all frequencies in the observed band B cause the same phase shift when the Centre Frequency (CF) $f_c \gg B$. This simplifies the construction of the steering vector given below in 6.4. At the sensor location, the electromagnetic field

induces a complex voltage v_m, which can be assumed to be a linear combination of the plane waves arriving at the mth antenna element. The open-circuit voltage at the mth antenna element from P transmitters can be expressed as [171],

$$v_m = \sum_{i=1}^{P} I_i^{inc} e^{-j\tau_m(\theta_i)} \tag{6.3}$$

where,

$$\tau_m(\theta_i) = \beta r \cos(\theta_i - \gamma_m) \tag{6.4}$$

and,

I_i^{inc} is the electric field associated with the ith impinging wave,

β is the angular wavenumber $(2\pi/\lambda)$,

r is the radius of the UCA,

θ_i is the angle of arrival of the ith incident wave,

γ_m is the angular position of the mth element,

λ is the free space wavelength of the wave.

τ_m is the phase shift of the incoming signal referred to the first element, while it is being received by the mth element of the UCA. A typical UCA geometry is shown in Fig. 6.1.

6.5 DOA estimation using Compressive Sensing

This section combines the received open-circuit voltage information at each antenna element to formulate a sparse matrix problem, which may be solved using CS techniques to identify the DOAs of target PUs in a CRN. To incorporate the architecture of CS into the system model, angular space is discretized into N possible DOAs, $\hat{\boldsymbol{\theta}} = \{\hat{\theta_n}, \quad 1 \leq n \leq N\}$, where N denotes the number of grid points. Suppose we have P target DOAs, $\bar{\boldsymbol{\theta}} = \{\bar{\theta_p}, \quad 1 \leq p \leq P\}$, where $P \ll N$. Considering the practical implementation of the

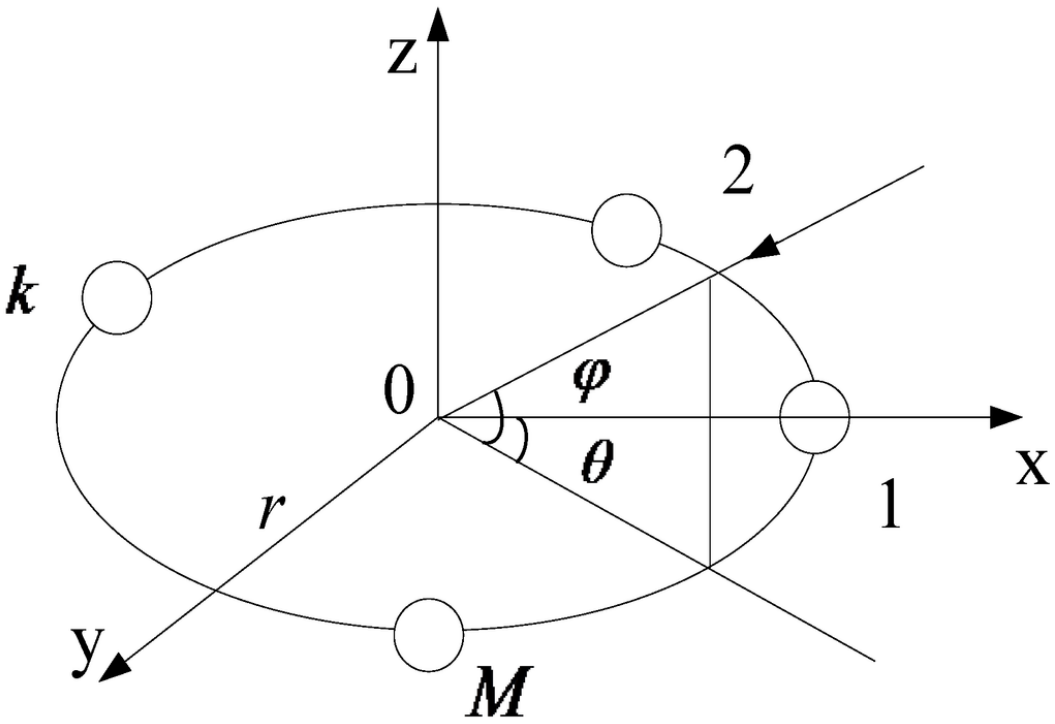

Fig. 6.1: A typical UCA with M elements, where θ and ϕ represent azimuth an elevation angles of a received signal.

model, P target sources are stationed randomly in a continuous angular domain. Unlike in other papers [174][107], PUs are not restricted to be positioned on grid points only, rather they can be positioned anywhere in a 360° angular region. Earlier, in Section 6.4, we established the relationship between the open-circuit voltage observation at each antenna element and the DOA from a target. In matrix form, (6.3) can be rewritten as

$$V = D(\hat{\boldsymbol{\theta}})I \tag{6.5}$$

where,

$$D(\hat{\boldsymbol{\theta}}) = \begin{pmatrix} e^{-j\tau_1(\hat{\theta}_1)} & e^{-j\tau_1(\hat{\theta}_2)} & \dots & e^{-j\tau_1(\hat{\theta}_N)} \\ e^{-j\tau_2(\hat{\theta}_1)} & e^{-j\tau_2(\hat{\theta}_2)} & \dots & e^{-j\tau_2(\hat{\theta}_N)} \\ \vdots & \vdots & \ddots & \vdots \\ e^{-j\tau_M(\hat{\theta}_1)} & e^{-j\tau_M(\hat{\theta}_2)} & \dots & e^{-j\tau_M(\hat{\theta}_N)} \end{pmatrix} \tag{6.6}$$

and, $V = \{v_m,\ \ 1 \leq m \leq M\} \in \mathbb{C}^{M\times 1}$, is a one dimensional column vector representing the complex voltage measurements at each antenna element of the UCA. $D(\hat{\boldsymbol{\theta}}) \in \mathbb{C}^{M\times N}$

is the dictionary matrix, where $\tau_m(\hat{\theta}_n)$ is calculated using (6.4). The entries of $D(\hat{\boldsymbol{\theta}})$ represent the phase shift introduced on the mth antenna element, for a wave arriving from the nth DOA. $I = \{I_n^{inc},\ \ 1 \leq n \leq N\} \in \mathbb{C}^{N\times 1}$ is the column vector, that is to be recovered using the CS technique. In a realistic scenario, the voltage observations in (6.5) are corrupted with a noise vector $P_n \in \mathbb{C}^{M\times 1}$. The entries of P_n are statistically independent and are extracted from a complex Gaussian distribution with zero mean and variance σ^2. The effect of noise on the voltage observations can be expressed as

$$V_n = D(\hat{\boldsymbol{\theta}})I + P_n. \tag{6.7}$$

Since the model assumes having only one PU ($N \gg P$) on a large angular grid of size N, we may consider $I_{N\times 1}$ as a sparse vector which satisfies the requirement for an accurate recovery using the CS algorithm. Due to the sparse nature of the solution, the vector will have only one nonzero element, representing the complex voltage induced by the impinging wave, while the index corresponding to the non-zero element indicates the angular grid on which the transmitting PU is located. Equation (6.7) can be formulated as a Second-order Cone Program discussed earlier in Section 6.3, to obtain an optimized solution for a user-defined threshold using (6.2).

6.6 Multi-resolution approach of DOA Estimation

The optimized sparse vector obtained in (6.7) enable us to detect the DOA of a PU located on the grid. However, it fails to detect a PU positioned in-between the quantized grid points. In such cases, due to dictionary mismatch, the optimized solution vector tends to generate peaks at neighboring grids, closer to the original off-grid DOA. This suggests that the solution in (6.7), converges to the closest neighboring grid points as shown in Fig. 6.2. The Weighted-centroid technique in [129] uses the peaks of two adjacent neighboring grids to estimate the original off-grid DOA. However, in cases when the two peaks (red) do not appear strictly on either side of the original peak (blue), the error in estimating off-grid DOA becomes significantly large. Our novel

Multi-Resolution based DOA algorithm (MRDOA) aims to exploit the peak with maximum amplitude to determine the DOA from an off-grid transmitter. In the first stage, MRDOA relies on open-circuit voltage information and the measurement matrix to obtain a sparse solution. The index corresponding to the maximum amplitude of the recovered sparse vector is considered to be the K_{max}, which can be expressed as

$$\mathrm{K_{max}} = max^{-1} I[n] : V_n = D(\hat{\boldsymbol{\theta}})I + P_n, \tag{6.8}$$

where, $I[n]$ is the n^{th} element of the recovered sparse vector obtained using CS. Given that the SNR is sufficiently high and the measurement matrix satisfies RIP condition, the first stage converges to the closest grid point. In such cases there is a high probability that the off-grid DOA is located anywhere in the angular grids between $[a, b]$, where $a = K_{max} + 1$ and $b = k_{max} - 1$. Let us assume that the two neighbouring grid points obtained from stage 1 are a and b. The new angular domain bounded by a and b is further sampled by fN, where f is the Resolution Constant (RC), such that $\frac{a-b}{fN} \geq \varepsilon$, where ε is a user-defined threshold. Due to the introduction of RC, the new angular domain (bounded by a and b) is discretized into L possible DOAs, $\acute{\boldsymbol{\theta}} = \{\acute{\theta}_l, \quad 1 \leq l \leq L\}$, where $L < N$. Using the new set of DOAs $\acute{\boldsymbol{\theta}}$, a refined measurement matrix is constructed similar to (7), which can expressed as

$$D^{ref}(\acute{\boldsymbol{\theta}}) = \begin{pmatrix} e^{-j\tau_1(\acute{\theta}_1)} & e^{-j\tau_1(\acute{\theta}_2)} & \dots & e^{-j\tau_1(\acute{\theta}_L)} \\ e^{-j\tau_2(\acute{\theta}_1)} & e^{-j\tau_2(\acute{\theta}_2)} & \dots & e^{-j\tau_2(\acute{\theta}_L)} \\ \vdots & \vdots & \ddots & \vdots \\ e^{-j\tau_M(\acute{\theta}_1)} & e^{-j\tau_M(\acute{\theta}_2)} & \dots & e^{-j\tau_M(\acute{\theta}_L)} \end{pmatrix} \tag{6.9}$$

where, $D^{ref}_{ml} \in \mathbb{C}^{M \times L}$ represents the phase shift of the waves impinging on the mth antenna element from the lth DOA. Combining (10) and voltage observations from (8), we can establish the following equation

$$V = D^{ref}(\acute{\boldsymbol{\theta}})I^{ref} \tag{6.10}$$

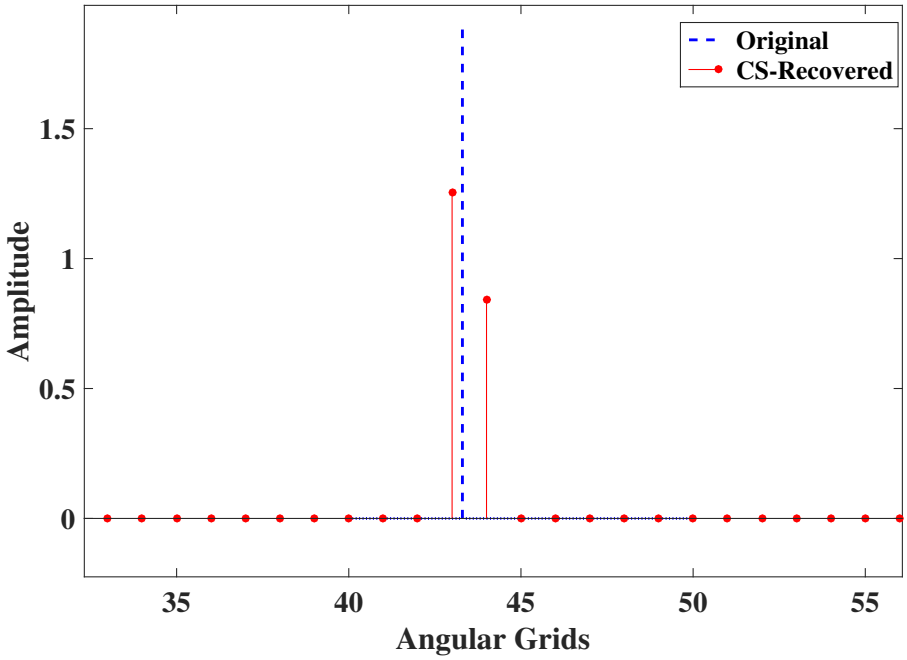

Fig. 6.2: First-stage DOA detection using MDROA. Blue peak indicates original off-grid DOA, whereas red peaks are the closest neighbouring grid points obtained using CS.

where, $I^{ref} = \{I_l^{inc}, 1 \leq l \leq L\} \in \mathbb{C}^{L\times 1}$, is the modified sparse vector which can be recovered using (3). As I^{ref} is sparse in the angular domain, the non-zero entries of the solution vector will indicate the accurate estimation of off-grid DOA.

6.7 Introduction of Transform Matrix

Based on the problem formulation in Section 6.5, when the 360° angular domain is sampled using large N, small grid separation may introduce a significant coherence between the columns of the measurement matrix, and this may violate the RIP condition [93]. To de-correlate, the columns of the measurement matrix a transform operation may be employed. The transform operation compacts the energy of a sequence into a very few component. The high compaction ability of transform function sparsifies the measurement matrix as well as the observation vector. The process of sparsifying the signal space results in a superior recovery with CS, allowing unique mapping between

the observation and the measurements. In this paper, we adopt a data-processing technique to increase the coherence between the rows, which are the observations of the complex open-circuit voltages from N angular grid points. Although similar work has been presented in [129], in this paper we extend the work to incorporate different transform matrices. Let X be a processing operator

$$X = YD^{+} \tag{6.11}$$

where $Y = (H^{*}D)$, and H is the $M \times M$ transform matrix and H^{*} is the conjugate transpose of H. $D^{+}$is the Moore-Penrose pseudoinverse of the measurement matrix D. Applying the operator X on both sides of (6.7) yields,

$$YD^{+}(V_n) = YD^{+}DI + YD^{+}P_n$$

$$\tilde{V} = BI + \omega. \tag{6.12}$$

Let $\tilde{V} = YD^{+}(V_n)$ be the noisy processed observation vector, and $B = YD^{+}D$ be the processed measurement matrix, while $\omega = YD^{+}P_n$ is the processed measurement noise. The entries of the row vectors are decorrelated by Y while the influence of $D^{+}D$ is negligible. Hence we can claim that matrix B satisfies the RIP condition. After applying the processing operator, CS may be used to recover the sparse vector from processed observations $\tilde{V}$, via a l_1-minimization program [162].

6.8 Simulation Results

The simulation in the following section is carried out on $N = 180$ angular grid points, with angular grid separation $w = \frac{360}{N} = 2^{\circ}$. The scanning angle ranges between $[-180^{\circ}, 180^{\circ})$. The UCA consists of $M = 9$ isotropic antenna elements distributed evenly on a circular ring with $r = 6\lambda$. The inter-element distance d between the antenna elements is approximately 4λ. For this simulation, f_c and r is considered to

be 750 MHz and 2.4 m respectively. The simulation scenario has one PU, randomly positioned among the 180 grid points. Signal power of the pth source $\mathbb{E}[|I_p^{inc}|^2]$ is uniformly distributed over the range [1, 3]. It has been assumed that the signal is arriving on the antenna with equal strength in order to perform an unbiased analysis of the accuracy of the method with respect to the angles of arrival. Section 6.8.1 assumes the transmitter to be located on the grid and off-grid DOA analysis is presented in Section 6.8.2. The simulations are carried out on a Intel(R) Core(TM) i7-4770 CPU with a clock rate of 3.40 GHz and on a 64-bit operating system. We relied on the MATLAB simulation platform to evaluate the performance of our algorithm.

6.8.1 Sensitivity Analysis of on-grid transmitter

This section considers having the transmitter on the angular grid points. In order to determine the robustness of our system model, the following noise sensitivity test has been considered. The Signal-to-Noise-Ratio (SNR) is calculated at the receiver as the ratio of the sum of the power received from m antenna elements to σ^2 where, σ^2 is the variance of the complex Gaussian noise. The measured data are characterized by $\text{SNR}_{\text{dB}} = [-10, -5, 0, 5, 10, 15, 20, 25, 30]$, defined as

$$\text{SNR}_{\text{dB}} = 10 \log_{10} \left[\frac{\sum_{m=1}^{M} |v_m|^2}{M\sigma^2} \right] \tag{6.13}$$

where, v_m, $m = 1, ...M$, is the noiseless complex voltage observation at each antenna element. Since the actual DOA and source power are selected randomly, $T = 500$ different scenarios have been considered, to give a consistent statistical validation. The results in this section aim to validate the effect of noise sensitivity on the performance parameters of two l_1-constrained optimization algorithms: Orthogonal Matching Pursuit (OMP) and Compressive Sampling Matching Pursuit (COSAMP) [66][67]. Performance parameters may be characterized as Mean Detection Ratio (MDR) and Mean

Square Sparse Error (MSSE) which can be expressed as,

$$\text{MDR} = \frac{\sum_{t=1}^{T} \frac{PU_{DET}^{t}}{PU_{TOTAL}^{t}}}{T} \tag{6.14}$$

$$\text{MSSE} = \frac{\sum_{t=1}^{T} \|I_{ORG}^{t} - I_{EST}^{t}\|_2^2}{T} \tag{6.15}$$

where PU_{DET}^{t} is the number of correct detections and PU_{TOTAL}^{t} is the total number of sources available at tth scenario. In order to be a correct detection, the amplitude of the peak at a DOA grid must be greater than some predefined threshold, in this case 1. Since we have just one PU, the detection can be a binary variable. MSSE is calculated as the square of the l_2-norm difference between the original sparse vector I_{ORG} and the estimated sparse vector I_{EST}. The MSSE of any unbiased estimator I_{EST} of I_{ORG} satisfies the Cramér-Rao bound, given in [181] as

$$\text{CRB} \triangleq \mathbb{E}[\|I_{ORG} - I_{EST}\|_2^2] \geq \sigma^2 Tr((\phi_a^T \phi_a)^{-1}), |a\|_0 = P.$$

Where, a is the index representing the PU position on the angular grid points. ϕ_a is the modified matrix constructed from the support set a of the original dictionary matrix ϕ. CRB will be used as a benchmark in the following simulation to validate the effectiveness of the model in recovering an accurate estimate of the original sparse vector. Fig. 6.3 and Fig. 6.4 show the impact of noise sensitivity on the performance of CS algorithms, in accurately recovering the sparse vector with minimum reconstruction error. Fig. 6.3 shows that CS algorithms integrated with the transform operation have a higher MDR. COSAMP and OMP with DCT outperformed conventional CS algorithms by achieving 30% more MDR. OMP with no transform has the worst performance among all, mainly due to the fact that OMP does not take the number of PU as an input while estimating the sparse vector. Fig. 6.4 illustrates the influence of the SNR on the MSSE of estimating the sparse vector. CS algorithms without any transform generated a higher MSSE compared to CS with DCT. COSAMP with DCT generated

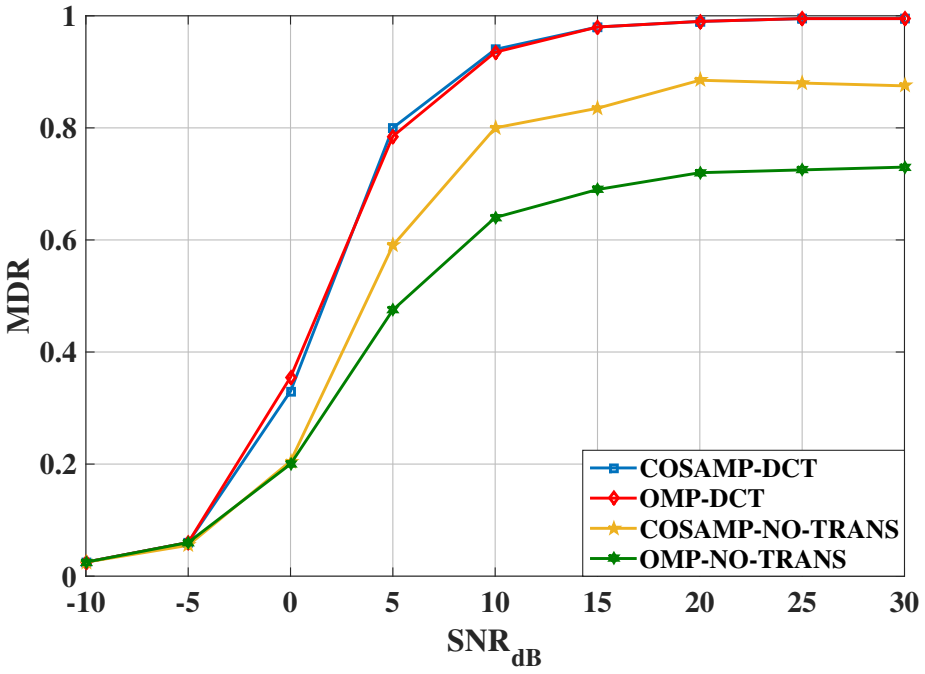

Fig. 6.3: MDR of two CS algorithms, OMP and COSAMP, in estimating on-grid DOA, with varying noise sensitivity.

the least error and performed very close to the CRB of sparse estimation. The result suggests that the transform operation enhances the overall performance of the CS algorithm. Moreover, for $\text{SNR}_{\text{dB}} > 10$, CS algorithms with DCT achieve accurate detection of the transmitter on quantized grids, for 90% of the trials.

6.8.2 Sensitivity Analysis of off-grid transmitter

In this section Multi-Resolution analysis has been carried out to estimate off-grid DOA using COSAMP algorithm with DCT as the transform matrix. The results in Fig. 6.3 suggests that for $\text{SNR}_{\text{dB}} < 10$, COSAMP fails to recover an unique solution that achieves the CRB. Such phenomenon shows the inefficiency of CS algorithms to recover accurate solution at low SNR. Therefore in case of $\text{SNR}_{\text{dB}} < 10$, the nearest grid search method will be used to estimate the DOA. To validate the effectiveness of our proposed MRDOA algorithm, MSE of DOA estimation will be compared with

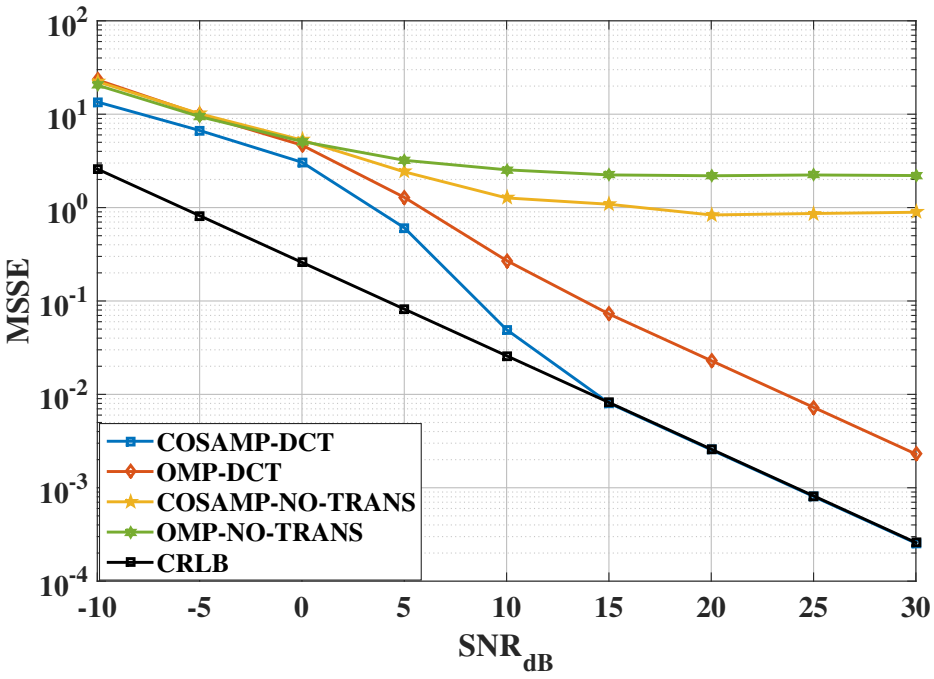

Fig. 6.4: Influence of SNR on the MSSE CS algorithms.

conventional Root-MUSIC, nearest-grid search method, Weighted-Centroid and high-resolution Beam-Scan search. The MSE is defined as

$$\text{MSE} = \frac{\sum_{t=1}^{T} |\bar{\theta}_{org} - \bar{\theta}_{est}|^2}{T}$$

where $\bar{\theta}_{org}$ is the original DOA of the source and $\bar{\theta}_{est}$ is the DOA of the source estimated using various algorithms. The simulation in Fig. 6.5 assumes $N_s = 1$ snapshot of the simulated signal. For cases with low SNR ($\text{SNR}_{\text{dB}} < 5$), both the Root-MUSIC and the Weighted-Centroid techniques have the lowest MSE. For higher SNR ($\text{SNR}_{\text{dB}} > 15$), however, we can clearly observe that MRDOA outperforms all the algorithms. The second stage of finer search in MRDOA, offers an added advantage over the conventional algorithms such as Beam-Scan, allowing MRDOA to obtain a better estimate of the original off-grid DOA.

Although MSE act as a good indicator DOA estimation, in some cases, the presence of outliers can push the MSE to the higher side. To further validate the claim that, MRDOA offers a better estimate, in Fig. 6.6 we analyzed the proportion of times

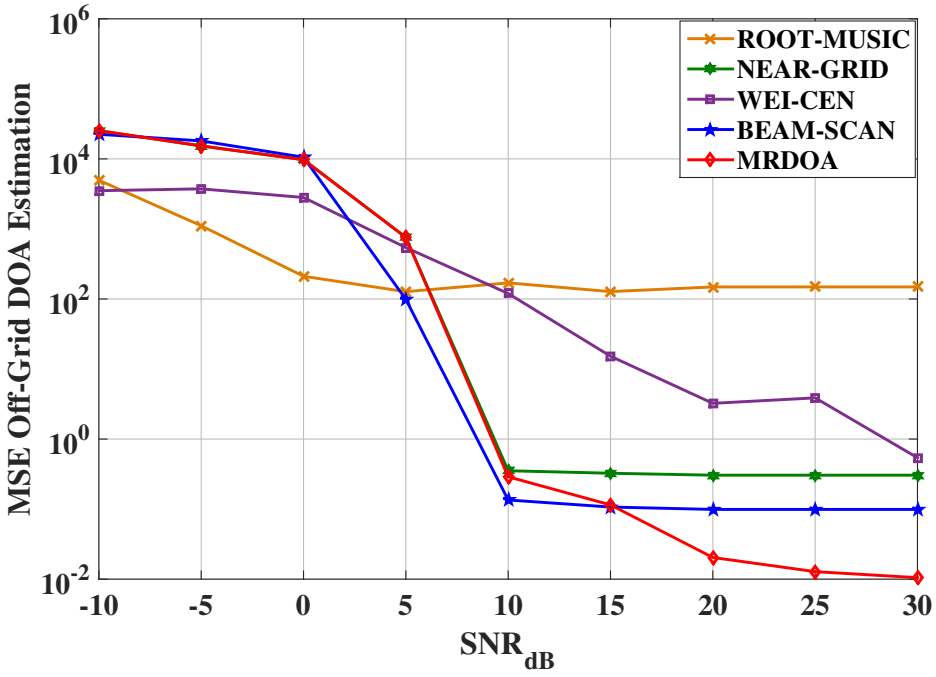

Fig. 6.5: MSE comparison plot for off-grid DOA estimation error of different algorithms.

each algorithm estimated off-grid DOA with absolute error $< 0.2°$. From the plots, it is clear that MRDOA has the largest proportion of accurate estimation followed by the Weighted-Centroid technique. Traditional Beam-Scan and Root-MUSIC algorithm failed to reach the mark, due to insufficient snapshots of the simulated signal. The results also demonstrate the ability of MRDOA to estimate off-grid DOA with minimum samples of the simulated signal, hence greatly reducing the computational complexity compared to conventional estimation algorithm. In Conventional CS, to obtain a DOA estimate with higher resolution, the angular domain of 360° is required to be discritized with large N. COSAMP algorithm has a complexity of $O(MN)$, and with an increase in N, the computational efficiency decreases. Fig. 6.7 indicates the influence of MRDOA in reducing the computational time compared to conventional CS based DOA algorithms. In comparison to traditional COSAMP techniques, MRDOA with COSAMP achieves a finer DOA estimate while reducing the computation time

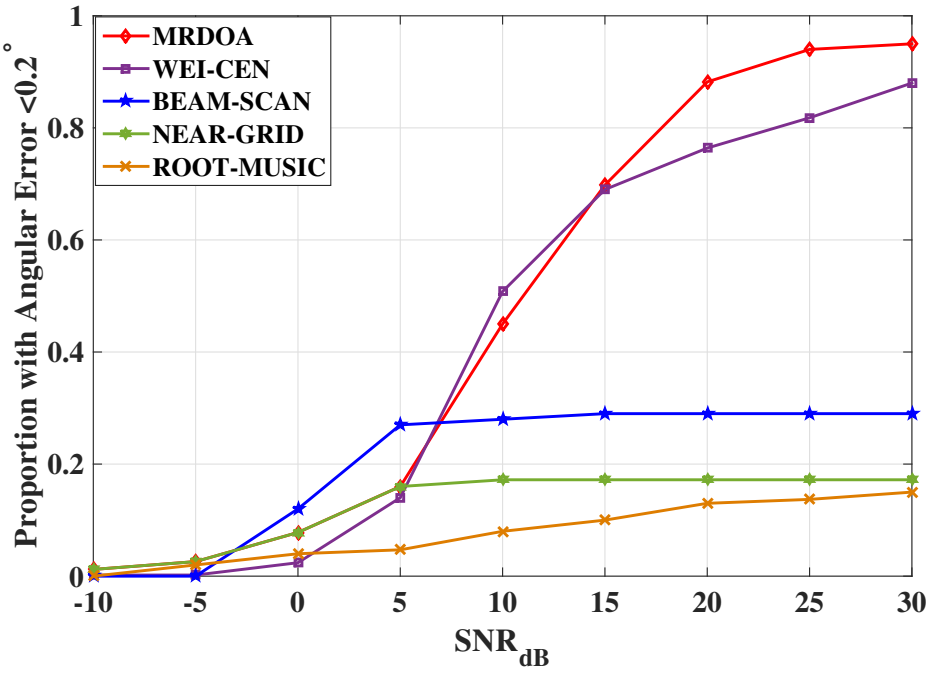

Fig. 6.6: Analysis to validate the proportion of accurate DOA estimate with |Error| < 0.2°.

by a factor of nine.

6.9 Conclusion

The paper discusses the formulation of a novel Multi-Resolution based CS algorithm to effectively estimate the DOA of a signal transmitted from an off-grid source. The algorithm exploits the neighboring grid point information to construct a refined search area from which the original off-grid DOA is estimated. Our novel MRDOA algorithm showed promising results by achieving significant improvements in estimating off-grid DOA with minimum MSE. Simulation results suggest that at a relatively high SNR, our proposed approach has reduced the MSE of off-grid DOA estimation approximately by a factor of 10, compared to traditional Beam-Scan and Weighted-Centroid techniques. The novel MRDOA outperformed other DOA estimation techniques considered while achieving an error of less than two tenths of a degree for 90% of the trials. Moreover, the results also indicate that MRDOA achieved a reduction in computation time by a

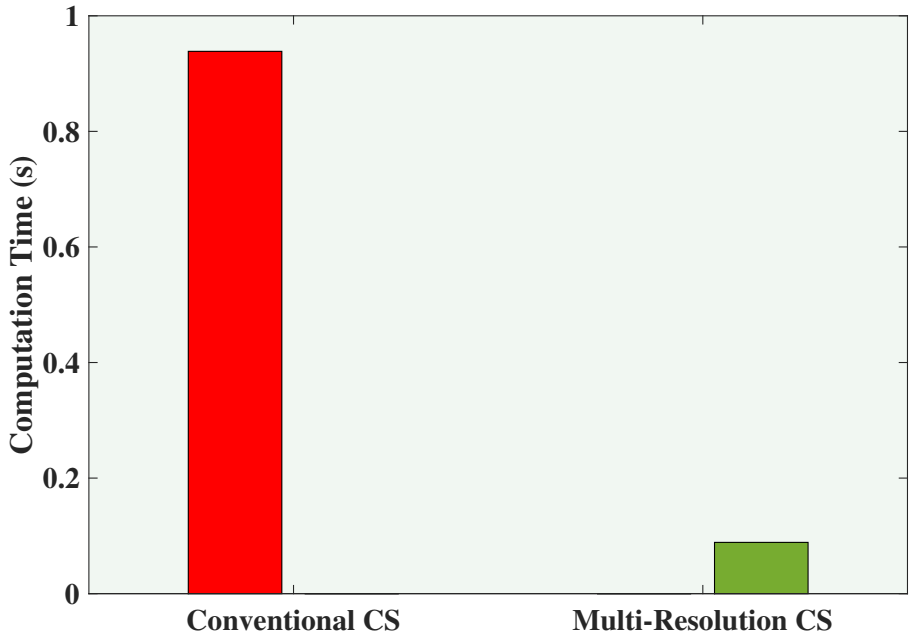

Fig. 6.7: Comparison of computation time between conventional CS and MDROA based DOA detection.

factor of 9 when compared to traditional CS algorithms using finer resolution. Future work will incorporate range measurement techniques to geographically locate multiple off-grid transmitters.

7

Effective Sensor Positioning to Localize Target Transmitters in a Cognitive Radio Network.

7.1 Abstract

Precise positioning of transmitting nodes enhances the performance of Cognitive Radio (CR) by enabling more efficient dynamic allocation of channels and transmit powers for unlicensed users. Most localization techniques rely on the random positioning of sensor nodes where a few sensor nodes may have a small separation between adjacent nodes. Closely spaced nodes introduce correlated observations affecting the performance of the Compressive Sensing (CS) algorithm. This paper introduces a novel minimum-distance

separation aided compressive sensing algorithm (MDACS). The algorithm selectively eliminates Secondary User (SU) power observations from the set of SU receiving terminals such that pairs of the remaining SUs are separated by a minimum geographic distance. We have evaluated the detection of multiple sparse target locations and error in l_2-norm of the recovery vector. The proposed method offers an improvement in the detection ratio of 20% while reducing the error in the l_2-norm by 57%.

7.2 Introduction

The spectrum scarcity along with inefficient spectrum usage has motivated the development of *Cognitive Radio* (CR). The increasing demand for high data rates due to large numbers of portable hand-held devices initiated significant research in the field of interference mitigation and effective spectral utilization. CR provides a promising solution to the existing problem by efficiently using the underutilized spectrum to facilitate services by *Dynamic Spectrum Sharing* (DSS) for both licensed and unlicensed users. CR technology is based on the concept of learning the state of channel use of *Primary Users* (PUs), and subsequent efficient allocation of channels and transmit parameters to *Secondary Users* (SUs). This allocation takes into account maximum acceptable interference levels to PUs and the throughput and performance requirements of SUs.

In a Cognitive Radio Network, both PUs and SUs share the same channels. Since SUs have lower priority, the channel use is constrained by a maximum acceptable level of interference to PUs. Many efforts have been made in previous literature [182][183] to tackle the issue of interference mitigation but only a few research papers have been published on channel collision avoidance based on the utilization of a *Radio Environment Map* (REM). To generate a REM, the locations of the transmitters and their transmit power levels need to be accurately estimated. From this estimation, the received power level throughout a two-dimensional area may be estimated. For the REM, the received power levels interpolated over a two-dimensional geographic area are obtained through the use of analytic equations for signal propagation.

In CR, the REM is extremely useful in secondary user channel and transmit parameter selection. This selection must be made with the dual requirements of SU communication effectiveness and bounded interference to PUs. The bounded interference to PUs can only be maintained if the PU locations and received power levels from other PUs are known by SUs. Therefore an accurate REM is crucial for effective CR operation.

In [75], a cooperative algorithm is formulated that takes the received signal strength at each SU to create a weighting function and uses it to compute the location of multiple PUs. Although this algorithm has relatively low computational complexity, it requires a high density of SUs, and the performance degrades with channel fading. The work in [184] and[185] is based on the concept of using sectorized antennas to detect the Direction of Arrival (DOA) of a signal. The phase information of a received signal is exploited to estimate the position of PUs. However, this technique might not be feasible for a practical CRN implementation due to antenna requirements which may be impractical for portable devices.

In this paper we adopt a Compressive Sensing (CS) technique to retrieve the locations of multiple transmitting PUs in a CRN. The approach relies on a location fingerprinting approach, where a certain geographic area is discretized into equally spaced grid points. The PUs are assumed to be positioned at a subset of the grid points. The SUs are also assumed to be positioned at some known locations in the area of interest. Each SU measures the Received Signal Strength (RSS) from target PUs. From this set of measurements, there is an attempt to recover the PU locations and the transmit power levels. It is usually the case that the number of PUs is much smaller than the number of grid points. Consequently, the set of equations for the power levels transmitted by PUs is under-determined and there are many possible solutions. When the number of PUs is much smaller than the number of grid points, the sparsest solution for the set of equations yields accurate power levels at the correct grid points. Compressive sensing can be used to obtain the data required for the formulation of the REM. Similar techniques were used in [129], [186], [187] and [188].

In a physical system, some of the SUs will be closely geographically located. Having

closely placed SUs introduces correlated observations which may increase the observation coherence. The performance of CS algorithms relies heavily on the coherence of measurement matrix constructed using the observations from SUs. The high coherence among the power measurements makes it difficult for matrix inversion, which may cause inaccurate recovery of the sparse vector. To improve the performance of the CS algorithm, we propose a novel minimum distance aided CS (MDACS) algorithm. The approach aims to improve the performance of CS algorithms by selectively removing measurements of closely spaced SUs from the set, such as to increase the minimum distance separation between adjacent SUs. The algorithm prioritizes the RSS of an SU before completely eliminating it from the set. The process generates a refined set of SUs with a certain distance separation and a high RSS. Our method achieved superior detection of multiple PUs with significantly fewer SU measurements than with random deployment of SUs.

In this paper, the locations of SUs are specified by two-dimensional vectors. Both uniform distribution and Gaussian distribution were considered for the random assignment of SU positions. Irrespective of distribution used, our novel approach of pre-selecting SU power measurements appears to achieve reliable detection ratios with fewer receiving nodes. Section 7.3 discusses the background of compressive sensing. Sections 7.4-7.6 describe the system model. Section 7.7 - 7.10 presents the simulation results which validate the effectiveness of our proposed method. The conclusion is given in Section 7.11.

7.3 Compressive Sensing

The CS technique is an approach for the solution of an underdetermined set of equations for which the solution vector is known to be sparse. Some data vectors are sparse while others can be made more sparse by an appropriate basis transformation. A typical example would be the time-frequency pair. A signal, which is a linear combination of several frequency components, can be easily retrieved by exploiting sparsity in the

frequency domain. The complex Fourier Transform basis functions can be used to represent the time domain signal with a few non-zero coefficients. In such case, the CS algorithm can be used to obtain the sparsest solution vector to a set of underdetermined equations. The sparse vector $x_{N\times 1}$ is the solution with the minimum number of non-zero elements. If $y_{M\times 1}$ is the raw observation vector obtained by the SU power measurements, there exists the relationship

$$y = \phi x, \tag{7.1}$$

where $\phi_{M\times N}$ is a measurement matrix, representing the power propagation losses from each grid point to each SU. In [186] it states that, if a matrix ϕ satisfies the *Restricted Isometry Property* (RIP) condition, then all subsets of S columns chosen from ϕ are nearly orthogonal. Once this is true, there is a high probability of completely recovering the sparse vector with at least $M = CK \times \log(N/K)$ measurements (where K is the number of PUs and C is a positive constant) using the l_1 -minimization algorithm [10]. This can be can be expressed as

$$min \left\|x\right\|_1 = min \sum_i |x_i|$$

subject to

$$y = \phi x. \tag{7.2}$$

This formulation is valid for a noiseless scenario, but when external noise is considered the algorithm is modified to a *Second-Order Cone Program* for an optimized solution for a defined threshold [64]. This can be stated as

$$min \left\|x\right\|_1 = min \sum_i |x_i|$$

subject to

$$\left\|y - \phi x\right\|_2 \leq \varepsilon, \tag{7.3}$$

where $\|\cdot\|_p$ is the l_p-norm and ε is the relaxation constraint for measurement errors. The sparsest solution for x is the solution with minimum $\|x\|_0$. However, the CS algorithm is effective because the same solution vector usually has a minimum l_0 norm and a minimum l_1 norm [64].

7.4 System Model

Let us consider a square area discretized into an equally spaced $P \times P$ grid, where K PUs are randomly positioned at unique grid points. For simplicity of illustration, we assume that each PU is assigned a single dedicated sub-channel to carry out duplex communication with the base station. Now, to observe the radio environment and detect the free spectrum, M SUs are deployed randomly in the area of interest. Unlike [129] and [187] the SUs are not placed on the grid points. We adopted a more realistic approach of allowing the SUs to be placed at some known locations in the area. They have the added flexibility of being positioned at non-discretized points on the map. The SUs are controlled and managed by a central node called the *Fusion Centre* (FC). There exists a common control channel between the central node and the SUs for effective communication of RSS observations and channel allocation information. The FC processes the signal-level measurements and manages SU channel allocation. The most crucial assumption in the model is that the spatial coordinates of both the grid points and the SUs are known *a priori* by the FC, which receives sensing information from each individual SU. The received power at an SU is a function of the distance between the PU and SU as well as shadowing loss. The wireless channels are corrupted by noise and are also considered to be affected by log-normal shadowing. The simplified path-loss model as a function of distance may be described as

$$Pathloss_{dB}(d) = K_1 + 10\eta \log_{10}(\frac{d}{d_0}) + \alpha, \tag{7.4}$$

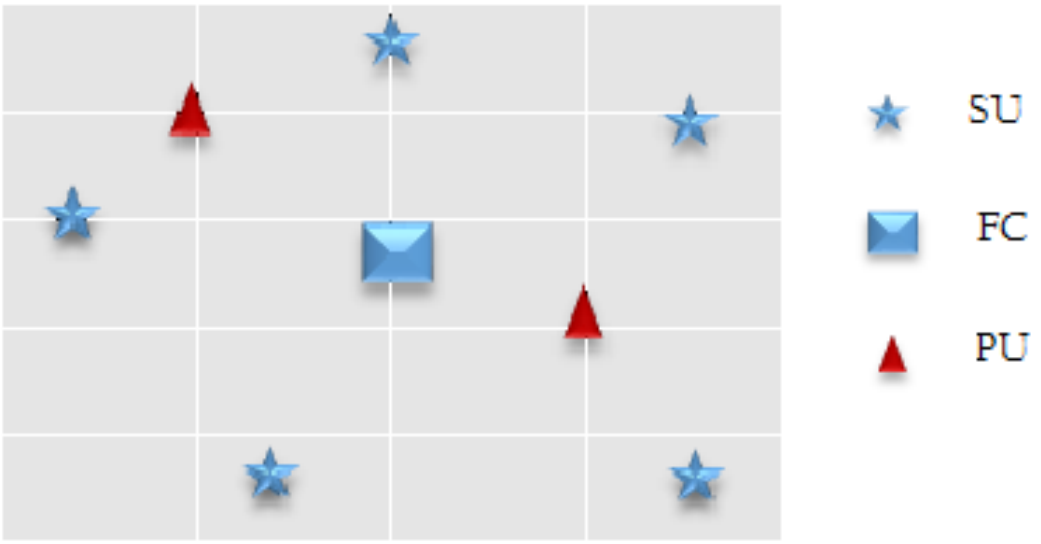

Fig. 7.1: System model demonstrating the positioning of PU, SU and FC

where

d is transmission distance in meters,

d_0 is the reference distance of the antenna far field,

K_1 is a dimensionless constant in dB,

η is the propagation loss exponent,

α is the shadowing loss in dB.

K_1 is a unit-less constant that relies on the antenna characteristics and the average channel attenuation and $K_1 dB = 10 \log_{10}(K_1)$ [74]. α accounts for the random attenuation of signal strength due to shadowing, where α, dB scale, is assumed to be a Gaussian random variable with zero mean and standard deviation $\sigma_{dB} = 5.5$ dB [75]. This model was used in [75] for both multipath and shadowing characterization.

7.5 Localization using compressive sensing

This section combines the location-dependent RSS information at each SU to formulate a sparse-matrix problem, which can then be solved using the CS method to obtain the

exact location of the PUs in a CRN. Our grid layout consists of N grid points, with grid resolution w in both x-axis and y-axis. The N grid points are located at $\{V_n, 1 \leq n \leq N\}$, where V_n is a two-dimensional position vector. The M SUs are located at $\{U_m, 1 \leq m \leq M\}$, where U_m is also a two-dimensional position vector. Earlier in Section 7.4 we mentioned that the K PUs are positioned only at K discrete grids where $K < N$. The FC is assumed to have prior knowledge of V_n and U_m. Using the distance information and signal propagation model described in (7.4) a measurement matrix Φ is constructed. The entries of the matrix are the channel gains and are expressed using

$$d_{mn} = \| U_m - V_n \|_2, \tag{7.5}$$

$$\Phi_{mn} = 10^{-Pathloss_{dB}(d_{mn})/10}, \tag{7.6}$$

where d_{mn} is the distance between the m^{th} SU and the n^{th} grid point and Φ_{mn} is the pathloss between the m^{th} SU and the n^{th} grid point. Let Y be a $M \times 1$ column vector where the m^{th} element, Y_m, represents the summation of the received power from the K PUs on them^{th} SU.

$$Y_m = \sum_{k=1}^{K} Q_{m,k}, \tag{7.7}$$

where

$$Q_{m,k} = 10^{\frac{Q_{m,k,dB}}{10}}$$

and

$$Q_{m,k,dB} = P_{k,t} - Pathloss_{dB}(d_{mk})$$

where $Q_{m,k}$ is the power received at SU m which

was transmitted by PU k,

$P_{k,t}$ is the power transmitted by user k,

and $d_{m,k}$ is the distance between SU m and PU k.

Equations (7.6) and (7.7) may be combined to formulate a CS problem similar to (7.3). It is assumed that the FC has complete knowledge of Φ. Therefore

$$Y = \Phi X \tag{7.8}$$

with $X_{N\times 1}$ being an $N \times 1$ column vector that is to be recovered using CS approach described in Section 7.3. In a realistic scenario, the observations are corrupted with noise-power vector P_n. The elements of P_n are statistically independent with variance σ_n^2, and are chi-square distributed with 1 degree of freedom. We can include the effect of additive noise by writing

$$Y_n = \Phi X + P_n. \tag{7.9}$$

Since the model assumes having only a few PUs on a large grid size N, the vector $X_{N\times 1}$ satisfies the sparsity requirement for accurate recovery using a CS algorithm. Due to the sparse condition, the recovered vector will have only a few nonzero elements representing the transmit powers while the indices corresponding to non-zero elements indicate the grid points on which transmitting PUs are located. Hence using a single-compressed sensing problem we can jointly estimate both the locations and the transmit powers of multiple PUs by solving (7.3) as described in Section 7.3. From the estimation, FS can approximate the received power level throughout a two-dimensional area, using the pathloss model in (7.4).

7.6 Data Processing

Based on the problem formulation in Section 7.5, $Y_{M\times 1}$ is a power observation vector with each row representing a sum of the RSS received from K PUs on the m^{th} SU, and $\Phi_{M\times N}$ is the measurement matrix with the channel gain from each grid point. The small grid separation ensures a large coherence between the columns of the measurement matrix, and this may violate the RIP condition [93]. A matrix transformation may be employed to increase the incoherence between the columns. We adopt a data-processing

technique described in [129] and [187] to decorrelate the rows which are the observation of the signal strengths from the grid points on each SU. Let T be a processing operator

$$T = SR^{+} \tag{7.10}$$

where $S = orth(\Phi^{T})^{T}$. The built-in function of MATLAB, $orth(B)$, returns an orthonormal basis of the range of B, and B^{T}returns the transpose of B. $R^{+}$is the Moore-Penrose pseudoinverse of a matrix R, where $R = \Phi$. Applying the operator T on both sides of (7.9) yields

$$SR^{+}(Y_n) = SR^{+}\Phi X + SR^{+}P_n = S\Phi^{+}\Phi X + SR^{+}P_n = Ax + \omega$$

$$Y^{'} = AX + \omega. \tag{7.11}$$

Let $Y^{'}$ be $SR^{+}(Y_n)$, the noisy processed observation vector. $A = S\Phi^{+}\Phi$ be the processed measurement matrix then $\omega = SR^{+}P_n$ is the processed measurement noise. The row vectors are orthogonalized by S while the columns are decorrelated by the influence of $\Phi^{+}\Phi$. Hence we can claim that matrix A satisfies the RIP condition. Note that [129] and [187] considered $\Phi^{+}\Phi = \mathbb{I}_N$ as a diagonal identity matrix. Although $\Phi^{+}\Phi$ acts like an identity on a portion of the space in the sense that it is symmetric, it is not an identity matrix. After applying the processing operator, CS may be used to recover the sparse vector from processed observation $Y^{'}$, via the l_1-minimization program [129].

7.7 Simulation And Results

The localization accuracy of the CS algorithm can be affected by certain external factors such as the *Signal to Noise Ratio* (SNR), shadowing, the density of SUs and the distribution of SUs. This section analyzes the dependency of these factors on the performance parameters of three l_1 constrained optimization algorithms (L1-Magic, OMP and CoSAMP) to produce an accurate result. L1 Magic, CoSaMP, and OMP are

three numerical algorithms for constrained l_1 vector optimization [65], [66] and [67]. The performance parameters may be categorized as

$$DetectionRatio = \left[\frac{PU_{Det}}{PU_{Total}}\right]$$

$$Normalized\ Error\ Per\ Grid\ Point = \frac{1}{N}\left\|X_{org} - X_{est}\right\|_2$$

where PU_{Det} is the number of detected PUs. PU_{Total} is the number of the PUs in the network. X_{org} is the original sparse vector and X_{est} the recovered vector using CS algorithms. The average absolute error between the vectors X_{org} and X_{est} is obtained by simulation. This is used to evaluate the accuracy of the algorithms to reconstruct a sparse vector with a minimum number of non-zero coefficients. Furthermore, to study the impact of each factor, the simulation is analyzed independently to demonstrate the robustness and reliability of the algorithms.

7.7.1 Simulation Setup

The simulation is carried out on a 43×43 (i.e. $N = 1849$) square grid with a grid separation of 80 m. Among the 1849 grid points, 10 PUs are uniformly distributed on the grid points. The transmit power is random and uniformly distributed over the range of 1 to 5 watts. The scenario consists of 160 SUs with a two-dimensional, zero mean, Gaussian spatial distribution with standard deviation σ_{sd}. The shadowing factor is log-normal distributed.

Simulation (I) - Impact of SNR

The Signal-to-noise ratio is a crucial factor affecting the performance of each algorithm. SNR is calculated at the receiver as the ratio of the average received power at an SU

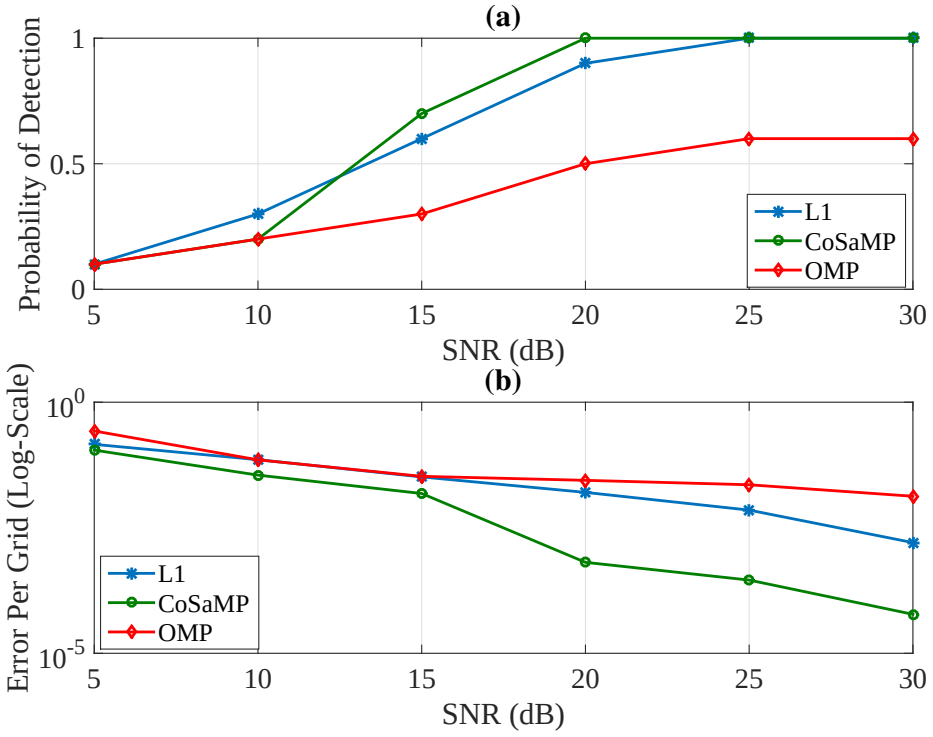

Fig. 7.2: (a) Detection ratio against SNR at the top (b) Error per grid against the SNR at the bottom.

to σ_n^2, where σ_n^2 is the variance of the additive, zero mean, Gaussian noise. Then

$$SNR(dB) = 10\log_{10}(\frac{1}{M}\sum_{i=1}^{M}\frac{Y_i}{\sigma_n^2}).$$

Y_i is the received RSS from all the transmitting PUs at the i^{th} SU. As the received signal power is position dependent, the SNR will vary with respect to the positioning of the SUs. This prompted us to take the average SNR over M elements of the observation vector. Fig. 7.2(a) and Fig. 7.2(b) show the plots for the detection ratio of the PUs and the normalized error per grid versus average received SNR in dB. As shown in 7.2(a) when SNR $<$ 12dB, L1-Magic performs better than CoSaMP, however when SNR $>$ 15dB, CoSaMP outperforms L1-Magic and OMP. At a higher SNR $=$ 25dB, both CoSAMP and L1-Magic achieve a detection ratio of 1 while OMP is at 0.6. Fig.7.2(b)

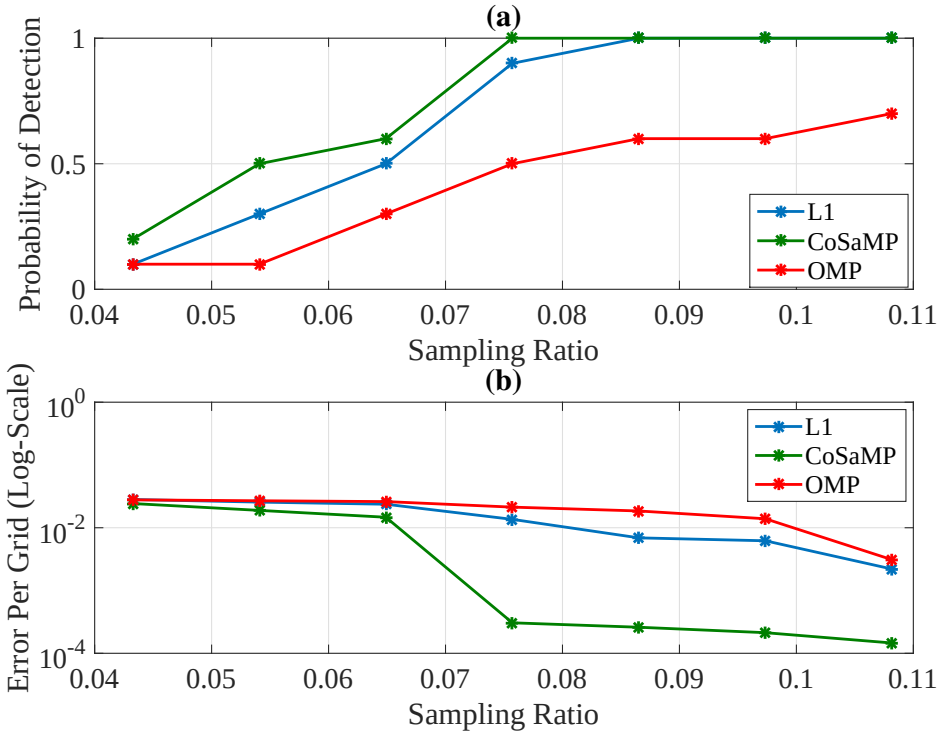

Fig. 7.3: (a) Sampling ratio vs detection ratio (b) sampling ratio vs normalized error per grid

shows that, with a gradual increase in SNR, CoSaMP generates fewer normalized errors per grid than L1-Magic and OMP. Even at a moderate SNR of 15 dB, CoSaMP produces 50% and 54% fewer errors than L1-Magic and OMP respectively.

Similation (II) - Sampling Ratio

Sampling ratio $\frac{M}{N}$ is another major factor that has a significant impact on the performance of these algorithms. In this simulation, we start with 200 SUs to detect the position of 10 PUs, where at each iteration 20 SUs are randomly removed to observe the effect of a reduced number of SUs. The SNR is kept constant at 25 dB. The plots in Fig. 7.3 follow a similar trend as in Fig.7.2. At the very low sampling ratio of 0.05, almost all three algorithms fail to recover an accurate sparse solution, as solving an under-determined system with such a small number of measurements is not feasible regardless of any methods used. However, with an increase in the sampling ratio,

CoSaMP achieves a detection ratio of 1 using 10% fewer SUs than L1-Magic as shown in 7.3(a) . OMP seems to require a higher number of SUs to meet the accuracy of CoSaMP and L1-Magic. Similar conclusions can be drawn from Fig. 7.3(b), where the graph of normalized error per grid for CoSaMP as a function of sampling ratio decreases much rapidly than the other two algorithms. Results from simulation (I) and (II) indicate that CoSaMP is more robust and can perform with superior results to the other two algorithms. The next set of simulations will be carried out using CoSaMP and L1-Magic only.

7.8 Impact of SU Distribution

In the previous section, the simulations were carried out using SU positions generated from a two-dimensional, zero mean, Gaussian spatial distribution only. This section analyzes the influence of the spread of a particular spatial distribution, used to obtain the location of SUs in a CRN. The two-dimensional SU positions are two-dimensional random vectors with statistically independent elements. Two cases were considered. In the first case each element is uniformly distributed over $[-X_{max}\sigma_{sd}, X_{max}\sigma_{sd}]$. In the second case, each element is zero mean Gaussian distributed with standard deviation $\{X_{max}\sigma_{sd}\}$. For each of the cases, simulations were carried out with 100 different scenarios. The PU positions are kept constant and the shadowing factor is log-normal distributed. The first set of simulations shows the detection ratio of the optimization algorithms, where uniform distribution and Gaussian distribution were considered for the random assignment of SU positions. The second set aims to provide a deeper insight into the effect of the spread of a particular spatial distribution on the coherence of the measurement matrix Φ and the average received SNR at each SU.

While keeping the SNR constant and the number of SUs and PUs constant, σ_{sd} is varied in the range [1.5, 6.5]. Fig. 7.4 shows the results for the first set of simulations. The figure illustrates the ability to detect the presence of PUs, for a set of SUs drawn from (a) Gaussian normal distribution and (b) uniform distribution respectively. The results

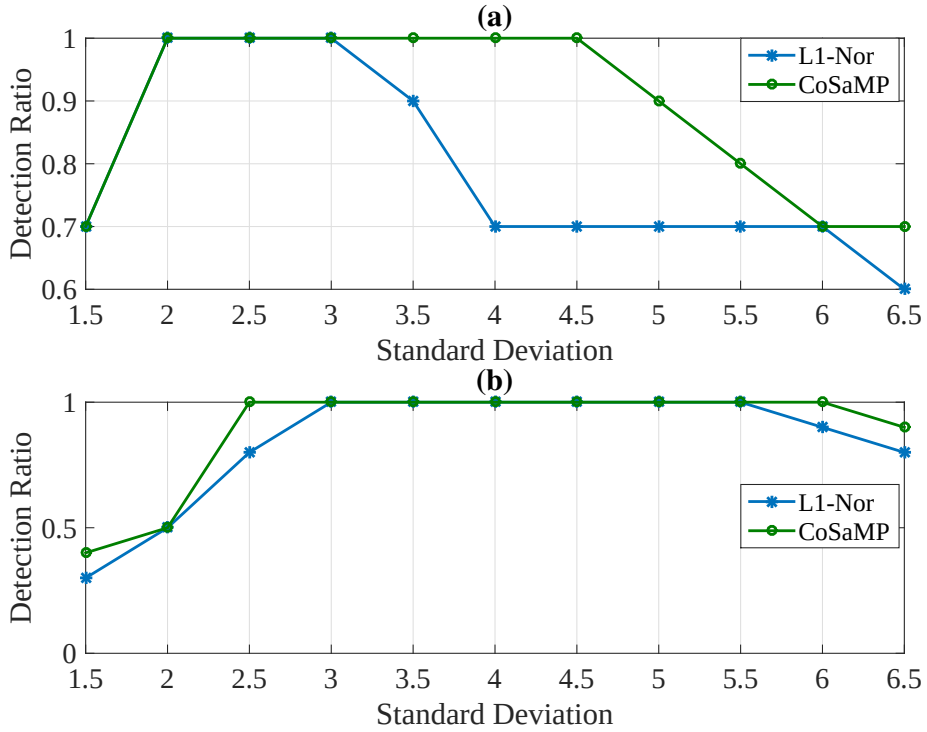

Fig. 7.4: (a) Detection ratio for SUs generated using normal distribution (b) detection ratio for SUs uniform distribution

are averaged out over 100 scenarios. In Fig. 7.4(a) the SU positions are extracted from a zero-mean Gaussian normal distribution. As σ_{sd} is varied, the detection ratio increases from 0.7 to 1 and maintains the maximum, until $\sigma_{sd} = 4$ for L1-Magic and $\sigma_{sd} = 5$ for CoSAMP. When $\sigma_{sd} > 5$, the detection ratio has a downward slope irrespective of the algorithms used, and at $\sigma_{sd} = 6.5$ it reaches a minimum point.

Further analysis is carried out to learn about the impact of the distribution of spread on the structure of the measurement matrix. Fig. 7.5 (a) shows the effect in mutual coherence of the measurement matrix when constructed using both normal and uniform distribution. On the other hand in Fig. 7.5(b), the average received SNR at SUs are observed simultaneously. It can be seen that with an increase in the spread of the distributions, the mutual coherence of the measurement matrices is decreasing monotonically. Especially, the measurement matrix constructed using normal distribution has a sharper drop than that of the uniform distribution. Similarly, at the same, the average SNR of the SUs are also decreasing, as the SUs are more spread

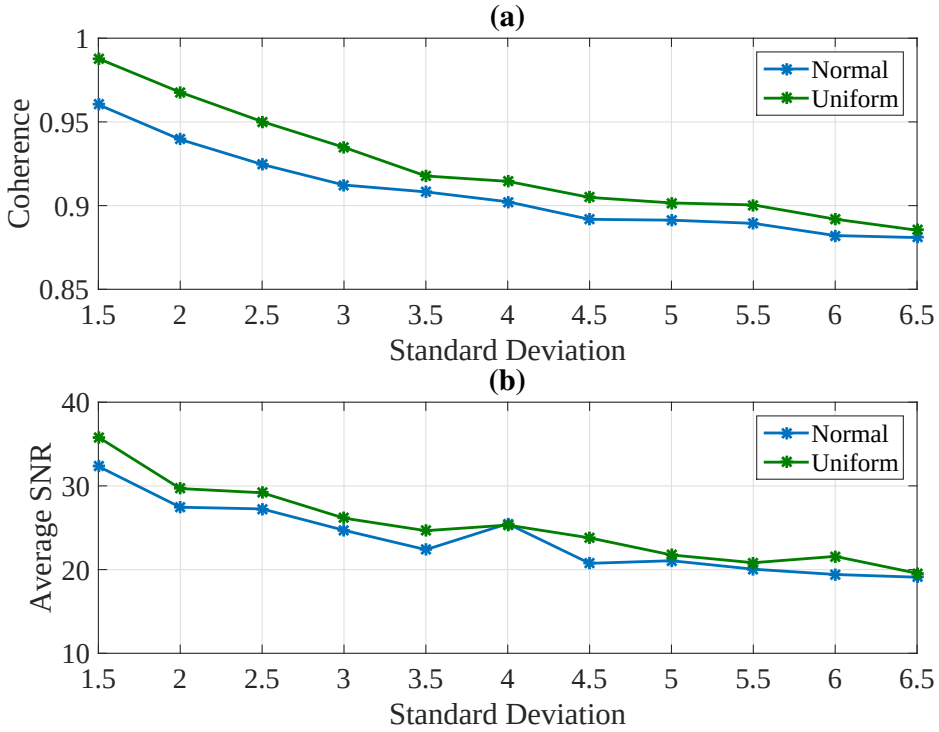

Fig. 7.5: (a) Impact on mutual coherence due to spread of distribution (b) Average SNR of the SUs as a function of the spread of the distribution.

across the network. The set of SUs extracted from a Gaussian normal distribution have a significant proportion of the SUs positioned around the origin. With the spread of the distributions gradually increasing, the SUs are pushed further away from the center. The sharp tail of Gaussian distribution, extending towards infinity, often forces some of the SUs to be positioned at a distance, where the channel noise is large with respect to received signal strength. This may cause significant errors in the construction of the measurement matrix, resulting in an incorrect recovery of the sparse vector. However, due to large distance separation from the transmitting node, the observations at receiving nodes becomes independent of each other. The independent observations are the reason behind the reduction in mutual coherence between the columns of the measurement matrices. This provides an explanation to the fact that, even with a smaller mutual coherence at high σ_{sd}, the SUs generated using normal distribution fails to accurately detect the PUs in the network. When looked back at Fig. 7.4, in case of normal distribution, the CS algorithms achieved detection ratio of 1 at σ_{sd}

= 2. On the other hand, uniform distribution requires $\sigma_{sd} = 2.5$, for at least one of the algorithms to hit a detection ratio of 1. This is solely due to higher coherence between the columns of measurement matrix as shown in Fig. 7.5(a). In spite of having relatively higher received SNR compared to a normal distribution, a large coherence resulted in a poor detection ratio < 0.5. However uniform distribution achieved to maintain the maximum detection ratio for a larger range of σ_{sd} [3, 5.5] compared to [2, 3] for normal distribution. This is due to higher received SNR as shown in Fig. 7.5(b). The working simulations clearly establishes a relationship between the geometry of the SU positions generated using two different distributions and the effectiveness of the CS algorithms. The plots also indicates that, with large σ_{sd} of the two distributions, CS fails to perform efficiently in spite of having a lower coherence between the columns of Φ.

7.9 Minimum distance aided CS algorithm (MDACS)

The following section introduces the Minimum distance aided CS algorithm (MDACS). The proposed modification incorporates the received SNR at each individual SU to deduce the perfect set of measurement nodes. The output of the algorithm is a set of selected SUs, which helps to enhance the performance of the CS algorithms. Prior to the improvements, the existing min-dist algorithm [189] relied on selecting a random pair of SUs with a specific distance separation between adjacent SUs. The value of separation can be pre-defined by the user. Once the pair is selected, the algorithm randomly removes an SU from the chosen pair. The method iterates through a loop and repeats the procedure until a refined set is generated such that all SUs are separated from the adjacent SUs by the specified value. With an incremental increase in distance separation, the algorithm sequentially eliminates SUs from a given set, until the l_2-norm error of the recovered sparse vector is greater than some predefined value. As the previous algorithm depends on random removal of SU nodes, there may be situations where SUs with higher RSS may be accidentally eliminated. As a result, corrupted measurement data may get included in the observation vector. Such scenarios may

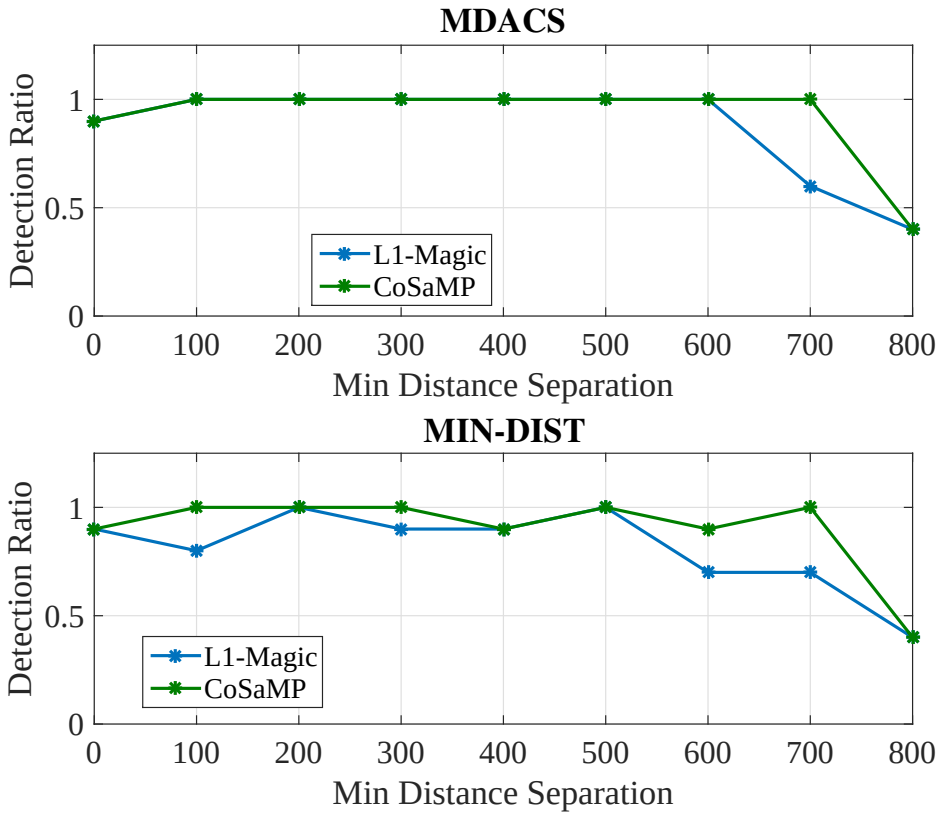

Fig. 7.6: (a) Detection ratio of MDACS ;(b) detection ratio of existing algorithm.

restrict CS algorithms from successfully retrieving the sparse vector. Considering the issues with the existing algorithm, our modification uses the RSS at each SU to produce a refined group of SUs with certain geometry. In other words, the algorithm selectively eliminates SUs with low received SNR and the outcome is a new set of SUs such that there average received SNR is greater than some user-defined value. Algorithm 1, provides an high-level description of the modified technique. The new set of SUs have the required minimum distance separation between each adjacent nodes as well as high RSS. The separation allows the observation to be independent reducing the coherence in the measurement matrix and high RSS reduces the chance of observations being corrupted by channel noise. Fig. 7.6 (a) and (b) evaluates the detection ratio of MDACS in comparison to the existing min-dist algorithm in [189]. In Fig. 6(a) the results for detection ratio shows a consistent pattern compared to the unusual pattern

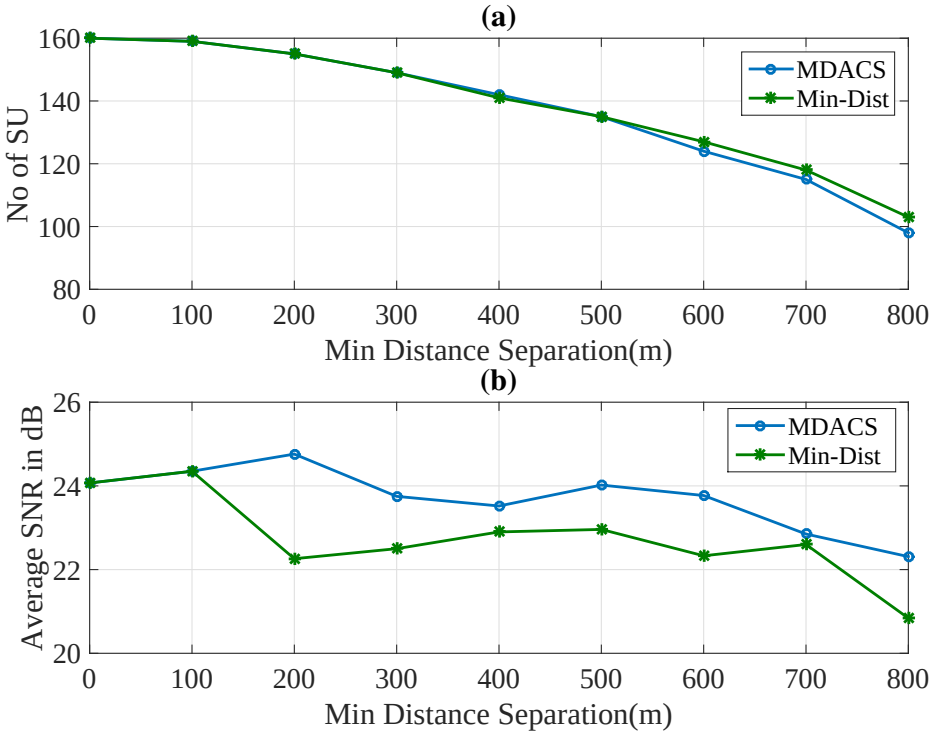

Fig. 7.7: (a) No of SU vs minimum distance separation; (b) Average received SNR vs minimum distance separation.

in Fig. 7.6(b). The inconsistency in case of the min-dist algorithm in Fig. 7.6(b), is due to random removal of SUs with higher RSS values. To further validate the impact of MDACS algorithm on the average SNR of the refined set, simulation results are presented in Fig. 7.7. The result shows that the reduction of the number of SUs for both the MDACS and min-dist algorithms are almost identical. However, in case of MDACS, the refined set of SUs have higher average received SNR than with the existing min-dist. The result presented in this section indicates that even with the selective elimination of SUs at each iteration, MDACS is able to maintain a set of SUs with relatively high average SNR. The gradual elimination of SUs helps to reduce the computational complexity while a high average SNR ensures accurate recovery of the sparse vector using CS algorithms.

Algorithm 1: Minimum distance aided CS algorithm

Input: $\{su\_pos,\ mindist,\ snr\_dB,\ error\}$
Output: $Refined\ set\ of\ SU$, $X_{M\times 1}$
Method:

$d \rightarrow mindist$;
$snr \rightarrow snr\_dB$;
$Q \rightarrow 0$;
$min\_dist \rightarrow min\{pdist(SU\_POS)\}$;

while (min_dist < d) **do**

(i) Find SU pair with separation less than d;
(ii) Extract the SU with higher SNR;
(iii) Create new set with extracted SUs;
(iv) Feed the refined set into CS algorithm;
(v) Q = (l_2-norm of recovery vector) - Q;

if $(Q > error)$,
break;
end

end while

Return SU_POS, $X_{M\times 1}$

7.9.1 Simulations

To verify the robustness of our proposed MDACS algorithm, the simulations were carried out for two different sets of distributions of the location of the secondary users, first for a Gaussian random distribution and second for uniform random distribution. In the previous section, the simulations were conducted with a set of SUs whose locations were generated from a two-dimensional Gaussian distribution. In Fig. 7.8 the effectiveness of our proposed MDACS algorithm is verified in order to successfully detect the presence of PUs using the L1-Magic and the CoSaMP algorithms. For each distribution, the spread of the distribution σ_{sd} is kept constant at 2.5. Fig. 7.8(a), shows the detection ratio plots for each of the MDACS algorithms with respect to the different sets of distributions used for SU positioning. The legend L1-Nor represents L1-Magic with SUs extracted from a Gaussian distribution; CoSaMP-Nor represents

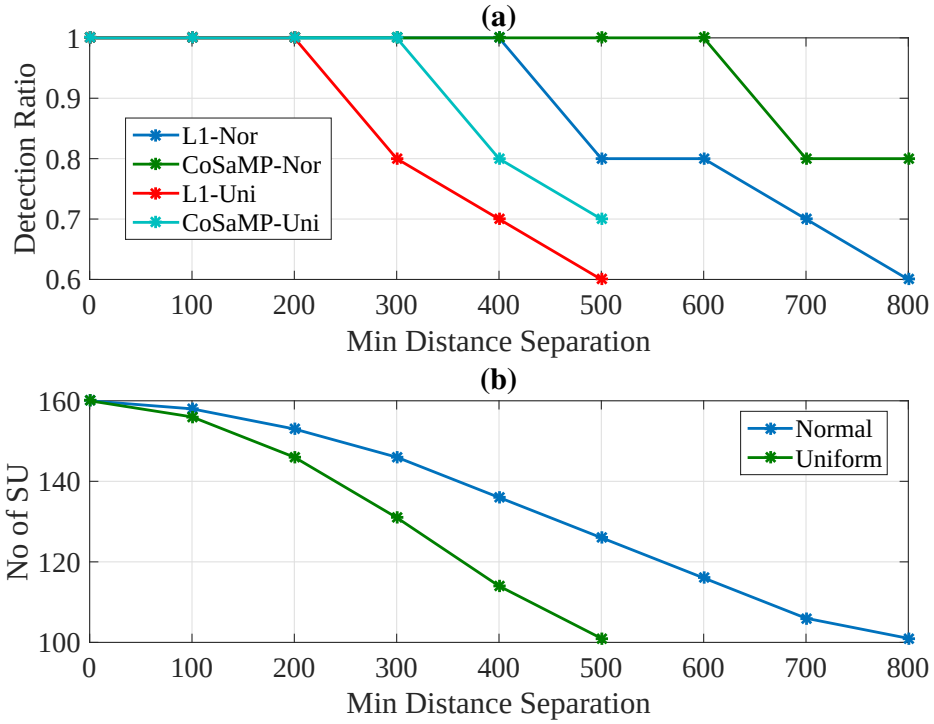

Fig. 7.8: (a) Detection ratio of minimum distance aided CS algorithms associated with two different sets of SUs. (b) Reduction in the number of SU with respect to increasing minimum distance separation.

the results for CoSaMP with SUs extracted from Gaussian distribution. On the other hand, the legend L1-Uni represents L1-Magic CS with SUs whose locations are generated from a two-dimensional uniform distribution; CoSaMP-Uni represents the results for CoSaMP with SUs extracted from a uniform distribution. In the x-axis, we gradually increase the minimum distance separation between the SUs until the detection ratio drops below a certain threshold. Fig. 7.8(a) shows that L1-Uni and CoSaMP-Uni have a detection ratio < 0.8, when minimum distance separation is greater than 300m and 400m respectively. A similar trend can be observed in case of normal distribution, where the detection ratio drops below 0.8 at a distance separation of 500 m and 700 m. From the results, it can be seen that the CS algorithms can maintain a higher detection ratio for a larger distance separation for normal distribution rather than uniform. Moreover in Fig. 7.8(b) it can be seen that, with systematic elimination of SUs from a random set, the proposed MDACS algorithm reduce the number of measurements

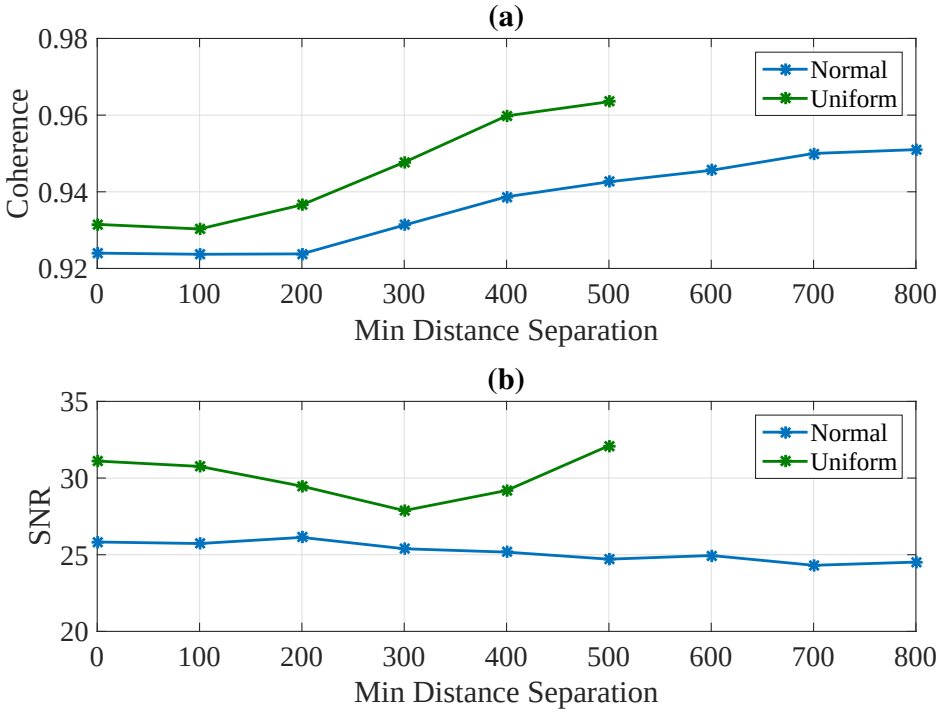

Fig. 7.9: (a) Impact of minimum distance separation on the coherence of the measurement matrix; (b) Average SNR of the refined set of SUs as a function of the minimum distance septation.

by 28% for a normal distribution and 21% for an uniform distribution. In both cases, CoSaMP outperformed L1-Magic in terms of achieving a higher detection ratio.

7.9.2 Effect on Characteristics of Measurement Matrix

The systematic removal of measurement nodes impacts the overall structure of the measurement matrix. Fig. 7.9 gives a deeper insight into the characteristics of each distribution by evaluating parameters, such as the coherence of measurement matrix and the average received SNR at SUs (observation vector). In the previous simulation, with an incremental increase in distance separation the number of SUs decreases. The reduction is due to the elimination of SUs by the MDACS algorithm. This has a direct impact on the coherence of the measurement matrix as shown in Fig. 7.9(a). The measurement matrix is a rectangular matrix, where the rows are the observations

from each SU. A reduction in the number of receiving nodes causes a rank deficiency, pushing the coherence of the measurement to a higher value. This makes the matrix inversion process difficult. For the uniform set, the matrix coherence reaches a maximum value of 0.9635 compared to 0.9510 for the normal set. According to the theory of CS, a successful recovery of a sparse vector is not feasible with the matrix having high coherence between the columns. From the working simulations and results, we can clearly conclude that the SU positions that are Gaussian distributed offer better recovery using the MDACS algorithm than for a uniform distribution.

7.9.3 Error in Recovery vector

On each iteration of the MDACS algorithm, it removes excess SUs until, the detection ratio or the l_2-norm of the recovered sparse vector drops below a certain threshold. The stopping criterion can be a user-defined threshold depending on the application. In scenarios where localization of nodes has a higher priority, the error threshold can be raised to a higher value. In Fig. 7.10, the y-axis represents the difference of the $l_2 - norm$ of the recovered vector and the original vector. A high $l_2 - norm$ error suggests that, REM created with the respective recovered sparse vector will have significant errors. Irrespective of the CS algorithms used, the sparse vector should have the same $l_2 - norm$, as the positioning of PUs and their transmit power level is constant for all. As can be seen in the figure, all the four plots have approximately similar starting points with slight variations, mainly due to minor errors in accurately determining the transmit powers. Although the plots for a uniform distribution have comparatively small errors at the start, with incremental distance separation, there is an exponential increase in the difference in l_2-norm. The plot of L1-Uni generates the maximum error with increasing distance separation followed by CoSaMP-Uni, L1-Nor and CoSaMP-Nor. The results indicate that the sparse vector recovered using CoSaMP algorithm associated with SUs extracted from a normal distribution have the least $l_2 - norm$ error. This makes CoSaMP-Nor a suitable option for an accurate generation of a Radio Environment Map.

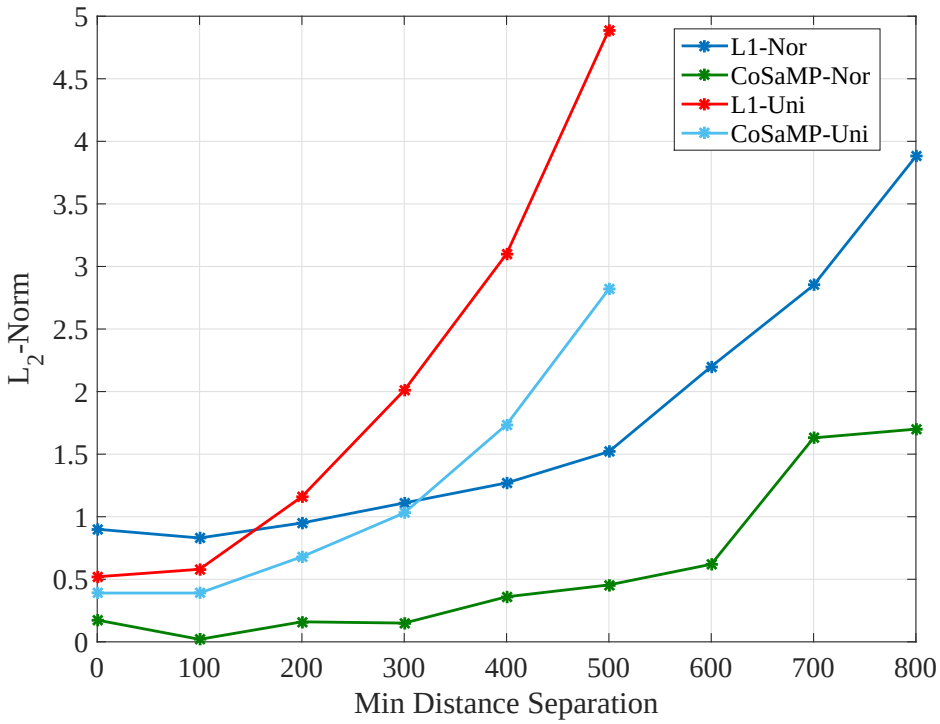

Fig. 7.10: Difference in l_2-norm of the recovery vector to the original vector.

7.10 Proposed Algorithm Comparison

The working solutions and results from the previous section, conclude that CoSAMP incorporated with MDACS algorithm with SU positions extracted from a Gaussian random distribution generates maximum detection ratio with the minimum error. The previous results (Fig.7.8) also show that, for our best case scenario, the CoSAMP-(MDACS) algorithm achieved a detection ratio of 1, with only 115 SUs. To validate the effectiveness of the proposed MDACS algorithm, we compared the performance with the original CoSAMP and L1-Magic CS algorithms (without the selective elimination feature for MDACS). In both cases, 115 SU positions were extracted from a Gaussian random distribution with $\sigma_{sd} = 2.5$. Fig. 7.11 illustrates the impact of our proposed method in enhancing the performance of the CS algorithms. Fig. 7.11(a) shows that our method allows 20% and 10% more detection for CoSAMP and L1-Magic respectively, especially when integrated with the MDACS algorithm. Even when evaluating the difference in l_2-norm error, Fig. 7.11(b) shows that the proposed technique reduce the

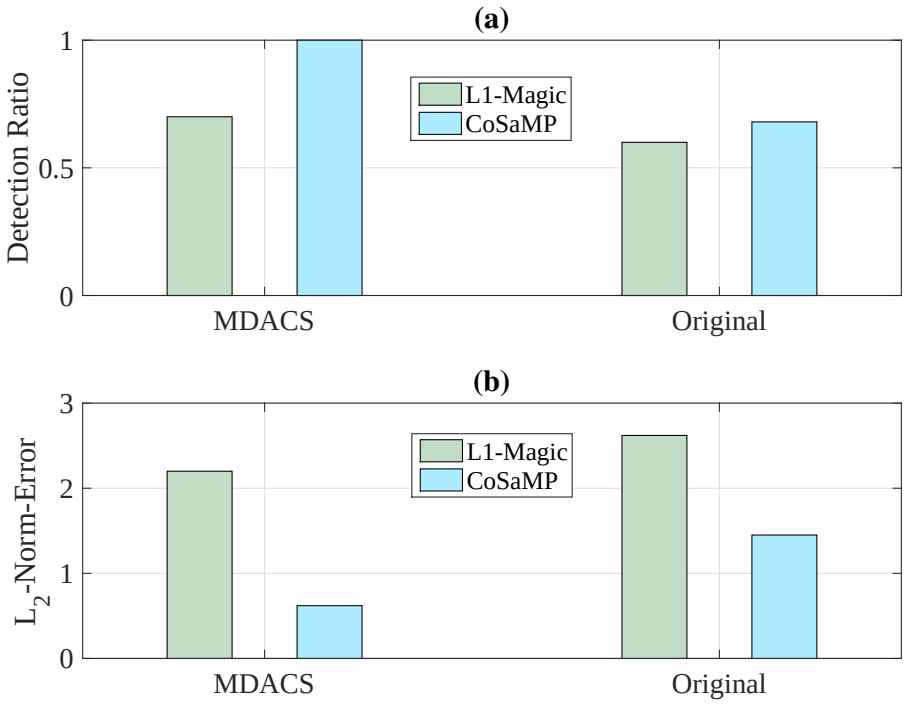

Fig. 7.11: Detection ratio and Error comparison of proposed algorithm compared to original CS algorithm .

error by 57% and 17% for CoSAMP and L1-Magic respectively. Moreover, Fig. 7.12(b), shows that the set of SU generated from the refinement technique has 3% less coherence than the randomly deployed set of SUs. Limited coherence between the columns allows better structure in the construction of a measurement matrix and enables the refined set of SUs to operate at a lower received SNR of 24.95 dB compared to 26.73 dB as shown in Fig. 7.12(a).

7.11 Conclusion

This paper discusses the formulation of a novel algorithm to jointly deduce the location and transmit power of PUs in a cognitive radio network. The algorithm exploits the geographic location of the SUs to extract useful information about the positioning of PUs in a network. The proposed method introduces a refinement technique to

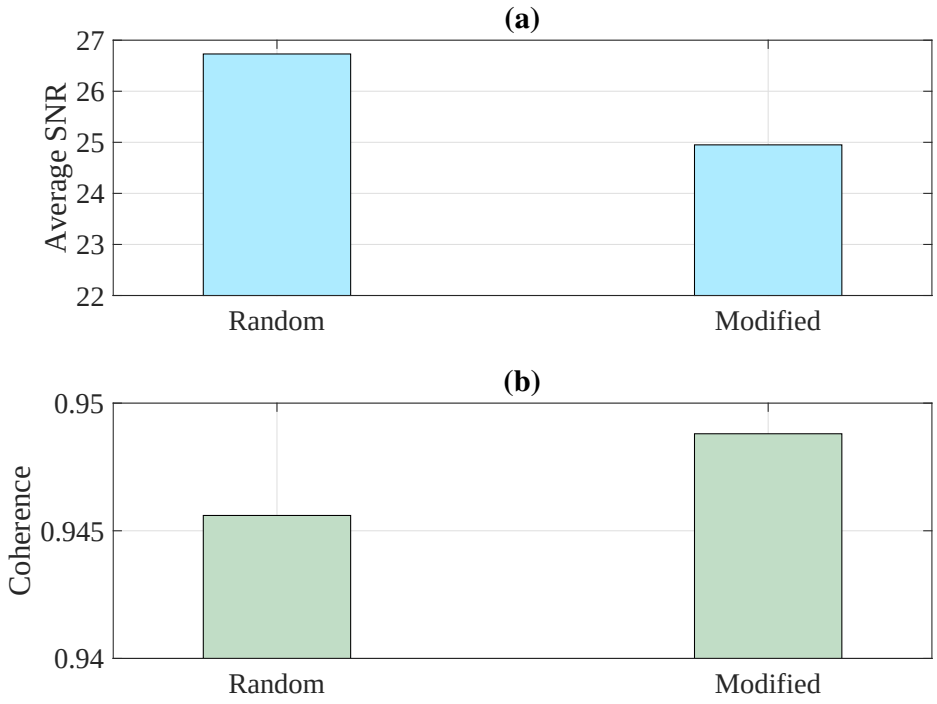

Fig. 7.12: Impact of proposed algorithm on coherence and received SNR at SUs.

selectively eliminate closely spaced SUs in order to reduce the number of correlated observations. The novel method allows adjacent SUs to have a minimum distance separation, such that the observations at each SUs are nearly independent. Simulation results show that our novel MDACS algorithm achieved significant improvements in the overall performance of CS algorithms. Simulation results indicate that our proposed approach has a 20% higher detection ratio, while reducing the l_2-norm error by 57%. Moreover, the results also show that our approach generates a set of selective SUs with lower coherence than with random positioning. This enables CS algorithms to offer perfect recovery at a comparatively lower received SNR. To verify the robustness of the algorithm, we tested our method for two spatial probability distributions for SU positions. In both cases, our algorithm achieved a maximum detection ratio with fewer secondary users as receive power sensing. Future work will incorporate the construction of an efficient Radio Environment Map, to detect free spectrum in a geographic area.

8

Conclusion and Future work

8.1 Conclusion

The dissertation presented detailed research on positioning techniques used to estimate the exact geographical location of a transmitting source. The techniques are developed based on the framework of Compressive Sensing (CS) an emerging method for signal acquisition. CS framework relies on discretizing continuous parameters such as geographical area and angular range to finite grid points in order to construct a finite dictionary matrix. In reality, when the sensing parameter is not exactly aligned to the finite grid points, the performance of CS degrades significantly. In this dissertation, we emphasized primarily upon innovating algorithms that can overcome the limitations of CS while accurately estimating the location information of a source. Several

novel positioning algorithms are proposed in this dissertation that utilize the properties of a signal such as direction of propagation and signal strength to determine the location of a transmitting source. The dissertation consists of two novel Direction of Arrival (DOA) estimation algorithms and one Received Signal Strength (RSS) based localization algorithms. Apart from the invention of the estimation algorithms, the dissertation unveils some open-ended issues that can have significant influence in the development of any CS based DOA estimation algorithms.

	MUSIC	**Root-MUSIC**	**ESPRIT**	**ICSDOA**.
SNR	High	High	High	Moderate
Snapshots(P)	High	High	Moderate	One
Antenna Elements (N)	High	High	Moderate	Moderate
Complexity	$O(PM^2N + N^2)$	$O(PM^2N + N^2)$	$O(PM^2 + M^3)$	$O(5MN)$

TABLE 8.1: Complexity comparison of DOA estimation algorithms.

The first novel algorithm ICSDOA proposed in chapter 3, 4 and 5 highlights a key innovation of a new signal processing paradigm that completely eliminates the quantization error in grid-based CS framework and allows the Mean Square Error (MSE) to be on the theoretical Cramér-Rao lower bound (CRLB) and no algorithm can perform better than the bound. The performance of the algorithm is demonstrated by applying it on two well-known antenna geometries, the Uniform Circular Array (UCA) and Uniform Linear Array (ULA). In both cases, the algorithm achieved the CRLB with moderate Signal-to-Noise Ratio (SNR). The underlying concept of the algorithm is based on a two-stage estimation process, where a coarse estimate is initially calculated to obtain the nearest quantized grid points. Later an iterative loop is initiated that exploits the two dominant complex envelopes of the reconstructed sparse signal to generate an error discriminant. Simulation results suggest that for both UCA and ULA, the algorithm converges to an accurate estimate using just two iterations. The iterative loop is designed to halt when the error discriminant converges to zero or some user defined threshold. The computational complexity of the algorithm is calculated to be O(5MN), where M and N represents the number of antenna elements in the antenna

geometry and M is the number of quantized angular grid points. Compared to the celebrated DOA techniques such as MUSIC, Root-MUSIC and ESPRIT, the computational complexity of ICSDOA is significantly lower. Table 8.1 presents a complexity comparison of the algorithms including ICSDOA.

The robustness of the proposed ICSDOA algorithm is validated by carrying out extensive statistical analysis with noise inherent to the UCA and ULA processing. Initial investigation suggest that ULA offers a better DOA estimate than UCA, given that the incoming DOA is in the broad-side region of the antenna geometry. This is supported by the CRLB derivation of DOA estimate using UCA and ULA. However, UCA has a broader range of azimuth angular coverage compared to ULA. Simulation results indicate that both UCA and ULA integrated with ICSDOA out-performs well Known Root-MUSIC, Beamforming and ESPRIT DOA estimation algorithms when single snapshot of the signal is considered. EVD-based techniques such as Root-MUSIC and ESPRIT relies on larger number of snapshots to obtain a an accurate estimate, whereas the performance of Beamforming is dependent on finer quantization of angular grid. Both large number of snapshots and finer grid quantization greatly increases the computational complexity of the algorithm, hence making them less attractive for practical application. On the other hand ICSDOA uses the advantages of both worlds to obtain a computationally effective accurate estimate. The CS framework of ICSDOA enables the algorithm to perform using a single snapshot whereas the iterative process (error discriminant calculation) allows the estimate to converge to the CRLB using a coarser grid quantization. The MSE comparison simulation result shows that UCA and ULA with ICSDOA offer 10 dB and 5 dB better estimate than the well-known techniques. It is worth noting that this performance is achieved using just a single snapshot of the incoming signal. To the best of our knowledge, no other computationally efficient algorithms have achieved such results using two completely different antenna geometries. The results also re-iterates the fact that the ICSDOA technique can be adapted for a wide range of antenna geometries, validating the robustness and compatibility of the algorithm.

In addition to the invention of the algorithm, the thesis provides an in-depth analysis

on the structure of the dictionary matrices for UCA and ULA antenna geometry and its impact on the estimation process. Due to the difference in antenna geometries, the structure of the dictionary matrices is vastly different. The entries of the dictionary matrix are a function of the number of antenna elements (M), the number of finite angular grid points (N) and the inter-element spacing of the antenna elements. It has been illustrated through simulation results and theoretical analysis that there exists a direct relationship between M and N that influences any CS based DOA estimation methods. The analysis concludes that both UCA and ULA constructed with larger M requires finer quantization of angular grid (i.e, large N) in order to achieve the CRLB of estimation error. However, it was found that ULA is more sensitive to a coarser grid quantization compared to UCA. Although a large M yields a better estimation accuracy of the DOA, at the same time it increases the computational complexity of the algorithm. Thus, there is a systematic trade-off of performance against computational complexity. It has been an open-ended issue in the framework of CS-based DOA techniques and according to our best knowledge, such analysis has not been addressed in any other prior literature.

Moreover, the dissertation also analyzes the impact of array geometry parameters such as the number of antenna elements and the radius of the UCA on the structure of the dictionary matrix. As the dictionary matrix is rectangular is shape, the mutual coherence property is used as an indicator of the fitness of the matrix. It was found that an increase in M improves the fitness of the matrix (low mutual coherence) especially in the case of UCA. However, on closer analysis, it was discovered that an increase in an odd number of M yields a lower mutual coherence compared to even M. This is due to the centro-symmetric property of the UCA, that causes UCA with even M to have indistinguishable observations hence reducing the dimensionality of the dictionary matrix. In the case of ULA, the increase M does not have any significant impact apart from a slight reduction in mutual coherence. On a separate analysis, the impact of inter-element spacing on the mutual coherence of the dictionary matrix of UCA and ULA are studied in detail. The study states that for UCA, there exists an optimum inter-element spacing greater than $\lambda/2$ that causes the mutual coherence

between the columns of the dictionary matrix to be significantly reduced. The analysis was supported by simulation results that show using the optimal radius, the MSE can be 16 dB lower than that with the traditional $\lambda/2$ element spacing. However, for a larger inter-element spacing, the array size also increases, hence there is a systematic trade-off between the size of UCA and the precision of the DOA estimation. In the case of ULA, the study found $\lambda/2$ to be the optimum inter-element spacing.

The dissertation also discusses a novel multi-resolution DOA (MRDOA) detection algorithm, based on CS technique, to estimate the DOA of a signal arriving from an off-grid source. Similar to the ICSDOA, MRDOA is based on a two-stage strategy, whereby in the first state an initial estimate is obtained using a single CS operation. Then in the next stage, a finer sequential search is carried out around the initial estimate. Compared to traditional CS based algorithm using finer grid quantization, MRDOA achieved a significant reduction in computation complexity. The complexity is calculated to be O(2MN) which is less than the complexity of ICSDOA (O(5MN)). Simulation results suggest that at a relatively high SNR, our MRDOA has reduced the MSE of off-grid DOA estimation approximately by a factor of 10, compared to traditional Beam-Scan and Weighted-Centroid techniques. However, unlike ICSDOA, MRDOA was unable to achieve the CRLB of estimation error. This is primarily because of the error induced due to grid quantization. Although in terms of computational complexity, MRDOA offers a feasible alternative, but in scenarios when estimation accuracy is a priority, ICSDOA is the best solution as it guarantees convergence to the correct estimate.

In addition to the two DOA techniques, the thesis discusses the formulation of a novel algorithm to jointly deduce the location and transmit power of a transmitting node in a cognitive radio network. The algorithm is also based on the framework of CS where RSS information at randomly positioned sensor nodes is used to estimate the location of a transmitting node. The proposed method introduces a refinement technique to selectively eliminate closely spaced sensor nodes so that the number of correlated observations are significantly reduced. Two spatial probability distributions namely Gaussian and Uniform distributions are used to randomly generate the location

of the sensor node. For each case, the impact of the two distributions on the mutual coherence of the dictionary matrix is analyzed in detail. The research suggests that Gaussian distribution of sensor nodes offers a better reduction of mutual coherence of the dictionary matrix than that uniform distribution. It was found that RSS observations among the sensor nodes are more independent in the case of Gaussian distribution compared to the uniform distribution. Simulation results indicate that our proposed refinement method coupled with the Gaussian distribution of sensor nodes achieved a 20% higher detection ratio while reducing the l_2-norm error by 57%, when compared to other techniques where nodes are randomly distributed without the refinement.

Overall, the thesis provided an in-depth analysis of the impact of measurement matrix on several estimation processes using CS framework. The fitness of the measurement matrix is an integral part of CS processing and requires finer tuning in order to achieve the expected result. The luxury of selecting a structured dictionary matrix is extremely limited in practical scenarios. And there are no such global formulas that would provide the perfect measurement matrix for all scenarios. The physical properties of the sensing process (e.g., the laws of wave propagation), as well as the constraints associated with the respective grid points, will always dictate the structure of the measurement matrix. Hence, each scenario requires specific manipulation of physical parameters in order for the underlying CS algorithms to achieve the best result. In addition to the three separate estimation algorithms, the thesis paved the path for new research towards manipulation of physical parameters in order to enhance the fitness of the measurement matrix.

8.2 Future Work

In future the following aspects can be considered for further research and developments:

- As part of future work, it is also of great interest to extend the algorithm using multiple receiving UCA and ULA antennas to deduce the location of the transmitting source in a network. We are also currently working on developing a working prototype to validate the performance of the algorithm in a realistic

environment.

- Incorporating ICSDOA into a wide range of antenna geometries to verify the performance. Our key interest is towards the X-array that has the precision of the ULA geometry and the 2π azimuth coverage of the UCA.

- Possible extension of the ICSDOA algorithm is to detect transmitting sources in 3D can be a future research topic. We have already initiated our research to cater for such scenarios and are in the simulation phase.

- Currently, using ICSDOA and two phased array antennas at two different location, we can position the source with extreme accuracy. The next phase of the work can focus on tracking the source using smart filtering techniques. As ICSDOA uses a single snapshot of the incoming signal, it can be a computationally efficient alternative to detect moving objects in an indoor and outdoor environment.

- In the analysis of antenna geometry (especially in the case of UCA), the relationship between grid quantization and inter-element spacing will be an interesting area of study. Our primary investigation suggested that the optimal radius varies with grid quantization. A detailed analysis may reveal some interesting answer leading to future research.

- The underlying concept of ICSDOA can be expanded to cater for various estimation processes using TOA, TDOA or RSS information of a received signal. A comparison study of three different estimation processes can provide worldview comparison among the different techniques.

- Currently the RSS based localization algorithm relies on having the transmitting source on the exact grid points. Using the concept of ICSDOA, the algorithm can be expanded to cater for off-grid scenarios. This will enable localization of transmitting sources anywhere on a specific geographic area. This can help future research towards identifying exclusion zones using the construction of an efficient REM.

A

Appendix A

A.1 List of Acronyms

1G	First Generation
2G	Second Generation
3G	Third Generation
4G	Third Generation
5G	Third Generation
ABS	Australian Bureau of Statistics
ACMA	Australian Communication and Media Authority
AN	Anchor Node

AOA	Angle of Arrival
AP	Access Point
ARV	Array Response Vector
CDMA	Beam-forming
CDMA200	Base Station
COSAMP	Base Station
CR	Base Station
CRLB	Base Station
CRN	Base Station
D2D	Base Station
BS	Base Station
DCT	Discrete Cosine Transform
DF	Direction Finding
DFT	Discrete Fourier Transform
DOA	Direction of Arrival
DoD	Department of Defence
DSA	Dynamic spectrum access
DSS	Dynamic Spectrum Sharing
EB	Exabyte
EDGE	Enhanced Data Rate for GSM Evolution
EL	Expected Likelihood
ER	Error Ratio
ESPRIT	Estimation of Signal Parameters via Rotational Invariance Techniques
EVD	Eigenvalue Decomposition

FC	Fusion Centre
FDMA	Frequency Division Multiple Access
GB	Gigabyte
GHz	Giga Hertz
GPS	Global Position System
GPS	Global Positioning System
GSM	Global System for Mobile Communication
HetNet	Heterogenous Networks
HSPDA	High Speed Packet Access
ICSDOA	Iterative Compressive Sensing based DOA estimation
IFF	Identification, Friend or Foe
KB	Kilobyte
Kbps	Kilo bits per second
KLT	Karhunen-Loeve Transform
LASSO	Least-Absolute Shrinkage And Selection Operator
LBE	Learning-by-example
LOB	Lines of Bearing
LOS	Line of Sight
LTE	Long Term Evolution
M2M	Machine to Machine
MB	Megabyte
Mbps	Mega bits per second
MDACS	Minimum-Distance Separation Aided Compressive Sensing Algorithm
MDR	Mean Detection Ratio

MIMO	Multiple In Multiple Out
ML	Maximum Likelihood
MRDOA	Multi-Resolution DOA
MSE	Mean Square Error
MSSE	Mean Square Sparse Error
MUSIC	Multiple Signal Classification
NAVSTAR	Navigation System with Timing and Ranging
OFDMA	Orthogonal Frequency Division Multiple Access
OMP	Orthogonal Matching Pursuit
P2P	Point-to-Point
PPS	Precise Positioning Service
PU	Primary User
QOS	Quality of Service
REM	Radio Environment Map
RFID	Radio Frequency Identification
RIP	Restricted Isometry Property
Root-MUSIC	Root Multiple Signal Classification
RSS	Received Signal Strength
RSSI	Received Signal Strength Indicator
RVM	Relevance Vector Machine
SBL	Sparse Bayesian learning
SDR	Software Defined Radio
SM	Spatial Multiplexing
SNR	Signal-to-Noise Ratio

SPS	Standard Positioning Service
SSR	Sparse Signal Representation
STLS	Sparse Total Least Squares
SU	Secondary Users
SVD	Singular Value Decomposition
TDMA	Time Division Multiple Access
TDOA	Time Difference of Arrival
TOA	Time of Arrival
UCA	Unifirm Circular Array
ULA	Uniform Linear Array
UTMS	The Universal Mobile Telecommunication System
WCN	Wireless Communication Network
WCS	Wireless Communication System
WLAN	Wireless Local Area Network
ZB	Zetabyte

B

Appendix

B.1 CRLB for UCA

The Cramér-Rao Lower bound determines the lower bound of the variance of an unbiased estimator. An estimator achieving the CRLB is considered to be efficient and it is not possible for any estimator to perform better than the theoretical CRLB. In this work, CRLB will be used verify the MSE of our DOA estimation algorithm compared to the theoretical bound. The single path cases with omni-directional antennas are only considered in this simulation; further information for a multi-path scenarios can be obtained from [149]. In this derivation of CRLB, we are not interested in the channel gain and phase of the incoming signal. Thus the output of the antenna array

for any incident angle ψ, at any time sample can be written as,

$$V = \alpha e^{jb}\Phi(\psi) + \eta \tag{B.1}$$

where, αe^{jb} is considered to be 1; $\Phi(\psi) = [\tau_1(\psi), \tau_2(\psi), \cdots, \tau_M(\psi)]^T$ and $\eta = [\eta_1, \eta_2, \cdots, \eta_M]$ is a noise vector with entries extracted from a zero-mean Gaussian random vector with variance σ^2. The probability density $f = f(\mathbf{V}|\psi)$ of the vector $\mathbf{V}$ is computed by

$$f(\mathbf{V}|\psi) = c \ \exp\left\{-\frac{(\mathbf{V} - \Phi(\psi))^H - (\mathbf{V} - \Phi(\psi))}{\sigma^2}\right\}. \tag{B.2}$$

The log-likelihood function is,

$$\ln(f(\mathbf{V}|\psi) = \ln(c) - \left\{\frac{(\mathbf{V} - \Phi(\psi))^H - (\mathbf{V} - \Phi(\psi))}{\sigma^2}\right\}. \tag{B.3}$$

After some mathematical manipulation and differentiating the log-likelihood function produces,

$$\begin{aligned}\frac{\partial \ln(f(\mathbf{V}|\psi)}{\partial\psi} = -\frac{1}{\sigma^2}\Bigg\{&\left(\frac{\partial\Phi}{\partial\psi}\right)^H \mathbf{V} + \mathbf{V}^H\left(\frac{\partial\Phi}{\partial\psi}\right) - \left(\frac{\partial\Phi}{\partial\psi}\right)^H \Phi(\psi) \\ &-\Phi^H(\psi)\left(\frac{\partial\Phi}{\partial\psi}\right)^H\Bigg\}\end{aligned} \tag{B.4}$$

and,

$$\begin{aligned}\frac{\partial^2 \ln(f(\mathbf{V}|\psi)}{\partial\psi^2} = -\frac{1}{\sigma^2}\Bigg\{&\left(\frac{\partial^2\Phi}{\partial\psi^2}\right)^H \mathbf{V} + \mathbf{V}^H\left(\frac{\partial^2\Phi}{\partial\psi^2}\right) \\ &- \left(\frac{\partial^2\Phi}{\partial\psi^2}\right)^H \Phi(\psi) - 2\left(\frac{\partial\Phi}{\partial\psi}\right)^H\left(\frac{\partial\Phi}{\partial\psi}\right) - \Phi^H(\psi) - \left(\frac{\partial^2\Phi}{\partial\psi^2}\right)\Bigg\}\end{aligned} \tag{B.5}$$

From the theory of CRLB [190], we know that,

$$\text{var}(\psi) \geq \frac{1}{-\mathbb{E}\left[\frac{\partial^2 \ln(f(\mathbf{V}|\psi)}{\partial\psi^2}\right]}. \tag{B.6}$$

From [191], we obtained a simplified form as,

$$\mathbb{E}\left[\frac{\partial^2 \ln(f(\mathbf{V}|\psi)}{\partial\psi^2}\right] = \frac{-2}{\sigma^2}\left\|\frac{\partial\Phi}{\partial\psi}\right\|^2 \tag{B.7}$$

where,

$$\left\|\frac{\partial\Phi}{\partial\psi}\right\|^2 = \sum_{i=1}^{M}\beta^2 r^2 sin^2\left(\psi - \frac{2\pi i}{M}\right) = \frac{M\beta^2 r^2}{2}. \tag{B.8}$$

By combining (24),(25) and (26), we compute the CRLB for angle estimation as,

$$\text{var}(\psi) \geq \frac{-1}{\left(\frac{-2}{\sigma^2}\right)\left(\frac{M\beta^2 r^2}{2}\right)} = \frac{\sigma^2}{M\beta^2 r^2}. \tag{B.9}$$

Bibliography

[1] *Heterogeneous 5g networks.* Open Air Interface URL http://www.openairinterface.org/?page_id=458. xxi, 6

[2] S. Haykin. *Cognitive radio: brain-empowered wireless communications.* IEEE journal on selected areas in communications **23**(2), 201 (2005). xxi, 9

[3] *Beyond 2020 heterogeneous wireless networks with millimeter-wave small cell access and backhauling.* MiWaveS URL http://www.miwaves.eu/index.html. xxi, 12

[4] K. Pahlavan. *Principles of wireless networks: A unified approach* (John Wiley & Sons, Inc., 2011). 1

[5] G. L. Stüber. *Principles of mobile communication*, vol. 2 (Springer, 2001). 2

[6] E. Perahia. *Ieee 802.11n development history, process, and technology.* IEEE Communications Magazine **46**(7) (2008). 2

[7] B. Sidhu, H. Singh, and A. Chhabra. *Emerging wireless standards-wifi, zigbee and wimax.* World Academy of Science, Engineering and Technology **25**(2007), 308 (2007). 2

[8] *The zettabyte era: Trends and analysis.* Cisco (2017). URL https://www.cisco.com/c/en/us/solutions/collateral/service-provider/visual-networking-index-vni/vni-hyperconnectivity-wp.html. 2

[9] *Cisco visual networking index: Forecast and methodology, 20162021.* Cisco (2017). URL https://www.cisco.com/c/en/us/solutions/collateral/service-provider/visual-networking-index-vni/complete-white-paper-c11-481360.html.

[10] *Cisco visual networking index: Global mobile data traffic forecast update, 20162021 white paper.* Cisco (2017). URL https://www.cisco.com/c/en/us/solutions/collateral/service-provider/visual-networking-index-vni/mobile-white-paper-c11-520862.html. 2

[11] *Main features - volume of data downloaded.* Australian Bureau of Statistics, Australian Government . 3

[12] *Main features - mobile handset subscribers.* Australian Bureau of Statistics, Australian Government .

[13] T. A. Communications and M. Authority. *Standard asset page.* Australian Government / ACMA (2016). URL http://www.acma.gov.au/theACMA/Newsroom/Newsroom/Media-releases/appetite-for-digital-content-drives-extensive-changes. 3

[14] D. Astély, E. Dahlman, A. Furuskär, Y. Jading, M. Lindström, and S. Parkvall. *Lte: the evolution of mobile broadband.* IEEE Communications magazine **47**(4) (2009). 4

[15] R. M. Whitaker and S. Hurley. *Evolution of planning for wireless communication systems.* In *36th Annual Hawaii International Conference on System Sciences, 2003. Proceedings of the*, pp. 10 pp.– (2003). 4

[16] *Ge, nokia and qualcomm unveil first private lte-based trial network customized for industrial iot.* Qualcomm Press Release (2017). URL https://www.qualcomm.com/news/releases/2017/02/22/ge-nokia-and-qualcomm-unveil-first-private-lte-based-trial-network. 4

[17] *A brief history of wi-fi.* The Economist (2004). URL http://www.economist.com/node/2724397. 5

[18] *Helping define 802.11n and other wireless lan standards.* Intel URL https://www.intel.com/content/www/us/en/standards/802-11-wireless-lan-standards-study.html. 5

[19] E. Hossain and M. Hasan. *5g cellular: key enabling technologies and research challenges.* IEEE Instrumentation & Measurement Magazine **18**(3), 11 (2015). 5

[20] W. H. Chin, Z. Fan, and R. Haines. *Emerging technologies and research challenges for 5g wireless networks.* IEEE Wireless Communications **21**(2), 106 (2014).

[21] H. S. Dhillon, H. Huang, and H. Viswanathan. *Wide-area wireless communication challenges for the internet of things.* IEEE Communications Magazine **55**(2), 168 (2017).

[22] S. Chen and J. Zhao. *The requirements, challenges, and technologies for 5g of terrestrial mobile telecommunication.* IEEE Communications Magazine **52**(5), 36 (2014).

[23] *5g systems- enabling the transformation of industry and society.* Ericsson White Paper URL http://www.abs.gov.au/ausstats/abs@.nsf/Latestproducts/8153.0Main%20Features5December%202016?opendocument&tabname=Summary&prodno=8153.0&issue=December2016&num=&view=. 5

[24] N. Bhushan, J. Li, D. Malladi, R. Gilmore, D. Brenner, A. Damnjanovic, R. Sukhavasi, C. Patel, and S. Geirhofer. *Network densification: the dominant theme for wireless evolution into 5g.* IEEE Communications Magazine **52**(2), 82 (2014). 5

[25] E. Hossain, M. Rasti, H. Tabassum, and A. Abdelnasser. *Evolution toward 5g multi-tier cellular wireless networks: An interference management perspective.* IEEE Wireless Communications **21**(3), 118 (2014). 6

[26] 3rd Generation Partnership Project. *Scenarios and requirements for small cell enahncement for e-utra and e-utran.* 3GPP TR36.932 V12.0.0 URL http://www.etsi.org/deliver/etsi_tr/136900_136999/136932/12.01.00_60/tr_136932v120100p.pdf. 6

[27] M. Eslami, R. C. Elliott, W. A. Krzymień, and M. Al-Shalash. *Location-assisted clustering and scheduling for coordinated homogeneous and heterogeneous cellular networks.* Transactions on Emerging Telecommunications Technologies **24**(1), 84 (2013). 6

[28] F. Boccardi, R. W. Heath, A. Lozano, T. L. Marzetta, and P. Popovski. *Five disruptive technology directions for 5g.* IEEE Communications Magazine **52**(2), 74 (2014). 6

[29] O. N. Yilmaz, Z. Li, K. Valkealahti, M. A. Uusitalo, M. Moisio, P. Lundén, and C. Wijting. *Smart mobility management for d2d communications in 5g networks.* In *Wireless Communications and Networking Conference Workshops (WCNCW), 2014 IEEE*, pp. 219–223 (IEEE, 2014). 6

[30] 3rd Generation Partnership Project. *Feasibility study for proximity services (prose).* 3GPP TR36.932 V12.0.0 URL http://www.tech-invite.com/3m22/tinv-3gpp-22-803.html. 7

[31] M. N. Tehrani, M. Uysal, and H. Yanikomeroglu. *Device-to-device communication in 5g cellular networks: challenges, solutions, and future directions.* IEEE Communications Magazine **52**(5), 86 (2014). 7

[32] Y. Ren, C. Wang, D. Liu, F. Liu, and E. Liu. *Applying lte-d2d to support v2v communication using local geographic knowledge.* In *Vehicular Technology Conference (VTC Fall), 2015 IEEE 82nd*, pp. 1–5 (IEEE, 2015). 7

[33] Q. Chen, G. Yu, H. Shan, A. Maaref, G. Y. Li, and A. Huang. *Cellular meets wifi: Traffic offloading or resource sharing?* IEEE Transactions on Wireless Communications **15**(5), 3354 (2016). 8

[34] M. Bennis, M. Simsek, A. Czylwik, W. Saad, S. Valentin, and M. Debbah. *When cellular meets wifi in wireless small cell networks.* IEEE Communications Magazine **51**(6), 44 (2013). 8

[35] S. Dimatteo, P. Hui, B. Han, and V. O. K. Li. *Cellular traffic offloading through wifi networks.* In *2011 IEEE Eighth International Conference on Mobile Ad-Hoc and Sensor Systems*, pp. 192–201 (2011). 8

[36] A. Pyattaev, K. Johnsson, S. Andreev, and Y. Koucheryavy. *3gpp lte traffic offloading onto wifi direct.* In *2013 IEEE Wireless Communications and Networking Conference Workshops (WCNCW)*, pp. 135–140 (2013). 8

[37] J. Mitola. *Cognitive radio—an integrated agent architecture for software defined radio* (2000). 8

[38] A. S. Margulies and J. Mitola. *Software defined radios: a technical challenge and a migration strategy.* In *Spread Spectrum Techniques and Applications, 1998. Proceedings., 1998 IEEE 5th International Symposium on*, vol. 2, pp. 551–556 (IEEE, 1998). 8

[39] I. F. Akyildiz, W.-Y. Lee, M. C. Vuran, and S. Mohanty. *Next generation/dynamic spectrum access/cognitive radio wireless networks: A survey.* Computer networks **50**(13), 2127 (2006). 10

[40] Q. Zhao and B. M. Sadler. *A survey of dynamic spectrum access.* IEEE signal processing magazine **24**(3), 79 (2007). 10

[41] W. Roh, J. Y. Seol, J. Park, B. Lee, J. Lee, Y. Kim, J. Cho, K. Cheun, and F. Aryanfar. *Millimeter-wave beamforming as an enabling technology for 5g cellular communications: theoretical feasibility and prototype results.* IEEE Communications Magazine **52**(2), 106 (2014). 10

[42] F. W. Vook, A. Ghosh, and T. A. Thomas. *Mimo and beamforming solutions for 5g technology.* In *2014 IEEE MTT-S International Microwave Symposium (IMS2014)*, pp. 1–4 (2014). 11

[43] J. C. Liberti and T. S. Rappaport. *Smart antennas for wireless communications: IS-95 and third generation CDMA applications* (Prentice Hall PTR, 1999). 11

[44] A. Paulraj, R. Nabar, and D. Gore. *Introduction to space-time wireless communications* (Cambridge university press, 2003). 11

[45] P. Kela, M. Costa, J. Turkka, M. Koivisto, J. Werner, A. Hakkarainen, M. Valkama, R. Jantti, and K. Leppanen. *Location based beamforming in 5g ultra-dense networks.* In *Vehicular Technology Conference (VTC-Fall), 2016 IEEE 84th*, pp. 1–7 (IEEE, 2016). 11

[46] M. Cheng and X. Fang. *Location information-assisted opportunistic beamforming in lte system for high-speed railway.* EURASIP Journal on Wireless Communications and Networking **2012**(1), 210 (2012). 11

[47] S. Sun, T. S. Rappaport, R. W. Heath, A. Nix, and S. Rangan. *Mimo for millimeter-wave wireless communications: beamforming, spatial multiplexing, or both?* IEEE Communications Magazine **52**(12), 110 (2014). 11

[48] W. Roh, J.-Y. Seol, J. Park, B. Lee, J. Lee, Y. Kim, J. Cho, K. Cheun, and F. Aryanfar. *Millimeter-wave beamforming as an enabling technology for 5g cellular communications: Theoretical feasibility and prototype results.* IEEE communications magazine **52**(2), 106 (2014). 11

[49] Q. Li, G. Li, W. Lee, M.-i. Lee, D. Mazzarese, B. Clerckx, and Z. Li. *Mimo techniques in wimax and lte: a feature overview.* IEEE Communications magazine **48**(5) (2010). 12

[50] Y. Zhang, G. Wang, and M. G. Amin. *Cooperative spatial multiplexing in multihop wireless networks.* In *Acoustics, Speech and Signal Processing, 2006. ICASSP 2006 Proceedings. 2006 IEEE International Conference on*, vol. 4, pp. IV–IV (IEEE, 2006). 12

[51] D. Adamy. *Introduction to electronic warfare modeling and simulation* (Artech House, 2003). 12

[52] F. C. C. E. Bureau. *Gps, wi-fi, and cell phone jammers frequently asked questions (faqs)* URL https://transition.fcc.gov/eb/jammerenforcement/jamfaq.pdf. 13

[53] B. Barshan and B. Eravci. *Automatic radar antenna scan type recognition in electronic warfare.* IEEE Transactions on Aerospace and Electronic Systems **48**(4), 2908 (2012). 13

[54] K. Pelechrinis, M. Iliofotou, and S. V. Krishnamurthy. *Denial of service attacks in wireless networks: The case of jammers.* IEEE Communications Surveys & Tutorials **13**(2), 245 (2011). 13

[55] B. Dunbar. *Global positioning system history.* NASA (2015). URL https://www.nasa.gov/directorates/heo/scan/communications/policy/GPS_History.html. 13

[56] M. G. Wing, A. Eklund, and L. D. Kellogg. *Consumer-grade global positioning system (gps) accuracy and reliability.* Journal of forestry **103**(4), 169 (2005). 14

[57] S. Kumar and J. Stokkeland. *Evolution of gps technology and its subsequent use in commercial markets.* International Journal of Mobile Communications **1**(1-2), 180 (2003). 14

[58] *Cisco global cloud index: Forecast and methodology, 20152020.* Cisco (2016). URL https://www.cisco.com/c/dam/en/us/solutions/collateral/service-provider/global-cloud-index-gci/white-paper-c11-738085.pdf. 14

[59] K. Pahlavan, F. Akgul, Y. Ye, T. Morgan, F. Alizadeh-Shabdiz, M. Heidari, and C. Steger. *Taking positioning indoors wi-fi localization and gnss.* Inside GNSS **5**(3), 40 (2010). 14

[60] S. P. Tarzia, P. A. Dinda, R. P. Dick, and G. Memik. *Indoor localization without infrastructure using the acoustic background spectrum.* In *Proceedings of the 9th*

international conference on Mobile systems, applications, and services, pp. 155–168 (ACM, 2011). 14

[61] K. Pahlavan, P. Krishnamurthy, and Y. Geng. *Localization challenges for the emergence of the smart world*. IEEE Access **3**, 3058 (2015).

[62] S.-H. Baeg, J.-H. Park, J. Koh, K.-W. Park, and M.-H. Baeg. *Building a smart home environment for service robots based on rfid and sensor networks*. In *Control, Automation and Systems, 2007. ICCAS'07. International Conference on*, pp. 1078–1082 (IEEE, 2007).

[63] S. C. Spinella, A. Iera, and A. Molinaro. *On potentials and limitations of a hybrid wlan-rfid indoor positioning technique*. International Journal of Navigation and Observation **2010** (2010). 14

[64] E. Candes and M. Wakin. *An introduction to compressive sampling*. Signal Processing Magazine, IEEE **25**(2), 21 (2008). 16, 39, 41, 52, 55, 99, 125, 162, 163, 164, 165, 183, 184

[65] E. Candes and J. Romberg. *l1-magic: Recovery of sparse signals via convex programming*. URL: www. acm. caltech. edu/l1magic/downloads/l1magic. pdf **4**, 14 (2005). 45, 52, 73, 101, 189

[66] J. Tropp and A. Gilbert. *Signal recovery from random measurements via orthogonal matching pursuit*. Information Theory, IEEE Transactions on **53**(12), 4655 (2007). 118, 172, 189

[67] D. Needell and J. A. Tropp. *Cosamp: Iterative signal recovery from incomplete and inaccurate samples*. Applied and Computational Harmonic Analysis **26**(3), 301 (2009). 16, 73, 93, 117, 118, 134, 142, 172, 189

[68] M. A. Herman and T. Strohmer. *General deviants: An analysis of perturbations in compressed sensing*. IEEE Journal of Selected topics in signal processing **4**(2), 342 (2010). 17

[69] Y. Chi, L. L. Scharf, A. Pezeshki, and A. R. Calderbank. *Sensitivity to basis mismatch in compressed sensing.* IEEE Transactions on Signal Processing **59**(5), 2182 (2011).

[70] T. Strohmer. *Measure what should be measured: progress and challenges in compressive sensing.* IEEE Signal Processing Letters **19**(12), 887 (2012). 17

[71] G. Mao. *Localization Algorithms and Strategies for Wireless Sensor Networks: Monitoring and Surveillance Techniques for Target Tracking: Monitoring and Surveillance Techniques for Target Tracking* (IGI Global, 2009). 26, 35, 36, 37

[72] *Wi-fi location-based services 4.1 design guide.* CISCO . 27

[73] R. Fuller and X. D. Koutsoukos. *Mobile Entity Localization and Tracking in GPS-less Environnments: Second International Workshop, MELT 2009, Orlando, FL, USA, September 30, 2009, Proceedings*, vol. 5801 (Springer, 2009). 27, 35, 36, 37

[74] A. Goldsmith. *Wireless Communications* (Cambridge University Press, New York, NY, USA, 2005). 28, 185

[75] A. Mariani, S. Kandeepan, A. Giorgetti, and M. Chiani. *Cooperative weighted centroid localization for cognitive radio networks.* In *Communications and Information Technologies (ISCIT), 2012 International Symposium on Communication*, pp. 459–464 (2012). 29, 181, 185

[76] P. Kumar, L. Reddy, and S. Varma. *Distance measurement and error estimation scheme for rssi based localization in wireless sensor networks.* In *Wireless Communication and Sensor Networks (WCSN), 2009 Fifth IEEE Conference on*, pp. 1–4 (IEEE, 2009). 29

[77] P. Kumar, L. Reddy, and S. Varma. *Distance measurement and error estimation scheme for rssi based localization in wireless sensor networks.* In *Wireless Communication and Sensor Networks (WCSN), 2009 Fifth IEEE Conference on*, pp. 1–4 (IEEE, 2009). 29

[78] G. Lui, T. Gallagher, B. Li, A. G. Dempster, and C. Rizos. *Differences in rssi readings made by different wi-fi chipsets: A limitation of wlan localization.* In *Localization and GNSS (ICL-GNSS), 2011 International Conference on*, pp. 53–57 (IEEE, 2011). 29

[79] N. A. Alsindi, B. Alavi, and K. Pahlavan. *Measurement and modeling of ultrawideband toa-based ranging in indoor multipath environments.* IEEE Transactions on Vehicular Technology **58**(3), 1046 (2009). 31

[80] F. Gustafsson and F. Gunnarsson. *Mobile positioning using wireless networks: possibilities and fundamental limitations based on available wireless network measurements.* IEEE Signal processing magazine **22**(4), 41 (2005). 32

[81] V. Y. Zhang, A. K.-s. Wong, K. T. Woo, and R. W. Ouyang. *Hybrid toa/aoa-based mobile localization with and without tracking in cdma cellular networks.* In *Wireless Communications and Networking Conference (WCNC), 2010 IEEE*, pp. 1–6 (IEEE, 2010). 32

[82] C. A. Balanis. *Antenna Theory: Analysis and Design* (Wiley-Interscience, 2005). 32, 78, 85, 149

[83] G. Di Stefano and A. Petricola. *A distributed aoa based localization algorithm for wireless sensor networks.* JCP **3**(4), 1 (2008). 34

[84] G. Sun, J. Chen, W. Guo, and K. R. Liu. *Signal processing techniques in network-aided positioning: a survey of state-of-the-art positioning designs.* IEEE Signal Processing Magazine **22**(4), 12 (2005). 34

[85] E. J. Candes and J. Romberg. *Quantitative robust uncertainty principles and optimally sparse decompositions.* Foundations of Computational Mathematics **6**(2), 227 (2006). 39

[86] E. J. Candes and T. Tao. *Near-optimal signal recovery from random projections: Universal encoding strategies?* IEEE transactions on information theory **52**(12), 5406 (2006).

[87] R. G. Baraniuk. *Compressive sensing [lecture notes].* IEEE signal processing magazine **24**(4), 118 (2007).

[88] D. L. Donoho. *Compressed sensing.* IEEE Transactions on information theory **52**(4), 1289 (2006). 39

[89] M. A. Davenport, M. F. Duarte, Y. C. Eldar, and G. Kutyniok. *Introduction to compressed sensing.* Preprint **93**(1), 2 (2011). 39, 42, 55, 56, 116, 141, 142

[90] M. Elad. *Optimized projections for compressed sensing.* IEEE Transactions on Signal Processing **55**(12), 5695 (2007). 42, 55

[91] R. S. Varga. *Geršgorin-Type Theorems for Partitioned Matrices*, pp. 155–187 (Springer Berlin Heidelberg, Berlin, Heidelberg, 2004). URL http://dx.doi.org/10.1007/978-3-642-17798-9_6. 42, 56

[92] F. R. Gantmakher. *The theory of matrices*, vol. 131 (American Mathematical Soc., 1998). 42, 56

[93] S. Foucart and H. Rauhut. *A mathematical introduction to compressive sensing* (Springer, 2013). 42, 43, 56, 57, 99, 143, 170, 187

[94] T. Strohmer and R. W. Heath. *Grassmannian frames with applications to coding and communication.* Applied and computational harmonic analysis **14**(3), 257 (2003). 42, 56

[95] D. Taubman and M. Marcellin. *Jpeg 2000: Image compression fundamentals, practices and standards.* Springer (2001). 42, 56

[96] D. G. Feingold and R. Varga. *Block diagonally dominant matrices and generalizations of the gerschgorin circle theorem.* Pacific Journal of Mathematics **12**(4), 1241 (1962). 43, 56

[97] R. Schmidt. *Multiple emitter location and signal parameter estimation.* IEEE Transactions on Antennas and Propagation **34**(3), 276 (1986). 44, 51, 99, 138, 163

[98] R. Roy and T. Kailath. *Esprit-estimation of signal parameters via rotational invariance techniques*. IEEE Transactions on Acoustics, Speech, and Signal Processing **37**(7), 984 (1989). 44, 51, 99, 138

[99] J. Capon. *High-resolution frequency-wavenumber spectrum analysis*. Proceedings of the IEEE **57**(8), 1408 (1969). 44, 51

[100] P. Stoica and A. Nehorai. *Music, maximum likelihood, and cramer-rao bound*. IEEE Transactions on Acoustics, Speech, and Signal Processing **37**(5), 720 (1989). 44

[101] D. H. Johnson and E. Dan. *De dudgeon array signal processing* (1993). 44

[102] M. Donelli, F. Viani, P. Rocca, and A. Massa. *An innovative multiresolution approach for doa estimation based on a support vector classification*. IEEE Transactions on Antennas and Propagation **57**(8), 2279 (2009). 44, 52, 100

[103] A. H. El Zooghby, C. G. Christodoulou, and M. Georgiopoulos. *Performance of radial-basis function networks for direction of arrival estimation with antenna arrays*. IEEE Transactions on Antennas and Propagation **45**(11), 1611 (1997).

[104] A. H. El Zooghby, C. G. Christodoulou, and M. Georgiopoulos. *A neural network-based smart antenna for multiple source tracking*. IEEE Transactions on Antennas and Propagation **48**(5), 768. 44

[105] D. Malioutov, M. Çetin, and A. S. Willsky. *A sparse signal reconstruction perspective for source localization with sensor arrays*. IEEE transactions on signal processing **53**(8), 3010 (2005). 44

[106] Y. Wang, G. Leus, and A. Pandharipande. *Direction estimation using compressive sampling array processing*. In *Statistical Signal Processing, 2009. SSP'09. IEEE/SP 15th Workshop on*, pp. 626–629 (IEEE, 2009). 100, 163

[107] M. Ibrahim, F. Roemer, and G. D. Galdo. *On the design of the measurement matrix for compressed sensing based doa estimation*. In *Acoustics, Speech and*

Signal Processing (ICASSP), 2015 IEEE International Conference on, pp. 3631–3635 (2015). 163, 167

[108] I. Bilik. *Spatial compressive sensing for direction-of-arrival estimation of multiple sources using dynamic sensor arrays.* IEEE Transactions on Aerospace and Electronic Systems **47**(3), 1754 (2011). 44, 52, 100, 139

[109] Z. Yang, C. Zhang, and L. Xie. *Robustly stable signal recovery in compressed sensing with structured matrix perturbation.* IEEE Transactions on Signal Processing **60**(9), 4658 (2012). 45

[110] H. Zhu, G. Leus, and G. B. Giannakis. *Sparsity-cognizant total least-squares for perturbed compressive sampling.* IEEE Transactions on Signal Processing **59**(5), 2002 (2011). 45

[111] A. C. Gurbuz, V. Cevher, and J. H. Mcclellan. *Bearing estimation via spatial sparsity using compressive sensing.* IEEE Transactions on Aerospace and Electronic Systems **48**(2), 1358 (2012). 45

[112] Z. Tan and A. Nehorai. *Sparse direction of arrival estimation using co-prime arrays with off-grid targets.* IEEE Signal Processing Letters **21**(1), 26 (2014). 45, 46, 53, 100

[113] A. Biswas, S. Reisenfeld, L. Goratti, M. Hedley, and Z. Chen. *Multiresolution compressive sensing algorithm to detect off-grid direction of arrival.* In *2016 10th International Conference on Signal Processing and Communication Systems (ICSPCS)*, pp. 1–6 (2016). 45, 52, 100

[114] M. Ibrahim, F. Roemer, and G. D. Galdo. *An adaptively focusing measurement design for compressed sensing based doa estimation.* In *2015 23rd European Signal Processing Conference (EUSIPCO)*, pp. 859–863 (2015). 45, 52, 100

[115] C. D. Austin, R. L. Moses, J. N. Ash, and E. Ertin. *On the relation between sparse reconstruction and parameter estimation with model order selection.* IEEE Journal of Selected Topics in Signal Processing **4**(3), 560 (2010). 45

[116] P. Stoica and P. Babu. *Sparse estimation of spectral lines: Grid selection problems and their solutions.* IEEE Transactions on Signal Processing **60**(2), 962 (2012). 45

[117] S. Ji, Y. Xue, and L. Carin. *Bayesian compressive sensing.* IEEE Transactions on Signal Processing **56**(6), 2346 (2008). 46

[118] M. Carlin, P. Rocca, G. Oliveri, F. Viani, and A. Massa. *Directions-of-arrival estimation through bayesian compressive sensing strategies.* IEEE Transactions on Antennas and Propagation **61**(7), 3828 (2013). 46, 53, 100

[119] D. P. Wipf and B. D. Rao. *Sparse bayesian learning for basis selection.* IEEE Transactions on Signal processing **52**(8), 2153 (2004). 100

[120] Z.-M. Liu, Z.-T. Huang, and Y.-Y. Zhou. *An efficient maximum likelihood method for direction-of-arrival estimation via sparse bayesian learning.* IEEE Transactions on Wireless Communications **11**(10), 1 (2012). 53, 100

[121] X. Wu, W.-P. Zhu, and J. Yan. *Direction of arrival estimation for off-grid signals based on sparse bayesian learning.* IEEE Sensors Journal **16**(7), 2004 (2016).

[122] M. Carlin and P. Rocca. *A bayesian compressive sensing strategy for direction-of-arrival estimation.* In *Antennas and Propagation (EUCAP), 2012 6th European Conference on*, pp. 1508–1509 (IEEE, 2012). 46

[123] Z.-M. Liu and Y.-Y. Zhou. *A unified framework and sparse bayesian perspective for direction-of-arrival estimation in the presence of array imperfections.* IEEE Transactions on Signal Processing **61**(15), 3786 (2013). 46

[124] Z. Yang, L. Xie, and C. Zhang. *Off-grid direction of arrival estimation using sparse bayesian inference.* IEEE Transactions on Signal Processing **61**(1), 38 (2013). 46

[125] H. Zhu, G. Leus, and G. B. Giannakis. *Sparsity-cognizant total least-squares for perturbed compressive sampling.* IEEE Transactions on Signal Processing **59**(5), 2002 (2011). 46

[126] Y. D. Zhang, S. Qin, and M. G. Amin. *Doa estimation exploiting coprime arrays with sparse sensor spacing*. In *Acoustics, Speech and Signal Processing (ICASSP), 2014 IEEE International Conference on*, pp. 2267–2271 (IEEE, 2014). 46, 53

[127] E. T. Northardt, I. Bilik, and Y. I. Abramovich. *Spatial compressive sensing for direction-of-arrival estimation with bias mitigation via expected likelihood*. IEEE Transactions on Signal Processing **61**(5), 1183 (2013). 46, 53, 77, 107

[128] I. Kazemi, M. R. Moniri, and R. S. Kandovan. *Optimization of angle-of-arrival estimation via real-valued sparse representation with circular array radar*. IEEE Access **1**, 404 (2013). 46, 53

[129] C. Feng, S. Valaee, and Z. Tan. *Multiple target localization using compressive sensing*. In *Global Telecommunications Conference, 2009. GLOBECOM 2009. IEEE*, pp. 1–6 (2009). 46, 53, 87, 104, 123, 163, 168, 171, 181, 184, 188

[130] R. Grabau and K. Pfaff. *Funkpeiltechnik*. Franckhsche Verlagshandlung, Stuttgart (1989). 50

[131] J. C. Liberti and T. S. Rappaport. *Smart antennas for wireless communications: IS-95 and third generation CDMA applications* (Prentice Hall PTR, 1999). 51

[132] J. Gammel. *Military radar or radio communication system* (1988). US Patent 4,761,813.

[133] J. Kennedy and M. C. Sullivan. *Direction finding and" smart antennas" using software radio architectures*. IEEE Communications Magazine **33**(5), 62 (1995).

[134] P. M. Kintner and B. M. Ledvina. *The ionosphere, radio navigation, and global navigation satellite systems*. Advances in Space Research **35**(5), 788 (2005).

[135] T. S. Rappaport, J. H. Reed, and B. D. Woerner. *Position location using wireless communications on highways of the future*. IEEE communications Magazine **34**(10), 33 (1996).

[136] J. Bergin, J. D. Halsey, and J. D. Carlos. *Intelligent passive navigation system for back-up and verification of gps* (2005). US Patent 6,917,880.

[137] P. Howland. *Target tracking using television-based bistatic radar.* IEE Proceedings-Radar, Sonar and Navigation **146**(3), 166 (1999).

[138] A. Lin and H. Ling. *Through-wall measurements of a doppler and direction-of-arrival (ddoa) radar for tracking indoor movers.* In *Antennas and Propagation Society International Symposium, 2005 IEEE*, vol. 3, pp. 322–325 (IEEE, 2005). 51

[139] J. B. Roes and D. Varshneya. *Secure covert combat identification friend-or-foe (iff) system for the dismounted soldier* (2007). US Patent 7,308,202. 51

[140] R. O. Schmidt. *Multilinear array manifold interpolation.* IEEE Transactions on Signal Processing **40**(4), 857 (1992). 51

[141] Q. H. Spencer, A. L. Swindlehurst, and M. Haardt. *Zero-forcing methods for downlink spatial multiplexing in multiuser mimo channels.* IEEE Transactions on Signal Processing **52**(2), 461 (2004). 51

[142] J. G. Andrews, W. Choi, and R. W. Heath. *Overcoming interference in spatial multiplexing mimo cellular networks.* IEEE Wireless Communications **14**(6), 95 (2007). 138

[143] D. J. Love and R. W. Heath. *Limited feedback unitary precoding for spatial multiplexing systems.* IEEE Transactions on Information theory **51**(8), 2967 (2005). 51

[144] M. Chryssomallis. *Smart antennas.* IEEE Antennas and Propagation Magazine **42**(3), 129 (2000). 51, 138

[145] D. Malioutov, M. Çetin, and A. S. Willsky. *A sparse signal reconstruction perspective for source localization with sensor arrays.* IEEE Transactions on Signal Processing **53**(8), 3010 (2005). 52, 107

[146] Y. Wang, G. Leus, and A. Pandharipande. *Direction estimation using compressive sampling array processing*. In *2009 IEEE/SP 15th Workshop on Statistical Signal Processing*, pp. 626–629 (2009). 100, 139

[147] M. Ibrahim, F. Roemer, and G. Del Galdo. *On the design of the measurement matrix for compressed sensing based doa estimation*. In *2015 IEEE International Conference on Acoustics, Speech and Signal Processing (ICASSP)*, pp. 3631–3635 (IEEE, 2015). 52, 100, 139

[148] F. Belloni and V. Koivunen. *Beamspace transform for uca: Error analysis and bias reduction*. Signal Processing, IEEE Transactions on **54**(8), 3078 (2006). 53, 163

[149] F. Bellili, S. Affes, and A. Stéphenne. *On the lower performance bounds for doa estimators from linearly-modulated signals*. In *Communications (QBSC), 2010 25th Biennial Symposium on*, pp. 381–386 (IEEE, 2010). 72, 118, 154, 219

[150] D. Xu, Z. Liu, Y. Xu, and J. Cao. *A unitary transformation method for doa estimation with uniform circular array*. In *2010 IEEE International Conference on Wireless Communications, Networking and Information Security*, pp. 142–145 (2010). 78

[151] I. Kazemi, M. R. Moniri, and R. S. Kandovan. *Optimization of angle-of-arrival estimation via real-valued sparse representation with circular array radar*. IEEE Access **1**, 404 (2013). 78

[152] R. Dony. *Karhunen-loeve transform*. In *The transform and data compression handbook* (CRC Press, 2000). 87, 123

[153] N. Ahmed, T. Natarajan, and K. R. Rao. *Discrete cosine transform*. IEEE transactions on Computers **100**(1), 90 (1974). 123

[154] S. Weinstein and P. Ebert. *Data transmission by frequency-division multiplexing using the discrete fourier transform*. IEEE transactions on Communication Technology **19**(5), 628 (1971). 87, 123

[155] W. Sun, J. Liu, and H. Zhang. *When smart wearables meet intelligent vehicles: Challenges and future directions.* IEEE Wireless Communications **24**(3), 58 (2017). 98

[156] S. M. Razavizadeh, M. Ahn, and I. Lee. *Three-dimensional beamforming: A new enabling technology for 5g wireless networks.* IEEE Signal Processing Magazine **31**(6), 94 (2014). 99

[157] N. Al-Falahy and O. Y. K. Alani. *The impact of higher order sectorisation on the performance of millimetre wave 5g network.* In *2016 10th International Conference on Next Generation Mobile Applications, Security and Technologies (NGMAST)*, pp. 1–5 (2016).

[158] F. Athley, M. N. Johansson, and A. Nilsson. *Increased sectorization: Horizontal or vertical?* In *2013 IEEE 78th Vehicular Technology Conference (VTC Fall)*, pp. 1–5 (2013).

[159] R. W. Heath, S. Sandhu, and A. Paulraj. *Antenna selection for spatial multiplexing systems with linear receivers.* IEEE Communications letters **5**(4), 142 (2001).

[160] Q. H. Spencer, A. L. Swindlehurst, and M. Haardt. *Zero-forcing methods for downlink spatial multiplexing in multiuser mimo channels.* IEEE Transactions on Signal Processing **52**(2), 461 (2004).

[161] H. Bolcskei, D. Gesbert, and A. J. Paulraj. *On the capacity of ofdm-based spatial multiplexing systems.* IEEE Transactions on communications **50**(2), 225 (2002). 99

[162] M. A. Davenport, M. F. Duarte, Y. C. Eldar, and G. Kutyniok. *Introduction to compressed sensing.* Preprint **93**(1), 2 (2011). 99, 163, 164, 171

[163] L. Anitori, A. Maleki, M. Otten, R. G. Baraniuk, and P. Hoogeboom. *Design and analysis of compressed sensing radar detectors.* IEEE Transactions on Signal Processing **61**(4), 813 (2013). 100, 163

[164] A. Biswas, S. Reisenfeld, L. Goratti, M. Hedley, and Z. Chen. *Multiresolution compressive sensing algorithm to detect off-grid direction of arrival*. In *Signal Processing and Communication Systems (ICSPCS), 2016 10th International Conference on*, pp. 1–6 (IEEE, 2016). 100

[165] W. Dai and O. Milenkovic. *Subspace pursuit for compressive sensing signal reconstruction*. IEEE Transactions on Information Theory **55**(5), 2230 (2009). 122

[166] S. Li and G. Ge. *Deterministic construction of sparse sensing matrices via finite geometry*. IEEE Transactions on Signal Processing **62**(11), 2850 (2014).

[167] A. Cohen, W. Dahmen, and R. DeVore. *Compressed sensing and best k-term approximation*. Journal of the American mathematical society **22**(1), 211 (2009). 122

[168] V. Abolghasemi, S. Ferdowsi, B. Makkiabadi, and S. Sanei. *On optimization of the measurement matrix for compressive sensing*. In *Signal Processing Conference, 2010 18th European*, pp. 427–431 (IEEE, 2010). 126

[169] J. Xu, Y. Pi, and Z. Cao. *Optimized projection matrix for compressive sensing*. EURASIP Journal on Advances in Signal Processing **2010**(1), 560349 (2010).

[170] G. Li, Z. Zhu, D. Yang, L. Chang, and H. Bai. *On projection matrix optimization for compressive sensing systems*. IEEE Transactions on Signal Processing **61**(11), 2887 (2013). 126

[171] C. A. Balanis. *Antenna theory: analysis and design* (John Wiley & Sons, 2016). 130, 166

[172] I. A. Junglas and R. T. Watson. *Location-based services*. Commun. ACM **51**(3), 65 (2008). URL http://doi.acm.org/10.1145/1325555.1325568. 138

[173] M. Sedehi, F. Colone, D. Cristallini, and P. Lombardo. *Reduced order jammer cancellation scheme based on double adaptivity*. IEEE Transactions on Aerospace and Electronic Systems **46**(4), 1762 (2010). 138

[174] M. Carlin, P. Rocca, G. Oliveri, F. Viani, and A. Massa. *Directions-of-arrival estimation through bayesian compressive sensing strategies.* IEEE Transactions on Antennas and Propagation **61**(7), 3828 (2013). 139, 163, 167

[175] P. Ioannides and C. A. Balanis. *Uniform circular arrays for smart antennas.* IEEE Antennas and propagation magazine **47**(4), 192 (2005). 139

[176] J.-A. Tsai, R. M. Buehrer, and B. D. Woerner. *Ber performance of a uniform circular array versus a uniform linear array in a mobile radio environment.* IEEE Transactions on Wireless Communications **3**(3), 695 (2004).

[177] P. Ioannides and C. A. Balanis. *Uniform circular and rectangular arrays for adaptive beamforming applications.* IEEE Antennas and Wireless Propagation Letters **4**(1), 351 (2005).

[178] Y. Wu and H. C. So. *Simple and accurate two-dimensional angle estimation for a single source with uniform circular array.* IEEE Antennas and Wireless Propagation Letters **7**, 78 (2008). 139

[179] A. Biswas and S. Reisenfeld. *New high resolution direction of arrival estimation using compressive sensing.* In *2017 IEEE 22nd International Workshop on Computer Aided Modeling and Design of Communication Links and Networks (CAMAD)*, pp. 1–6 (2017). 139, 154

[180] H. L. Van Trees. *Detection, estimation, and modulation theory, optimum array processing* (2004). 163

[181] Z. Ben-Haim, Y. C. Eldar, and M. Elad. *Coherence-based performance guarantees for estimating a sparse vector under random noise.* Signal Processing, IEEE Transactions on **58**(10), 5030 (2010). 173

[182] S. Wang, Q. Yang, W. Shi, and C. Wang. *Interference mitigation and resource allocation in cognitive radio-enabled heterogeneous networks.* In *Global Communications Conference (GLOBECOM), 2013 IEEE*, pp. 4560–4565 (2013). 180

[183] D. Hu and S. Mao. *Co-channel and adjacent channel interference mitigation in cognitive radio networks.* In *Military Communications Conference, 2011 - MILCOM 2011*, pp. 13–18 (2011). 180

[184] J. Werner, J. Wang, A. Hakkarainen, M. Valkama, and D. Cabric. *Primary user localization in cognitive radio networks using sectorized antennas.* In *Wireless On-demand Network Systems and Services (WONS), 2013 10th Annual Conference on*, pp. 155–161 (2013). 181

[185] I. Arambasic, J. Q. Casajus, I. Raos, M. Raspopoulos, and S. Stavrou. *Anchor-less self-positioning in rectangular room based on sectorized narrowband antennas.* In *Wireless Conference (EW), Proceedings of the 2013 19th European*, pp. 1–6 (2013). 181

[186] X. Li, S. Hong, Z. Han, and Z. Wu. *Bayesian compressed sensing based dynamic joint spectrum sensing and primary user localization for dynamic spectrum access.* In *Global Telecommunications Conference (GLOBECOM 2011), 2011 IEEE*, pp. 1–5 (2011). 181, 183

[187] B. Jayawickrama, E. Dutkiewicz, I. Oppermann, G. Fang, and J. Ding. *Improved performance of spectrum cartography based on compressive sensing in cognitive radio networks.* In *Communications (ICC), 2013 IEEE International Conference on*, pp. 5657–5661 (2013). 181, 184, 188

[188] H. Jamali-Rad, H. Ramezani, and G. Leus. *Sparse multi-target localization using cooperative access points.* In *Sensor Array and Multichannel Signal Processing Workshop (SAM), 2012 IEEE 7th*, pp. 353–356 (2012). 181

[189] A. Biswas, S. Reisenfeld, M. Hedley, Z. Chen, and P. Cheng. *Localization of primary users by exploiting distance separation between secondary users.* In *Cognitive Radio Oriented Wireless Networks - 10th International Conference, CROWNCOM 2015, Doha, Qatar, April 21-23, 2015, Revised Selected Papers*, pp. 451–462 (2015). 195, 196

[190] S. M. Kay. *Fundamentals of statistical signal processing* (Prentice Hall PTR, 1993). 220

[191] B. R. Jackson, S. Rajan, B. J. Liao, and S. Wang. *Direction of arrival estimation using directive antennas in uniform circular arrays.* Antennas and Propagation, IEEE Transactions on **63**(2), 736 (2015). 221